

JOURNAL OF

CHROMATOGRAPHY A

INCLUDING ELECTROPHORESIS AND OTHER SEPARATION METHODS

EDITORS

U.A.Th. Brinkman (Amsterdam)
 R.W. Giese (Boston, MA)
 J.K. Haken (Kensington, N.S.W.)
 L.R. Snyder (Orinda, CA)
 S. Terabe (Hyogo)

EDITORS, SYMPOSIUM VOLUMES,
 E. Heftmann (Orinda, CA), Z. Deyl (Prague)

EDITORIAL BOARD

D.W. Armstrong (Rolla, MO)
 W.A. Aue (Halifax)
 P. Boček (Brno)
 A.A. Boulton (Saskatoon)
 P.W. Carr (Minneapolis, MN)
 N.H.C. Cooke (San Ramon, CA)
 V.A. Davankov (Moscow)
 G.J. de Jong (Weesp)
 Z. Deyl (Prague)
 S. Dilli (Kensington, N.S.W.)
 Z. El Rassi (Stillwater, OK)
 H. Engelhardt (Saarbrücken)
 F. Erni (Basle)
 M.B. Evans (Hatfield)
 J.L. Glajch (N. Billerica, MA)
 G.A. Guiochon (Knoxville, TN)
 P.R. Haddad (Hobart, Tasmania)
 I.M. Hais (Hradec Králové)
 W.S. Hancock (Palo Alto, CA)
 S. Hjerten (Uppsala)
 S. Honda (Higashi-Osaka)
 Cs. Horváth (New Haven, CT)
 J.F.K. Huber (Vienna)
 K.-P. Hupe (Waldbronn)
 J. Janák (Brno)
 P. Jandera (Pardubice)
 B.L. Karger (Boston, MA)
 J.J. Kirkland (Newport, DE)
 E. sz. Kováts (Lausanne)
 K. Macek (Prague)
 A.J.P. Martin (Cambridge)
 L.W. McLaughlin (Chestnut Hill, MA)
 E.D. Morgan (Keele)
 J.D. Pearson (Kalamazoo, MI)
 H. Poppe (Amsterdam)
 F.E. Regnier (West Lafayette, IN)
 P.G. Righetti (Milan)
 P. Schoenmakers (Amsterdam)
 R. Schwarzenbach (Dübendorf)
 R.E. Shoup (West Lafayette, IN)
 R.P. Singhal (Wichita, KS)
 A.M. Siouffi (Marseille)
 D.J. Strydom (Boston, MA)
 N. Tanaka (Kyoto)
 K.K. Unger (Mainz)
 R. Verpoorte (Leiden)
 Gy. Vigh (College Station, TX)
 J.T. Watson (East Lansing, MI)
 B.D. Westerlund (Uppsala)

EDITORS, BIBLIOGRAPHY SECTION

Z. Deyl (Prague), J. Janák (Brno), V. Schwarz (Prague)

ELSEVIER

JOURNAL OF CHROMATOGRAPHY A

INCLUDING ELECTROPHORESIS AND OTHER SEPARATION METHODS

Scope. The *Journal of Chromatography A* publishes papers on all aspects of **chromatography, electrophoresis** and related methods. Contributions consist mainly of research papers dealing with chromatographic theory, instrumental developments and their applications. In the *Symposium volumes*, which are under separate editorship, proceedings of symposia on chromatography, electrophoresis and related methods are published. *Journal of Chromatography B: Biomedical Applications*—This journal, which is under separate editorship, deals with the following aspects: developments in and applications of chromatographic and electrophoretic techniques related to clinical diagnosis or alterations during medical treatment; screening and profiling of body fluids or tissues related to the analysis of active substances and to metabolic disorders; drug level monitoring and pharmacokinetic studies; clinical toxicology; forensic medicine; veterinary medicine; occupational medicine; results from basic medical research with direct consequences in clinical practice.

Submission of Papers. The preferred medium of submission is on disk with accompanying manuscript (see *Electronic manuscripts* in the Instructions to Authors, which can be obtained from the publisher, Elsevier Science B.V., P.O. Box 330, 1000 AH Amsterdam, Netherlands). Manuscripts (in English; four copies are required) should be submitted to: Editorial Office of *Journal of Chromatography A*, P.O. Box 681, 1000 AR Amsterdam, Netherlands, Telefax (+31-20) 5862 304, or to: The Editor of *Journal of Chromatography B: Biomedical Applications*, P.O. Box 681, 1000 AR Amsterdam, Netherlands. Review articles are invited or proposed in writing to the Editors who welcome suggestions for subjects. An outline of the proposed review should first be forwarded to the Editors for preliminary discussion prior to preparation. Submission of an article is understood to imply that the article is original and unpublished and is not being considered for publication elsewhere. For copyright regulations, see below.

Publication information. *Journal of Chromatography A* (ISSN 0021-9673): for 1994 Vols. 652–682 are scheduled for publication. *Journal of Chromatography B: Biomedical Applications* (ISSN 0378-4347): for 1994 Vols. 652–662 are scheduled for publication. Subscription prices for *Journal of Chromatography A*, *Journal of Chromatography B: Biomedical Applications* or a combined subscription are available upon request from the publisher. Subscriptions are accepted on a prepaid basis only and are entered on a calendar year basis. Issues are sent by surface mail except to the following countries where air delivery via SAL is ensured: Argentina, Australia, Brazil, Canada, China, Hong Kong, India, Israel, Japan, Malaysia, Mexico, New Zealand, Pakistan, Singapore, South Africa, South Korea, Taiwan, Thailand, USA. For all other countries airmail rates are available upon request. Claims for missing issues must be made within six months of our publication (mailing) date. Please address all your requests regarding orders and subscription queries to: Elsevier Science B.V., Journal Department, P.O. Box 211, 1000 AE Amsterdam, Netherlands. Tel.: (+31-20) 5803 642; Fax: (+31-20) 5803 598. Customers in the USA and Canada wishing information on this and other Elsevier journals, please contact Journal Information Center, Elsevier Science Inc., 655 Avenue of the Americas, New York, NY 10010, USA. Tel. (+1-212) 633 3750, Telefax (+1-212) 633 3764.

Abstracts/Contents Lists published in Analytical Abstracts, Biochemical Abstracts, Biological Abstracts, Chemical Abstracts, Chemical Titles, Chromatography Abstracts, Current Awareness in Biological Sciences (CABS), Current Contents/Life Sciences, Current Contents/Physical, Chemical & Earth Sciences, Deep-Sea Research/Part B: Oceanographic Literature Review, Excerpta Medica, Index Medicus, Mass Spectrometry Bulletin, PASCAL-CNRS, Referativnyi Zhurnal, Research Alert and Science Citation Index.

US Mailing Notice. *Journal of Chromatography A* (ISSN 0021-9673) is published weekly (total 52 issues) by Elsevier Science B.V., (Sara Burgerhartstraat 25, P.O. Box 211, 1000 AE Amsterdam, Netherlands). Annual subscription price in the USA US\$ 4994.00 (US\$ price valid in North, Central and South America only) including air speed delivery. Second class postage paid at Jamaica, NY 11431. **USA POSTMASTERS:** Send address changes to *Journal of Chromatography A*, Publications Expediting, Inc., 200 Meacham Avenue, Elmont, NY 11003. Airfreight and mailing in the USA by Publications Expediting.

See inside back cover for Publication Schedule, Information for Authors and information on Advertisements.

© 1994 ELSEVIER SCIENCE B.V. All rights reserved.

0021-9673/94/\$07.00

No part of this publication may be reproduced, stored in a retrieval system or transmitted in any form or by any means, electronic, mechanical, photocopying, recording or otherwise, without the prior written permission of the publisher, Elsevier Science B.V., Copyright and Permissions Department, P.O. Box 521, 1000 AM Amsterdam, Netherlands.

Upon acceptance of an article by the journal, the author(s) will be asked to transfer copyright of the article to the publisher. The transfer will ensure the widest possible dissemination of information.

Special regulations for readers in the USA - This journal has been registered with the Copyright Clearance Center, Inc. Consent is given for copying of articles for personal or internal use, or for the personal use of specific clients. This consent is given on the condition that the copier pays through the Center the per-copy fee stated in the code on the first page of each article for copying beyond that permitted by Sections 107 or 108 of the US Copyright Law. The appropriate fee should be forwarded with a copy of the first page of the article to the Copyright Clearance Center, Inc., 27 Congress Street, Salem, MA 01970, USA. If no code appears in an article, the author has not given broad consent to copy and permission to copy must be obtained directly from the author. The fee indicated on the first page of an article in this issue will apply retroactively to all articles published in the journal, regardless of the year of publication. This consent does not extend to other kinds of copying, such as for general distribution, resale, advertising and promotion purposes, or for creating new collective works. Special written permission must be obtained from the publisher for such copying.

No responsibility is assumed by the Publisher for any injury and/or damage to persons or property as a matter of products liability, negligence or otherwise, or from any use or operation of any methods, products, instructions or ideas contained in the materials herein. Because of rapid advances in the medical sciences, the Publisher recommends that independent verification of diagnoses and drug dosages should be made.

Although all advertising material is expected to conform to ethical (medical) standards, inclusion in this publication does not constitute a guarantee or endorsement of the quality or value of such product or of the claims made of it by its manufacturer.

Ⓢ The paper used in this publication meets the requirements of ANSI/NISO Z39.48-1992 (Permanence of Paper).

Printed in the Netherlands

CONTENTS

(Abstracts/Contents Lists published in *Analytical Abstracts*, *Biochemical Abstracts*, *Biological Abstracts*, *Chemical Abstracts*, *Chemical Titles*, *Chromatography Abstracts*, *Current Awareness in Biological Sciences (CABS)*, *Current Contents/Life Sciences*, *Current Contents/Physical, Chemical & Earth Sciences*, *Deep-Sea Research/Part B: Oceanographic Literature Review*, *Excerpta Medica*, *Index Medicus*, *Mass Spectrometry Bulletin*, *PASCAL-CNRS*, *Referativnyi Zhurnal*, *Research Alert* and *Science Citation Index*)

REGULAR PAPERS

Column Liquid Chromatography

- Use of system peaks for the determination of the distribution of resorcinol, catechol and phenol in liquid chromatography
by S. Levin and S. Abu-Lafi (Jerusalem, Israel), S. Golshan-Shirazi (Wilmington, NC, USA) and G. Guiochon
(Knoxville and Oak Ridge, TN, USA) (Received 21 March 1994) 213
- Column efficiency and radial homogeneity in liquid chromatography
by T. Farkas, J.Q. Chambers and G. Guiochon (Knoxville and Oak Ridge, TN, USA) (Received 16 March 1994) 231
- Metaphosphates as packing materials for biochromatography
by S. Inoue and N. Ohtaki (Saitama, Japan) (Received 27 May 1994) 247
- Choice of a tracer for external porosity measurement in ion-exchange resin beds
by M.-L. Lameloise and V. Viard (Massy, France) (Received 19 May 1994) 255
- Analytical method optimization for protein determination by fast high-performance liquid chromatography
by I. Gaillard, A. Martial, A. Marc, J.-M. Engasser and M. Fick (Vandoeuvre-lès-Nancy, France) (Received
26 April 1994) 261
- Extraction, purification by solid-phase extraction and high-performance liquid chromatographic analysis of taxanes from
ornamental *Taxus* needles
by M.J.I. Mattina and G.J. MacEachern (New Haven, CT, USA) (Received 21 June 1994) 269
- Liquid chromatography of antihistamines using post-column tris(2,2'-bipyridine) ruthenium(III) chemiluminescence de-
tection
by J.A. Holeman and N.D. Danielson (Oxford, OH, USA) (Received 8 June 1994) 277
- Characterisation of electron beam generated transformation products of Irganox 1010 by particle beam liquid chromatog-
raphy-mass spectrometry with on-line diode array detection
by D.W. Allen, M.R. Clench, A. Crowson, D.A. Leathard and R. Saklatvala (Sheffield, UK) (Received
13 June 1994) 285

Gas Chromatography

- Effect of detector temperature on the flame ionization detector response
by M. Dressler and M. Cigánek (Brno, Czech Republic) (Received 26 May 1994) 299
- Gas chromatographic determination of vapour pressures of pheromone-like compounds. II. Alcohols
by B. Koutek, A. Hoskovec, P. Vrkočová, K. Konečný and L. Feltl (Prague, Czech Republic) (Received
21 April 1994) 307
- Carbon dioxide supercritical fluid extraction of incinerator fly ash with a reactive solvent modifier
by J.W. Hills and H.H. Hill, Jr., (Pullman, WA, USA) and D.R. Hansen and S.G. Metcalf (Richland, WA, USA)
(Received 30 November 1993) 319

Supercritical Fluid Chromatography

- Supercritical fluid chromatographic determination of tocopherols on an ODS-silica gel column
by T. Yarita and A. Nomura (Ibaraki, Japan) and K. Abe and Y. Takeshita (Tokyo, Japan) (Received 26 May 1994) 329

Electrophoresis

- Suggested definition of zone resolution and zone capacity in separations of weak electrolytes or ampholytes by steady-state
electrophoretic methods
by K. Šlais (Brno, Czech Republic) (Received 2 May 1994) 335

Contents (continued)

Time course of formation of inositol phosphates during enzymatic hydrolysis of phytic acid (myo-inositol hexaphosphoric acid) by phytase determined by capillary isotachopheresis
by P. Blatný (Vienna, Austria), F. Kvasnička (Prague, Czech Republic) and E. Kenndler (Vienna, Austria)
(Received 22 June 1994) 345

Sensitive and selective method for the separation of organic acids by capillary zone electrophoresis
by O. Devèvre (Champenoux, France), D.P. Putra and B. Botton (Vandoeuvre-Les-Nancy, France) and J. Garbaye
(Champenoux, France) (Received 1 June 1994) 349

Use of selectively methylated β -cyclodextrin derivatives in chiral separation of dansylamino acids by capillary zone electrophoresis
by M. Yoshinaga and M. Tanaka (Osaka, Japan) (Received 1 June 1994) 359

Chiral high-performance liquid chromatography methodology for quality control monitoring of dexfenfluramine
by L. Dou, J.-N. Zeng, D.D. Gerochi, M.P. Duda and H.H. Stuting (Raritan, NJ, USA) (Received 16 May 1994) 367

SHORT COMMUNICATIONS

Column Liquid Chromatography

Application of normal- and reversed-phase high-performance liquid chromatography for monitoring the progress of reactions of anthraquinone manufacturing processes
by S. Husain, R. Narsimha, S. Khalid and R. Nageswara Rao (Hyderabad, India) (Received 14 June 1994) 375

High-performance liquid chromatographic determination of carnosic acid and carnosol in *Rosmarinus officinalis* and *Salvia officinalis*
by N. Okamura, Y. Fujimoto, S. Kuwabara and A. Yagi (Hiroshima, Japan) (Received 14 June 1994) 381

Dynamic ion-exchange chromatography for the determination of lanthanides in rock standards
by N.M.P. Moraes and H.M. Shihomatsu (São Paulo, Brasil) (Received 8 June 1994) 387

Gas Chromatography

Experimental method to distinguish column dead time from system dead time for the accurate determination of gas chromatographic void volumes: simultaneous pre- and post-column injection
by Y. Liu, K.S. Yun and J.F. Parcher (University, MS, USA) (Received 28 June 1994) 392

Quantitative determination of pivalic acid in dipivefrin-containing ophthalmic solutions by gas chromatography
by L. Hall (Irvine, CA, USA) (Received 13 June 1994) 397

BOOK REVIEWS

Electrophoresis in Practice —A Guide to Theory and Practice (by R. Westermeier), reviewed by Petr Boček (Brno, Czech Republic) 402

Mass Spectrometry for the Characterization of Microorganisms (edited by C. Fenselau), reviewed by Emilo Gelpí (Barcelona, Spain) 404

AUTHOR INDEX 406



ELSEVIER

Journal of Chromatography A, 679 (1994) 213–229

JOURNAL OF
CHROMATOGRAPHY A

Use of system peaks for the determination of the distribution of resorcinol, catechol and phenol in liquid chromatography

Shulamit Levin^{a,*}, Saleh Abu-Lafi^a, Sadroddin Golshan-Shirazi^b,
Georges Guiochon^{c,d}

^a*School of Pharmacy, Hebrew University of Jerusalem, Jerusalem 91120, Israel*

^b*AAI, Wilmington, NC, USA*

^c*Department of Chemistry, University of Tennessee, Knoxville, TN 37996-1600, USA*

^d*Division of Chemical and Analytical Sciences, Oak Ridge National Laboratory, Oak Ridge, TN 37863, USA*

First received 24 November 1993; revised manuscript received 21 March 1994

Abstract

The single-component adsorption isotherms of resorcinol, catechol and phenol between aqueous solutions and LiChrosorb RP-18 were determined using the system peaks of these components. The single-component isotherms obtained agree well with those derived by frontal analysis. For multi-component solutions at low concentrations, the system peaks obtained are the combination of those observed for the different single-component systems (linear range). When the concentration increases, the retention times and the areas of the different system peaks depend on the nature and concentration of all the system components (non-linear range). The experimental results agree well with the results predicted using the Langmuir competitive isotherms derived from the single-component isotherms. The dependence of the system peak areas on these concentrations is especially complex. The experimental results agree well, however, with those of calculations based on the use of the equilibrium-dispersive model.

1. Introduction

In a number of cases involving most modes of liquid chromatography, the mobile phase contains additives that are retained on the stationary phase [1]. In such cases, an equilibrium is reached between the additive composition of the two phases, and this equilibrium can be perturbed by changes in the column temperature or in the composition of the mobile phase. These perturbations can be used to study the thermodynamics and kinetics of the phase equilibrium.

A typical perturbation is the injection of a sample which does not have exactly the composition of the mobile phase. Upon such an injection, two sets of bands migrate along the column and more peaks are recorded than there are sample components. The first set corresponds to the elution of these sample components. The second set corresponds to the perturbation of the additive equilibria. These peaks are called system peaks.

The appearance of system peaks was reported over 20 years ago [2,3]. Systematic investigations of system peaks have been performed by several groups, from different viewpoints [4–11]. The

* Corresponding author.

origin and characteristics of system peaks, and the variety of information which can be derived from their study, were discussed by Levin and Grushka [12–14]. Theoretical discussions regarding the fundamentals of system peaks were given by Helfferich and Klein [15], Golshan-Shirazi and Guiochon [16] and Riedo and Kováts [17]. Although there is an abundance of papers regarding the observation and the practical uses of system peaks [1], there are few systematic experimental investigations related to the theoretical aspects of the problem.

System peaks are relaxation signals whose study permits an investigation of the underlying equilibria of the additives between the two phases [12]. According to the system peak theory [1,15–17], when the mobile phase contains N components, a weak solvent considered as not adsorbed [18] and $N - 1$ retained additives, we observe $N - 1$ additive system peaks on injection of a sample pulse or of a vacancy. These peaks propagate at a velocity characteristic of the additives. Note that some of these peaks may not be detectable for a number of reasons [1]. If a P -component sample is injected, we obtain also for each component a peak that moves at a velocity characteristic of the analyte. In this work, we used mainly vacancy chromatography, a technique in which samples of the pure weak solvent are injected. In some experiments, solutions containing mobile phase components of composition different from that of the mobile phase were also injected. Therefore $P = 0$, and we have only $N - 1$ system peaks. For the sake of simplicity, they are referred to as the system peaks.

An important feature of system peaks is that when the sample size and hence the system perturbation are small, their retention time is independent of the nature of the sample injected. However, the size of the perturbation caused by a given amount of sample depends on the nature of the injected sample. The system peaks can even be positive or negative, depending on the nature of the sample and on the detection mode. Each of these $N - 1$ peaks can be assigned to one and only one component of the system only if there is no competition between them for retention. Conversely, when

there is competition for retention between the components of the system, the migration of a particular system peak can no longer be related to a specific component. Further, the system peaks are not pure, and each peak contains all of the components involved in the competition, in variable amounts. The migration of each system peak is related to the combination of the influence of all the components. Accordingly, it is difficult to deconvolute or predict the chromatograms.

The object of our work is the investigation of the relationships between the retention times and areas of system peaks and the equilibrium isotherms of all the compounds involved. We used simple, non-ionic systems, with one to three additives, under linear and non-linear conditions. We measured the isotherms by the classical frontal analysis method, and from recorded system peaks under a variety of experimental conditions [19]. The experimental results are compared with those of the theory of system peaks reported previously [1,16].

2. Theory

Assuming the equilibrium-dispersive model which lumps the band broadening effects of finite axial dispersion and a finite kinetics of mass transfer in the column into an apparent dispersion coefficient, the mass balance is written

$$u \cdot \frac{\partial C_j}{\partial z} + \frac{\partial C_j}{\partial t} + F \cdot \frac{\partial q_j}{\partial t} = D_a \cdot \frac{\partial^2 C_j}{\partial t^2} \quad (1)$$

where u is the mobile phase velocity, z is the distance along the column, t is the time, F is the phase ratio [with $F = (1 - \epsilon)/\epsilon$ and ϵ is the total column porosity] and D_a is the apparent dispersion coefficient. At equilibrium between the two phases, the concentration of component j in the stationary phase, q_j , is related to the mobile phase concentrations of all the components of the mobile phase by the equilibrium isotherm. Assuming the competitive Langmuir isotherm model for the present case, we have

$$q_j = \frac{a_j C_j}{1 + \sum_i b_i C_i} \quad (2)$$

where a_j and b_j are the numerical coefficients of the pure component Langmuir isotherm of component j . The apparent dispersion coefficient is related to the column HETP by

$$D_a = \frac{Hu}{2} \quad (3)$$

The initial condition is that the concentration of the additive in the mobile phase throughout the column is constant and equal to C_j^0 :

$$C_j(z, t = 0) = C_j^0 \quad (4)$$

The boundary conditions correspond to a perturbation of the equilibrium at the column inlet:

$$\begin{aligned} C_j(z = 0, t) &= C_j^p & 0 \leq t \leq t_p \\ C_j(z = 0, t) &= C_j^0 & t_p < t \end{aligned} \quad (5)$$

where t_p is the duration of the injection pulse and C_j^p is the additive concentration in the injected sample, or perturbation. This latter concentration depends on the experimental conditions. It is zero for a vacancy, but it can be smaller or larger than C_j^0 .

According to the theory of system peaks [16], unless the concentrations of all additives are extremely low, the response of the column to a perturbation is complex. It involves the formation of as many peaks as there are additives in the system, even if the perturbation entails a change in the concentration of a single additive. The velocities of the peaks formed are given by the eigenvalues of the matrix of the differentials, $\partial q_i / \partial C_j$, of the competitive isotherm. If the perturbation affects the concentrations of several additives, e.g., of k additives, k series of j system peaks are formed, and the k system peaks formed for each component of the system interfere [16].

3. Experimental

3.1. Instrumentation

Experiments were carried out on an HP1050 (Hewlett-Packard, Palo Alto, CA, USA) liquid chromatograph equipped with a diode-array UV

detector and an HPCHEM data station. Injections were done using a Rheodyne (Cotati, CA, USA) injection valve with a 20- μ l loop. The temperature was kept constant at $30 \pm 0.1^\circ\text{C}$, by placing the column in the stream of a circulating water-bath. The UV spectra were recorded using a Uvikon 930 instrument (Kontron, Zurich, Switzerland).

3.2. Choice of detection wavelength

Chromatographic detectors are very sensitive. At the concentrations used in this work, the baseline becomes very noisy at the wavelengths of the adsorption maxima in the spectrum which are traditionally used. The precision of the measurements of the retention times and areas of the system peaks is then poor. The wavelength was selected to optimize the signal-to-noise ratio of the system peaks. For all mixtures, detection was carried out at 240 nm for concentrations below 0.01 M and at 298 nm for higher concentrations, as the molecular absorptivities of resorcinol and phenol are negligible and that of catechol is much smaller. In single-component cases, detection was carried out at 240 nm for all concentrations.

3.3. Column

A 125 \times 4 mm I.D. LiChrosorb RP-18 cartridge (Merck, Darmstadt, Germany) was used for all the experiments.

3.4. Chemicals

Water (HPLC grade) was used as the weak solvent in the mobile phase. The additives, phenol, (Merck), catechol and resorcinol (Sigma, St. Louis, MO, USA), were used as received.

3.5. Methods

Experiments were carried out at a flow-rate of 2 ml/min. The chromatographic system was washed with an acetonitrile–water solution between any change in the mobile phase composi-

tion. The data station provided retention times and peak areas.

4. Results and discussion

We studied three binary systems, with water and each of the three additives, resorcinol (a), catechol (b), and phenol (c). One system peak was obtained in each instance (chromatograms 1–3, Fig. 1-I and 1-II). We also studied one ternary system [a 1:1 mixture of resorcinol (a') and catechol (b') in water] and one quaternary system [a 1:1:1 mixture of resorcinol (a''), catechol (b'') and phenol (c'') in water]. We obtained two system peaks in the former instance (chromatogram 4, Fig. 1-I and 1-II), and three in the later (chromatogram 5, Fig. 1-I and 1-II). The experiments reported in Fig. 1-I and 1-II were performed under the same experimental conditions, except for the additive concentrations, 0.0005 M in Fig. 1-I and 0.01 M in Fig. 1-II. The elution order of the three components is resorcinol, catechol and phenol under the analytical conditions.

4.1. Retention of the system peaks

We measured the retention factors of the system peaks [$k' = (t_R - t_0)/t_0$] and compared them with the theoretical values derived from the isotherms. For binary mobile phases, the retention time of the system peak is easily predicted from the adsorption isotherm of the additive in the weak solvent and its concentration. The area of the system peak is simply equivalent to the sample size, and is proportional to $\Delta n/F_v$, where F_v is the flow-rate and Δn is the amount of additive injected (positive for a pulse, negative for a vacancy). The systematic determination of the system peak retention time as a function of the additive concentration provides a simple method of isotherm determination [19].

When the mobile phase contains several additives, the situation is more complicated, and it is not possible to derive simply the multi-component isotherms from systematic determinations of the retention times of the system peaks.

Theory indicates that, under non-linear conditions, the composition of these peaks is mixed, so none of the system peaks in a multi-component mixture can be ascribed strictly to any component of the mixture. The retention times of these system peaks depend on the competitive isotherms of all the additives involved in the competition and on their concentration.

Experimental measurements of the retention factors of system peaks

Measurements of system peak retention times and areas were done for the different binary mobile phases (solutions of phenol, resorcinol or catechol in water), one ternary mobile phase (1:1 resorcinol–catechol mixtures at different total concentrations) and one quaternary mobile phase (1:1:1 phenol–resorcinol–catechol mixtures at different total concentration). The technique of vacancy chromatography was used for the measurements, with injection of small amounts of water.

In the linear range, at concentrations below ca. 0.5 mM, two system peaks were recorded for the ternary and three for the quaternary mobile phase (Fig. 1-I). Their retention times were constant, and the same as those of small sample pulses in elution, under linear conditions. As the additive concentrations were increased above 1 mM, the retention times of the system peaks began to decrease with increasing additive concentration (Fig. 1-II). This indicates the onset of non-linear behavior, and of competitive interactions between the components of the multi-component mixtures.

Fig. 2-I–III illustrate the dependence of the retention factors of the additives on the concentration of the solutions for resorcinol (Fig. 2-I), catechol (Fig. 2-II) and phenol (Fig. 2-III). The retention factors decrease rapidly with increasing concentration in the range 1–20 mM. They continue to decrease, more slowly but steadily, for concentrations up to 100 mM. The retention times of the three system peaks were slightly, but significantly, different from those of the pure compounds, demonstrating interactions and hence competition between these components. Thus, the system peaks can no longer be

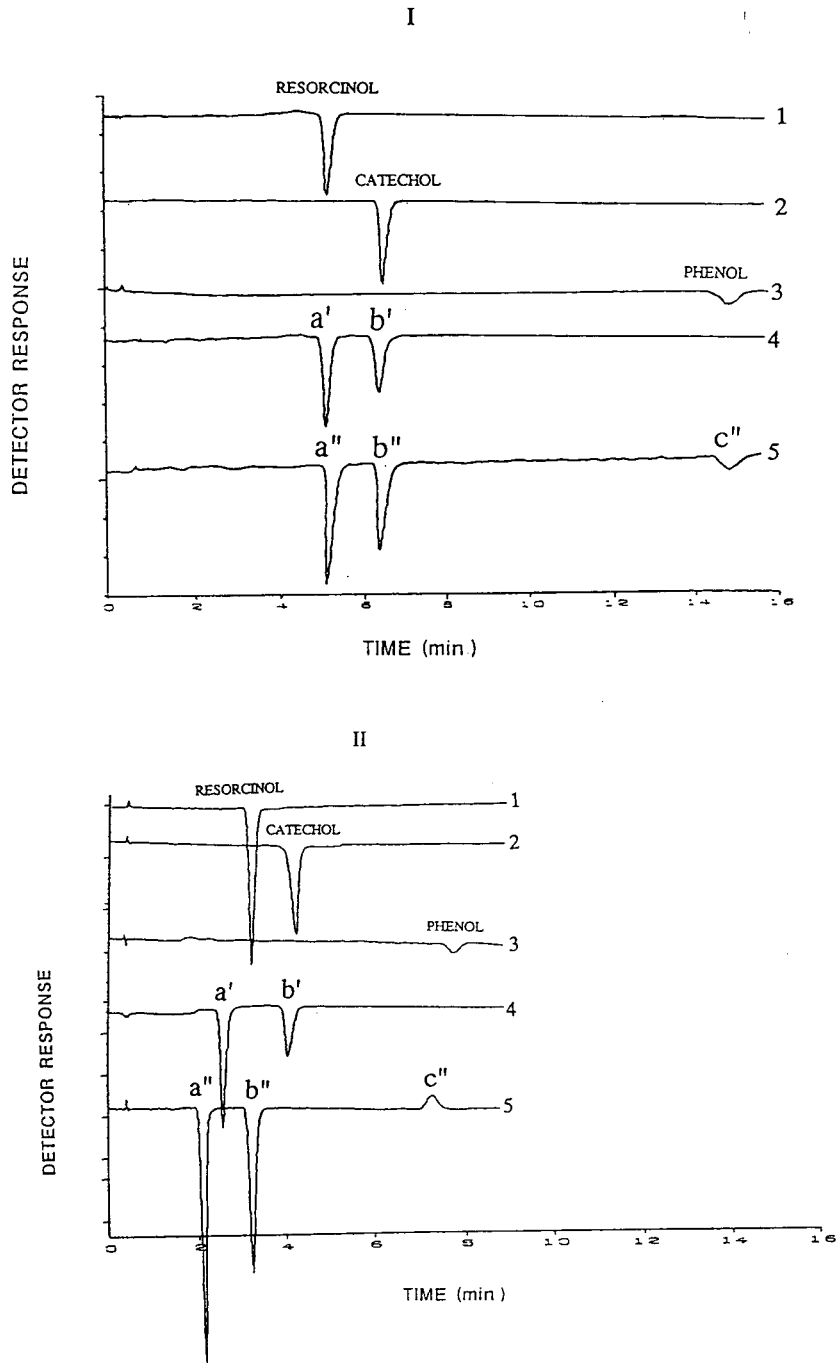


Fig. 1. System peaks obtained on injection of pure water into the following mobile phases: (1) water–resorcinol; (2) water–catechol; (3) water–phenol; (4) water + resorcinol–catechol (1:1); and (5) water + resorcinol–catechol–phenol (1:1:1). Detection at 240 nm in I and II, chromatograms 1–3, and at 298 nm in II, chromatograms 4 and 5. Concentrations: (I) phenol, resorcinol and catechol, 0.5 mM each; (II) phenol, resorcinol and catechol, 10 mM each.

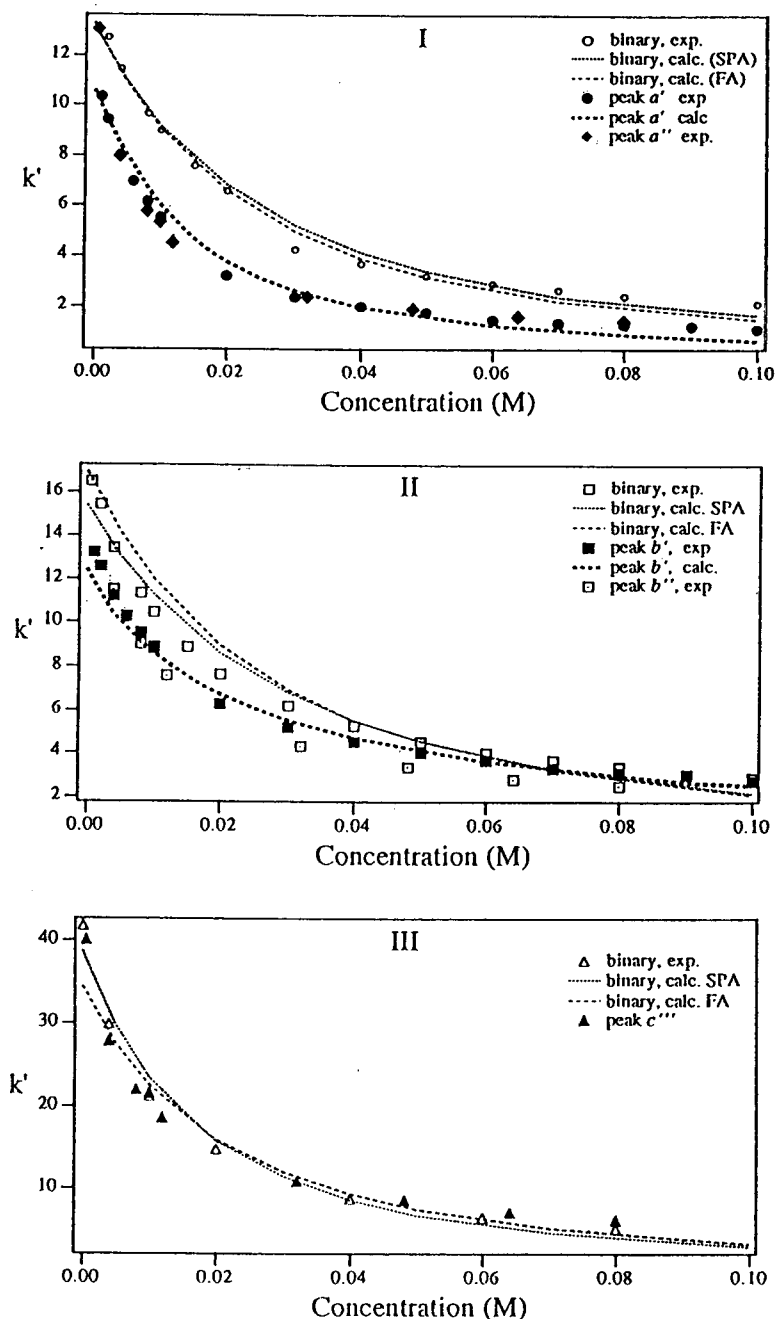


Fig. 2. Retention factors, k' , of the system peaks as a function of the concentration of the mobile phase additives. (I) Retention factor of the first peak versus concentration of resorcinol in the binary, ternary (a') and quaternary (a'') mobile phases; (II) retention factor of the second peak versus concentration of catechol in the binary, ternary (b') and quaternary (b'') mobile phases; (III) retention factor of the third peak versus concentration of phenol in the binary and quaternary (c'') mobile phases. Experimental results (symbols) and dependences calculated in the binary and ternary systems (lines), using the Langmuir coefficients in Table 1. Sample volume, 20 μ l; concentration, 0; column length, 12.5 cm; phase ratio, 1.24; flow-rate, 2 ml/min; t_0 , 21 s; column efficiency, 1000 plates.

related to specific compounds. Their migration rates depend on a combination of velocities. Further, the composition of the material transported with the system peaks in ternary and quaternary systems is a mixture of all components, in different concentrations.

In the quaternary mobile phase, for example, each peak contains a certain amount of each of the three additives involved in the competition. This effect is well illustrated in Fig. 1-II, chromatogram 5. As the injection is a vacancy, while all system peaks in linear chromatography are negative (Fig. 1-I, trace 5), the third peak, c'' in this chromatogram, is positive. The signal recorded is the sum of the detector response to the concentration signals of the three additives, resorcinol, catechol and phenol. The balance in peak c'' gives a positive signal. This positive signal is in agreement with the prediction of the system peak theory [16] because phenol and resorcinol do not give a significant detector response at 298 nm. In this instance, the area of peak c'' represents only the excess amount of catechol eluted, and is positive as required by theory.

Determination of adsorption isotherms

The single-component adsorption isotherms were determined by frontal analysis and the

Table 1

Parameters of the best fit of the adsorption isotherms to the Langmuir equation

Solute	System peaks		Frontal analysis	
	<i>a</i>	<i>b</i>	<i>a</i>	<i>b</i>
Resorcinol	10.6	20.5	10.7	22.2
Catechol	12.4	17.7	13.7	19.8
Phenol	31.2	29.9	27.9	24.7

results are reported in Fig. 3. This method is accurate, and its results are independent of any assumption regarding the theory of chromatography, provided that the adsorption isotherms are convex upwards, and the band front exhibits a shock layer. The isotherms were also derived by integration of the plots of the system peak retention factor, k' , versus the additive concentration, C , obtained for each single-component mixture. The results are also shown in Fig. 3. There is an excellent agreement between the two sets of results.

The isotherm data were fitted to the Langmuir equation. The best coefficients are reported in Table 1 and the corresponding curves are plotted in Fig. 3 (lines). The experimental data (symbols) do not exhibit any systematic deviations from the model at high concentrations. The low

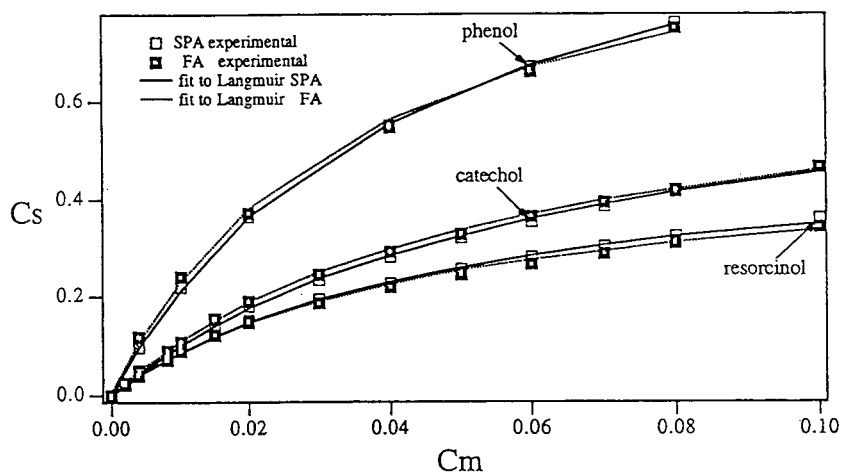


Fig. 3. Adsorption isotherms of resorcinol, catechol and phenol, measured by frontal analysis (FA) and by system peak analysis (SPA). The best values of the parameters of the Langmuir model are given in Table 1.

concentration results (retention times of small pulses in water, initial slopes of the isotherms) are also in satisfactory agreement.

The first parameter, a , of the Langmuir isotherm can also be derived easily from the retention factor of a very small size sample of the additive injected in the pure solvent [$a = k'_0/F = (t_{R,0} - t_0)/(Ft_0)$, where F is the phase ratio]. These values of a are 11.0, 13.3 and 33.5 for resorcinol, catechol and phenol, respectively. Although the experimental isotherm data fitted the Langmuir model well, the values of a derived from the three methods, the fit of the frontal analysis and of the system peak data to the Langmuir model and the measurement of k'_0 under linear conditions, were slightly different for resorcinol. The difference was larger for phenol. This observation is not uncommon and illustrates the sensitivity of the isotherm determination, the problem of fitting experimental data to a two-parameter model [1] and, possibly, the lack of homogeneity of the surface of adsorbents, which are often more active at very low surface coverages.

Validity of the Langmuir competitive isotherm model

The column saturation capacities for resorcinol and catechol are close (Table 1). Thus, the competitive Langmuir model (Eq. 2) is expected to account properly for the competitive adsorption behavior of the two components [16]. Introducing in this equation the coefficients given in Table 1 permits the calculation of the apparent retention factor of a small pulse or vacancy of component j . Using the approach described previously [16], and taking the coefficients of the single component Langmuir isotherms in the calculation, we calculated the retention factors of the three system peaks, a , b , and c , in the binary mixtures and of the system peaks a' and b' in the ternary mixtures.

The results of the calculation made for the ternary mobile phase (resorcinol, catechol and water) are shown as the lines in Fig. 2-I and 2-II. These lines are the plots of the retention factors of the two system peaks a' and b' , versus the concentration of the 1:1 mixture used. As can be

seen, there is a substantial agreement between the experimental data and the retention factors derived from the competitive Langmuir isotherm model. This justifies the theoretical approach [16], and the use of the Langmuir competitive model to account for the adsorption behavior of the two components in the present experimental case.

A similar approach could not be extended to the competitive adsorption behavior between phenol and resorcinol and catechol. The saturation capacities of the adsorbent for phenol and the other two components are too different to allow the use of the competitive Langmuir model to account for their competitive interactions.

4.2. System peak areas

Although the retention of system peaks has already been used extensively in their study in connection with isotherm determination, for example, their areas have been far less systematically investigated. Peak areas were measured under non-competitive and competitive conditions for the various system peaks recorded. We assumed that the detector response is linear.

System peak areas under non-competitive conditions

Under linear conditions, each system peak can be ascribed to one mobile phase component, hence the peak area is proportional to the size of the disturbance, i.e., to the extent of the vacancy created by the injection provided that the detector response is linear. The peak area is independent of the nature and concentration of the other components of the sample. The spectra of the three components studied are given in Fig. 4-I and 4-II. The positive spectra in Fig. 4-I were recorded from the top of small elution peaks and the negative spectra were recorded from the trough of the vacancy peaks. Fig. 4-I(1) shows the spectra obtained with binary mixtures, i.e., with pure additives at a concentration of 0.5 mM. Fig. 4-I(2) shows the spectra in the case of the quaternary mixture, with concentrations of 0.1 mM for each additive. There are virtually no

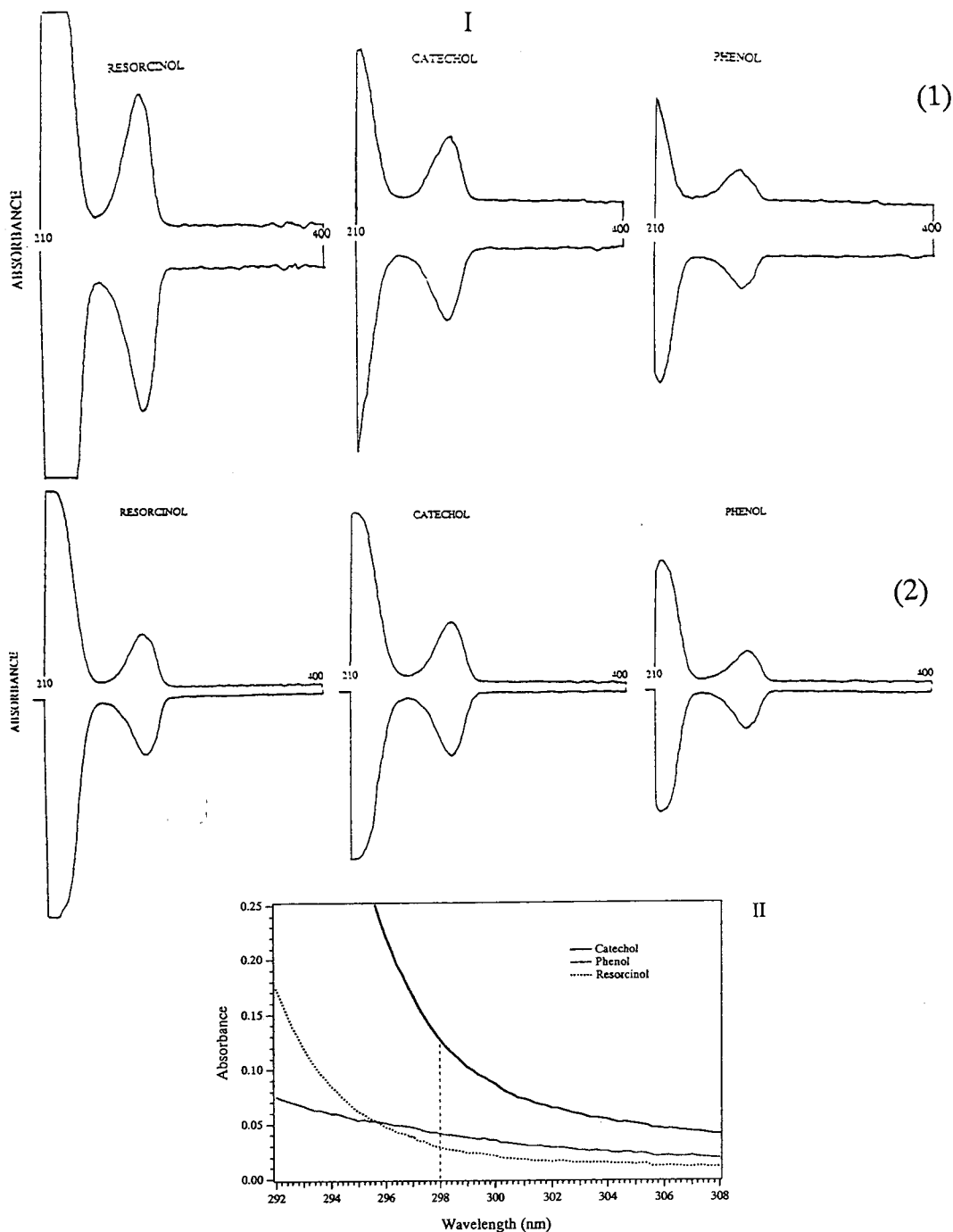


Fig. 4. UV spectra of the compounds studied. (I) Spectra (210–400 nm) recorded with the diode-array detector on the top of the peaks of resorcinol, catechol and phenol, in the case of analytical-size injections (positive peaks) and vacancy injections (negative peaks). 1 = Binary systems; 2 = quaternary system. Reference, baseline. (II) UV spectra of resorcinol, catechol and phenol (10 mM each), recorded with a UV spectrophotometer and overlaid, in the region 292–308 nm, showing the low response for resorcinol and phenol at 298 nm.

differences, and the positive (elution in water) and negative (vacancy) spectra are mirror images. These observations confirm our earlier conclusions regarding the lack of competitive interactions between these components at low concentrations (below 1 mM).

Small samples of water containing only one of the three additives in the quaternary mixture were injected, instead of the standard vacancy injected in previous experiments. The concentration of this single additive was increased while the vacancy of the other two components remained constant. The peak area was plotted versus the amount injected. The experiment was repeated for each additive. The results are plotted in Fig. 5-I–III. They are in agreement with similar, previous results obtained with ionic systems [12–14]. As expected, the peak area of only one additive changes during these experiments. It is the area of the additive whose concentration in the sample was changed during the series of experiments. The calibration line intersects the abscissa axis at $C = 0.5$ mM, the additive concentration in the mobile phase.

System peak areas under competitive conditions

Experimental results with the ternary mobile phase. At high additive concentrations, competitive adsorption behavior results in a more complex situation [16]. The chromatogram obtained depends on the number of components and their elution order compared with the additive system peak itself [1]. If the detector responds only to the additive (indirect detection), the system peaks associated with each component are positive when the components are eluted before the additive system peak and negative when they are eluted later [16,17]. The additive system peak is negative if all the components are eluted before it, and positive if they are all eluted after it. If some components are eluted before the additives and others are eluted later, the sign and size of the additive system peak result from a mass balance of all the perturbations, positive or negative, caused by the injection of the sample. The total algebraic area of these perturbations is

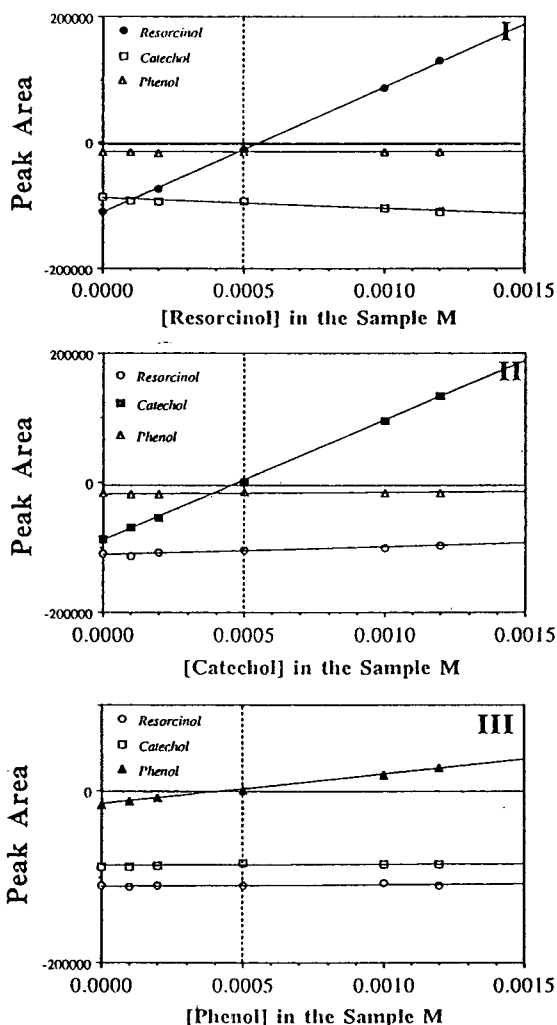


Fig. 5. Plots of the areas of the three system peaks as a function of the additive concentrations. (I) Resorcinol; (II) catechol; (III) phenol. Mobile phase, resorcinol–catechol–phenol (0.5 mM each) (1:1:1). Detection at 240 nm.

equivalent to the detector response for the amount Δn of additive.

As seen in Fig. 6, the areas of all the system peaks vary with increasing concentration of any one of the additives in the sample volume. This is simply explained by the fact that at high concentration each system peak contains every component of the system, albeit in varying amounts. The results shown in Fig. 6 were obtained with the ternary mobile phase (1:1

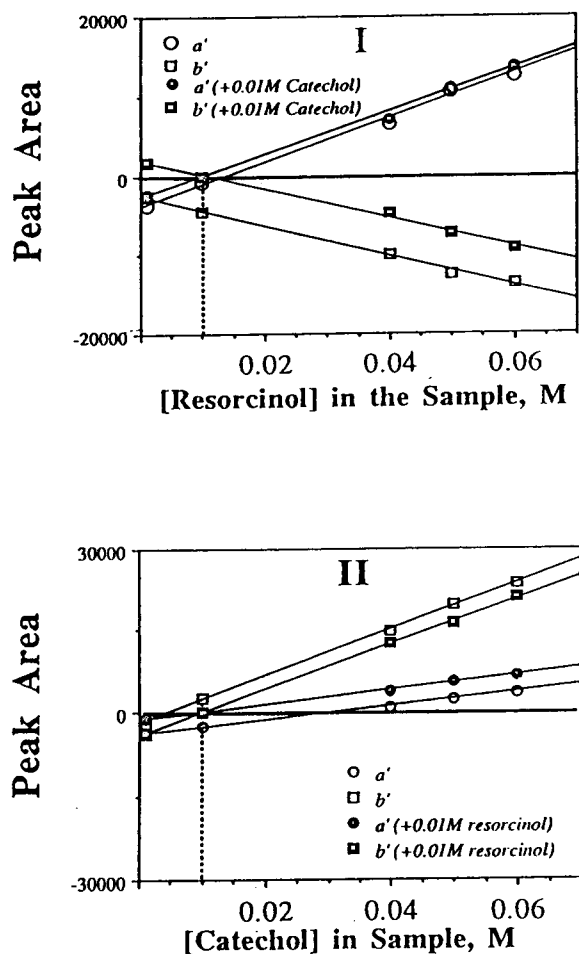


Fig. 6. Plots of the areas of the two system peaks, a' (circles) and b' (squares), as a function of the additive concentrations. (I) Resorcinol at various concentrations (open symbols) and same resorcinol solutions with 10 mM catechol (solid symbols). (II) Catechol at various concentrations (open symbols) and same catechol solutions with 10 mM resorcinol (solid symbols). Mobile phase, resorcinol–catechol (10 mM each) (1:1). Detection at 298 nm.

resorcinol–catechol at 10 mM each). When solutions of increasing concentrations in resorcinol were injected, the area of the first system peak (a') increased linearly, whereas the area of the second system peak (b') decreased linearly. Adding a constant concentration, 10 mM, of catechol to the sample shifted the response curve of the second system peak by a fixed, positive

amount, whereas it hardly changed the response for the first system peak. Conversely, when solutions of catechol of increasing concentrations were injected, the areas of both system peaks increased linearly. Adding a 10 mM resorcinol concentration to the sample shifted the first peak response upwards and the second peak response downwards by fixed amounts.

If a sample of one of the two additives having a concentration equal to the additive concentration in the mobile phase is injected, the corresponding system peak does not vanish. Its area does not become zero (Fig. 6), in contrast to what happens under linear conditions (Fig. 5). Only when the sample and the mobile phase have the same composition does the system peaks vanish. This effect is due to the presence of both additives in each of the two system peaks.

The influence of competitive adsorption behavior on the area of system peaks becomes noticeable at concentrations above 0.5 mM. We also measured UV spectra as in Fig. 4-I(2) in a quaternary system at 0.5 mM each. The spectra were no longer exact mirror images of each other. This demonstrates the occurrence of some non-linear effects at a concentration of 0.5 mM in each of the three additives.

Calculated chromatograms for the ternary mixture. The chromatograms from which Fig. 6 was derived were calculated using the algorithms described previously [16] and the competitive Langmuir isotherm derived above, for a 10 mM mobile phase concentration. The chromatograms obtained are given in Fig. 7-I–VII. The concentrations of the two components (resorcinol and catechol, respectively) in the samples were lower than in the mobile phase in the chromatograms in Fig. 7-I and 7-VI, and higher in the chromatograms in Fig. 7-III and 7-VI. In the chromatograms in Fig. 7-II and 7-V these concentrations were the same. The vacancy chromatogram was also calculated, and is shown in Fig. 7-VII.

Although both phenol and resorcinol absorb at 298 nm (see Fig. 4-II), their response factors are low compared with that of catechol. For the sake

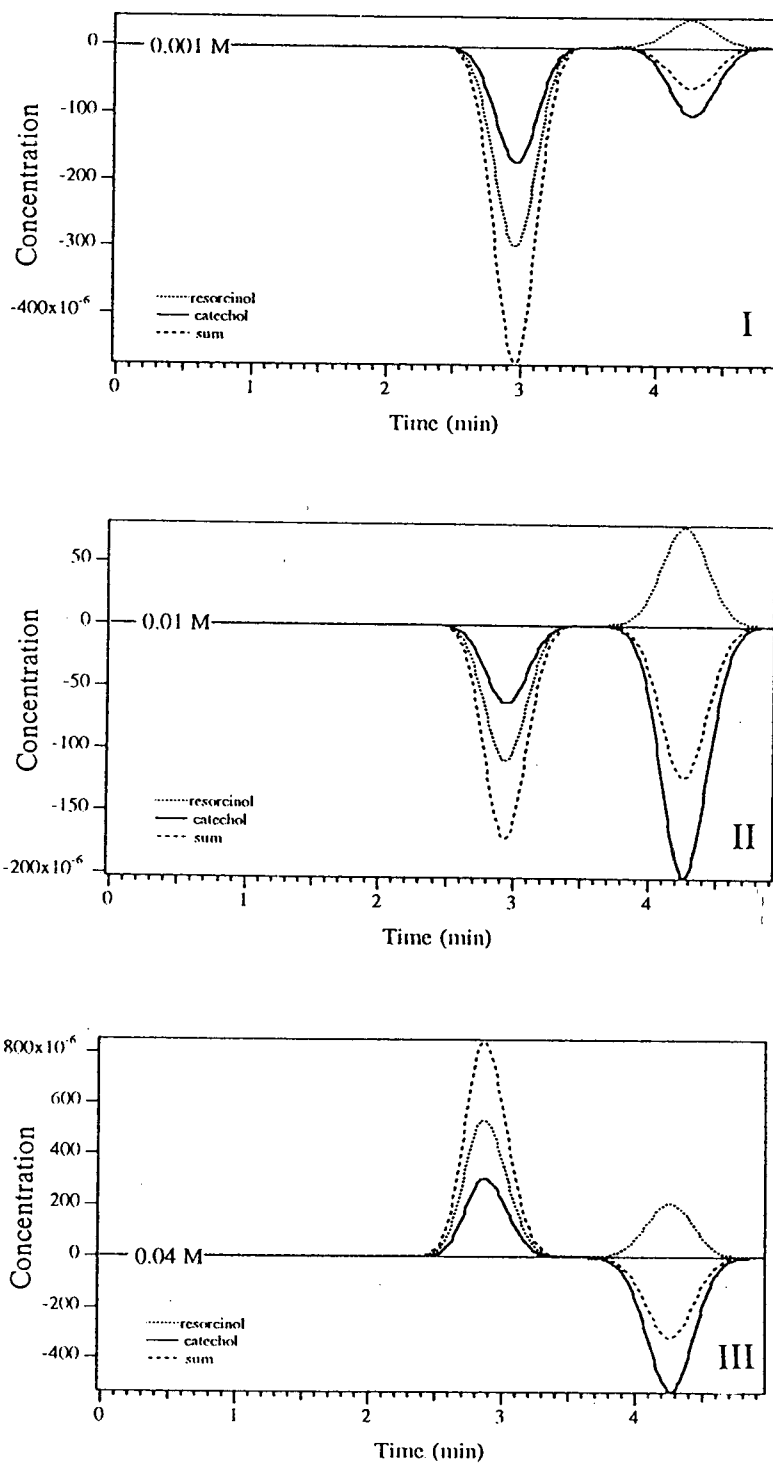


Fig. 7.

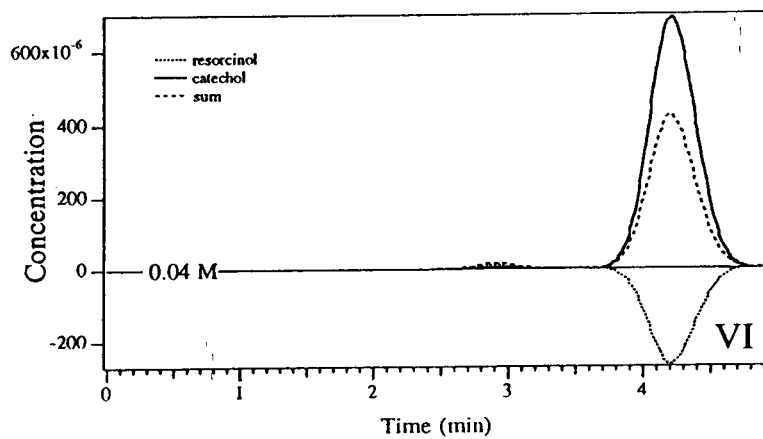
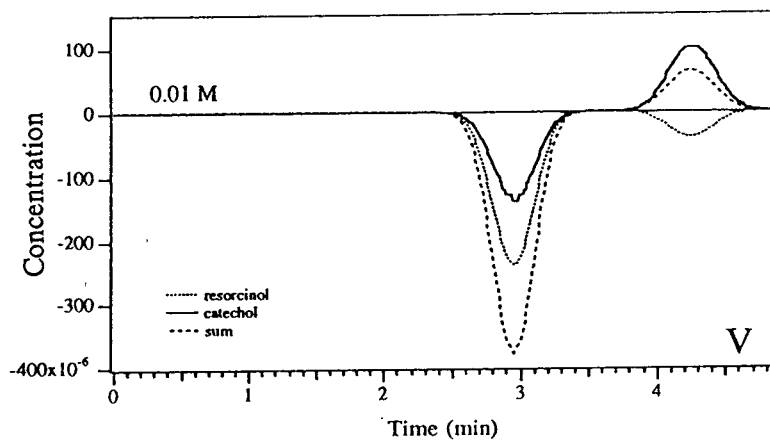
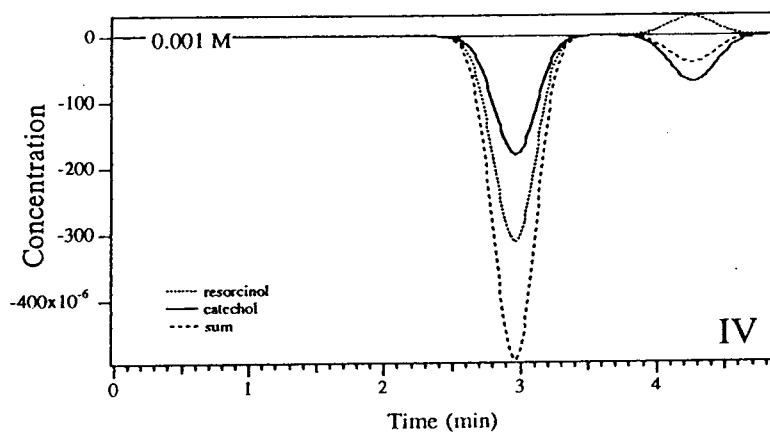


Fig. 7. (Continued on p. 226)

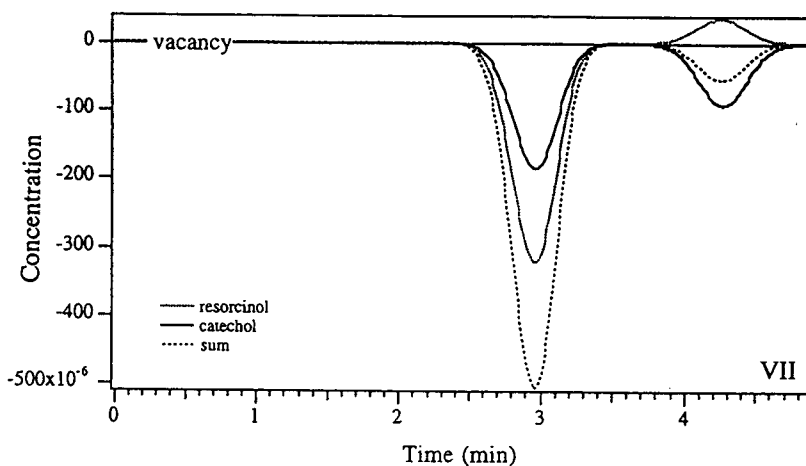


Fig. 7. Calculated chromatograms showing the system peaks predicted by the system peak theory for the ternary mixture, with a mobile phase containing 10 mM each of resorcinol and catechol. Samples: I–III, resorcinol; IV–VI, catechol; VII, pure water. Sample volume, 20 μ l; concentrations as indicated. L , F , F_v , t_0 , N and sample volumes as in Fig. 2.

of simplicity in the following discussion, we assume that the responses of phenol and resorcinol are negligible compared with that of catechol. This is not entirely true and a small correction should be applied to the quantitative results. The nature of the argument would remain unchanged, however. The comparison of Figs. 1-II (chromatogram 4) and 7-VII shows clearly that the profiles calculated for catechol, the only compound which is detected by the UV detector at 298 nm (Fig. 4-II), are nearly identical with the experimental chromatograms. The same agreement was observed in all other experiments (not reported). The areas of the system peaks were derived and are plotted against the sample concentration of resorcinol and catechol in Fig. 8-I–III and 8-IV–VI, respectively. The plots of the experimental data in Fig. 6-I–II and of the calculated data in Fig. 8-IV–VI are very similar. The experimental results reported in Fig. 6 can now be explained in detail, assuming that catechol is the detection agent for the system peaks recorded at 298 nm, and that the “resorcinol” peak recorded is in fact due to its catechol content. The small contribution of the UV absorbance of resorcinol is neglected.

When resorcinol was injected, the detected signals are the two perturbations to the catechol equilibrium, the one which travels with the catechol vacancy and the one which travels with

the resorcinol pulse. When the injected amount of resorcinol increases (Fig. 6-I), the amount of catechol expelled from the stationary phase by the competitive effect of the increasing amount of resorcinol also increases, and the absolute value of the area of the corresponding (negative, b') peak increases, hence the area of the first system peak (peak a'), increases (Figs. 6-I and 8-I–III). Assuming that catechol is the only detection agent of peaks a' and b' , the area of peak b' can be determined by observing that the sum of the areas of the peaks a' and b' is equivalent to the injected amount Δn of catechol, i.e., to the difference between the amounts of catechol in the vacancy pulse injected and in an equal volume of mobile phase. Similarly, when the injected amount of catechol increases, the areas of all recorded peaks increase (Fig. 6-II), although the amount of resorcinol in the second system peak actually decreases (Fig. 8-IV–VI), but the resorcinol response is negligible in these experiments.

As seen in Fig. 6, the slopes of the plots of the peak areas versus injected amounts of resorcinol or catechol were the same whether the injected pulse contained or not a constant amounts of the other hydroxyphenol. The addition of the other component merely caused a vertical shift in the position of the straight line obtained. The addition of a constant amount of catechol to the

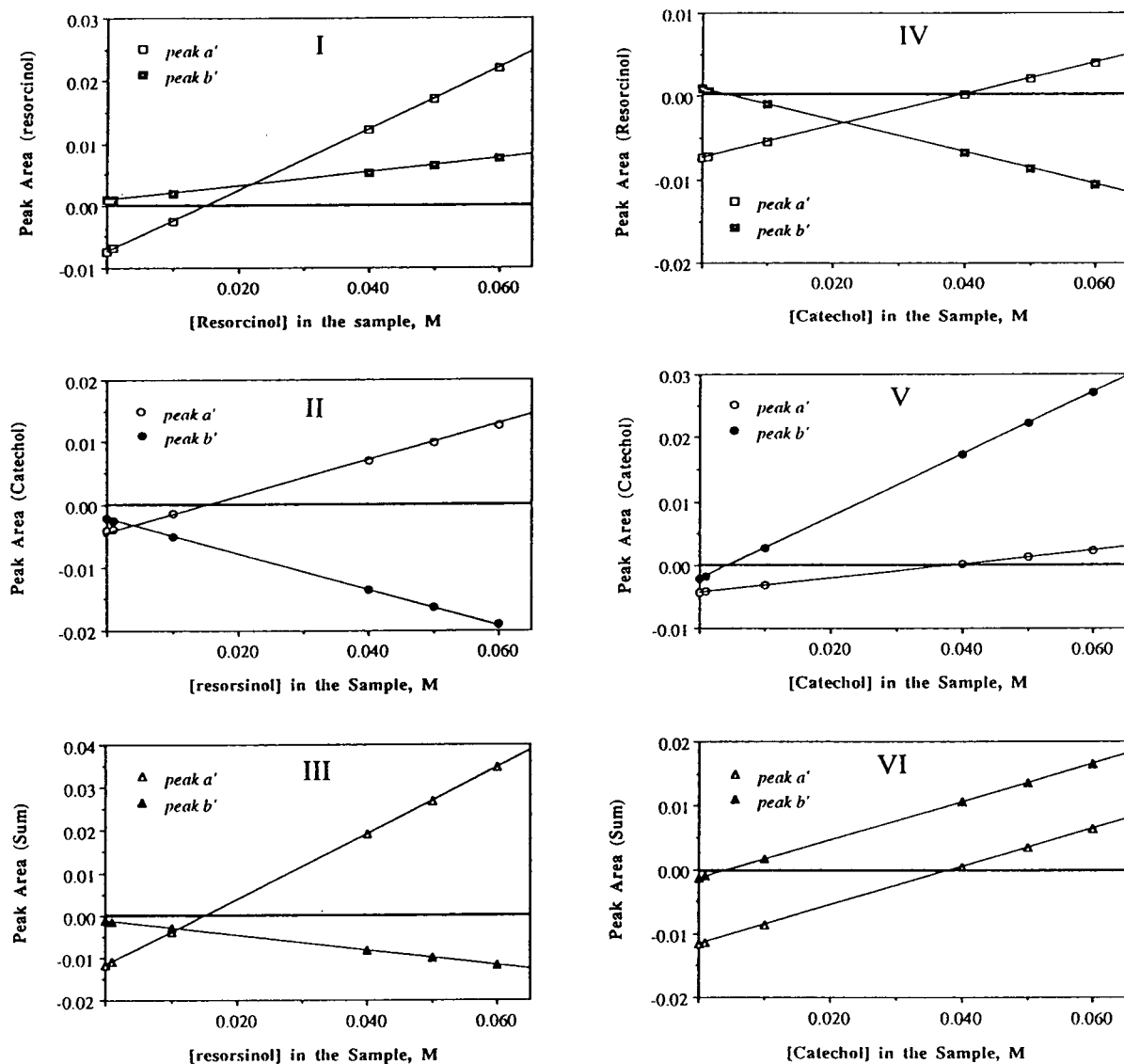


Fig. 8. Plots of the area of the calculated system peaks versus the sample concentration. Samples: I–III, resorcinol; IV–VI, catechol. Mobile phase composition as in Fig. 6.

resorcinol pulses caused a positive shift on the two response curves, confirming the distribution of catechol between the two peaks, and the fact that it is the catechol response which is recorded. The addition of a constant amount of resorcinol to the catechol pulses caused a positive shift of the first and a negative shift of the second peak response factor. This illustrates the influence of resorcinol on the distribution of catechol be-

tween the two system peaks, and further confirms the presence of both components in both system peaks.

Study of a quaternary mobile phase. The dependence of the system peak areas on the sample size was also studied for the quaternary mobile phase. Constant volumes of samples of increas-

ing concentrations in resorcinol, catechol or phenol were injected in a mobile phase containing an equal concentration (10 mM) of each of the three phenols. The results are shown in Fig. 9-I–III. The interpretation of the results is greatly simplified by the assumption that in each instance the signal recorded is the variation of the catechol concentration, and that the small contributions of phenol and resorcinol are negligible. Because the concentrations of the components of the mobile phase are high enough for the equilibrium behaviour to be non-linear, a change in the catechol concentration is associated with each of the three system peaks. This change gives rise to the three peaks observed and measured. The same three system peaks also appeared in vacancy chromatography, when a sample of pure water was injected, but the first two were negative and the third one positive (Fig. 1-II, chromatogram 5). This result is in agreement with the system peak theory [16], since the UV detector responds mainly to catechol at this wavelength (Fig. 4-II).

When a sample of resorcinol is injected (Fig. 9-I), the area of the third peak remains nearly constant, whereas the areas of the other two peaks follow the same trend as for the ternary mixture (Fig. 6-I). The area of the first peak increase whereas that of the second peak decreases with increasing sample size, in agreement with the system peak theory [16]. This confirms that the competition between resorcinol and catechol is intense, as demonstrated above. Because the response of resorcinol is negligible, however, no further conclusions can be derived from the fact that the area of the third peak, i.e., the amount of catechol travelling with it, is constant. Especially, we cannot draw conclusions regarding the lack of competition between phenol and the other two additives.

The injection of catechol samples leads to very similar conclusions (Fig. 9-II). The area of the third peak is small and remains nearly constant. The area of the other two peaks increase, the first more slowly than the second, which is to be expected as catechol contributes much more to the second than to the first peak. Finally, the injection of phenol samples results in a marked

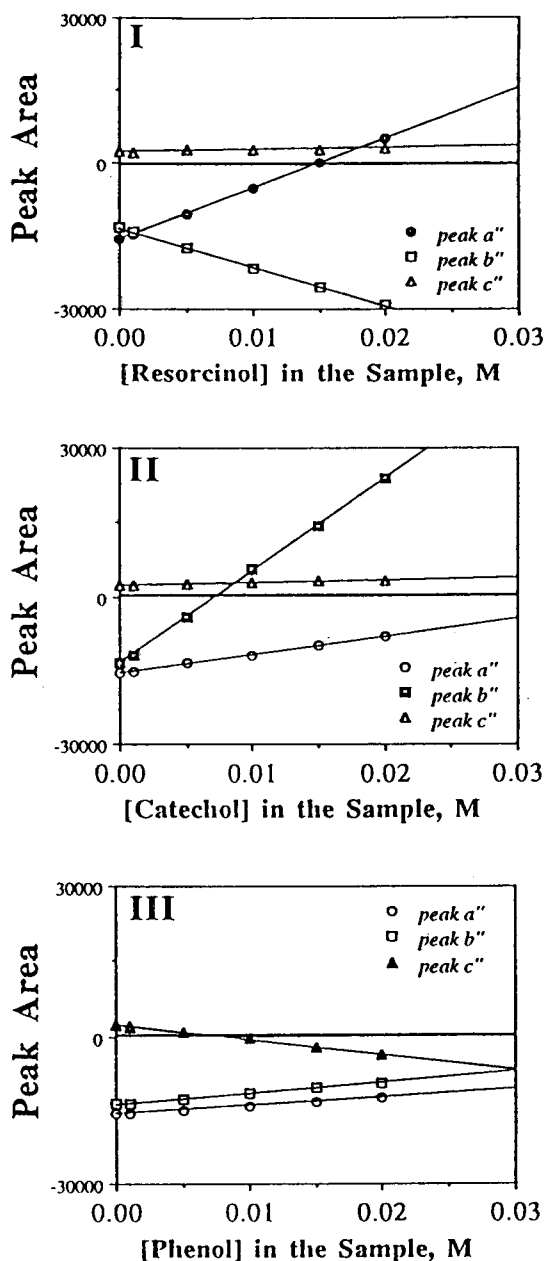


Fig. 9. Plots of the areas of the three system peaks versus the sample concentration. Sample: I, resorcinol; II, catechol; III, phenol. Mobile phase, resorcinol–catechol–phenol (10 mM each) (1:1:1). Detection at 298 nm.

decrease in the area of the third system peak, which, initially positive (for a vacancy, see Fig. 1-II, chromatogram 5), becomes negative for a

phenol concentration slightly lower than 10 mM. The areas of the first two peaks, initially negative, increase slowly with increasing sample size, i.e., decrease in absolute terms. The catechol concentration in the third peak decreases with increasing phenol sample size, while the catechol concentration increases in the second peak. This result is again in agreement with the system peak theory. It shows also that there is competition between phenol and the two hydroxyphenols, as phenol is not detected at 298 nm. This competition explains the decrease in the catechol content of the third system peak.

5. Conclusions

The experimental results presented above validate earlier theoretical developments regarding the behavior of system peaks in multi-component chromatographic mobile phases [1,16]. The equilibrium of the retained additives between the mobile and the stationary phases is perturbed by the injection of any sample having a composition different, however slightly, from that of the mobile phase. The study of these perturbations can provide useful information on the nature of the equilibrium. It is important to recognize that, because the equilibrium isotherms are not linear, and that they are coupled in multi-component systems, the retention times of the pulses, and also their areas, depend on the mobile phase composition, and each system peak is actually a local perturbation of all the equilibria involved.

Acknowledgements

This work was supported in part by the Peter Hylston Foundation for Medical Research from the mutual funds of the Hebrew University of Jerusalem, and by grant Che-9201663 of the National Science Foundation. We are grateful to

the Pharmaceutical Chemistry Department of the Hebrew University for giving us unlimited use of the departmental HP 1050 HPLC system. We acknowledge fruitful discussions with Martin Czok of the School of Pharmacy, Université Paris-Sud, Chatenay-Malabry, France.

References

- [1] G. Guiochon, S. Golshan-Shirazi and A.M. Katti, *Fundamentals of Non-Linear and Preparative Chromatography*, Academic Press, Boston, 1994, Ch. XIII.
- [2] N. Fornstedt and J. Porath, *J. Chromatogr.*, 42 (1969) 376.
- [3] D.J. Solms, T.W. Smuts and V.J. Pretorius, *J. Chromatogr. Sci.*, 9 (1971) 600.
- [4] R.M. McCormick and B.L. Karger, *J. Chromatogr.*, 199 (1980) 259.
- [5] F. Riedo and E. sz Kováts, *J. Chromatogr.*, 239 (1982) 91.
- [6] W.R. Melander, F.F. Erard and Cs. Horváth, *J. Chromatogr.*, 282 (1983) 229.
- [7] J.H. Knox and R. Kaliszan, *J. Chromatogr.*, 349 (1985) 211.
- [8] J. Crommen, G. Schill and P. Herne, *Chromatographia*, 25 (1988) 397.
- [9] A. Sokolowski, *Chromatographia*, 22 (1986) 177.
- [10] J. Stahlberg and M. Almgren, *Anal. Chem.*, 61 (1989) 1109.
- [11] E. Arvidsson, J. Crommen, G. Schill and D. Westerlund, *J. Chromatogr.*, 461 (1989) 429.
- [12] S. Levin and E. Grushka, *Anal. Chem.*, 58 (1986) 1602.
- [13] S. Levin and E. Grushka, *Anal. Chem.*, 59 (1987) 1157.
- [14] S. Levin and E. Grushka, *Anal. Chem.*, 61 (1989) 2428.
- [15] F.G. Helfferich and G. Klein, *Multicomponent Chromatography. A Theory of Interference*, Marcel Dekker, New York, 1970.
- [16] S. Golshan-Shirazi and G. Guiochon, *Anal. Chem.*, 62 (1990) 924.
- [17] F. Riedo and E. sz Kováts, in F. Dondi and G. Guiochon (Editors), *Proceedings of the NATO ASI on Advancements in Chromatography and Related Separation Methods, Ferrara, August 1991*, Kluwer, Delft, 1992, p. 211.
- [18] E. sz Kováts, in F. Bruner (Editor), *The Science of Chromatography*, Elsevier, Amsterdam, 1985, p. 205.
- [19] S. Levin and S. Abu-Lafi, *J. Chromatogr.*, 556 (1991) 277.



ELSEVIER

Journal of Chromatography A, 679 (1994) 231–245

JOURNAL OF
CHROMATOGRAPHY A

Column efficiency and radial homogeneity in liquid chromatography

Tivadar Farkas, James Q. Chambers, Georges Guiochon*

Department of Chemistry, University of Tennessee, 575 Buehler Hall, Knoxville, TN 37996-1503, USA
Division of Analytical Chemistry, Oak Ridge National Laboratory, Oak Ridge, TN, USA

Received 16 March 1994

Abstract

Local, on-column electrochemical detection was carried out in the amperometric mode at different points of the column outlet cross-section. This permitted the determination of the spatial distribution of analyte molecules within the chromatographic zone at the column exit. The radial distribution of the peak-maximum velocity, the local efficiency and the analyte concentration were determined for a commercial column and for several laboratory-packed columns made with different solid particles and with a commercial silica-based stationary phase. An important region of the packing close to the wall is denser, has a lower permeability and a lower efficiency than the core of the packing. The concentration along the wall is lower than average, in part because of the lower efficiency.

1. Introduction

In the entire chromatography literature, with only very few exceptions [1–5], most of them nearly twenty years old, columns are seen as unidimensional. This means that their radial homogeneity is assumed to be sufficiently high on the scale of the column radius for minor radial fluctuations of the packing density not to cause any problems. The analyte bands are assumed to exhibit a constant concentration over the entire column cross-section. Similarly, if a preparative column is overloaded, the degree of overload, or loading factor, is assumed to be constant in the radial direction. There is little experimental evidence in support of these assumptions, except for the feeling, not entirely unjustified, that should it be otherwise, column

performance would be drastically decreased compared to what is routinely achieved.

In the early development stage of high-performance liquid chromatography, Knox and co-workers [1,2] showed that packed columns are not radially homogeneous, but that there is a wall region, extending to ca. 30 particle diameters from the wall, which is less homogeneous than the column core. If the column is sufficiently wide in relation to its diameter and to the particle size, the molecules of a sample injected in the center of the column would not have time to reach the wall region before they elute. Thus, the zone would move in a highly homogeneous packing and the column performance would be as good as if the wall region did not exist and the packing was entirely homogeneous. By contrast, if a sufficient proportion of the molecules in a zone can reach the wall region and experience the dispersive effect of this different and less

* Corresponding author.

homogeneous part of the packing, the apparent column efficiency drops markedly [2]. Knox and co-workers [1,2] recommended the use of columns having a diameter in excess of four standard deviations of the radial dispersion. For all practical purposes, these columns would be equivalent to "infinite diameter columns" [1].

The technological developments of liquid chromatography have made this approach practically impossible to follow. Conventional 1/4 in. O.D. (1 in. = 2.54 cm) columns are somewhat long and narrow, making marginal the achievement of the infinite column diameter condition. A 250 × 4.6 mm column packed with 10- μm particles has to be operated at a reduced velocity, ν , in excess of 5 (ν should exceed 20 with $d_p = 20 \mu\text{m}$, 2 with $d_p = 5 \mu\text{m}$) to satisfy the infinite diameter column condition [2]. Since these columns are usually operated at reduced velocities of around 8 in most analytical applications, the condition would be satisfied provided the injection is made at the very column center and the diameter of the injected pulse is very small. However, syringe injection has been universally replaced by valve injection. The sample band is carried into the column by the mobile phase stream which flushes the content of the sample loop. This makes it impossible to perform an axial injection. On the contrary, the injection pulse is spread over the entire column cross-section area. Similarly, in preparative chromatography injection is made by switching, for a given period of time, the sample solution for the mobile phase as the pump feed. The use of valve injection is not compatible with the operation of any column under the "infinite diameter column" mode.

Later, Eon [3] studied radial dispersion in chromatographic columns. He showed that radial dispersion proceeds at a slower pace than axial dispersion. This is in agreement with the results of Knox et al. [2] and with the general results derived from thin-layer chromatography [6]. However, his careful measurements demonstrated that, as a larger and larger fraction of the sample penetrates into the wall region, the column height equivalent to a theoretical plate

(HETP) appears to increase with increasing column length instead of remaining constant, which is a basic tenet of the theory of linear chromatography. This fact may explain various inconsistencies found in the literature regarding the plate height equations and, in Eon's opinion, casts some serious doubts regarding the validity of the conclusions of many publications made in this area [3]. Finally, Eon [3] showed that radial compression improves markedly column performance, presumably because it reduces the density difference between the wall region and the column core.

Recently, Baur et al. [4] have investigated the radial distribution of analyte molecules in chromatographic bands by means of electrochemical detection in the amperometric mode, using carbon fiber electrodes placed close behind the column outlet frit. They found that the radial distribution of the analyte concentration across narrow analytical columns (ca. 3.2 mm I.D.) was surprisingly uneven, although valve injection was used which obviously should prevent the achievement of an axial injection. The retention time is a few percents larger along the wall than in the center. They also showed that the coefficient of axial dispersion and the column efficiency depends strongly on the radial position. The reduced plate height may be four times as large along the wall than in the center part of the column. The radial concentration profiles measured were used to reconstruct the band profiles recorded with a bulk detector. This work demonstrates that at least a large part of the residual tailing observed in cases where there can be little polar interaction between solutes and stationary phase is due to the wall effects.

In spite of their clarity and importance, these results have not yet been assimilated in the culture of chromatographers. For the last twenty years, analysts have generally assumed that wall effects are negligible in analytical columns. It seems strange to them that any significant fluctuations of the packing density may arise over distances as short as the column radius, cause an uneven radial distribution of the concentration of analytes, and have major effects on the column

efficiency. The packing material does look homogeneous, and unpacking columns does not show any difference between core and wall regions. Finally, it is not easy to detect the effects shown by Knox and co-workers [1,2], Eon [3] and Baur et al. [4]. Conventional detectors determine the cross-section average concentration of the mobile phase and are useless for the purpose. Knox et al. [2] and Eon [3] used a dual polarographic detector for their experimental studies. This is not an easy technique. Injections have to be repeated many times since the chromatogram in one single point of the column cross-section can be recorded. Finally, and most importantly, the range of column efficiencies currently achieved seems satisfactory to most users.

The problem of column homogeneity is becoming relevant again, however. There is growing evidence that preparative columns are at least moderately inhomogeneous [7,8] and should be considered as two-dimensional packed beds, i.e., cylindrical, rather than one-dimensional ones, i.e., linear. Recent modeling studies have shown that the long-range fluctuation of the mobile phase velocity in a radially compressed preparative column may exceed 5%, but does not probably reach 10%, except in really bad situations [5]. In conventional packed columns, voids are known to appear at the top of the column after some period of time. This formation is blamed on the lack of “wall support” of the packing [9]. It is certainly due, at least in most part, to a progressive settling of the packing particles, accompanied by a decrease in the column porosity [7–9]. The cause of this phenomenon, and the factors which influence its kinetics are unknown at present. The packing homogeneity and stability of preparative columns needs systematic investigations [8].

Because even the packing structure of analytical columns is still poorly known and understood, it seems interesting to investigate it again in this context. In this first paper, we report on the results of systematic measurements of the radial distribution of the mobile phase velocity and the radial shape of the elution band of a

compound on various analytical columns by means of on-column electrochemical detection. Simultaneous measurements were carried out at different locations.

2. Experimental

2.1. Detection device

Conventional detectors measure the cross-section average composition of the eluent at column outlet. The distribution of the analyte molecules along the column axis is classical. The determination of the radial distribution requires local, on-column determination of the concentration of the eluent at different points of the cross-sectional area, allowing for mapping the analyte distribution over this area before all molecules reunite in the effluent, heading then for the post-column bulk detector.

Like Baur et al. [4], we used electrochemical detection in the amperometric mode, with gold electrodes rather than carbon fiber electrodes placed close behind the column outlet frit. The gold microelectrodes were prepared by inserting a 50- μm nominal diameter gold wire into a 25–30 mm long section of fused-silica capillary tubing 150 μm I.D. (Polymicro Technologies, Phoenix, AZ, USA). The space between the gold wire and the inner wall of the tube was filled with an epoxy resin (Epon Resin 828; Shell, Houston, TX, USA). The tips of the electrodes were polished with diamond paste (sizes 1 then 1/4). The other end of the gold wire was connected to a copper conductor by means of a silver epoxy connection (Epo-tek H20E; Epoxy Technology, Billerica, MA, USA), insulated with the same epoxy resin. Cyclic voltammograms were run with a BAS 100 electrochemical analyzer (Bioanalytical Systems, West Lafayette, IN, USA) in order to assess for the actual area of the electrodes.

To avoid obvious electrical problems, the electrodes were inserted in holes drilled into a non-metallic frit (Upchurch Scientific, Oak Harbor, WA, USA) placed at the outlet end of the

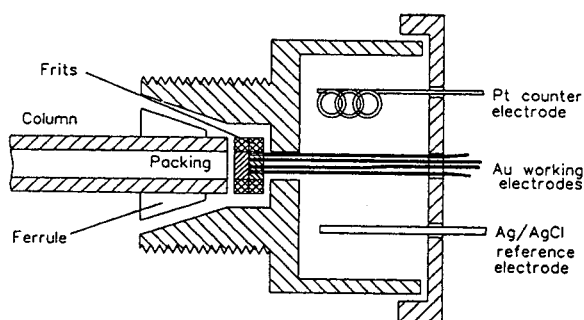


Fig. 1. Schematic of the detector arrangement for four gold working electrodes, a platinum counter electrode and a reference electrode.

chromatographic column. Four electrode tips are placed at different radial positions, facing a second, identical frit placed against the column packing and holding it when the external frit is rotated to permit the acquisition of other sets of data (Fig. 1). One electrode is placed near the center of the frit, two other electrodes are at equal distance from the axis, at about $r_c/2$ (r_c = column radius), in perpendicular directions, and a fourth electrode is close to the wall (Fig. 2). In order to acquire more data points over the column cross-section area, each experi-

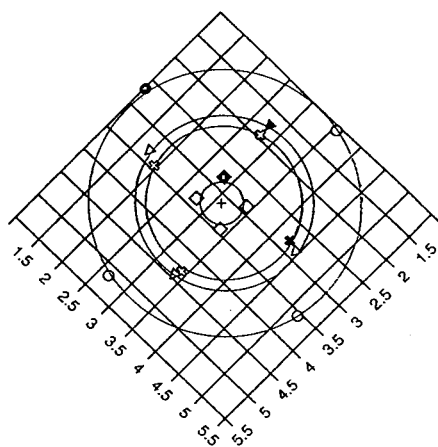


Fig. 2. Position of the electrodes at the column end (solid symbols) and successive positions during a measurement cycle (solid and open symbols).

ment was done four times, and the frit was rotated by 90° steps around the column axis between successive experiments. Thus, 16 data points are collected in each case. The electrode positions are shown in Fig. 2, with the four solid black symbols corresponding to the points collected at one position of the frit.

The aspect of the polished electrode surface was investigated under microscope. All four electrode tips protruding slightly from the frit could be brought together into focus under a high-resolution microscope. Thus, the four electrode tips were in the same plane perpendicular to the column axis. The outlet fitting of the column was modified in order to allow for a four-electrode set-up, for the amperometric detection of electroactive compounds. A platinum counter electrode, and an Ag/AgCl reference electrode were placed behind the outlet frit in the cup-shaped fitting (Fig. 1). The output of each electrode was amplified by means of a Voltammograph Model CV-37 (Bioanalytical Systems). Systematic electrode fouling was experienced. The electrode tips were cleaned before each experimental run by means of sweeping the applied potential from -1 to $+1$ V (electrolytic polishing).

2.2. Liquid chromatography equipment

The chromatographic system consisted of a Waters (Milford, MA, USA) HPLC Pump Model 510, a Spectraflow Model 575 absorbance detector (Applied Biosystems, Ramsey, NJ, USA) as the bulk detector, when needed, and a Rheodyne (Cotati CA, USA) HPLC injection valve Model 7010. The data of either the UV detector or the four electrochemical detectors were acquired using a Waters system interface module with two A/D convertor boards permitting the simultaneous monitoring of four detectors. Waters Maxima 820 version 3.3 software was used to collect the data at a rate of 10 data points per second. The data files were uploaded to one of the computers of the University of Tennessee Computer Center for further calculations.

2.3. Injection profile

The shape of the injection profile has a critical importance in this work. Significant spacial deviations of the profile of the injected plug of sample from the shape of a rectangular band propagating under piston flow conditions would affect the elution profile as much as the lack of radial homogeneity in the column packing that we try to investigate. It is important to determine the possible contribution of the injection profile to our results. The problem of the influence of the design and operating conditions of the injection device on the band profile has been lucidly discussed by Kirkland et al. [10]. Only the considerable improvements made during the last twenty years to the chromatographic equipment have affected the conclusions of this work. Modern columns are closed with a low porosity frit which is tightly crimped at the column inlet. A distributor is placed on the top of the column, above the frit. This provides a relatively flat profile for the front of the injection band when it reaches the column inlet. Because of the parabolic profile of the flow velocity across an empty tube such as the sample loop, the rear of the injection profile tends to assume also a parabolic shape. The use of a narrow, coiled capillary tube as sample loop enhances the radial diffusion in this tube by triggering a secondary circulation. This contributes to alleviate the curved rear of the injection profile.

Measurements of the electrode responses to the injection of samples in a column of length $L=0$, obtained by putting the assembly of electrodes described later directly against an inlet frit and a distributor has given results showing an almost flat injection band, although its axial profile is far from rectangular. Fig. 3 shows typical injection profiles recorded under the same conditions as those used for the chromatograms discussed later in this report and obtained with real columns having 15 to 25 cm in length. The sample concentration rises and decays slightly more slowly along the column wall than in its center. However, there is little difference between the maxima of the two profiles and the delay between the maxima of the profiles

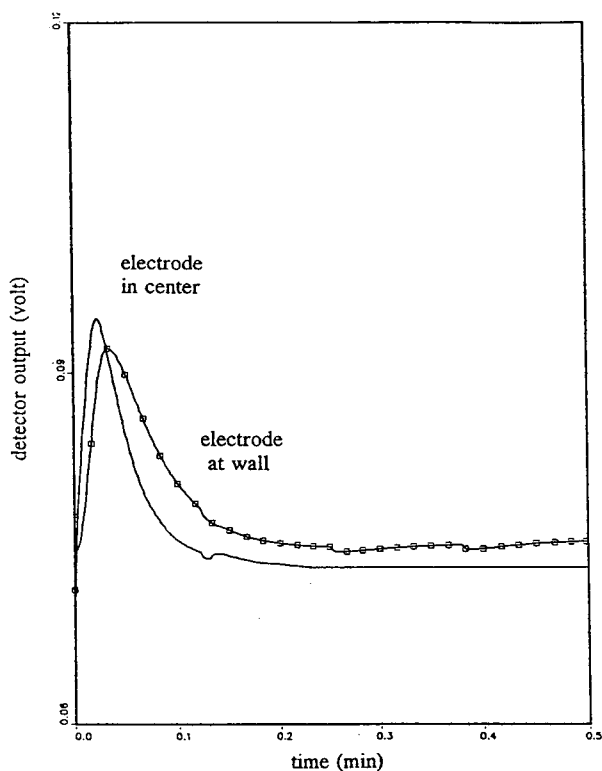


Fig. 3. Injection profiles recorded without column, using the center and wall electrodes.

recorded at the column center (first arrived) and along the column wall is of the order of 0.5 s only, to be compared with values of the order of 12 s observed at the column exit between the retention times of the corresponding profiles at the column center and along its wall.

This demonstrates that the results reported below are due essentially to phenomena taking place inside the column. The contribution of the equipment and, more specifically, of the injection device to these results is essentially negligible.

2.4. Chromatographic columns

Most of the investigated columns (200×4.6 mm) were packed in the laboratory with commercially available packing materials; $40\text{-}\mu\text{m}$ glass beads (EM Separations, Gibbstown, NJ,

USA), 10- and 16- μm porous silica and C_{18} -silica (PQ Corp., now BTR Separation, Wilmington, DE, USA) were used. A Kromasil (Eka Nobel, Bohus, Sweden) KR10-16- C_{18} column packed by the manufacturer was also studied.

2.5. Chromatographic mobile phase

A 0.1 M KCl aqueous electrolyte solution was used as the mobile phase, except for the reversed-phase columns packed with C_{18} silica. Since this material is poorly wet by water [11], 20% methanol was added to the mobile phase. This concentration was chosen because it was the highest for which the amperometric detector worked satisfactorily. It was insufficient, however, to achieve good efficiencies with the reversed-phase column. Fig. 4 shows a conventional plot of the reduced height equivalent to a theoretical plate for benzoquinone (see next section) on this column as a function of the

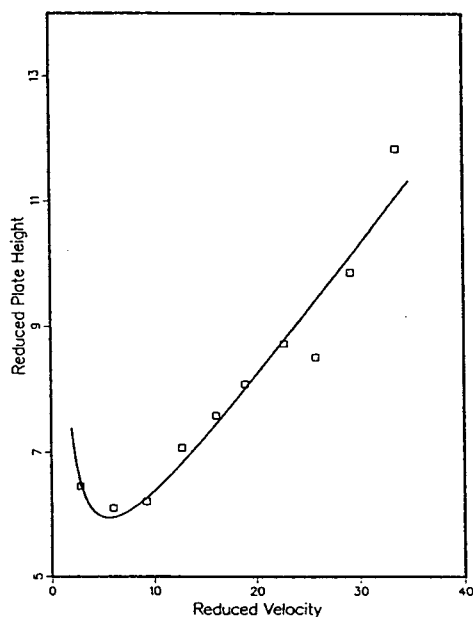


Fig. 4. Plot of the reduced plate height versus the reduced velocity for the Kromasil KR100-16- C_{18} column. Column dimensions, 100×4.6 mm; particle size, 16 μm ; mobile phase, methanol-0.1 M aqueous KCl (20:80). Sample, benzoquinone, 0.1 M solution.

reduced velocity. The data in Fig. 4 were obtained with the UV detector, measuring the column efficiency from the concentration profile in the bulk stream of mobile phase. A value nearly half as large was observed for the minimum plate height with the same column and compound but a water-methanol (40:60) solution as the mobile phase. This suggests that this commercial column is well packed.

The use of a saline, water-rich solution as eluent of a silica column guarantees low or negligible retention factors for most analytes. This is not a problem in the present work, as we study the hydrodynamic properties of the packed bed. Their effects on band profiles is expected to be independent of the possible retention, and to contribute to the total band width following the rule of variance additivity [12]. The influence on the analyte retention of local fluctuations of the stationary phase density will be studied separately.

2.6. Samples

As explained above, the effect studied is clearer on a non-retained peak. Sensitive detection is not an issue either. The samples were chosen to optimize the behavior of the amperometric detector. Several compounds, potassium ferricyanide, hydroquinone and benzoquinone could easily be detected electrochemically under conditions satisfactory for our purpose. However, the electrolyte mobile phase is corrosive and dissolved enough Fe^{2+} from the stainless-steel column wall to cause rapid fouling and clogging of the column and exit frit by deposition of Prussian Blue. This ruled out the use of the ferricyanide/ferrocyanide redox couple.

Dilute solutions of benzoquinone in the electrolyte solution used as the mobile phase proved to be much more stable than the too readily oxidizable hydroquinone solutions. Because of the poor solubility of benzoquinone in electrolyte solution used as mobile phase, $1 \cdot 10^{-3}$ to $1 \cdot 10^{-4}$ M solutions were used. The applied potential difference between the working electrode and the reference electrode for optimum

benzoquinone detection was -0.45 V. Samples of $20 \mu\text{l}$ were injected for each experiment.

2.7. Calibration

Calibration proved to be the most difficult task of this work. It was only partly successful, as we were able to measure only the relative concentrations of the tracer. In order to calculate the local concentration of analyte from the value of the current drawn during the experiment, the response factor for each microelectrode has to be determined. Cyclic voltammograms were run as mentioned previously, and from the value of the resulting limiting current, the actual area of the electrode could be calculated. This parameter cannot be used in the calibration for two reasons.

First, the gold surface of the electrode proved to be highly sensitive to electrochemical fouling that could not be entirely removed by rinsing or ultrasonication. This fouling reduces the active area of the electrode, hence diminishes the response factor. Thus, a frequent, systematic electrochemical cleaning is necessary. However, each cycle of electrolytic polishing removes also a thin metal layer from the fresh gold surface that could not be removed and later small pieces of epoxy insulation around the electrode tip. As a consequence, the active area of the electrode increases in time. These two phenomena have opposite effects. Overall, we found that the limiting current increased significantly during the first week of using the electrode, and then decreased gradually to very small values due to irreversible surface deactivation. The cyclic voltammograms run before using the electrode, and after one week of usage are shown in Fig. 5, demonstrating the effects of an initial increase of the active electrode area, followed by electrochemical fouling of the electrode tip.

The electrode response factor could not be determined by elution experiments because, although the initial concentration of the injected sample is known, the local, actual concentration at the electrode tip is unknown as a consequence of the radial distribution of analyte concentration

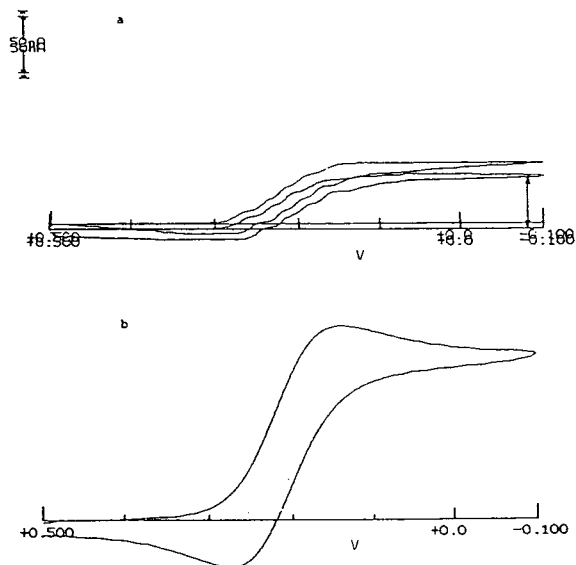


Fig. 5. Cyclic voltammograms run (a) with the electrodes in their initial clean state; (b) after 1 week of experiments. Solution, 0.05 M benzoquinone in 0.1 M KCl. Scan rate, 20 mV/s.

within the component zone. Recalculating the actual electrode area after every short series of experiments by running cyclic voltammograms under steady-state conditions is not practical because of the poor mechanical resistance of the electrodes.

Frontal analysis provides the only practical solution. In this case, the four electrodes are measuring the concentration of the same solution when the plateau at the injection concentration has been reached. This permits the calibration of each electrode relative to the others at the beginning and end of each such experiment. However, the method is quite time consuming, and the extent to which it can be used is limited by fouling, so only a small number of calibration points can be acquired. Accordingly, it was carried out only in connection with the measurements made for the determination of the radial distribution of the analyte concentration. Other experiments were performed without relating the signals of the individual electrodes to the solute concentration.

2.8. Procedures and reproducibility

Each experiment consists in the injection of a small, known amount of benzoquinone as a dilute solution, and the recording of the four electrode signals. The experiment is repeated a number of times, with rotation of the electrode holder by an angle of 90° between successive determinations.

The repeatability of the experiment is assessed periodically by performing series of injections without intermediate rotations, with successive rotations of 360° angles, and with successive rotations of 90° angles. The first series of such experiments gives the repeatability of the injection and detection systems. The results of one such experiment are reported in Fig. 6a. The profiles obtained are identical. The slight shift between the successive signals is due to fluctuations in the delay between the manual actuation of the injection valve and the data acquisition device. Table 1 shows the reproducibility of the differences between the retention times measured with two different electrodes (6 different pairs). Since the two electrodes at $r_c/2$ from the column center are at 90° angle, the difference between their peak maxima is small and less reproducible than for the other five pairs.

The second series of experiments includes the contribution of the additional error made in repositioning the electrodes. Typical results are given in Fig. 6b which shows essentially the same degree of repeatability. The results of the third series of experiments are illustrated in Fig. 6c, as plots of the difference between the retention times measured from the signal of the central electrode and from each of the three other electrodes. The repeatability of the signal of the central electrode is the same as in Fig. 6b, and its fluctuations are due to errors in the timing of the initial data point. This error does not affect the differences shown in Fig. 6c. The repeatability of this difference under the conditions of Fig. 6a is 0.005 min. The fluctuations seen in Fig. 6c, especially at the wall, demonstrate that the velocity distribution is not exactly cylindrical. Obviously, the fluctuations of the retention time observed across the column exceeds largely the errors of measurements.

3. Results and discussion

3.1. Radial distribution of the mobile phase velocity

It would be difficult and meaningless to measure the velocity in any given point of the column. This velocity is chaotic, not only in space, but also in time, because of the eddies which form between particles. The velocity varies rapidly and considerably from the wall of a particle to the center of each interparticle channel. Some averaging is necessary. The cross-section averaged velocity, $u = L/t_0$, is widely used to characterize the convective transport along the column. To study the packing homogeneity we need to average the velocity over a distance which is short compared to the column diameter, but large compared to the particle size. The electrode diameter ($50 \mu\text{m}$) is barely larger than the coarser particles used in this work ($40 \mu\text{m}$), but the electrode is placed in a silica sleeve ($150 \mu\text{m}$) which causes the formation of a local eddy, hence averaging on a space scale of the order of a few particle diameters, which seems to be sufficient. In the plots presented here we give the relative difference, $(u - \bar{u})/\bar{u}$, between this local average velocity and the cross-section averaged velocity, $\bar{u} = L/t_0$.

In an homogeneously packed tube, the radial profile of the velocity averaged over a few particle diameters should be essentially constant, from the axis to the wall. The effect of a lower packing density at the very wall, because particles cannot penetrate into a smooth wall, would be averaged out if the velocity measured is an average calculated over a few particle diameters. The classical Poiseuille parabolic velocity profile applies to empty tubes, to some extent to the interparticle channels (which have too small an aspect ratio for this law to apply strictly), but not to packed columns. Experimental results, however, deviate from this ideal model of the velocity profile.

The plots in Figs. 7a–d show the results obtained for the distribution of the mobile phase velocity in the different columns studied. Fig. 7a shows a three-dimensional plot of the velocity versus the position of the electrodes in the 40-

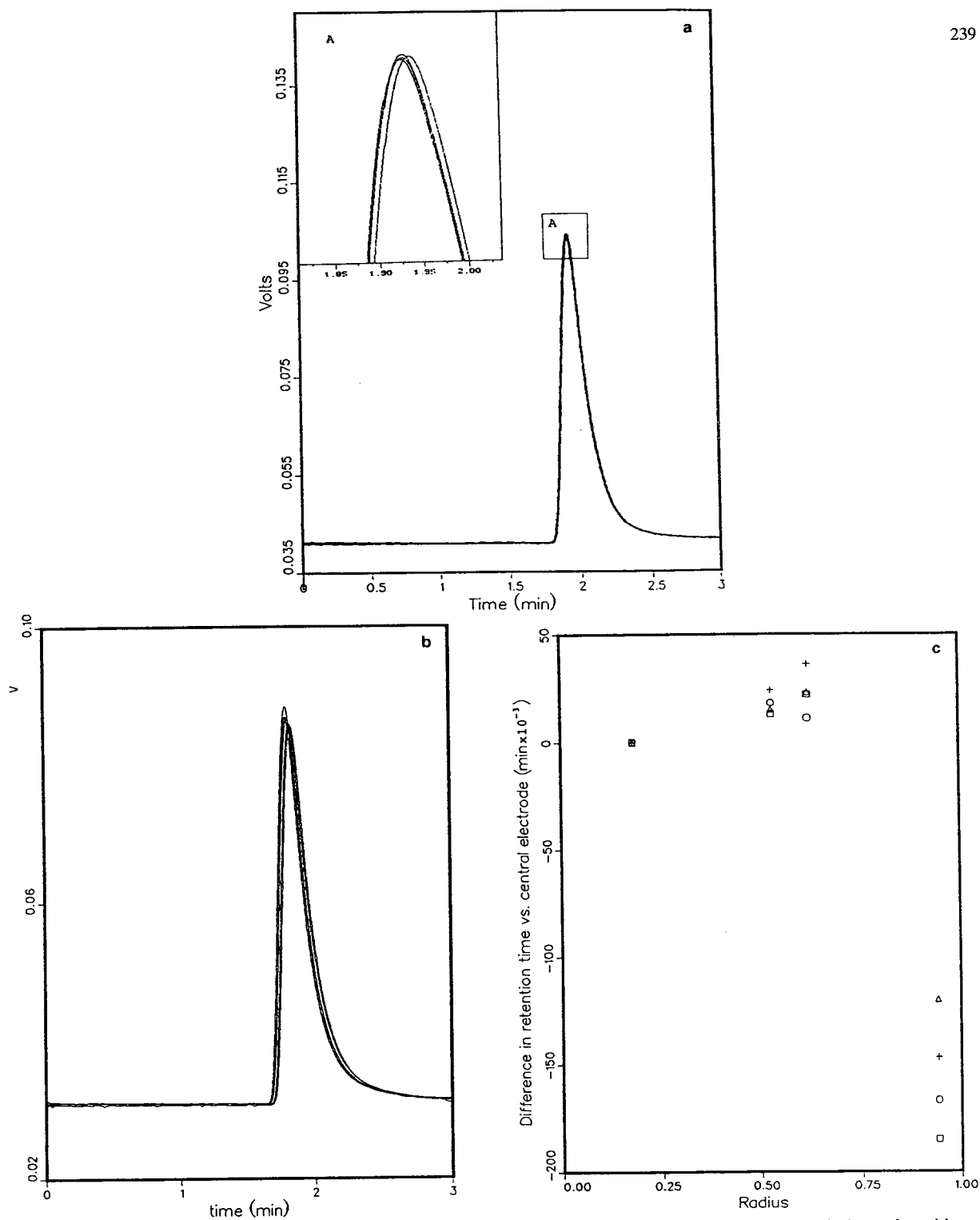


Fig. 6. Reproducibility of the measurements. (a) Four successive chromatograms obtained with the central electrode, without moving the electrode assembly between successive measurements, overlaid. (b) As (a), but the electrode assembly is rotated one full turn between two successive measurements. (c) Differences between the retention times measured by the central electrode and any of the other three electrodes at four different positions (0° , 90° , 180° and 270°) of the electrode assembly. "Radius" indicates relative radius, r/r_c .

Table 1
Reproducibility of retention time differences

Electrode pair ^a	Δt_R (s)	σ (s)	σ/t_R (%)
C-W	7.23	0.53	7.2
C-M1	2.10	0.10	2.8
C-M2	3.90	0.25	6.5
M1-M2	1.15	0.36	32
M1-W	10.5	0.48	4.6
M2-W	7.80	0.40	5.0

The injections were done without moving the electrodes between successive injections. Average and relative standard deviation (σ/t_R) of 8 experimental results.

^a C = Center electrode; M1 = electrode at $r_c/2$, in the plane of C and W; M2 = other electrode at $r_c/2$; W = electrode at the wall (see Fig. 2).

μm glass bead column. It is obvious that the mobile phase velocity is systematically lower close to the wall than in the center of the column. There is a high velocity ridge about half-way through the column, where the velocity is maximum. This ridge is more clearly visible in Fig. 7b, which is a projection of the data in Fig. 7a on the z, y plane of Fig. 7a. The velocity is nearly constant over a core section of the packing which has a diameter of nearly a third of the column inner diameter. The diameter of the ridge is equal to approximately two third of the column diameter.

The phenomenon is unambiguous. The time differences observed are important, much larger than the experimental errors, as shown in the section on reproducibility (see Figs. 6a–c). For example, the delay between the elution of the fastest peak (electrodes half way from the center to the wall) and the slowest peak (along the wall) is of the order of 14 s (12% of t_R), while the band width at half-height of these peaks does not exceed 10 s, and the standard deviation on the retention time of a peak is between 0.1 and 0.5 s, depending on experimental conditions (table or figure).

The glass bead column was unpacked, then repacked twice. The new results are shown in Fig. 7c, as a plot of the relative velocity differences versus the radial position of the electrode

for all measurements made on these columns. This plot shows that the velocity distribution is highly repeatable, except, may be, at the very wall, where angular fluctuations do exit (Fig. 7c). This result demonstrates that the packing method used provides column beds which are highly reproducible, even though they are not ideal. Finally, Fig. 7d compares the results obtained with one of the 40- μm glass bead columns, and a 10- μm silica particle column also packed by us. The radial distributions obtained are nearly identical, although the retention factor of benzoquinone in this case was different from 0 ($k' = 0.22$). This shows that the phenomenon observed does not strongly depends on the solute retention, as expected from its hydrodynamic nature.

This phenomenon was not observed by Knox et al., who report “little [radial] variation of peak-maximum velocity” [2, summary] for an 11 mm I.D. column, but still a 4% *higher* velocity at the wall than at the center [2, Fig. 6b]. Eon [3] obtained similar results with two 17 mm I.D. columns, one made of steel, the other of PTFE (for radial compression). The velocity near the wall is 3 to 4% *higher* than in the column center. In neither case is there any velocity ridge around the column core region. Results similar to ours were reported by Baur et al. [4] who used a 3.2 mm I.D. column, and found that the retention time increases by a few percents close to the wall (2% at 0.2 mm from the wall, i.e., at 65 particle diameters). In our columns, the thickness of the wall region seems to be ca. 15% of the column diameter, or 30 particle diameters, a figure in excellent agreement with the values reported by Knox et al. [2] and by Eon [3] for the thickness of the wall region in their columns. Opposite to these authors’ findings, however, and in agreement with Baur et al., we observe that the velocity is lower at the wall, by up to 12%, and not higher.

3.2. Radial distribution of the column efficiency

For the sake of providing proper reference, we have shown in Fig. 4 the conventional plots of the reduced column efficiency versus the reduced mobile phase velocity, as measured with the UV

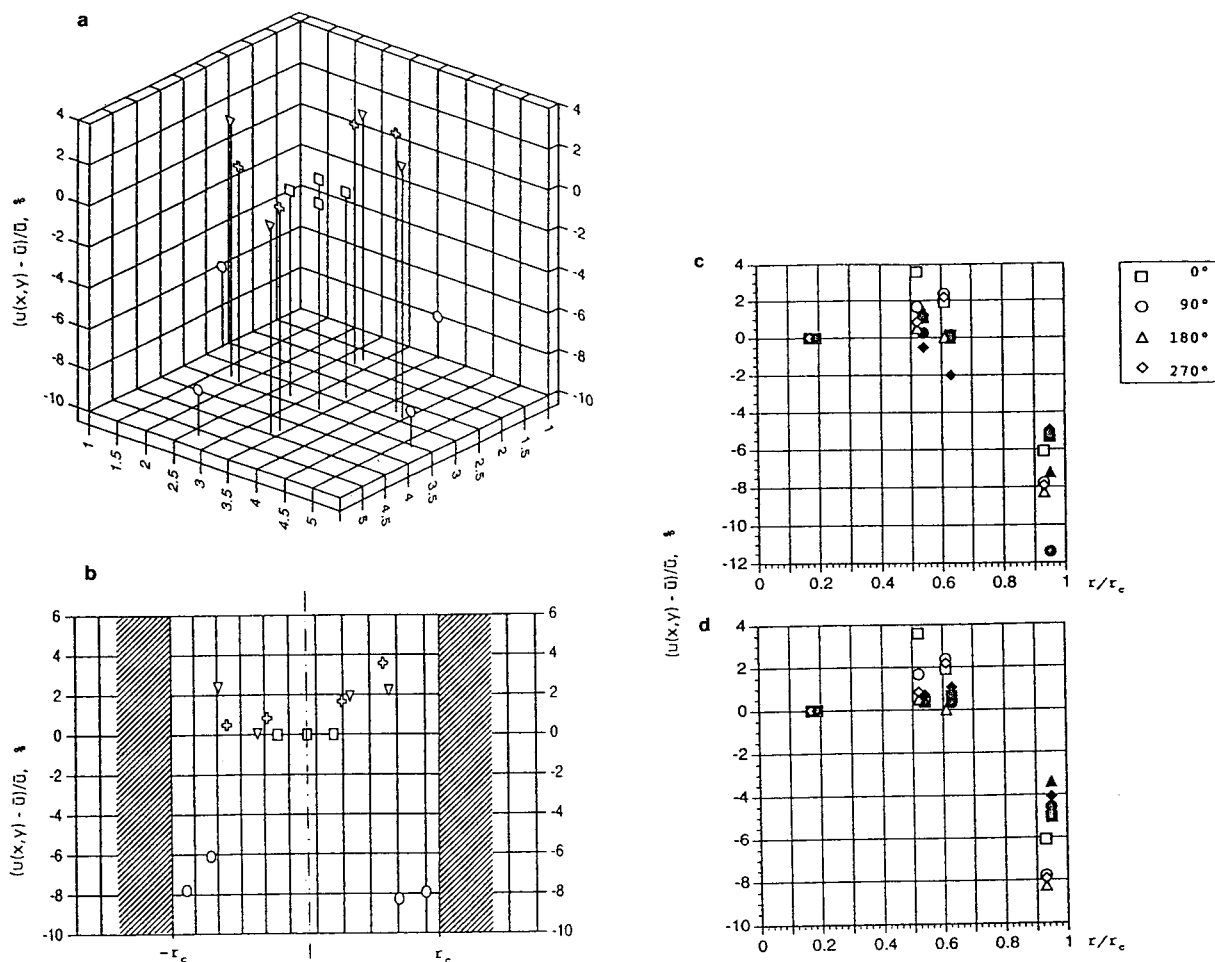


Fig. 7. Plot of the relative velocity difference, $[u(x,y) - \bar{u}]/\bar{u}$, versus the position of the electrode. (a) False three-dimensional plot of the relative velocity difference versus the coordinates of the electrode at the column exit. Column packed with $40\text{-}\mu\text{m}$ glass beads. (b) Projection of the three-dimensional plot in (a) on the y,z plane. Figs. 7a and b, symbols as in Fig. 2. (c) Plot of the relative velocity difference between the radial distance of the electrode. Data obtained with two different columns packed with the same $40\text{-}\mu\text{m}$ glass beads, overlaid. (d) Plot of the relative velocity difference between the radial distance of the electrode. Data obtained with one column packed $40\text{-}\mu\text{m}$ glass beads and with one column packed with $10\text{-}\mu\text{m}$ porous silica particles, overlaid.

detector for the commercial column. As benzoquinone is practically not retained on any of the columns, the slope of the curve at high reduced velocities is essentially due to mass transfer resistances in the mobile phase. It is smaller for glass bead columns than for conventional silica columns, as the beads are not porous. Note, however, that because of its definition, the cross-sectional average velocity depends on the internal porosity of the particles. For a given flow-

rate, the hold-up time is approximately twice as large for a porous silica particle (with total porosity = 0.8) as for non-porous glass beads, hence \bar{u} is twice smaller, while the actual values of the solvent velocities around the particles are the same.

The width recorded for an elution band depends considerably on the position of the electrode. As seen in the Figs. 8a–c, the column efficiency calculated from the width of the band

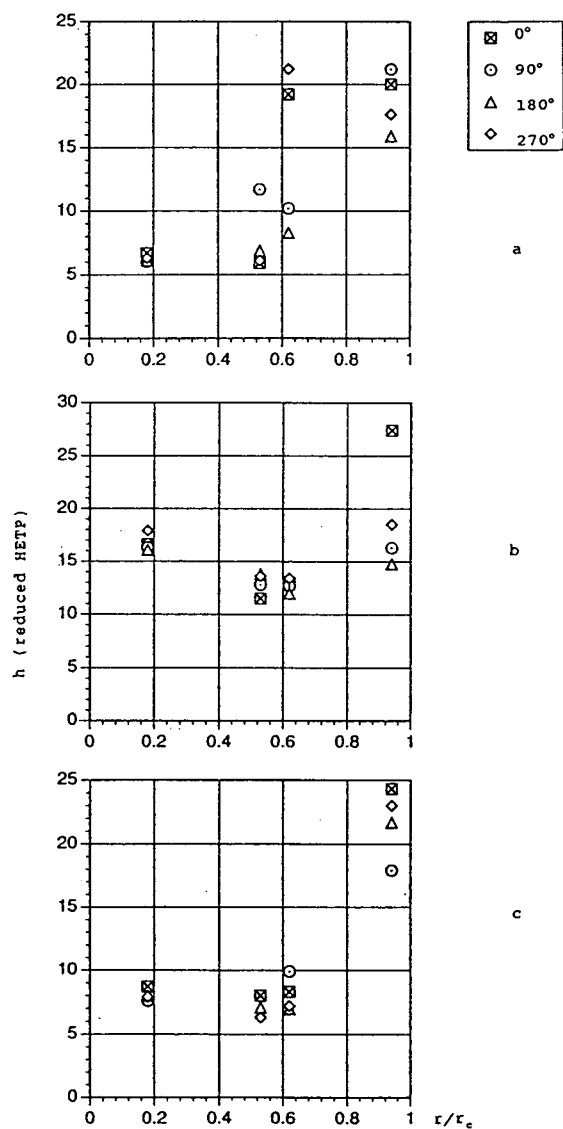


Fig. 8. Plot of the column reduced HETP versus the radial position of the electrode tip. (a) Column packed with 40- μm glass beads. (b) Column packed with 10- μm porous silica particles. (c) Kromasil column, 10 cm long, packed with 16- μm porous particles of octadecyl silica.

at half-height depends much upon the radial position of the electrode. However, the results obtained with the different columns show more variability for the efficiency than for the mobile phase velocity distribution.

Fig. 8a illustrates the dependence of the ef-

iciency on the electrode position in the exit cross-section for the column packed with 40- μm glass beads. The most efficient section of this column seems to involve the core and the intermediate region corresponding to the velocity ridge. Within this center, most of the data points are around 900 theoretical plates, corresponding to a reduced plate height of ca. 5.5 (for a reduced velocity of ca. 90). However, some data points in this region can be as low as 300 plates, which is very poor, and unexpected. The efficiency drops sharply in the region close to the column wall, where all the data points are below 350 plates. Furthermore, peaks recorded at radial positions close to the wall show strongly distorted and wide band shapes. Examples are shown in Fig. 9.

Fig. 8b shows a plot of the column HETP versus the radial position of the electrode for the column packed with 10- μm particles. The result is quite similar, but with the notable difference of a clear maximum at the velocity ridge, where the efficiency is nearly three times larger than along the wall, against 2.5 times in the center. As in the other column (Fig. 8a), the efficiency drop is precipitous around two-thirds of the distance between the center and the wall. As seen in both Fig. 8a and b, it seems that the column is not exactly cylindrical, but that the "wall region" is thicker along some directions than along others.

As seen in Fig. 8c, the commercial column, packed with 16- μm particles, seems to be somewhat more homogeneous than our packed columns, although the results are substantially the same. The shape of the plot of the column efficiency versus the radial position is quite similar to those seen in Fig. 8b, and to that of the plot of the peak-maximum velocity versus the radius (Fig. 7d). The column efficiency is poor at the column wall, maximum along the velocity ridge, and lower at the center. However, the efficiency drop observed near the column wall is much less important than in the other columns. The efficiency at the wall is about 60% of the maximum, along the velocity ridge, and, quite surprisingly, more than 90% of the efficiency in the core region. This column is

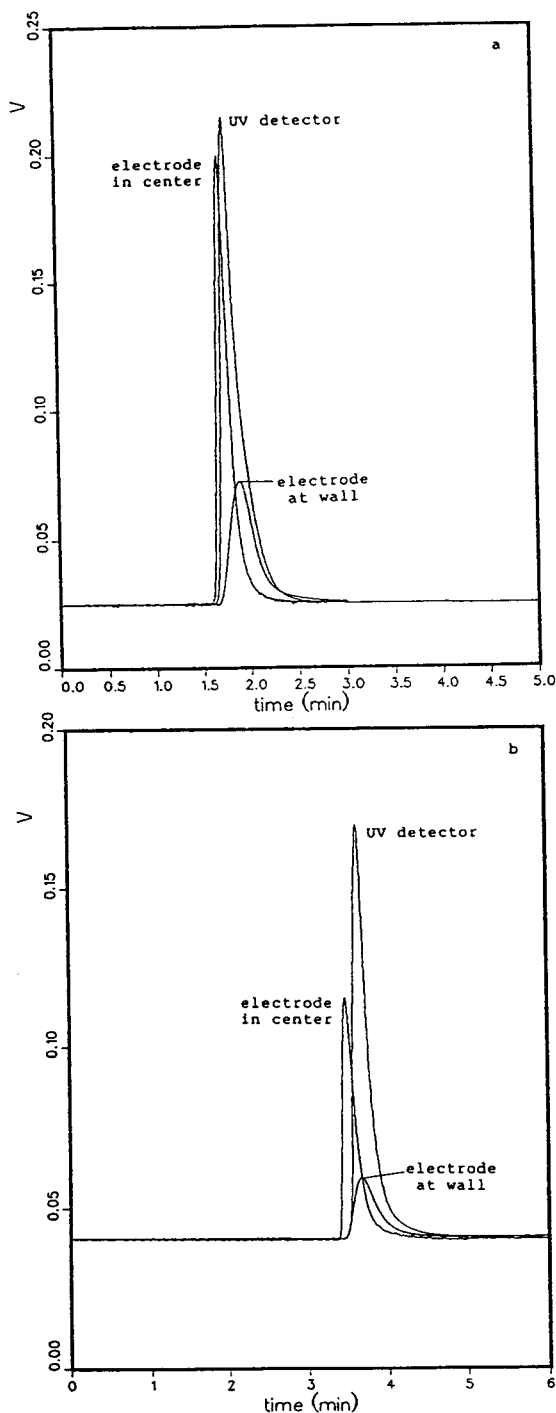


Fig. 9. Comparison between chromatograms recorded with the central and the wall electrodes. (a) Column packed with 40- μm glass beads. (b) Column packed with 10- μm porous silica particles.

certainly much more homogeneously packed than those made in our laboratory.

These results agree with those previously published, but only to a point. As reported here, Knox et al. [2], Eon [3], and Baur et al. [4] found that the column efficiency is much better at the center than along the wall. The profiles of the radial distribution of the column efficiency shown by Knox and co-workers [2], by Eon [3] and by Baur et al. [4] are similar to those shown in Fig. 8. In all these cases and in the present work, the maximum efficiency is two to three times higher than the efficiency near the wall. However, all these authors found the column efficiency to be constant in the central core region. This is not the case for the different columns studied here, even for the commercial column. This shows that more work is necessary to develop an improved packing technology which could reduce or eliminate the wall region and give a more homogeneous, more efficient packed bed.

A consequence of the experimental results of previous authors, confirmed by our own results, is that markedly better separations could be performed by HPLC if only on-column detection were used. A three-fold gain in column efficiency is a major achievement, translating into a 70% better resolution, or three times faster analyses. If this approach is used, however, the positioning of the detecting sensor should be carefully chosen, inside the core area within half a column radius from the column axis, or better, along the velocity ridge.

3.3. Radial distribution of analyte concentration

Fig. 10a shows the distribution of the signal maximum over the column cross-section corrected for the differences in response compared to the electrode placed close to the column axis. Despite the relative lack of precision in the determination of the local concentrations at different values of the column radius, we see that the maximum concentration of the peaks is largest at the column center and in the core region, while it is three to four times lower along the column wall.

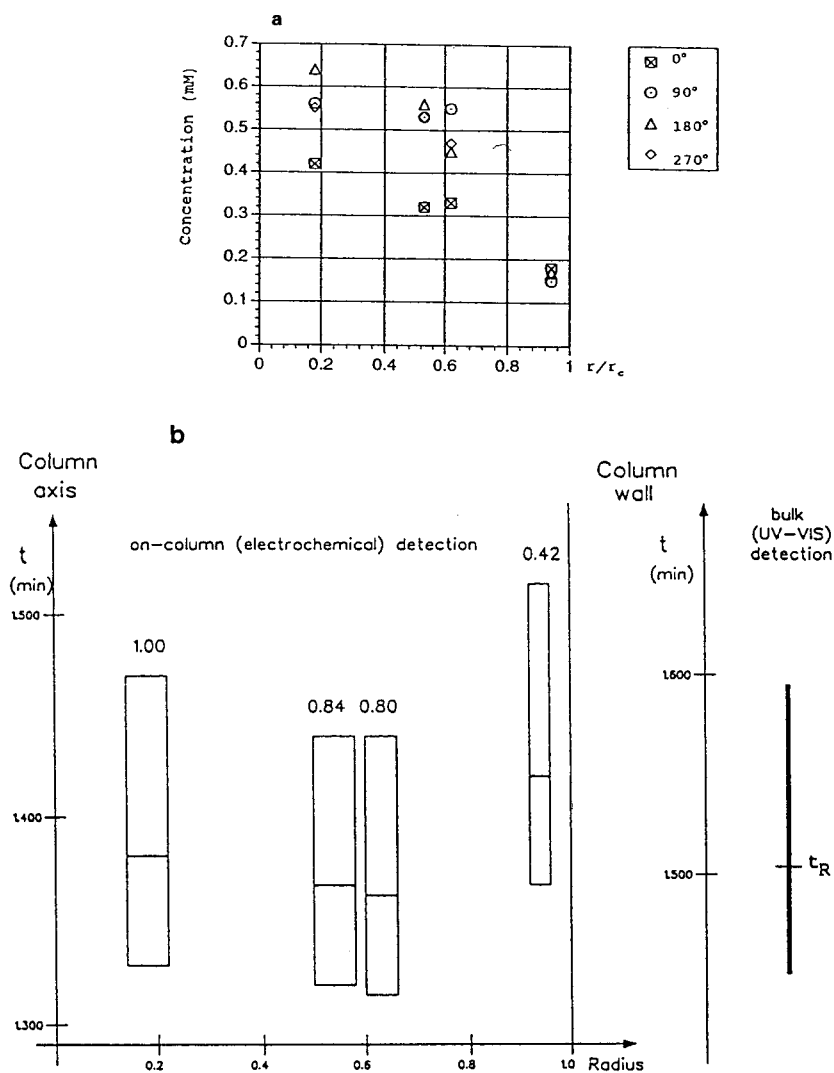


Fig. 10. Radial distribution of the concentration and amount of solute in the column. (a) Maximum concentration of the chromatograms. Kromasil column. (b) Amount of material accounted for by the chromatogram. Abscissa: radial position, as r/r_c .

This result is in agreement with our previous findings. Since the bands are wider and the column efficiency is poorer at the wall than in the core region, the same amount of material injected per unit surface area will give a peak shorter along the wall than in the center. However, multiplying the peak height and its width at half-height gives a figure which is proportional to the peak area. This value is not constant across the column, but increases, albeit much less

rapidly than the peak height, from the column wall to its center (Fig. 10b). This latter finding explains why the large peak width recorded at the column wall does not contribute more to the overall peak width observed with a bulk detector. The results shown in Fig. 10a are in excellent agreement with those of Baur et al. [4]. The ratio of the maximum peak concentrations at the column center and along its wall is ca. 5 in their case, about 3 to 4 in ours.

As shown in the Experimental section, it is possible to rule out any significant contribution of the injection band profile to the radial distribution of the solute concentration. The principle, design and mode of operation of the sampling valve and its connection to the column permit the achievement of almost flat injection profiles. Because the concentration profile of an analyte along the wall passes later and is wider and shorter than in the column center, the signal of a bulk detector is bound to exhibit some degree of tailing, even if the peak profile at any point of the column cross-section is Gaussian. This phenomenon could provide a likely explanation to the puzzling tailing exhibited by weakly polar or non-polar compounds on well-deactivated, end-capped, carefully bonded octadecyl silica packings.

4. Conclusions

Although the details of our results are different from those obtained by previous workers [1–4], there is a substantial agreement regarding the nature of the phenomenon. Analytical HPLC columns are not radially homogeneous. On the contrary, a rather homogeneous core is surrounded by a thick layer of packing along the wall. The thickness of this layer is around 30 to 50 particle diameters. Why this layer is sometimes less permeable and probably denser than the core, as in our experiments and those of Baur et al. [4], while in other cases it is more permeable, as in the experiments of Knox and co-workers [1,2] and Eon [3], and why this is so, remains open for discussion. This observation is important as it does not seem to be consistent with the conventional explanation regarding the low stability of the beds in preparative columns, that these beds are lacking “wall support”. The wall region contributes more to band broadening than the core region. Band profiles recorded at the column wall are later eluted, more dilute and

wider than those recorded in the center during the same experiment.

As a consequence, analytical columns are operated under experimental conditions where a significant fraction of their potential performance is wasted. A small concentration sensor placed at the column axis would see narrower, better resolved and more concentrated bands. Recent progress in the realization of microelectrodes and optical fibers could permit the design of improved chromatographs. The fact that the analyte is more concentrated in the areas where the efficiency is higher renders this approach more attractive.

The behavior of packed column beds and the dynamics of the packing methods are still poorly understood [7–9]. Further progress in the performance of analytical as well as preparative columns could be expected from research done in these areas.

References

- [1] J.H. Knox and J.F. Parcher, *Anal. Chem.*, 41 (1969) 1599.
- [2] J.H. Knox, G.R. Laird and P.A. Raven, *J. Chromatogr.*, 122 (1976) 129.
- [3] C.H. Eon, *J. Chromatogr.*, 149 (1978) 29.
- [4] J.E. Baur, E.W. Kristensen and R.M. Wightman, *Anal. Chem.*, 60 (1988) 2338.
- [5] T. Yun and G. Guiochon, *J. Chromatogr. A*, 672 (1994) 1.
- [6] F. Geiss, *Fundamentals of Thin Layer Chromatography*, Hüthig, Heidelberg, 1987.
- [7] M. Sarker and G. Guiochon, *LC·GC*, 12 (1994) 300.
- [8] M. Sarker and G. Guiochon, *J. Chromatogr. A*, in press.
- [9] H. Colin, in G. Ganetsos and P.E. Barker (Editors), *Preparative and Production Scale Chromatography*, Marcel Dekker, New York, 1992, p. 47.
- [10] J.J. Kirkland, W.W. Yau, H.J. Stoklosa and C.H. Dilks, Jr., *J. Chromatogr. Sci.*, 15 (1977) 303.
- [11] G. Körösi, A.M. Siouffi and G. Guiochon, *J. Chromatogr. Sci.*, 18 (1980) 324.
- [12] J.C. Sternberg, *Adv. Chromatogr.*, 2 (1966) 205.



ELSEVIER

Journal of Chromatography A, 679 (1994) 247–253

JOURNAL OF
CHROMATOGRAPHY A

Metaphosphates as packing materials for biochromatography

Senya Inoue*, Nobuyuki Ohtaki

Central Research Laboratory, Kanto Chemical Co., Inc., 1-7-1, Inari, Soka-City, Saitama 340, Japan

First received 15 March 1994; revised manuscript received 27 May 1994

Abstract

The chromatographic properties of metaphosphates of Mg, Ca, Sr, Mn, Fe, Al and Y prepared as crystalline particles of 4–10 μm were studied. Each metaphosphate (MPi) column except the $\text{Mn}_2[\text{P}_4\text{O}_{12}]$ column showed similar retentions and elution orders of all the basic proteins tested and retention of only a few acidic proteins such as γ -globulins and some iron-binding proteins. The $\text{Mn}_2[\text{P}_4\text{O}_{12}]$ column retained most acidic and all the basic proteins used. The difference in the conformation between the iron-complexed and iron-poor proteins was discriminated in transferrin chromatography using the MPi columns, except for the $\text{Mn}_2[\text{P}_4\text{O}_{12}]$ column, and in conalbumin using the $\beta\text{-Ca}(\text{PO}_3)_2$ and $\beta\text{-Sr}(\text{PO}_3)_2$ columns. The $\text{Mg}_2[\text{P}_4\text{O}_{12}]$ and $\text{Mn}_2[\text{P}_4\text{O}_{12}]$ columns retained DNA, whereas the other MPi columns could not retain all the nucleotides and nucleic acids tested. The MPi columns studied had excellent mechanical strength and thermal and chemical stability. The zeta potentials of all the MPi materials studied were negative over a wide pH range of 0.01 *M* sodium phosphate solution.

1. Introduction

In a previous study [1], pyrophosphate (PPi), one of the condensed phosphates, was found to have interesting chromatographic properties: the retention properties of basic proteins of various PPi materials with different crystal systems and metals were similar to each other and to those of hydroxyapatite (HAP), but those for acidic proteins, nucleotides and nucleic acids were different, depending on the kind of PPi column. PPi materials and orthophosphates such as HAP can be used as packing materials for high-performance liquid chromatography.

The condensed phosphates form a very large group of pentavalent phosphorus compounds. A

metaphosphate (MPi) is also a form of a typical condensed phosphate. Although the type of phosphate group mainly dominates the physical and chemical properties of the condensed phosphates, the component metal ion may also be important [2,3]. Various metaphosphates of alkaline earth metals, transition metals and other polyvalent metals display excellent resistance to dissolution in acidic and alkaline solutions [4]. Moreover, they are inorganic salts, so that it is possible to work in a wide temperature range. Taking into account these properties, MPis are expected to be promising packing materials for chromatographic applications. This paper reports the chromatographic properties of various MPi materials including long-chain polyphosphates which approximate the MPi composition, which were all prepared as crystalline particles.

* Corresponding author.

2. Experimental

2.1. Materials

All proteins, nucleotides and nucleic acids used in this study, purchased from Sigma (St. Louis, MO, USA), were the same as those used previously [1].

2.2. Preparation of metaphosphates

The seven metaphosphates listed in Table 1 were synthesized by a solid-state reaction as follows. $Mg_2[P_4O_{12}]$ (MgMP), $Mn_2[P_4O_{12}]$ (MnMP), $Fe(PO_3)_3(C)$ [FeMP(C)] and $Y(PO_3)_3$ (YMP) were prepared by mixing the corresponding metal oxides and ammonium dihydrogenphosphate (molar ratio of divalent metal to phosphorus = 1:2, trivalent metal to phosphorus = 1:3, respectively), heating at 600°C in air, grinding and reheating at 800°C. $Al_4[P_4O_{12}]_3(A)$ [AIMP(A)], β -Ca $(PO_3)_2$ (β -CaMP) and β -Sr $(PO_3)_2$ (β -SrMP) were prepared by the same method, except that the corresponding metal hydroxides instead of oxides were used as raw materials.

These products were classified using an air classifier, and particles of 4–10 μ m were used as packing materials.

2.3. Analysis of products

The crystalline phases, morphology, pore-size distribution and specific surface area of the MPi products were measured by the methods described previously [1]. The zeta potentials of the MPi products were measured by a streaming potential technique [8] using a 0.01 M solution of sodium phosphate with a ZP-10B streaming potential analyser (Shimadzu, Kyoto, Japan). The zeta potential and also the pH of the supernatant solution after allowing the MPi products to settle were measured periodically until an apparent equilibrium was attained.

2.4. Chromatographic procedure

The MPi products (4–10 μ m) were packed in a stainless-steel tube (100 mm \times 8 mm I.D.) under a 300 kg/cm² pressure using the slurry packing method. The chromatographic procedures were the same used previously [1], and the experimental conditions will be only briefly summarized here: eluent, sodium phosphate buffer (pH 6.8); gradient, $5.00 \cdot 10^{-3}$ M/min from 0.001 to 0.3 M for proteins and from 0.001 to 0.8 M for nucleotides and nucleic acids; flow-rate, 1 ml/min; detection, UV at 280 nm for proteins and 260 nm for nucleotides and nucleic acids.

Table 1
Metaphosphates prepared in this study

Metaphosphate	Abbreviation	Crystal system	Linkage of PO ₄ tetrahedra
$Mg_2[P_4O_{12}]$	MgMP	Monoclinic	Ring
β -Ca $(PO_3)_2$	β -CaMP	Monoclinic	Long chain
β -Sr $(PO_3)_2$	α -SrMP	Monoclinic	Long chain
$Mn_2[P_4O_{12}]$	MnMP	Monoclinic	Ring
$Fe(PO_3)_3(C^a)$	FeMP(C)	Monoclinic	Long chain ^b
$Al_4[P_4O_{12}]_3(A^a)$	AIMP(A)	Cubic	Ring
$Y(PO_3)_3$	YMP	Monoclinic	Long chain

^a According to the notation of d'Yvoir [5] and Remy and Bulle [6].

^b According to Ref. [7].

3. Results and discussion

3.1. Properties of metaphosphates

MgMP, MnMP and AIMP(A) have a tetrametaphosphate ring structure and β -CaMP, β -SrMP, FeMP(C) and YMP have a long-chain structure of PO₄ tetrahedra. Although the latter should be polyphosphates, they can be interpreted as being approximately represented by a metaphosphate composition because of the chain being extremely large. Hence these polyphosphates were included in the MPi class in this study.

All MPi products were virtually non-porous

materials: pores with diameters larger than 60 Å, which affect the diffusion of large-sized samples such as biomolecules in a column, were not recognized by mercury porosimetry, and specific surface areas less than 1 m²/g were measured by the BET method.

The zeta potential of the studied MPi materials in 0.01 M sodium phosphate solution is given as a function of pH in Fig. 1a–g. For comparison, the zeta potential of the HAP measured under the same solution conditions, using the HAP powder prepared in the previous study [1], is given in Fig. 1h. The data were obtained after equilibration for 1 week. All the MPi materials studied showed negative zeta potentials in a solution of pH > 5. During the measurements, it was also found that addition of the MPi samples to 0.01 M sodium phosphate solution of pH in the range 6–8 caused no net change in the pH of the supernatant solution. Moreover, regarding MnMP and FeMP(C), even in the experiments involving an extended pH range of the solution

from 5 to 9, only a small pH change was observed. Hence the MPi materials are considered to be chemically stable under the chromatographic conditions of this study.

YMP was also similar to the other MPi materials concerning the above-described properties. However, an unusual rise in the back-pressure of the YMP column occurred during the chromatographic experiments, the reason for which was not clear. Hence the data on the elution of proteins obtained using the YMP column are not given in Table 2. However, the column showed some interesting chromatographic properties such as a very high retention ability for basic proteins (even higher than that of the HAP column), elution of γ -globulins over a very wide molarity range and an elution behaviour of transferrin similar to that obtained using the other MPi columns.

All these MPi materials had great mechanical strength and a sufficiently high thermal stability to withstand heating above 600°C.

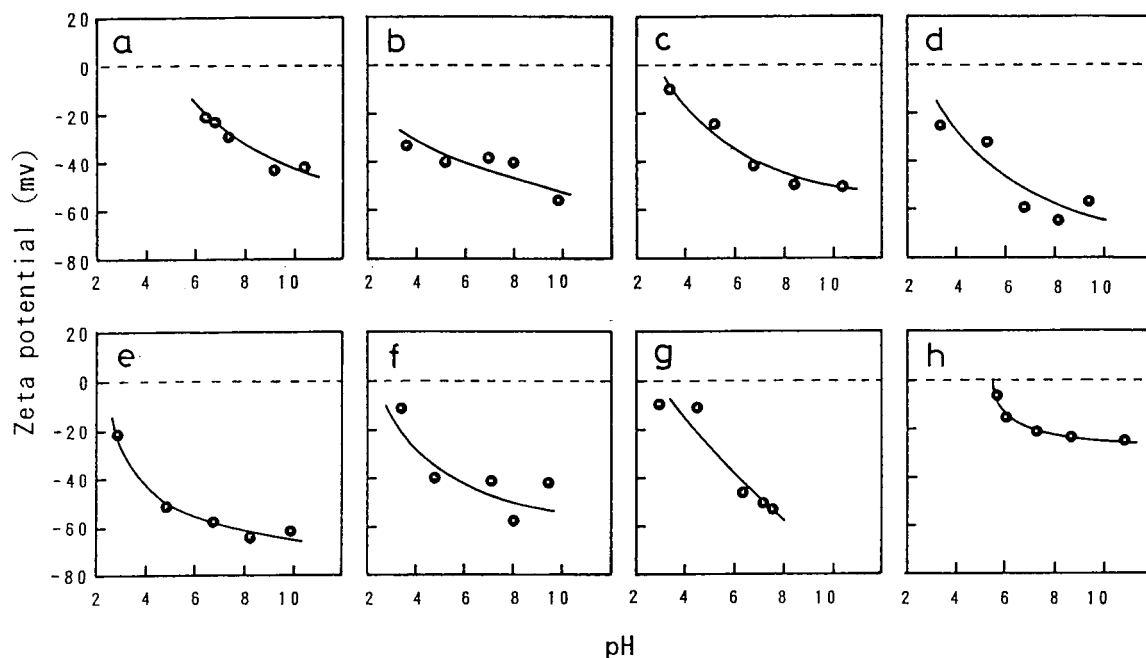


Fig. 1. Zeta potential of metaphosphates as a function of pH after equilibration for 1 week in 0.01 M sodium phosphate solution, obtained using (a) MgMP, (b) β -CaMP, (c) β -SrMP, (d) MnMP, (e) FeMP(C), (f) AlMP(A), (g) YMP and (h) HAP particles.

3.2. Chromatography of proteins

Elution of basic proteins

As Table 2 reveals, all the MPi columns retained the basic proteins with values of the isoelectric point (*pI*) larger than 7.0. The elution order of these basic proteins obtained using each MPi column was similar to that obtained using the HAP and PPi columns [1]. The difference in the elution molarity of a basic protein among the MPi columns except for the YMP column was very small. For the elution of cytochrome *c*, the chromatographic resolution of two peaks based on the reduced and oxidized forms obtained using the β -CaMP and β -SrMP columns was superior to that obtained using the other MPi columns. FeMP(C) and AIMP(A) showed chromatographic similarity, despite the fact that their

properties in the crystal system and linkage of PO₄ tetrahedra are different.

Elution of acidic proteins

The MPi columns except for the MnMP column showed weak retention for acidic proteins with *pI* values of 5.0–7.0 and no retention for the most acidic proteins with *pI* < 5.0. Although MnMP and MgMP are crystalline isomorphs [9], the MnMP column showed a higher retention ability than the MgMP column for usual acidic proteins.

Phosphoproteins and β -lactoglobulins are considered to be special acidic proteins that interact strongly with HAP [10,11] and with most PPi materials [1]. In contrast, the β -CaMP, β -SrMP and AIMP(A) columns showed no retention of the phosphoproteins tested (i.e., α - and β -casein

Table 2
Elution of proteins from metaphosphates

Protein	<i>pI</i>	Elution molarity					
		MgMP monoclinic	β -CaMP monoclinic	β -SrMP monoclinic	MnMP monoclinic	FeMP(C) monoclinic	AIMP(A) cubic
Trypsin inhibitor	4.3–4.6	N.r. ^a	N.r.	N.r.	N.r.	N.r.	N.r.
α -Lactalbumin	4.5	N.r.	N.r.	N.r.	0.02	N.r.	N.r.
Ovalbumin	4.6	N.r.	N.r.	N.r.	N.r.	N.r.	N.r.
β -Casein		N.r.	N.r.	N.r.	>0.3	>0.3	N.r.
α -Casein		N.r.	N.r.	N.r.	>0.3	N.r.	N.r.
Phosvitin	4.8	N.r.	N.r.	N.r.	>0.3	N.r.	N.r.
Albumin	4.7–4.9	N.r.	0.01	0.01	0.02	N.r.	N.r.
β -Lactoglobulin A	5.1	0.08	N.r.	N.r.	0.12	0.04	N.r.
β -Lactoglobulin B	5.2	0.1	N.r.	N.r.	0.13	0.06	N.r.
holo-Transferrin (human)	5.2	N.r.	N.r.	N.r.	0.02	N.r.	N.r.
apo-Transferrin (human)	5.5	0.01	0.02	0.01	0.02	0.01	0.01
holo-Transferrin (bovine)		N.r.	N.r.	N.r.	0.02	N.r.	N.r.
apo-Transferrin (bovine)		0.01	0.04	0.04	0.02	0.01	0.02
Catalase	5.5	N.r.	N.r.	N.r.	0.04	N.r.	N.r.
Conalbumin (iron-complexed)	6.0–6.8	0.05	0.01	0.02	0.06	0.04	0.02
Conalbumin (iron-poor)	6.0–6.8	0.04	0.06	0.06	0.05	0.04	0.03
Haemoglobin	6.8–7.0	0.03	0.01	0.01	0.04	0.02	0.01
Myoglobin	7.2	0.02	0.01	0.01	0.02	0.02	0.01
α -Chymotrypsin	8.1–8.6	0.08	0.07	0.07	0.06	0.07	0.07
Papain	8.8–9.5	0.04	0.04	0.04	0.05	0.04	0.03
α -Chymotrypsinogen A	9.5	0.07	0.08	0.07	0.07	0.08	0.07
Ribonuclease A	9.5–9.6	0.07	0.10	0.10	0.06	0.07	0.07
Cytochrome <i>c</i> (reduced)	10.1	0.13	0.12	0.12	0.12	0.16	0.14
Cytochrome <i>c</i> (oxidized)		0.14	0.14	0.14	0.13	0.16	0.15
Lysozyme	11.0–11.4	0.09	0.11	0.11	0.07	0.08	0.08

For details of measurements, see Experimental section.

^a N.r. = No retention under the experimental conditions.

and phosphitin) and β -lactoglobulin A and B. The MgMP column showed no retention of phosphoproteins and retention of β -lactoglobulins. The FeMP(C) column eluted only α -casein and phosphitin without retention in the column. On the other hand, the MnMP column strongly retained both phosphoproteins and β -lactoglobulins, similarly to the cases in HAP and PPI chromatography.

γ -Globulin was retained on all the MPi columns. This may be because γ -globulin, in general, is a mixture of a large number of immunoglobulin species and has a wide range of pI values even involving the basic range.

Elution of iron-binding proteins

It was found that the MPi columns except for the MnMP column discriminated the difference in conformation between Fe-bound and Fe-unbound transferrins: holo-transferrins (both human and bovine) were not retained on the MPi columns, and the apo-transferrins were retained to and eluted from the column at phosphate concentrations higher than 0.01 M. In contrast, in MnMP chromatography, transferrins with different conformations were eluted at the same molarities.

The retained apo-transferrin showed one peak in MPi chromatography except for the β -CaMP and β -SrMP columns. However, three peaks of apo-transferrin (bovine) were obtained when using the β -CaMP column, as shown in Fig. 2a. Rechromatography of each of the three fractions showed that they appeared again at the same three different positions as in the first experiment, although the first peak became very small and the other two peaks became large. Because transferrin is reported to be capable of binding various metal ions [12], the three peaks may be based on the uptake of calcium ions in apo-transferrin from the β -CaMP crystal, followed by the formation of different forms of the protein; the first peak is probably a form with actually no metal ion in both the N- and C-sites in transferrin, and the protein of this form may have a chance to take up metal ions in rechromatography. This may be the reason why the first peak becomes small in rechromatography. On the

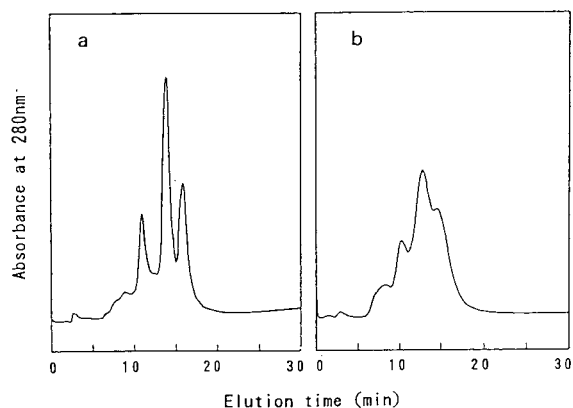


Fig. 2. Chromatograms of apo-transferrin (bovine) obtained using (a) β -CaMP and (b) β -SrMP columns. Elution conditions: gradient, $5.00 \cdot 10^{-3}$ M/min from 0.001 to 0.3 M sodium phosphate buffer (pH 6.8); flow-rate, 1 ml/min.

other hand, the other two peaks are probably forms in which metal ions in part occupied the N-site and/or C-site. In addition to rechromatography, the uptake of calcium ion in transferrin was confirmed by inductively coupled plasma emission spectrometry. Calcium ion was detected in each of the three fractions, but detection in the first fraction was weaker than that in the other fractions.

A chromatogram similar to Fig. 2a was obtained in β -SrMP chromatography, as shown in Fig. 2b, although the resolution was inferior to that with the β -CaMP column.

With regard to conalbumin also being an iron-binding protein, elution similar to that of transferrin was obtained using the β -CaMP and β -SrMP columns; holo-type conalbumin was eluted at a molarity lower than that of apo-type conalbumin. The reverse result, however, was obtained when using the MgMP and MnMP columns: the elution molarity of holo-type conalbumin was slightly higher than that of apo-type conalbumin. In AIMP(A) chromatography, the dependence of elution on the iron-binding state was hardly recognized.

Fig. 3a and b illustrate chromatograms of holo- and apo-type conalbumins obtained using the MnMP column. In the chromatogram of apo-type conalbumin two peaks were observed,

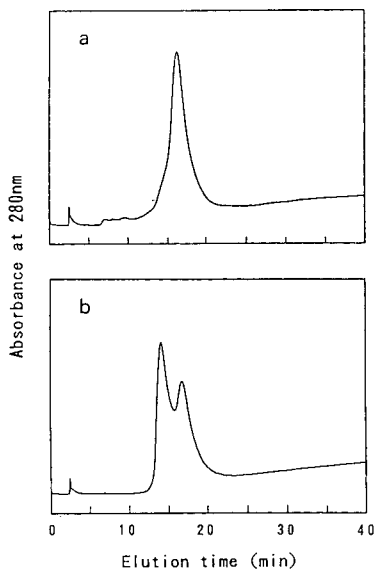


Fig. 3. Chromatograms of (a) iron-complexed conalbumin and (b) iron-poor conalbumin, obtained using the MnMP column. Elution conditions as in Fig. 2.

in which the latter peak was eluted at a molarity that agreed with that of holo-type conalbumin. Hence this peak might be based on the uptake of manganese ions in conalbumin from the MnMP crystal.

From the above-mentioned results for the chromatography of transferrin and conalbumin, the uptake of metal ions in some metalloproteins was shown to be influenced by the kind of metal ion composing the MPi crystal.

3.3. Chromatography of nucleotides and nucleic acids

The chromatographic properties of MPi for nucleotides and nucleic acids were also studied. Based on the experiment, the MPi columns studied except for the MgMP and MnMP columns were found not to retain all tested nucleotides and nucleic acids. The MgMP and MnMP columns could retain DNA. However, even when using these two columns, the retention of RNA was incomplete and nucleotides were not retained at all. Fig. 4a–c illustrate

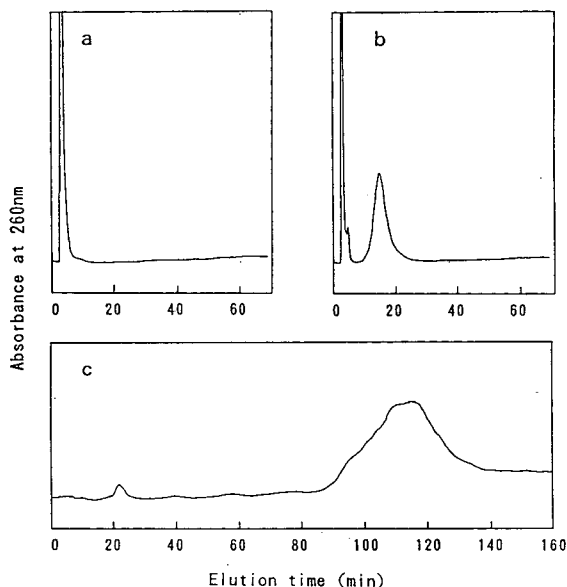


Fig. 4. Chromatograms of (a) ADP, (b) tRNA and (c) DNA, obtained using the MnMP column. Elution conditions as in Fig. 2, except that buffer concentration was from 0.001 to 0.8 *M*.

typical chromatograms for ADP, tRNA and DNA obtained using the MnMP column.

3.4. Chromatographic properties of the MPi column

In β -CaMP, β -SrMP and MnMP, their metal ions can form pure single-cation HAP, leading to the possibility of alternation in surface composition due to hydrolysis of the MPi in solution and formation of HAP on the MPi crystal. If that is the case, then the chromatographic properties would be expected to be similar among these MPi columns. However, as described above, the retention properties of the MnMP column for acidic proteins were different from those for the other two columns. Hence the metal arrangement in the crystal surface, which depends on both the type of anion (i.e., ortho-, pyro- or metaphosphate ion) and the linkage of PO_4 tetrahedra (i.e., ring or chain structure and its configuration), may influence the adsorption of acidic proteins. On the other hand, in MgMP, FeMP(C) and AlMP(A), their metal ions cannot

form pure single-cation HAP, so their surfaces probably maintain their intrinsic crystal structures or change, if at all, to compounds other than HAP. Nevertheless, similar elution behaviour for basic proteins was found among all studied MPi columns. Hence it is considered that the difference in the component metal and crystal structure of MPi does not greatly influence the adsorption of basic proteins on the MPi column.

As with the HAP crystal, there may be two types of adsorbing sites on the MPi crystal surface: one is the negatively charged sites formed by phosphorus ions and oxygen ions, and the other is positively charged sites related to the metal ions of the MPi crystal. The adsorption of biomolecules on the MPi crystal is considered to take place fundamentally because of the electrostatic interaction between the adsorption groups of these molecules and the adsorbing sites of the MPi crystal. However, the chemical properties of the MPi surface in a solution are dependent not only on the MPi's crystallographic properties but also on the solution conditions such as pH and ions present in the system as a result of the various hydrolytic reactions. From the fact that the MPi's zeta potential shows a negative values near neutral pH (Fig. 1), the positively charged sites which are available to adsorb acidic molecules (acidic proteins, nucleic acids and nucleotides) are probably partly or nearly saturated with the phosphate ions of the buffer under the chromatographic conditions in this study. To be adsorbed on the HAP surface an acidic molecule requires a contact area of fixed adsorbing sites that are free of adsorbed phosphate ions [13]. Hence, if the contact area contains less than fixed free sites, then no adsorption will take place. This may be one of the reasons why the MPi columns show weak or no retention of most acidic molecules. This interpretation is not inconsistent with the findings that the HAP with affinity for most acidic proteins has a pI of about pH 6 in 0.01 M potassium dihydrogenphosphate solution [14]. Almost the same result for the pI of HAP was also obtained under the present solution conditions (i.e., 0.01 M sodium phosphate solution), as shown in Fig. 1h.

Transferrin is known to have two conformations [15,16]: one is the conformation of apo-transferrin in which the iron-binding site is in an open cleft near the protein surface and is exposed to the surrounding solution, and the other is the conformation of holo-transferrin in which the iron-binding site is in a closed cleft and is buried under the protein surface so that it cannot approach interacting agents. Hence, on the basis of the chromatographic results obtained in this study and the published findings on the conformation of proteins, it is suggested that the elution of iron-binding proteins may be the result of the main interaction between the metal-binding site or other negative adsorption groups of the protein and the metal ion of the MPi crystal. Moreover, the difference in chromatographic resolution of iron-binding proteins among MPi columns may be the result of the different metal uptake in a protein, which depends on both the protein and the metal of the MPi crystal.

References

- [1] S. Inoue and N. Ohtaki, *J. Chromatogr.*, 645 (1993) 57.
- [2] J.R. Van Wazer, *Phosphorus and Its Compounds*, Vol. 1, Interscience, New York, 1958.
- [3] E. Thilo and I. Grunze, *Z. Anorg. Allg. Chem.*, 290 (1957) 209 and 223.
- [4] J.R. Van Wazer and E. Karl-Kroupa, *J. Am. Chem. Soc.*, 78 (1956) 1772.
- [5] F. d'Yvoir, *Bull. Soc. Chim. Fr.*, (1962) 1237.
- [6] P. Remy and A. Bulle, *Bull. Soc. Chim. Fr.*, (1972) 2213.
- [7] F. d'Yvoir, *Bull. Soc. Chim. Fr.*, (1962) 1243.
- [8] P. Somasundaran and G.E. Agar, *J. Colloid Interface Sci.*, 24 (1967) 433.
- [9] M. Beucher and J.C. Grenier, *Mater. Res. Bull.*, 3 (1968) 643.
- [10] G. Bernardi and T. Kawasaki, *Biochim. Biophys. Acta*, 160 (1968) 301.
- [11] M.J. Gorbunoff, *Anal. Biochem.*, 136 (1984) 425.
- [12] J.P. Harrington, *Int. J. Biochem.*, 24 (1992) 275.
- [13] E. Glueckauf and L. Patterson, *Biochim. Biophys. Acta*, 351 (1974) 57.
- [14] P. Somasundaran, *J. Colloid Interface Sci.*, 27 (1968) 659.
- [15] E.N. Baker, B.F. Anderson and H.M. Baker, *Int. J. Biol. Macromol.*, 13 (1991) 122.
- [16] E.N. Baker and P.F. Lindley, *J. Inorg. Biochem.*, 47 (1992) 147.



ELSEVIER

Journal of Chromatography A, 679 (1994) 255–259

JOURNAL OF
CHROMATOGRAPHY A

Choice of a tracer for external porosity measurement in ion-exchange resin beds

Marie-Laure Lameloise*, Virginie Viard

ENSIA (Ecole Nationale Supérieure des Industries Agricoles et Alimentaires), 1 Avenue des Olympiades, 91305 Massy, France

First received 10 January 1994; revised manuscript received 19 May 1994

Abstract

The external porosity of a gel-type resin bed was evaluated from the mean residence time of a non-adsorbing solute. In order to select a tracer that does not penetrate inside the resin, the resin porosity available to the solute was evaluated by fitting breakthrough curves with a model accounting for diffusion in particles and axial dispersion in a column. Examples are given of the applicability of the method.

1. Introduction

External porosity, ε , is involved in all calculations with column applications. However, it is given far less attention than solid-phase internal porosity and most of the time, its value is arbitrarily taken to be within the range 0.38–0.4. Although this blanket estimate is reasonable in some situations, it would fail in many instances, e.g., a bed consisting of a very polydisperse particle size population, a poorly packed system such as could be encountered in routine preparative systems or a gel bed under compressive conditions (high throughput, for example); also, shrinkage and swelling of gel type resin, which occur when the bed is submitted to large variations in concentrations, may significantly affect the external porosity of the bed.

A direct and simple way to measure ε consists in purging the column: however, care must be exercised to avoid drawing off some of the liquid

contained in the stationary phase, which could alter the result. Actually, the most reliable method consists in measuring t_0 , the mean retention time of an external tracer, and calculating ε from $\varepsilon = t_0(Q/V_b)$.

A non-adsorbing solute has to be found, of course. To evaluate if a solute penetrates or not inside the resin beads, we propose to identify the dynamic response of the column with a model accounting for adsorption. A pore diffusion model is often used to describe mass transfer in macroreticular resins [1] or molecular sieve adsorbents [2]. It will be tried here on a gel-type resin in order to evaluate the internal porosity available to a solute.

2. Model and resolution

The model accounts for column hydrodynamics, axially dispersed plug-flow characterized by the column Peclet number Pe and possible diffusion of the tracer in the resin void

* Corresponding author.

volume, characterized by an internal porosity χ and apparent diffusion coefficient in the pores D_p . Negligible external fluid film resistance is assumed.

This system can be described by the following equations:

(i) mass balance in liquid:

$$\frac{1}{Pe} \cdot \frac{\partial^2 x}{\partial z^2} = \frac{\partial x}{\partial z} + \frac{\partial x}{\partial \theta} + \chi \cdot \frac{1-\varepsilon}{\varepsilon} \cdot \frac{\partial \bar{x}_p}{\partial \theta} \quad (1)$$

(ii) mass balance in particles:

$$\frac{\partial x_p}{\partial \theta} = R_t \left(\frac{\partial^2 x_p}{\partial \rho^2} + \frac{2}{\rho} \cdot \frac{\partial x_p}{\partial \rho} \right); \quad R_t = \frac{D_p t_0}{R^2} \quad (2)$$

(iii) mean concentration of solute in particles:

$$\frac{\partial \bar{x}_p}{\partial \theta} = 3R_t \left(\frac{\partial x_p}{\partial \rho} \right)_{\rho=1} \quad (3)$$

(iv) boundary conditions:

$$\left(\frac{\partial x_p}{\partial \rho} \right)_{\rho=0} = 0 \quad (4)$$

$$\rho = 1; \quad x_p(\rho, z, \theta) = x(z, \theta) \quad (5)$$

The analytical resolution of this set of equations is performed in the Laplace domain according to a methodology described by Wilhelm [3]. The following column transfer function $H(s)$ is obtained:

$$H(s) = Pe \cdot \frac{\exp V}{U} \quad (6)$$

with

$$U = \frac{Pe}{2} \left\{ 1 + \sqrt{1 + \frac{4}{Pe} [s - g(s)]} \right\} \quad (7)$$

$$V = \frac{Pe}{2} \left\{ 1 - \sqrt{1 + \frac{4}{Pe} [s - g(s)]} \right\} \quad (8)$$

and

$$g(s) = -3\chi \cdot \frac{1-\varepsilon}{\varepsilon} \cdot R_t \left(\sqrt{\frac{s}{R_t}} \coth \sqrt{\frac{s}{R_t}} - 1 \right) \quad (9)$$

where $g(s)$ is the transfer function characteristic of the intraparticle transport. It should be noted that the mathematical expression reached

in this way is slightly different from that given by Costa and Rodrigues [4], which included a series term.

The time domain solution of the model (pulse response) for a set of parameters χ , D_p , Pe is obtained by numerical inversion of the transfer function $H(s)$ with a fast Fourier transform algorithm. Numerical integration of the pulse response is then performed, allowing the model breakthrough curve to be obtained. Identification of the parameters and especially χ is performed by fitting the theoretical solution to the experimental breakthrough curve of a solute with the Rosenbrock optimization method [5] (square differences sum as optimized function).

As shown in Fig. 1, the model pulse response is very sensitive to χ , at least above 0.01; below this value, the pulse response seems to merge with the residence time distribution of a non-retained solute. In order to define more precisely the specification of a non-adsorbing tracer, it is interesting to evaluate the influence of χ on the precision of the external porosity determination.

The external porosity ε is obtained from the mean residence time t_0 of a non-retained solute by the well known equation

$$\varepsilon = t_0 \cdot \frac{Q}{V_b}$$

If any solute is used as a tracer, an "apparent" external porosity ε_a should be defined in place of ε :

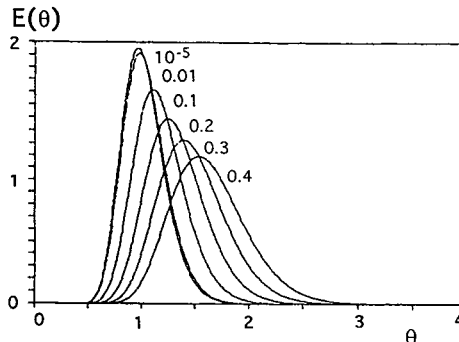


Fig. 1. Model pulse response showing the effect of varying internal porosity χ ($Pe = 50$, $R_t = 5$).

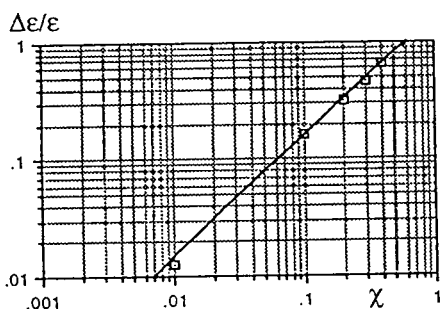


Fig. 2. Influence of χ on the relative error on external porosity measurement. Determination coefficient: $r^2 = 0.999$.

$$\varepsilon_a = \bar{t} \cdot \frac{Q}{V_b} \quad (10)$$

Then

$$\frac{\varepsilon_a - \varepsilon}{\varepsilon} = \frac{\bar{t}}{t_0} - 1 = \bar{\theta} - 1 \quad (11)$$

Hence $\bar{\theta} - 1$ measures the relative error $\Delta\varepsilon/\varepsilon$.

The parameter θ is readily calculated from model pulse responses for several values of χ . A linear relationship is obtained when $\bar{\theta} - 1$ is plotted versus χ in a logarithmic diagram (Fig. 2). A precision of better than 1% on external porosity is obtained when the solute has a χ value lower than $7 \cdot 10^{-3}$.

3. Application of the method

3.1. Systems under investigation

In order to validate the method and test its efficiency, we give two examples of its application to the choice of an external tracer for porosity measurement on a gel-type sulfonated polystyrene resin in the Ca^{2+} form; this resin is commonly used in our laboratory to perform the separation of glucose and fructose mixtures. Two possible tracers for external fluid phase were selected: (i) a calcium salt, at relatively low concentration in order to take advantage of Donnan ion exclusion; calcium chloride was chosen; (ii) a dye whose high molecular mass

prevents it from penetrating into the resin beads; Blue Dextran was chosen.

If we may reasonably expect Blue Dextran to be a good candidate for an external tracer, it is a more tenuous prediction for calcium chloride: because of the sensitivity of the analytical measurements, concentration should be sufficiently high; however, ion exclusion decreases with increasing concentration.

3.2. Experimental

The laboratory-scale column used was obtained from Pignat (France). It was a jacketed column, 50 cm \times 5.3 cm² section, with a piston allowing feeding of solutions exactly at the top of the resin bed through a PTFE frit. Feed solution was pumped from a thermostated bath (Gilson Minipuls peristaltic pump) to the top of the bed through the piston. Electric valves ensured flexibility of use of the apparatus. A purge line was used to obtain a perfect and non-delayed step signal at the entrance of the bed. A Gilson Model 201 fraction collector was connected to the exit of the bed.

Calcium chloride was of Rectapur grade from Prolabo. Blue Dextran was for laboratory use from Sigma (M_r 2 000 000). Calcium chloride concentration was measured by conductimetry (Tacussel). Blue Dextran solutions were analysed with a Carl Zeiss PMQII spectrophotometer at a wavelength of 635 nm. Duolite C204F/2115 resin with a mean bead diameter of 471 μm was supplied by Rohm and Haas.

3.3. Results and discussion

Fig. 3 shows the breakthrough curves of CaCl_2 and Blue Dextran at 10 ml/min. Obviously, CaCl_2 is more retained than Blue Dextran and therefore cannot be considered as a good external tracer, at least at concentrations compatible with our detection means; modelling was undertaken to confirm this and to conclude that Blue Dextran was superior. All curves are well fitted by the model, as shown in Fig. 4, and allow internal porosities to be obtained (see Table 1). The very low particle internal porosity available

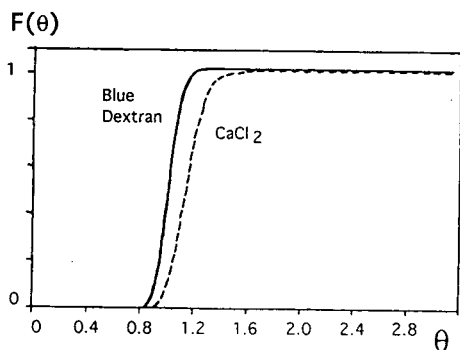


Fig. 3. Comparison of experimental breakthrough curves of CaCl_2 (dashed line) and Blue Dextran (solid line).

for Blue Dextran confirms that this solute does not penetrate into the resin and may be considered as a good tracer for an external liquid phase. In contrast, the value reached for calcium chloride, significantly higher than $7 \cdot 10^{-3}$, makes it inappropriate for this purpose. Fig. 2 indicates

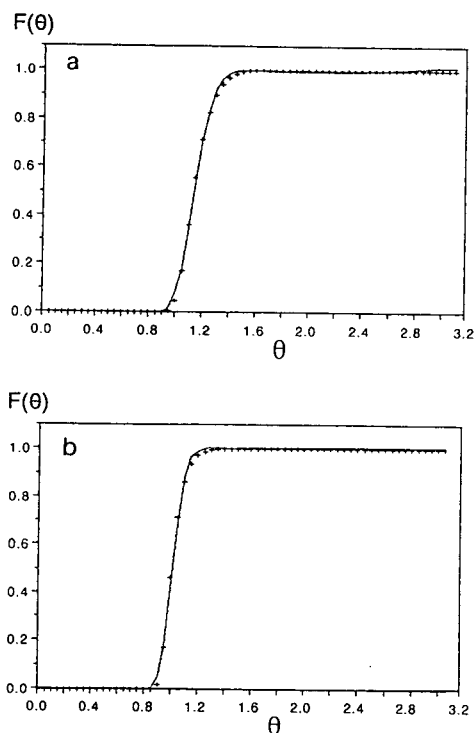


Fig. 4. Adjustment of the model (+) with experimental breakthrough curves: (a) CaCl_2 ; (b) Blue Dextran.

Table 1

Internal porosities obtained from identification of tracer breakthrough curves with the model (several runs performed for each tracer)

Run No.	χ	
	Calcium chloride	Blue Dextran
1	0.08	$0.44 \cdot 10^{-7}$
2	0.07	$0.62 \cdot 10^{-5}$
3	0.09	10^{-8}
4		$0.19 \cdot 10^{-4}$

that an error of more than 10% would be expected.

Blue Dextran breakthrough curves were recorded at different flow-rates ranging from 10 to 33 ml/min for the same bed volume, $V_b = 239 \pm 2$ ml, in order to evaluate ε . The value of t_0 can be determined either from the mass balance over the breakthrough curves or from identification with a J mixing cells in series model (parameters t_0 and $J = Pe/2$). Both methods were applied here. As shown in Fig. 5, the results obtained by either of the two methods are fully consistent and the plot of t_0 versus $1/Q$ is linear. The external porosity ε can be calculated from the slope, given the bed volume. The value obtained is $\varepsilon = 0.41 \pm 0.01$, which is in good agreement

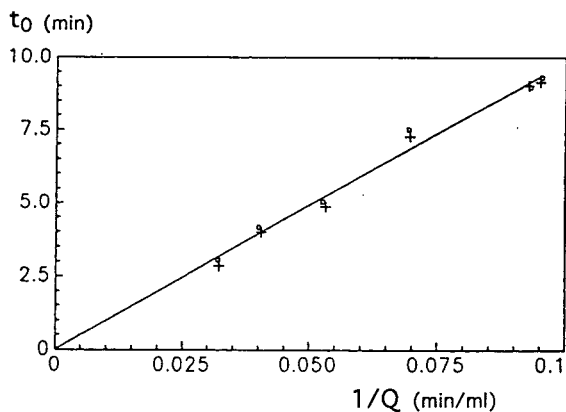


Fig. 5. Residence time t_0 plotted against $1/Q$. \square = Values obtained from mass balance over breakthrough curves; $+$ = values obtained from identification with a mixing cells in series model. Determination coefficient: $r^2 = 0.985$.

with general knowledge about the porosity of random packing of spheres.

4. Conclusions

A model accounting for axial dispersion in the external fluid phase and diffusion in the void volume of particles has been demonstrated to be efficient for selecting an appropriate tracer for an external liquid phase in a fixed bed of a gel-type ion-exchange resin. The external porosity could then be easily and accurately calculated by plotting the mean residence time against the reciprocal of flow-rate.

Symbols

D_a	axial dispersion coefficient
D_p	apparent diffusion coefficient in the pores
$E(\theta)$	column pulse response
$F(\theta)$	column step response
$H(s)$	column transfer function
L	column length
Pe	column Peclet number = uL/D_a
Q	flow-rate
R	particle radius
r	radial coordinate in particle
s	Laplace variable
t_0	mean residence time of a non-retained solute = L/u

t	time
\bar{t}	mean retention time
u	interstitial velocity
V_b	bed volume
x_p	concentration in particle pores
\bar{x}_p	mean concentration in particle
x	concentration in liquid phase
z	dimensionless abscissa in column

Greek letters

ϵ	external porosity
ϵ_a	apparent external porosity
ρ	dimensionless radial coordinate in particle = r/R
θ	dimensionless time = t/t_0
χ	particle porosity

References

- [1] A. Rodrigues, C. Costa, J. Loureiro, A. Leitaö and R. Ferreira, in A.E. Rodrigues, M.D. Le Van and D. Tondeur (Editors), *Adsorption: Science and Technology; NATO ASI Series, E158*, Kluwer, Dordrecht, 1989, p. 239.
- [2] L.K. Lee and D.M. Ruthven, *Ind. Eng. Chem., Fundam.*, 16 (1977) 290.
- [3] A.M. Wilhelm, *Thèse de Docteur-Ingénieur*, INP, Toulouse, 1983.
- [4] C. Costa and A. Rodrigues, *AIChE J.*, 31 (1985) 1645.
- [5] H.H. Rosenbrock, *Comput. J.*, 3 (1960) 175.



ELSEVIER

Journal of Chromatography A, 679 (1994) 261–268

JOURNAL OF
CHROMATOGRAPHY A

Analytical method optimization for protein determination by fast high-performance liquid chromatography

I. Gaillard, A. Martial, A. Marc, J.-M. Engasser, M. Fick*

*Laboratoire des Sciences du Génie Chimique, INPL, ENSAIA, CNRS UP 6811,
2 Avenue de la Forêt de Haye, B.P. 172, 54 505 Vandoeuvre-lès-Nancy Cedex, France*

First received 18 January 1994; revised manuscript received 26 April 1994

Abstract

A method based on fast HPLC allowing the rapid and efficient determination of proteins in mammalian cell cultures is proposed, involving the use of two chromatographic modes, RP-HPLC and high-performance liquid affinity chromatography. These two sequential chromatographic analyses separate the proteins most often used as supplements in serum-free media such as bovine serum albumin, insulin and transferrin, and also monoclonal antibodies secreted by hybridoma in cultures. Rapidity, reliability and flexibility are the main characteristics of the method. The monitoring of proteins in the course of a discontinuous hybridoma culture is presented.

1. Introduction

HPLC has made major advances over the past 10 years, especially in applications to protein determination and purification. The technological improvements to and the theoretical knowledge of this technique have widened its area of application. As the analytical level, HPLC ensures qualitative and quantitative control of protein molecules [1]. Among HPLC techniques, fast HPLC with a non-porous stationary phase has permitted the analytical separation of various proteins [2–6].

The need to associate efficient and reliable analytical methods with production and purification bioprocesses is a major concern of recent research in biotechnology [7]. Efficient analytical control of a given production process contributes

to improving the productivity and the understanding of physiological and metabolic mechanisms. Moreover, once the molecule of interest has been produced, analytical control has to be performed in each step of its purification. These requirements are principally encountered when high-value molecules are produced by bioprocesses.

Qualitative analysis of a protein secreted by recombinant microorganism may be checked by HPLC based on the detection of undesirable protein variants [8–10]. Peptide mapping may be considered as the most efficient method for determining the biochemical quality of proteins to be used in medicine [11–13]. This technique is widely employed for rt-PA and hGH determinations [1].

The use of HPLC as a quantitative tool is becoming more widespread. Notably, HPLC allows the establishment of the evolution of

* Corresponding author.

protein concentrations. The integration of HPLC in an automated system interfaced with a bioreactor in order to monitor on-line the evolution of protein concentrations is of current interest [14–16].

Concerning hybridoma cultures performed to produce monoclonal antibodies, studies dealing with the monitoring of proteins in the medium are scarce. However, the use of serum-free media characterized by an accurately defined formulation makes easier the specific determination of each protein added as a supplement [17–19]. Some examples of chromatographic modes accurately applied to determine secreted IgG may be noted [20–24]. Nevertheless, this field of application does not fully take advantage of the overall potential of HPLC.

The aim of this study was to develop a rapid and accurate chromatographic method for measuring proteins encountered in hybridoma cultures. The method involves the use of two chromatographic modes, RP-HPLC and high-performance liquid affinity chromatography (HPLAC). Optimization of each chromatographic mode and the parameters that influence them are presented. The use of the optimized method to determine proteins during a hybridoma culture is described to illustrate its potential in this area of application.

2. Experimental

2.1. HPLC method

Instrumentation

Chromatography was performed with an HP 1090 liquid chromatography (Hewlett-Packard) with a ternary DR5 solvent-delivery system, a diode-array detector (400–600 nm) and an auto-sampler. The chromatographic system and data evaluation were controlled by an HP 9000 Chem Station computer.

The reversed-phase column used was a Hy-Tach C₁₈ micropellicular reversed-phase column provided by Professor Cs. Horváth (Yale University). This column (30 × 4.6 mm I.D.) consists of non-porous silica microspheres ($d_p = 2 \mu\text{m}$)

coated with C₁₈-alkyl chains. The affinity column used was a Perstorp Biolytica (Lund, Sweden). ProAnaMabs column. This column (50 × 5.6 mm I.D.) is packed with 10- μm Selectispher silica particles covalently linked to a proprietary Fc receptor (protein A + protein G).

Reagents

RP-HPLC mobile phase and standard proteins. The mobile phase consisted of an aqueous phase (A) and an organic (B) phases with the following compositions: A = 0.1% trifluoroacetic acid (TFA) (Sigma) in water and B = 0.1% TFA + 95% acetonitrile (Prolabo). The aqueous and organic phases were filtered through a 0.45- μm filter (Interchim) on a Millipore filtration system and degassed by sparging with helium before use. Standard proteins to be measured by RP-HPLC (albumin, insulin, transferrin) were purchased from Sigma.

HPLAC mobile phase and standard IgG. The binding solution consisted of 100 mM citrate buffer (pH 5), obtained by mixing equimolar solutions of citric acid and sodium citrate and adjusting the pH by the addition of an acidic solution. The eluent solution was 100 mM citric acid adjusted to pH 1.6 with concentrated HCl. Both solutions were filtered through a 0.2- μm filter (Sartorius) and degassed by sparging with helium before use. Both solutions are stable for over 1 week at 4°C. Two standard monoclonal antibodies were used for calibration: mouse IgG₁ with 80% purity (Sigma) and mouse IgG₁ with 100% purity (Zymed).

Calibration procedure

Sample preparation. The require concentration range of each protein was obtained by dilution of a 1 mg/ml solution. This concentrated solution and all dilutions were made with the appropriate phase: water for BSA, insulin and transferrin and binding solution for IgG. Both BSA and transferrin concentrated solutions (1 mg/ml) are stable for over 1 month at 4°C but IgG concentrated solutions are stable for over only 1 week

at 4°C. Insulin concentrated solutions used for dilutions have to be freshly prepared. Calibration graphs were obtained according to the concentration of each protein in the serum-free medium: 10–50 µg/ml for transferrin, 5–50 µg/ml for insulin, 10–300 µg/ml for BSA and several levels for IgG and BSA–IgG mixture.

Precision determination. The reliability of each calibration graph was established by a statistical study. The calculation of each standard deviation relative to one protein concentration permits the determination of the precision of quantitative measurements by HPLC. Each standard sample corresponding to a defined protein concentration was injected ten times. By pooling the results obtained over several analyses, standard deviations were determined. A typical calibration graph for each protein assay was established. The reproducibility of the measurements and the influence of various parameters were tested by comparison with the calibration graphs.

Analytical conditions

The conditions for RP-HPLC and HPLAC were optimized in order to achieve a rapid and reliable determination of the proteins albumin, transferrin, insulin and IgG. Consequently, several parameters were studied such as flow-rate and gradient shape for RP-HPLC and time of the adsorption phase for HPLAC. This optimization investigation resulted in the following operating conditions.

RP-HPLC. The temperature is maintained at 80°C during the stabilization phase, the analysis phase and the washing phase. The volume taken is 25 µl and is injected automatically into the chromatographic system. Absorbance at 215 nm was chosen. Protein separation was performed with an organic solvent gradient in 5 min with a flow-rate optimized at 1.5 ml/min. Further details of the conditions for RP-HPLC are discussed under Results.

HPLAC. The temperature is controlled at 25°C. The volume of each sample injected is 250 µl and IgG is detected at 280 nm. An equilibration

phase is proposed in which binding solution is run for 45 min. Determination of IgG is achieved by changing the mobile phase pH: after 2 min of running 100% binding solution, IgG desorption is induced by injecting 100% eluent solution for 2 min. In both binding and elution phases the flow-rate is 3 ml/min.

2.2. Hybridoma cultures

Cell line and medium

Mouse hybridoma cells VO 208 secreting IgG₁ of unknown specificity were provided by Bertin. The line results from the fusion of mouse BALB/C spleen cells with myeloma cells. The serum-free medium used was optimized in our laboratory [17]. The basal medium consists of 50% IMDM (Iscove Modified Dubelco Medium) + 50% Ham F12 with 18 mM glucose, 3 mM glutamine (Intermed); the supplements were 4 mg/l insulin, 25 mg/l transferrin saturated with iron, 0.2% (w/v) polyethylene glycol, 20 mM aminoethanol, 50 mM β mercaptoethanol, 12 nM sodium selenite, 20 mg/l ascorbic acid, 18 mg/l liposomes containing cholesterol, oleic acid, dipalmitoyl-L-α-phosphatidylcholine and 180 mg/l BSA (Sigma).

Culture operating conditions

For batch operation, a 250-ml spinner flask (Techne) was used, containing 200 ml of medium with an inoculum cell density of $2 \cdot 10^5$ cells/ml. Twice a day, 8-ml aliquots are collected from the spinner. Cells count and viability were determined by the Trypan Blue dye exclusion method using a haemocytometer. The remaining sample was centrifuged and the supernatant was divided into aliquots and stored at –20°C until protein analyses. Proteins were determined by RP-HPLC and HPLAC.

3. Results

3.1. Method optimization

The principal of the proposed method is based on the complementary performances of two

Table 1
Optimum RP-HPLC conditions for the determination of insulin, transferrin and BSA + IgG mixture

Aqueous phase (A)	0.1% TFA in water
Organic phase (A)	95% acetonitrile in water containing 0.1% TFA
Gradient	From 0 to 60% B in 5 min
Flow rate	1.5 ml/min
Temperature	80°C
Volume injected	25 μ l

analytical columns, RP-HPLC and HPLAC. This sequential analysis allows the four proteins of interest to be accurately measured: proteins added to the serum-free medium (insulin, transferrin, BSA) and monoclonal antibodies secreted by hybridoma.

The test of several operating parameters (flow-rate, gradient shape, temperature) on the improvement of the resolution between BSA and IgG by RP-HPLC did not give satisfactory results. Consequently, to overcome these limitations, the RP-HPLC conditions were optimized in order to obtain the determination of insulin, transferrin and the mixture of BSA and IgG, whereas IgGs were determined by HPLAC. The albumin concentration was deducted from these two types of measurement; the BSA concentration resulted from subtraction from the total BSA + IgG concentration obtained by using the RP column of the IgG concentration determined with the affinity column.

Protein determination by RP-HPLC

The optimized conditions allowing the simultaneous determination of insulin, transferrin and BSA + IgG are reported in Table 1. The optimization criteria were essentially rapidity and resolution. Protein determinations were realized in less than 6 min with optimum resolutions between each protein pool considered (insulin, transferrin and BSA + IgG). Under these conditions BSA and IgG have the same retention time and their total peak allows the concentration of their mixture to be obtained. Fig. 1 illustrates chromatograms obtained for proteins determined by RP-HPLC under the optimized operating conditions.

Three calibration graphs were established with the appropriate range of concentration of each protein, insulin, transferrin and BSA + IgG (Figs. 2 and 3).

To assess the precision of the method, standard deviations (S.D.) of the protein concentrations were determined. The error range of BSA and transferrin measurements increased from 1.5% at the higher concentrations (200 and 50 μ g/ml, respectively) to 6% at lower concentrations (10 μ g/ml). The precision of insulin determination is not so good, especially for low concentrations which make the integration of the peaks difficult (the S.D. varies from 30 to 10% for the concentration range 5–50 μ g/ml). Consequently, the threshold of sensitivity for insulin determination was estimated to be 10 μ g/ml.

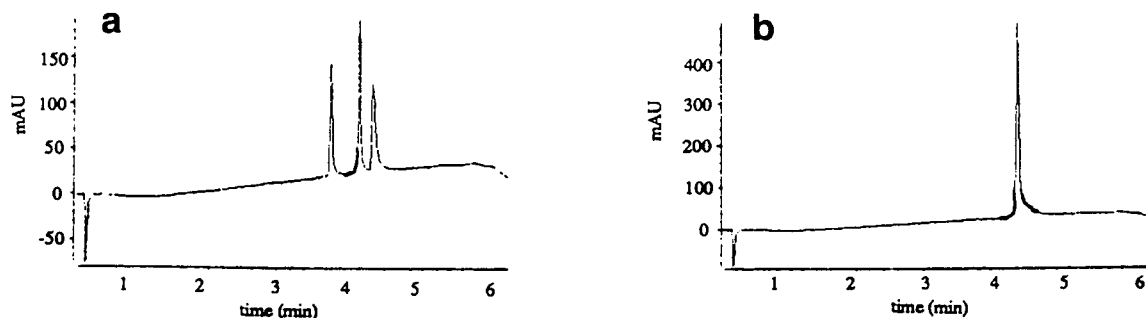


Fig. 1. Chromatograms for a protein mixture obtained by RP-HPLC. Column, 30 \times 4.6 mm I.D. packed with 2- μ m spherical silica particles having covalently bound octadecyl functions at the surface. Analytical conditions as in Table 1. Sample components: (a) insulin 50 μ g/ml, transferrin 50 μ g/ml, BSA 50 μ g/ml; (b) BSA 200 μ g/ml, IgG 40 μ g/ml.

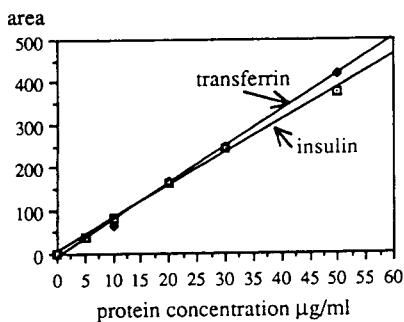


Fig. 2. Calibration graphs for transferrin and insulin. Calibration by RP-HPLC under the operating conditions given in Table 1.

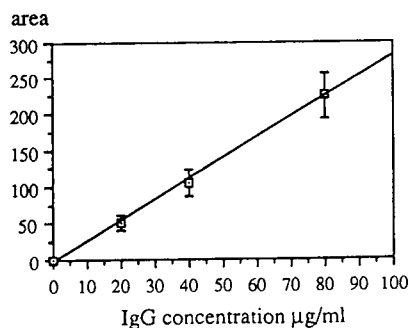


Fig. 4. IgG calibration with the affinity column under the optimized conditions given in Table 2. Vertical bars indicate confidence intervals.

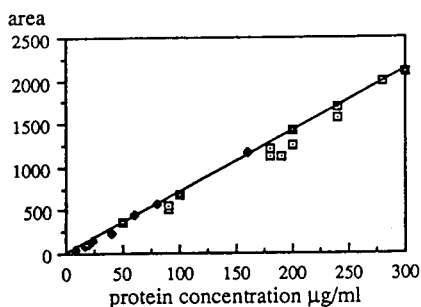


Fig. 3. Calibration graph for BSA + IgG established by RP-HPLC under the operating conditions given in table 1. Three ranges of dilution were used: \blacksquare = calibration with BSA; \blacklozenge = calibration with IgG; \square = calibration with BSA + IgG mixtures.

IgG determination by HPLAC

The affinity column used for IgG measurement consists of a protein A and protein G stationary

phase. Under the optimized operating conditions presented in Table 2, this column allowed the efficient determination of IgG.

The calibration of the method was defined within confidence intervals related to IgG concentrations (Fig. 4). The standard deviation varied from 7 to 15% for concentrations between 80 and 10 $\mu\text{g/ml}$, respectively. This calibration graph established with the precision lines was considered as a reference plot and, consequently, allowed the study of the influence of various parameters on the performance of the method. For testing the flexibility of the calibration method, the influence of various parameters involved in the protocol was investigated, viz., the nature of the dilution buffer, the source of standard IgG and the methods of conservation of standard solutions.

The results of these experiments compared

Table 2
Optimum conditions for the determination of IgG by HPLAC

Binding solution	100 mM citric acid (pH 5)
Eluent solution	100 mM citric acid (pH 1.6, adjusted with HCl)
Flow-rate	3 ml/min
Time of adsorption phase	2 min
Time of desorption phase	2 min
Temperature	Ambient (25°C)
Volume injected	250 μl
IgG standard	IgG ₁ , 80% purity
IgG diluted in	Binding solution

with the standard calibration graph showed that: serum-free medium, phosphate-buffered saline (PBS) and water could be used as dilution solutions for standard IgG; IgG₁ 80% pure and IgG₁ 100% pure could equally be chosen as standard monoclonal antibodies; fresh and unfrozen concentrated solutions used to prepare the range of dilutions could equally be adopted.

Further, the reproductibility of the measurements with repeated injections of one supernatant with unknown IgG concentrations was checked (Fig. 5).

Overall, the studies show that this method for IgG determination can be considered to be reproducible and flexible with regard to the analytical conditions.

3.2. Method application

This method was used as an efficient and fast means of monitoring the evolution of protein concentrations during cultures. A batch culture of hybridoma VO 208 was carried out with a serum-free medium in a spinner flask and with initial concentrations of protein supplements of insulin 4, transferrin 25 and BSA 180 $\mu\text{g}/\text{ml}$. Direct analysis of cell culture supernatants were performed on the RP-HPLC and HPLAC columns. No problem with column fouling was noticed.

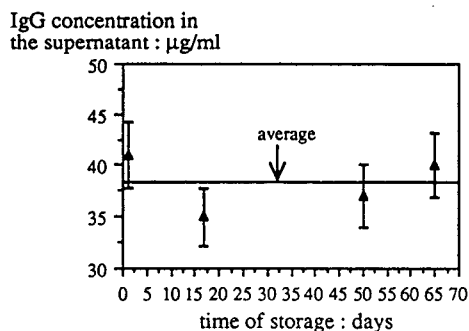


Fig. 5. Reproducibility of IgG determination tested by HPLAC. An aliquot of supernatant stored at -20°C was analysed four times over a period of 65 days. Vertical bars indicate the confidence interval relative to the measured concentrations (\blacktriangle) (S.D. = 8%). Operating conditions are given in Table 3.

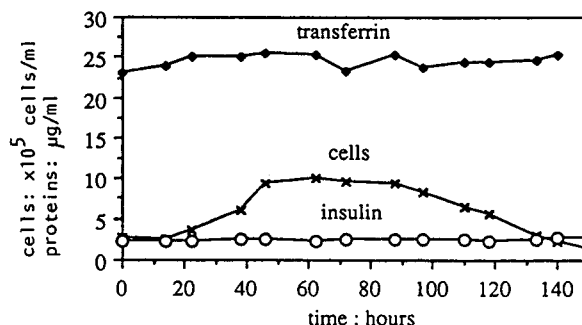


Fig. 6. Evolution with time of (\times) viable cell density, (\circ) insulin concentration and (\diamond) transferrin concentration during a discontinuous hybridoma (VO 208) culture. Proteins were determined by RP-HPLC under the operating conditions given in Table 1.

Figs. 6 and 7 show the kinetics of viable cell density and of each protein encountered in samples taken during the overall culture and analysed by the proposed method.

The transferrin concentration obtained by RP-HPLC does not change during the course of the culture, the measured concentration being equal to the initial concentration added to the medium (25 $\mu\text{g}/\text{ml}$). The insulin concentration seems to be stable during the culture and to remain lower than the initial concentration. However, this result has to be treated with caution because of the poor precision of the method at low concentrations of insulin. The albumin concentra-

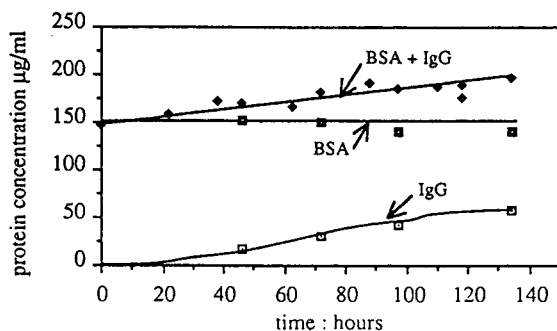


Fig. 7. Evolution with time of the BSA + IgG mixture and BSA and IgG concentrations during the discontinuous hybridoma culture. The BSA + IgG mixture (\diamond) was determined by RP-HPLC under the operating conditions given in Table 1 and the IgG concentration (\square) by HPLAC under the operating conditions given in Table 2. \square = BSA kinetic results from the first two analyses.

tion is deduced from the two consecutive chromatographic measurements, BSA + IgG determination by RP-HPLC and IgG determination by HPLAC. The determination albumin concentration in the supernatants indicated its kinetic stability at 155 $\mu\text{g/ml}$. The measured concentration is 10% below the initial concentration (180 $\mu\text{g/ml}$). Finally, the kinetics of monoclonal antibodies measured by HPLAC indicated a final concentration of ca. 50 $\mu\text{g/ml}$.

4. Discussion

The proposed method using two sequential chromatographic columns is considered to be suitable for the determination of the four proteins encountered in hybridoma cultures performed with a serum-free medium. Experiments were carried out in order to optimize the operation conditions and to investigate the characteristics of the method. The relative flexibility and rapidity of this technique can be emphasized: each analysis is completed in less than 6 min and the preparation of standards and samples is easy.

Concerning the determination of monoclonal antibodies, the specificity of the affinity column and the reproducibility of the measurements were checked. TEDESCO et al. [24] also investigated these interesting column characteristics. The precision of the determination of monoclonal antibodies varied from 7 to 15% for concentrations between 80 and 10 $\mu\text{g/ml}$, respectively. For comparison the enzyme-linked immunosorbent assay (ELISA) used for measuring monoclonal antibodies in cultures has a ca. 10–20% error. Other immunoassay methods have been proposed to overcome the limitations of ELISA [25,26].

The precision of the measurements of proteins added to the medium was studied. The standards deviation of transferrin and BSA measurements were in the range 2–6%. The precision for insulin was in the range 10–30% for concentrations varying from 50 to 5 $\mu\text{g/ml}$. Consequently, the results for insulin should be treated with caution.

The application of the method to discontinu-

ous culture monitoring allowed us to establish the kinetics of the proteins and to obtain interesting data. According to the culture analysed, the transferrin concentration remained stable. Martial et al. [27] also showed the stability of transferrin by employing a nephelometric technique. However, they observed some consumption of insulin for several cultures of hybridoma cells. This difference may be explained by the limit of validity of the chromatographic method for measuring insulin accurately at low concentrations (<10 $\mu\text{g/ml}$). Concerning the determination of albumin, the stability of its concentration was noted. The difference between the measured and the theoretical concentration (180 $\mu\text{g/ml}$) may be explained by the fact that albumin is employed in the preparation of liposomes. This observation indicates that ca. 10% of albumin is incorporated into the lipidic vesicles. The measurement of IgG concentrations by using the chromatographic method allowed the production kinetics to be established with rapidity and reliability.

This study has demonstrated the interest and potential of the method in the context of hybridoma cultures, especially concerning IgG kinetics. Its applications could be widened to other cultures such as continuous cultures, cultures with serum or cultures with other hybridoma cell lines. Moreover, a completely automated bioreactor–HPLC interface with a sampling device could be considered for the on-line monitoring of IgG concentrations during hybridoma cultures.

Acknowledgement

The authors thank Professor Cs. Horváth, Department of Chemical Engineering, Yale University, New Haven, CT, USA, for helpful advice and collaboration.

References

- [1] R.L. Garnick, N.J. Solli and P.A. Papa, *Anal. Chem.*, 60 (1988) 2546.

- [2] K. Kalghatgi and Cs. Horváth, *J. Chromatogr.*, 398 (1987) 335.
- [3] K. Kalghatgi, *J. Chromatogr.*, 499 (1990) 267.
- [4] M.A. Rounds and F.E. Regnier, *J. Chromatogr.*, 443 (1988) 73.
- [5] Y. Kato, S. Nakatani, T. Kitamura, Y. Yamasaki and T. Hashimoto, *J. Chromatogr.*, 502 (1990) 416.
- [6] N. Nimura, H. Itoh and T. Kinoshita, *J. Chromatogr.*, 585 (1991) 207.
- [7] S. Borman, *Anal. Chem.*, 59 (1987) 969A.
- [8] S.E. Builder and W.S. Hancock, *Chem. Eng. Prog.*, 84 (1988) 42.
- [9] V.R. Anicetti, B.A. Keyt and W.S. Hancock, *Tibtech*, 7 (1989) 342.
- [10] L.J. Janis and F.E. Regnier, *J. Chromatogr.*, 444 (1988) 1.
- [11] Y.F. Maa and Cs. Horváth, *J. Chromatogr.*, 445 (1988) 71.
- [12] M.W. Dong and A.D. Tran, *J. Chromatogr.*, 499 (1990) 125.
- [13] T. Isobe, K. Uchida, M. Taoka, F. Shinkai, T. Manabe and T. Okuyama, *J. Chromatogr.*, 588 (1991) 115.
- [14] E. Favre, P. Pugeaud and P. Péringier, *Biotechnol. Tech.*, 4 (1990) 315.
- [15] H. Lundström, M. Brobjer, B. Osterlöf and T. Moks, *Biotechnol. Bioent.*, 36 (1990) 1056.
- [16] D. Picque and G. Corrieu, *Biotechnol. Bioeng.*, 40 (1992) 919.
- [17] A. Martial, *Thèse*, Institut National Polytechnique de Lorraine, Vandoeuvre-lès-Nancy (1991).
- [18] M.C. Glassy, J.P. Tharakan and P.C. Chau, *Biotechnol. Eng.*, 32 (1988) 1015.
- [19] E. Shacter, *Tibtech.*, 7 (1989) 248.
- [20] M.C. Flickinger, N.K. Goebel and M.A. Bohn, *Bioprocess Eng.*, 5 (1990) 155.
- [21] R.F. Hammen, D. Pang K. Remington, H. Thompson, R.C. Judd and J. Szuba, *Biochromatography*, 3 (1988) 54.
- [22] S. Ohlson and J. Wieslander, *J. Chromatogr.*, 397 (1987) 207.
- [23] G. Schuler and M. Reinacher, *J. Chromatogr.*, 587 (1991) 61.
- [24] J.L. Tedesco, S. Ohlson, A. Holmberg and R. Rupp, *Biochromatography*, 4 (1989) 216.
- [25] P.I. Lindell, L. Hall, T.G. Wu and C.L. Cooney, *Biotechnol. Tech.*, 5 (1991) 187.
- [26] D. Velez, S. Reuveny, L. Miller, and J.D. Macmillan, *J. Immunol. Methods*, 86 (1986) 45.
- [27] A. Martial, P. Nabet, J.-M. Engasser and A. Marc, in R.E. Spier, J.B. Griffiths and B. Meignier (Editors), *Production of Biologicals from Animal Cells in Culture*, Butterworth, London, 1991, p. 454.



ELSEVIER

Journal of Chromatography A, 679 (1994) 269–275

JOURNAL OF
CHROMATOGRAPHY A

Extraction, purification by solid-phase extraction and high-performance liquid chromatographic analysis of taxanes from ornamental *Taxus* needles

M.J.I. Mattina*, G.J. MacEachern

Department of Analytical Chemistry, Connecticut Agricultural Experiment Station, 123 Huntington Street,
New Haven, CT 06511, USA

First received 3 May 1994; revised manuscript received 21 June 1994

Abstract

Needles from ornamental yews (*Taxus* spp.) are known to contain significant amounts of the anticancer agent Taxol (paclitaxel), as well as other analogous taxane compounds. Methanol extracts the taxanes from the needles efficiently, but the crude methanolic extract contains large amounts of co-extractives in addition to the taxanes of interest. The crude extract may be fractionally partitioned using C_{18} solid-phase extraction (SPE), permitting the collection of a fraction in which the taxanes elute quantitatively. This fraction can then be analyzed directly by means of high-performance liquid chromatography. We have successfully scaled-up the quantity of crude extract partitioned by means of the SPE technique, using larger SPE cartridges prepared in our laboratory as well as using Empore extraction disks. SPE using the Empore disks permits us to collect large quantities of the taxane fraction for studies on its cytostatic effect on non-mammalian eukaryotic cells.

1. Introduction

Studies on the chemistry of Taxol (paclitaxel, Bristol-Myers-Squibb, New York, NY, USA) and analogous taxane compounds span four decades, beginning in 1963 with the observation that extracts from the Pacific yew (*Taxus brevifolia*) were cytotoxic [1], up to the present attempts to elucidate paclitaxel's mode of action [2]. The structures of some diterpenoid taxanes are shown in Fig. 1. The magnitude of current interest in taxanes is attested to by symposia dedicated to paclitaxel chemistry [3], as well as by the increased magnitude of the taxane litera-

ture. By far the main focus of this literature is the interaction of taxanes with mammalian cells. In contrast, the number of reports on the effects of taxanes on non-mammalian, eukaryotic systems is few. For example, limited studies of paclitaxel effects on frog eggs [4], on sea urchin eggs [5], on hemoflagellates [6], on higher plants [7] and on fungi [8–11] have been reported.

All of the reports in the literature to date and alluded to above have utilized pure, authentic taxanes, e.g. paclitaxel, cephalomannine and baccatin III, from Pacific yew bark. Data from our earlier investigations [12] indicated that the needles from ornamental yew (*Taxus* spp.) shrubs contain paclitaxel and other taxanes in quantities equal to or higher than the amounts

* Corresponding author.

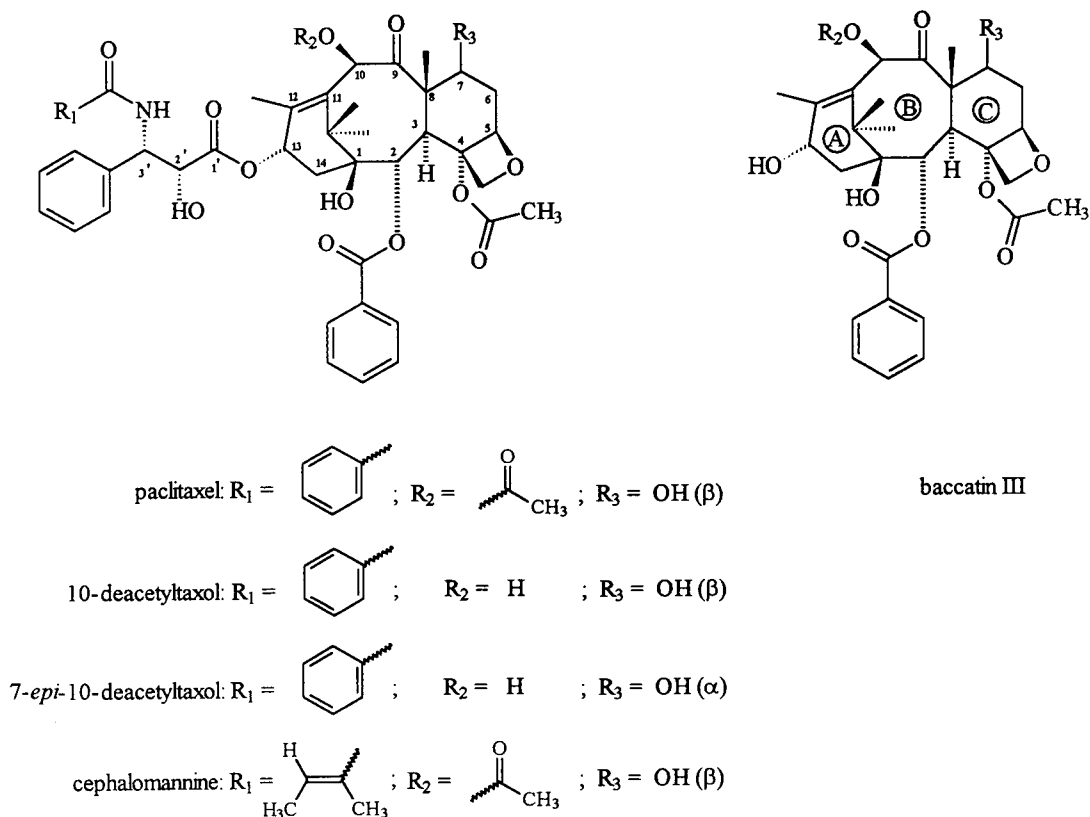


Fig. 1. Structures of taxane diterpenoids.

typically found in Pacific yew bark (i.e., 400 ppm). The development of taxanes as agrochemicals must not compete with supplies of these compounds destined for application as chemotherapeutic anticancer agents. In addition there is considerable expense entailed in the purification of a single, pure taxane, a necessary procedure for pharmaceuticals, which may be unnecessary in the production of taxane agrochemicals. Annual prunings of *Taxus* shrubs, which are a waste product of commercial nursery operations, can serve as the source of yew needles destined for extraction to produce bio-fungicides. Our studies [13] suggest that the fungitoxic efficacy of a mixed-taxane fraction may exceed that of a single pure taxane. These studies on potential taxane bio-fungicides extracted from yew needles require that we improve our methods for obtaining large quantities

of the partially purified taxanes. Solid-phase extraction membrane technology permits us to achieve this objective rapidly and economically.

2. Experimental

2.1. Extraction

The extraction procedure has not been altered substantially since our initial report [12]. Clippings from ornamental yew cultivars, such as *Taxus* \times *media* "Hicksi" and *T. \times media* "Nigra" from commercial plantings in Connecticut and Rhode Island, USA, from field research plots at The Connecticut Agricultural Experiment Station's Lockwood Farm, and from greenhouse-rooted cuttings, were collected and stored in plastic bags at 4°C. Within one week of collection the needles were stripped from the twigs. A

small sub-sample of the whole needles was dried to constant mass (typically 16 h) in an oven at 95–100°C solely for moisture determination. The remaining needles were reduced to 3 mm or smaller in size using a laboratory blender. A 3–4-g sub-sample of the well mixed, ground needles was weighed, transferred to an Erlenmeyer flask, and extracted with 100 ml of methanol at ambient temperature for 16 h on a wrist-action shaker. We have observed that 4 g of biomass/100 ml of extraction solvent results in the quantitative extraction of the taxanes. The resulting solution was filtered through Whatman 1 or 2 filter paper, the needles were washed with 25 ml of methanol, and the combined methanolic solution was evaporated to dryness on a rotovap at 40–43°C. The dried residue was reconstituted in 10 ml methanol and 1 ml distilled–deionized water. All water used in our procedures is distilled prior to finishing in a NANOpure II four-cartridge system (Barnstead/Thermolyne Corporation, Dubuque, IA, USA), and is referred to as distilled–deionized (DI-DI) water.

2.2. SPE Partitioning

Three C₁₈ SPE techniques were compared for their partitioning efficiency of the crude extract. The eluents for the SPE methods in their order of usage are DI-DI water, 20% methanol, 45 or 50% methanol, and 80% methanol. Most taxanes selectively elute in the methanol–water (80:20) fraction (hereafter referred to as the taxane fraction).

Method 1

High-capacity 6-ml C₁₈ disposable extraction columns (7020-07; J.T. Baker, Phillipsburg, NJ, USA) containing 1000 mg of sorbent have been routinely used in our laboratory for clean-up of the crude extract. The cartridge was conditioned with 10 ml ethyl acetate, 10 ml methanol and 10 ml DI-DI water. It is critical that a minimum of 2 mm of water remain above the top frit in the cartridge at the time the crude extract is transferred to the cartridge. After transfer of 0.5 ml of crude extract, the cartridge was eluted with 5

ml DI-DI water, 10 ml 20% methanol, 10 ml 50% methanol and 10 ml 80% methanol.

Method 2

Ultra-high-capacity C₁₈ columns have been prepared in our laboratory by packing 4 g of C₁₈ 40 μm sorbent (7025-00, J.T. Baker) into a 6-ml disposable polypropylene filtration column (7121-06, J.T. Baker). The sorbent bed is fitted with 20-μm polyethylene frits at the top and bottom. Conditioning was accomplished with 40 ml ethyl acetate, 40 ml methanol and 40 ml DI-DI water. Once again a sufficient layer of DI-DI water must remain above the top frit at the time of addition of < 4.0 ml of crude extract to the cartridge. The cartridge is then eluted with 20 ml DI-DI water, 40 ml 20% methanol, 40 ml 50% methanol and 40 ml 80% methanol.

Method 3

Empore (3M Corp., St. Paul, MN, USA) extraction disks, 47 mm size (7460-06, J.T. Baker) are used in conjunction with a Millipore all-glass filtration apparatus (XX15 047 00; Millipore, Bedford, MA, USA). To avoid clogging the Empore disk with particulate matter from the crude extract, a 47-mm polypropylene separator with 10-μm pore size (61757; Gelman Sciences, Ann Arbor, MI, USA) is placed on top of the Empore disk before the top reservoir is clamped in place. Conditioning is accomplished with 15 ml ethyl acetate, 15 ml methanol and 15 ml DI-DI water under gentle vacuum. Under very gentle vacuum (e.g., 1–2 mmHg; 1 mmHg = 133.322 Pa) 10 ml DI-DI water are added to the reservoir followed immediately by 7 ml of crude extract. Partitioning was accomplished under gentle vacuum with 15 ml DI-DI water, 15 ml 20% methanol, 15 ml 45% methanol and 20 ml 80% methanol.

2.3. HPLC Analysis

The taxane fraction was well shaken and filtered through a 2-μm external filter tip (FT

4004; Centaur West, Sparks, NV, USA) into an automatic liquid sampler vial. The HPLC system consists of a Perkin-Elmer (Norwalk, CT, USA) binary LC250 pump, fitted with a ISS-100 auto-sampler and LC235 dual-channel photodiode array detector. The peaks recorded at 230 nm are used for quantitation; the LC trace at 280 nm is also recorded. Separation is achieved on a MetaChem (Torrance, CA, USA) 250 × 4.6 mm, 5 μm Taxsil analytical column (0335-250 × 046) preceded by a Taxsil guard cartridge (0335-CS). The column oven is maintained at 32°C, the flow-rate at 1 ml/min, reservoir A contains 100% acetonitrile (Omnisolv; EM Science, Gibbstown, NJ, USA), and reservoir B contains water–methanol (70:30) (Omnisolv, EM Science). The injection volume is 10 μl and the following linear gradient elution program is used (program A):

0 to 15 min: isocratic at 41% A
 15 to 20 min: ramped to 65% A
 20 to 30 min: isocratic at 65% A
 30 to 35 min: ramped to 41% A
 35 to 40 min: isocratic at 41% A

Alternatively, paclitaxel can be resolved from 7-*epi*-10-deacetyltaxol on the MetaChem Taxsil analytical column if the following parameters are employed: 100% acetonitrile, in reservoir A, water–methanol (90:10) in reservoir B; and the following linear gradient elution program (program B):

0 to 15 min: isocratic at 43% A
 15 to 20 min: ramped to 65% A
 20 to 30 min: isocratic at 65% A
 30 to 35 min: ramped to 43% A
 35 to 40 min: isocratic at 43% A

Stock standard solutions in methanol (Omnisolv, EM Science) are prepared from authentic compounds received from the National Cancer Institute. Quantitation is by external standard using software on the PE Nelson 1020 personal integrator with 10-μl injections of either two or three standard solutions plus the origin. Day-to-day variation of the response factors for the three taxanes, paclitaxel, cephalomannine, and baccatin III, is typically <10% and the correlation coefficient for the calibration curves is typically >0.995.

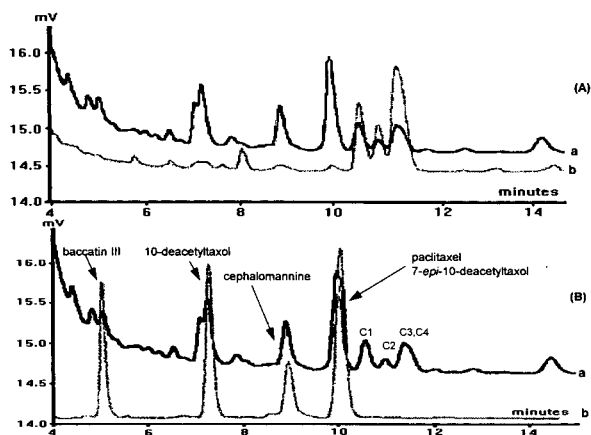


Fig. 2. LC traces using program A of (A) taxane fraction recorded at 230 nm (a) and 280 nm (b) and (B) taxane fraction (a) vs. 5-taxane standard (b) at the following concentrations: baccatin III, 16.06 ng/μl; 10-deacetyltaxol, 24.99 ng/μl; cephalomannine, 14.32 ng/μl; paclitaxel, 15.67 ng/μl; 7-*epi*-10-deacetyltaxol, 23.64 ng/μl. Peaks C₁, C₂, C₃, C₄ are assumed to be cinnamyl taxanes.

3. Results

It is well known that HPLC on C₁₈ analytical columns fails to resolve paclitaxel (with λ_{max} = 230 nm) from cinnamyl taxanes (with λ_{max} = 280 nm) [14–16]. Fig. 2A shows the LC traces of the taxane fraction recorded at both 230 and 280 nm using program A. Fig. 3 shows the UV spectra of relevant peaks in the taxane fraction (peaks B and C) and the authentic paclitaxel standard

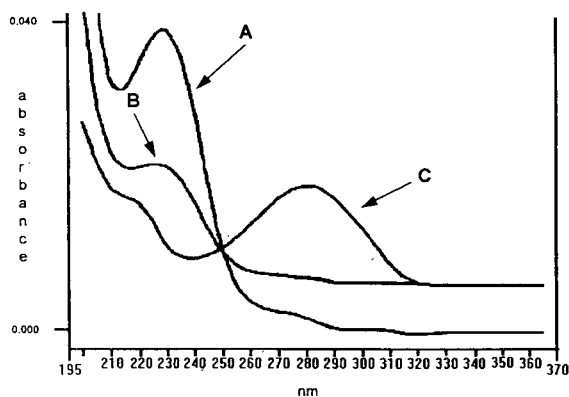


Fig. 3. UV spectra: A = paclitaxel from authentic standard; B = paclitaxel from taxane fraction; C = cinnamyl taxane from taxane fraction.

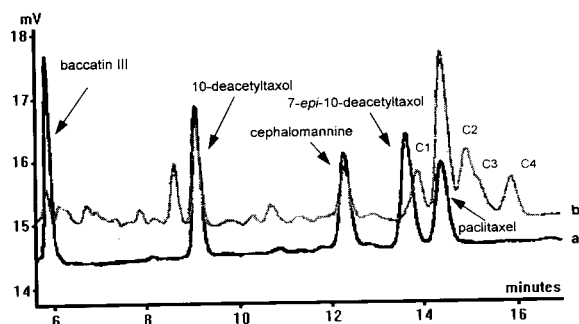


Fig. 4. LC traces using program B recorded at 230 nm of taxane fraction (b) and 5-taxane standard (a).

(peak A). The absence of any significant absorption at 280 nm in the paclitaxel peak in the taxane fraction (Fig. 2A; Fig. 3) confirms that the MetaChem Taxsil column together with program A not only provides rapid analysis times, but also resolves paclitaxel from the cinnamyl derivatives. Under these conditions, however, the retention times of paclitaxel and 7-*epi*-10-deacetyltaxol are equal (Fig. 2B). Fig. 4 shows that changing to the conditions given above in program B resolves these two compounds. Since the use of program B permits us to conclude that the amount of 7-*epi*-10-deacetyltaxol typically found in *Taxus* needles is quite small, our routine quantitation of the taxane fractions by means of program A gives accurate values of paclitaxel and taxane ana-

logues. Program A is the quantitation program of choice since it permits baseline resolution of paclitaxel from the cinnamyl derivatives. Using the procedures above more than 1000 injections have been made on the system with only three changes of the Taxsil guard column.

Table 1 compares relevant parameters for the different SPE techniques. In our earlier studies [12] we showed by means of spiking that recovery of paclitaxel is quantitative on the high-capacity C₁₈ cartridges within the limits given in the table. By using the ultra-high-capacity cartridges prepared in our laboratory, the volume of crude extract which may be partitioned is increased. Once again spiked recoveries and HPLC analysis of all eluates indicate that the less polar taxanes elute quantitatively from these ultra-high-capacity cartridges in the methanol-water (80:20) fraction within the limits given in Table 1, second column. The data in the third column of Table 1 show that the C₁₈ Empore extraction disks significantly increase the volume of crude extract which may be partitioned, while maintaining quantitative recovery of the less polar taxanes.

4. Discussion

Quantitative extraction of the taxanes from *Taxus* needles must obviously be followed by

Table 1
Comparison of parameters for C₁₈ SPE partitioning of crude extract from *Taxus* needles

	High-capacity cartridge	Ultra-high-capacity cartridge	47-mm Disk
Volume crude (ml)	0.5	3.5–3.9	7.0
Volume water (ml)	5	20	15
Volume 20% methanol (ml)	10	40	15
Volume 45% methanol (ml)	0	0	15
Volume 50% methanol (ml)	10	40	0
Volume 80% methanol	10	40	20
Paclitaxel recovery (%) ^a	104.0 ± 4.0 (n = 4)	103.5 ± 13.0 (n = 2)	115.8 ± 5.3 (n = 2)
Paclitaxel recovery (%) ^b			89.5 ± 0.1 (n = 2)
Estimated cost/ml of crude extract (US\$)	5.70	2.80	1.00

^a Authentic paclitaxel spiked directly into crude extract prior to partitioning on SPE.

^b Recovery based on paclitaxel concentration calculated from partitioning on J.T. Baker 7020-07 high-capacity cartridge.

removal of co-extractives without loss of the target compounds. Although liquid–liquid partitioning of the crude *Taxus* extract has been used [14], fractional elution on SPE cartridges has distinct advantages, saving time and reducing solvent usage [17]. Our investigations into the effects of taxanes on non-mammalian cells demanded that we produce large quantities of the taxane fraction efficiently and economically. SPE membrane technology permits us to achieve these goals.

SPE cartridges have been in use since 1978 [18]. In typical environmental applications 1 l of water can be extracted on the reversed-phase high-capacity C_{18} cartridges. When used in our laboratory to partition the crude *Taxus* extract, however, the optimum capacity of the high-capacity C_{18} cartridges for the methanolic crude extract is 0.5 ml. Larger volumes of the crude extract, up to 1 ml, may be partitioned on this cartridge. However, taxane breakthrough is possible close to this upper volume limit. Similarly, the ultra-high-capacity C_{18} cartridges prepared in our laboratories limit the volume of crude partitioned, are expensive, and even with vacuum filtration assist, tend to be slow because of the large amount of flocculate in the crude extract. Although, after adequate washing of the C_{18} sorbent, reloading of the crude extract on both cartridge types may be feasible, the additional time and solvent usage required reduces the practicality of this approach compared with the SPE membrane procedure.

Membrane SPE is a relatively new technique [19] introduced in 1989, which we decided to explore in our attempt to partition larger quantities of the crude *Taxus* extract more rapidly and economically. Some modifications of the cartridge approach were necessary to achieve quantitative recovery of the principal taxanes in the methanol–water (80:20) eluate from the Empore disk. First, a 10- μm pore size polypropylene separator was necessary to prevent the flocculate's clogging the 0.006- μm pores of the Empore disk. Rapid clogging of smaller pore size glass microfilters, e.g. Whatman GMF150 1 μm (1841-047; Whatman LabSales, Hillsboro, OR,

USA) and glass bead filtration aids, e.g. 3M Empore filter aid 400 (Varian 1214-6005 or J.T. Baker 7467-01), by the crude extract rendered these products useless for our application. Although we are able to partition 7 ml of the crude extract on a single 47-mm disk without taxane breakthrough, it is essential that approximately 10 ml of water be maintained in the reservoir during the addition of the crude extract under very gentle vacuum. Furthermore, the 50% methanol eluent, which results in small but measurable breakthrough of the taxanes, must be replaced by a methanol–water (45:55) eluent. Under these conditions HPLC analysis of the loading solution eluate, the water eluate, the methanol–water (20:80) eluate, and the methanol–water (45:55) eluate shows no breakthrough of taxanes with retention times > 6 min, namely, 10-deacetyltaxol, cephalomannine and paclitaxel. The HPLC analyses of these eluates did indicate, however, that small amounts of baccatin III are present, with the major amount in the methanol–water (45:55) or in the methanol–water (80:20) eluates. Finally, recovery of authentic paclitaxel spiked into the crude extract prior to partitioning on the Empore disk was quantitative in the taxane fraction (methanol–water, 80:20).

In summary, as may be seen in Table 1, there are several advantages of the SPE membrane versus cartridge methodology: total solvent volume/ml crude extract processed is reduced by more than 80%; a significant reduction in the cost of processing a given volume of crude, significant reduction in sample processing time, and a consistently high spike recovery are all achieved. Also, the LC traces of the taxane fraction from the cartridge and the Empore disk methods, shown in Fig. 5, are identical. Therefore, qualitatively and quantitatively SPE membrane technology provides the same taxane fraction as does the SPE cartridge.

We anticipate that this approach may be enhanced by stacking the 47-mm disks and/or using the 90-mm disks now available. Together with the three- and six-position filtration manifolds available from several manufacturers, SPE membrane technology will permit us to collect

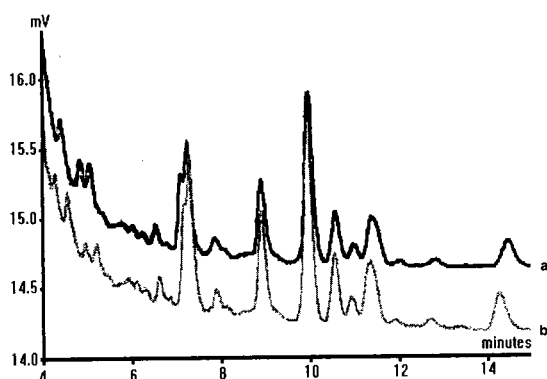


Fig. 5. Overlay of taxane fraction eluted from high-capacity C_{18} cartridge (a) with taxane fraction eluted from 47-mm Empore disk (b).

sufficient amounts of a multi-taxane fraction for examination of its effects on non-mammalian eukaryotic systems.

Acknowledgements

We should like to thank the National Cancer Institute for supplying the taxane standards, and Imperial Nurseries (Granby, CT, USA) and Rhode Island Nurseries (Middletown, RI, USA) for supplying *Taxus* rooted cuttings. We should also like to express our thanks to Chuck Haskins and Susan Price of 3M Corporation for helpful discussions and donations of certain supplies. This research was supported in part by a grant from the Horticultural Research Institute.

References

- [1] D.G.I. Kingston, in A.D. Kinghorn and M.F. Balandrin (Editors), *Human Medicinal Agents from Plants (ACS Symposium Series, No. 534)*, American Chemical Society, Washington, DC, 1993, Ch. 10, p. 138.
- [2] S. Rao, S.B. Horwitz and I. Ringel, *J. Natl. Cancer Inst.*, 84 (1992) 785.
- [3] *American Chemical Society 207th National Meeting, San Diego, CA, 13–17 March, 1994.*
- [4] S.R. Heidmann and P.T. Gallas, *Dev. Biol.*, 80 (1980) 489.
- [5] G. Schatten, H. Schatten, T.H. Bestor and R. Balczon, *J. Cell Biol.*, 94 (1982) 445.
- [6] W. Herth, *Protoplasma*, 115 (1983) 228.
- [7] A.S. Bajer, C. Cypher, J. Mole-Bajer and H.M. Howard, *Proc. Natl. Acad. Sci. U.S.A.*, 79 (1982) 6569.
- [8] H.C. Hoch and R.C. Staples, *Protoplasma*, 124 (1985) 112.
- [9] H. Lataste, V. Senilh, M. Wright, D. Guenard and P. Potier, *Proc. Natl. Acad. Sci. U.S.A.*, 81 (1984) 4090.
- [10] M. Wright, A. Moisan and M.L. Oustrin, *Protoplasma*, 113 (1982) 44.
- [11] D.H. Young, E.L. Michelotti, C.S. Swindell and N.E. Krauss, *Experientia*, 48 (1992) 882.
- [12] M.J.I. Mattina and A. A. Paiva, *J. Environ. Hort.*, 10 (1992) 187.
- [13] W.H. Elmer, M.J.I. Mattina and G.J. MacEachern, *Phytopathology*, 1994, in press.
- [14] T.P. Castor and T.A. Tyler, *J. Liq. Chromatogr.*, 16 (1993) 723.
- [15] R.E.B. Ketchum and D.M. Gibson, *J. Liq. Chromatogr.*, 16 (1993) 2519.
- [16] B. Alvarado-Lindner, M. McGuire, G. Chmurny, J. Paukstelis, J. Roman, J. Klose, B. Hilton, C. Metral and G. Muschik, presented at the *2nd National Cancer Institute Workshop on Taxol and Taxus*, 23–24 September, 1992, poster D-6.
- [17] N. Vidensek, P. Lim, A. Campbell and C. Carlson, *J. Natl. Prod.*, 53 (1990) 1609.
- [18] N. Simpson, *Am. Lab.*, Aug. (1992) 37.
- [19] D.F. Hagen, C. Markell and J. Schmitt, *Anal. Chim. Acta*, 236 (1990) 157.

Liquid chromatography of antihistamines using post-column tris(2,2'-bipyridine) ruthenium(III) chemiluminescence detection

John A. Holeman, Neil D. Danielson*

Department of Chemistry, Miami University, Oxford, OH 45056, USA

First received 24 November 1993; revised manuscript received 8 June 1994

Abstract

The separation and detection of five antihistamine drugs commonly found within over-the-counter allergy and cold pharmaceutical products was performed by HPLC with chemiluminescence (CL) detection. Comparable detection limits at 5–10 pmol were found for the antihistamines by both UV at 214 nm and tris(2,2'-bipyridine) ruthenium(III) CL. However, urine samples were found not to generate as large an unretained peak by CL detection as compared to those peaks by UV detection at 214 and 254 nm. For example, the pheniramine peak representing 0.15 $\mu\text{g/ml}$ was almost totally obscured at 214 nm. Quantitative results received for three antihistamine commercial samples ranged from 4 to 8% error in accuracy when an internal standard was used to compensate for short term detector drift.

1. Introduction

Chemiluminescence (CL) has been applied to a wide variety of compounds and ions as a means of detection for chromatography [1]. Recently, several studies have utilized tris(2,2'-bipyridine) ruthenium(III) $[\text{Ru}(\text{bpy})_3^{3+}]$ as an CL reagent that oxidizes various organic amines. This reagent will in general react best with tertiary, then secondary, and finally primary alkyl amines [2,3]. Studies have utilized this reagent to quantify antibiotic compounds like erythromycin and clindomycin which both have a reactive tertiary amine [4,5]. Recently, diuretic hydrothiazide compounds such as hydrochlorothiazide and hy-

droflumethiazide were found to chemiluminesce even at the 1–2 pmol level [6]. Amino acids were found to vary greatly in reactivity depending upon the R group. In particular, proline [7] and tryptophan [8] which have the more reactive secondary amine substituent can be detected in the pmole range. Detection limits for primary alkyl amino acids can be improved under basic conditions [9,10]. Dansylated amino acids having a tertiary amine group attached to an aromatic ring can be determined after HPLC separation at the 2 pmol level by $\text{Ru}(\text{bpy})_3^{3+}$ CL [11]. Oxidation of $\text{Ru}(\text{bpy})_3^{2+}$ immobilized on a Nafion-coated electrode in a flow cell mounted in front of a photomultiplier tube (PMT) permits reuse of $\text{Ru}(\text{bpy})_3^{3+}$ but analyte detection limits are only in the nmole range [12]. Electrochemical

* Corresponding author.

generation of $\text{Ru}(\text{bpy})_3^{3+}$ in solution on-line at either a Pt [13] or glassy carbon [14] electrode has been demonstrated but the limited concentration of oxidizing agent formed could deleteriously affect detection limits.

Antihistamines are found within a wide variety of over-the-counter cold and allergy medication products. Potential side effects caused by antihistamines when accompanied with alcohol, hypnotic agents, and antianxiety drugs are drowsiness and depression of the central nervous system [15]. Antihistamines are also sometimes used in combination with other drugs to treat adverse side effects. For instance, diphenhydramine is sometimes used to treat acute dystonic symptoms brought about by antipsychotic drugs used to treat patients with Parkinson disease [16].

In this paper, the determination of five antihistamines brompheniramine, chlorpheniramine, pheniramine, diphenhydramine, and pyrilamine (structures shown in Fig. 1) by $\text{Ru}(\text{bpy})_3^{3+}$ CL after HPLC separation is described. The quantitative analysis of three cold medication products and the potential of $\text{Ru}(\text{bpy})_3^{3+}$ CL for the

determination of drugs in urine samples is provided.

2. Experimental

2.1. Equipment

A Waters Model 510 HPLC pump (Milford, MA, USA) was used to transport the sample under chromatographic and flow injection analysis (FIA) modes. The $\text{Ru}(\text{bpy})_3^{2+}$ solution was oxidized to $\text{Ru}(\text{bpy})_3^{3+}$ with a Princeton Applied Research (Princeton, NJ, USA) Model 174A polarographic analyzer using a platinum gauze working electrode, a platinum wire auxiliary electrode, and a silver wire reference electrode. The reagent reservoir was continuously bubbled with helium gas for 30 min before applying a +950-mV potential across the electrodes. A magnetic stir bar was also used during the purging, reagent oxidation, and analysis processes. A Rheodyne Model 7010 injector (Cotati, CA, USA) with a 20- μl loop was used throughout all the studies. The $\text{Ru}(\text{bpy})_3^{3+}$ oxidizing reagent was transported by an Alita peristaltic pump (Medina, WA, USA) that utilized 1.0 mm (0.040 inch) I.D. Tygon pump tubing. The reagent flow stream connection between a diagonally cut PTFE tube (0.5 mm I.D. \times 1.5 mm O.D.) inserted in the Tygon pump tube to the fused-silica capillary utilized a male/male union in which a Kel-F ferrule and graphite ferrule sealed the PTFE and capillary lines, respectively.

A modified Waters 420-AC fluorometer was used to detect the CL reaction within the 8- μl flow cell. A stainless-steel tube (O.D. = 1.6 mm; I.D. = 1.0 mm) leading out of the top of the 8- μl flow cell to a stainless-steel tee was fitted with a fused-silica capillary (I.D. = 317 μm ; O.D. = 427 μm) coaxially with enough excess space available to allow waste to exit between the tubing walls and out through one branch of the tee. Introduction of the $\text{Ru}(\text{bpy})_3^{3+}$ occurred through this capillary that was fixed in position by a PTFE ferrule in the stainless-steel tee. The polyamide coating of the capillary within the quartz flow

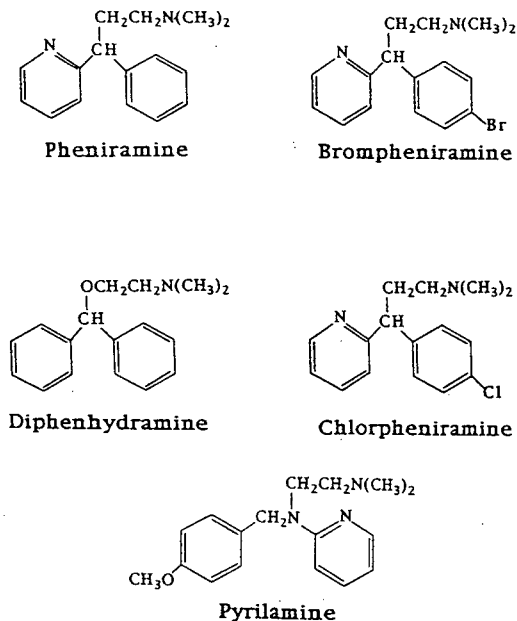


Fig. 1. Structures of five tertiary antihistamines.

cell was removed by burning the capillary tip with a match and wiping away the carbon coating. No modification was made on the inlet portion of the fluorometer. The excitation source of the fluorometer was removed but the position of the flow cell, optics, and PMT remained unchanged. A Hamamatsu PMT Model R928YP2547 with maximum sensitivity in the visible light region was substituted. Characterization of this flow cell design which ensures the CL light signal (about 1 s in duration) occurs in front of the PMT has been carried out previously [5]. The data were collected with a Shimadzu Chromatopac C-R6A integrator (Kyoto, Japan). UV analysis was performed on an Applied Biosystems (Ramsey, NJ, USA) Model 757 variable wavelength absorbance detector.

The chromatographic column used to separate the antihistamines was a 150 × 4.6 mm I.D. Asahipak ODP-50 C₁₈ column purchased from Keystone Scientific (Bellefonte, PA, USA). Flow-rates used for all experiments were 0.80 ml/min and 0.28 ml/min for the chromatographic and reagent streams, respectively. These flow-rates are in the optimum range found previously in another study [5].

2.2. Reagents

A 1 mM tris(2,2'-bipyridine) ruthenium(II) hexachloride solution (salt obtained from Aldrich in Milwaukee, WI, USA) was prepared with either a 0.05 M acetate-buffered supporting electrolyte (pH 5.5) or 0.05 M sodium sulfate. Although a 2 mM Ru(bpy)₃³⁺ solution when oxidized provided a somewhat greater CL signal, the 1 mM solution was used to conserve reagent.

Buffer solutions were prepared at concentrations of 0.2 M at pH values of 5.5, 7.0, 8.0, 9.0, and 10.0. A phosphate salt along with the borate salt was required for buffers pH 9.0 and 10.0 to maintain a consistent molarity to other buffers. An acetate salt was used for pH 5.5 and a phosphate salt for 7.0 and 8.0 buffers. The acetonitrile was supplied from Burdick and Jackson, (Muskegon, MI, USA). The antihistamines brompheniramine, chlorpheniramine, diphenhydramine, pheniramine, and pyrilamine were pur-

chased through Sigma (St. Louis, MO, USA). In-house water was purified with a Barnstead E-Pure system (Dubuque, IA, USA).

Pharmaceutical samples Benadryl (diphenhydramine), Chlor-Trimeton (chlorpheniramine) tablets, and Dimetapp (brompheniramine) grape flavor cough syrup were analyzed. The antihistamine tablets were prepared by crushing and grinding the tablet contents within a polystyrene weighing dish. The crushed contents were transferred into a volumetric flask with 100 ml of water along with 30–40 ml of acetonitrile to assist in dissolving the antihistamines. These solutions were diluted to 250 or 500 ml with water. A 10- to 20-ml portion of each of these tablet solutions was then centrifuged to remove any undissolved solids. A known quantity of the centrifuge supernatant was quantitatively diluted to a calculated concentration determined by the manufacturer's cited active ingredient amount. All standards and samples were spiked with N,N-dimethylbenzylamine as an internal standard.

3. Results and discussion

The optimum CL pH values for all five antihistamines were determined by FIA methodology. A comparison of the change in chemiluminescence intensity with pH is shown in Fig. 2. Pheniramine, chlorpheniramine, and brompheniramine are found to be the most reactive at pH 9.0. This alkaline pH optimum agrees with previous work involving amino acids [9] and supports the general trend of greater reactivity for compounds having unprotonated amine functional groups. The like reactivity of pheniramine, chlorpheniramine, and brompheniramine is reasonable since all three have similar structures. The tertiary nitrogen not the pyridine nitrogen is reasonable for the CL reaction. The diphenhydramine reactivity loss may be due to the ether functional group within the alkyl chain between the tertiary amine and aromatic rings. A similar trend involving polar side chains has been proposed to explain the different Ru(bpy)₃³⁺ CL responses for amino acids [10]. Pyrilamine is less

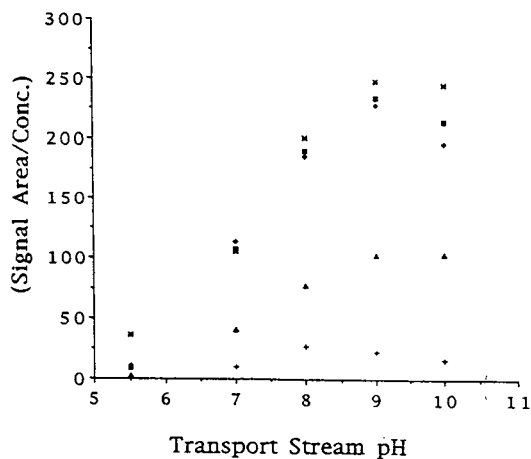


Fig. 2. CL response vs. pH for five antihistamines. Sample concentrations (M): (□) chlorpheniramine $6.3 \cdot 10^{-6}$, (◇) brompheniramine $4.4 \cdot 10^{-6}$, (▲) diphenhydramine $5.9 \cdot 10^{-6}$, (×) pheniramine $3.9 \cdot 10^{-6}$, (+) pyrilamine $4.3 \cdot 10^{-6}$.

reactive when compared to the other four antihistamines (about a factor of 4 and 9 less compared to diphenhydramine and pheniramine, respectively). A CL reactivity study was done on two model compounds, 2-dimethylaminopyridine and 2-benzylaminopyridine. The latter compound was ten times less reactive than pyrilamine indicating the benzyl group may be quenching. However this compound is a secondary amine and is expected to generate a weaker CL signal. 2-Dimethylaminopyridine was found to be seven times more reactive than pyrilamine even though pyrilamine has 2 tertiary nitrogens and this model compound has only one. This lends support back to the idea that this electron withdrawing benzyl group is probably quenching the pyrilamine CL signal. We also know that nitro groups can quench the CL signal since N,N-dimethylaniline can be detected at the 5 pmol level at pH 3 but N,N-dimethyl-3-nitroaniline does not react.

3.1. Chromatography

Reversed-phase separation of these antihistamines using a polymeric C_{18} column under basic and neutral conditions requires a moderate quantity of an organic solvent. Previous studies showed acetonitrile caused less quenching of the

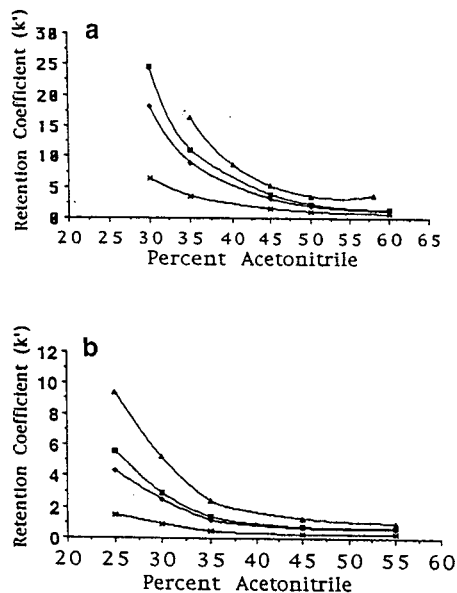


Fig. 3. Retention factor curves for changes in % acetonitrile for four antihistamines at (a) pH 9.0 and (b) pH 7.0. □ = Brompheniramine, ◇ = chlorpheniramine, ▲ = diphenhydramine and × = pheniramine.

$Ru(bpy)_3^{3+}$ CL reaction as compared to methanol [5]. Fig. 3 shows the retention factors of four antihistamines under neutral and basic conditions as a function of percent acetonitrile. Under neutral pH conditions the antihistamines become more protonated and k' values are about a factor of 7 less. The optimum acetonitrile–water ratios when separating these four antihistamines were 47:53 at pH 9.0 and 35:65 at pH 7.0. A fifth compound pyrilamine is retained similarly to brompheniramine but all five drugs can be separated upon reduction of the acetonitrile content in the mobile phase under neutral pH conditions (Fig. 4).

3.2. Detection limits

Good detection limits have been cited for these antihistamines. Detection limits for chlorpheniramine of about 0.5 pmol within 1-ml samples of plasma or saliva after extraction with diethylether and preconcentration were reported at a 254 nm wavelength [17]. Optimum UV wavelength conditions have been reported for

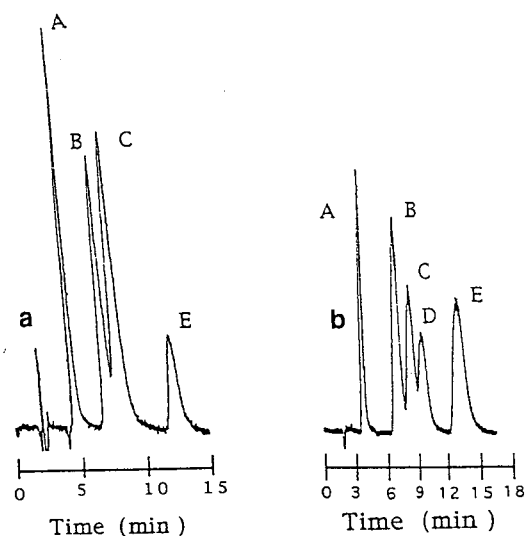


Fig. 4. Chromatograms for the separation of (a) four and (b) five antihistamines. (a) Acetonitrile–0.05 M borate buffer, pH 9.0 (47:53). (b) Acetonitrile–0.2 M phosphate buffer, pH 7.0 (27:73). A = Pheniramine, B = chlorpheniramine, C = brompheniramine, D = pyrilamine, E = diphenhydramine.

brompheniramine and pheniramine at 254 nm, and 214 nm for diphenhydramine, but no detection limits were provided [18]. A fluorometric method involving the derivatization of chlorpheniramine with benzyl chloroformate was able to determine 0.1 ng/ml within whole blood samples [19]. Although this derivatization procedure is general for tertiary amines, it only works with dry sample residues.

A detection limit comparison at pH 9 was made between the CL detector and the UV detector (Table 1). Comparable results (5–10 pmol) are achieved for the CL detector and the UV detector at 214 nm for pheniramine and

brompheniramine. Chlorpheniramine and diphenhydramine can be detected somewhat better at 214 nm than by CL. However, the CL response shows a 2–3 times improvement in detection limits for brompheniramine, chlorpheniramine, and pheniramine when compared to UV at 254 nm. Diphenhydramine at 254 nm exhibits a dramatic fall off in detectability by one order of magnitude compared to the CL detector. The pyrilamine CL detection limit is about one order of magnitude less responsive than that of the other antihistamines. The antihistamine CL detection limits shown in Table 1 are slightly better than the values reported for dipropylamine (16 pmol) but not as low as that for tripropylamine (0.2 pmol). This tends to indicate that tertiary amines with large bulky aromatic functional groups (brompheniramine, chlorpheniramine, and pheniramine) react similarly to secondary amines. Using a 100- μ l injection loop, concentration CL detection limits can be reduced to 0.01–0.03 μ g/ml for all four compounds in Table 1.

3.3. Quantitative analysis

To alleviate CL detector drift observed after 2–3 h, internal standards were chosen for their strong reactivity to the oxidizing reagent and ability to be separated from most of the antihistamines. One internal standard (N,N-dimethylbenzylamine) was added to the standards and samples of diphenhydramine, chlorpheniramine, and brompheniramine to compensate for the CL drift. *tert*-Butylbenzylamine could be used as an alternative internal standard for pheniramine although it happens to coelute near

Table 1
Detection limit comparison between UV detector and a chemiluminescence detector

Detector	Pheniramine	Brompheniramine	Chlorpheniramine	Diphenhydramine
Chemiluminescence	0.09 μ g/ml (8 pmol)	0.14 μ g/ml (9 pmol)	0.14 μ g/ml (10 pmol)	0.21 μ g/ml (16 pmol)
UV 214 nm	0.07 μ g/ml (6 pmol)	0.13 μ g/ml (8 pmol)	0.07 μ g/ml (5 pmol)	0.10 μ g/ml (8 pmol)
UV 254 nm	0.20 μ g/ml (17 pmol)	0.41 μ g/ml (26 pmol)	0.29 μ g/ml (21 pmol)	2.4 μ g/ml (290 pmol)

Table 2
Linear least square regression data

Compound	$Y = A + BX$	Correlation coefficients (No. data points)	Linear range studied ($\mu\text{g/ml}$)
Brompheniramine	$A = 1.1 \cdot 10^{-1} \pm 3.2 \cdot 10^{-2}$ $B = 2.7 \cdot 10^{-1} \pm 2.9 \cdot 10^{-2}$	0.999 (12)	0.5-22
Chlorpheniramine	$A = 1.4 \cdot 10^{-1} \pm 5.6 \cdot 10^{-2}$ $B = 3.0 \cdot 10^{-1} \pm 6.7 \cdot 10^{-3}$	0.997 (15)	0.3-15
Diphenhydramine	$A = 2.5 \cdot 10^{-2} \pm 3.2 \cdot 10^{-2}$ $B = 1.8 \cdot 10^{-1} \pm 7.6 \cdot 10^{-3}$	0.993 (10)	0.5-7.5

Y = Peak area sample/peak area internal standard. X = $\mu\text{g/ml}$.

chlorpheniramine and brompheniramine. Linear least squares regression analysis data are provided in Table 2. Reproducibility of duplicate or triplicate data points is about 2-10% R.S.D. With the internal standard, percent errors from the label values of 5-6% for diphenhydramine and 4-8% for chlorpheniramine and brompheniramine in three pharmaceutical products are calculated.

3.4. Matrix effects

Chromatograms of the three pharmaceutical samples with detection at 214 nm and CL were compared. Only single peaks due to diphenhydramine are observed in the Benadryl chromatograms regardless of detection method. An unretained peak which did not interfere with the chlorpheniramine peak is noted for both Chlor-Trimeton chromatograms. The Dimetapp sample matrix did cause some interference for the brompheniramine analyte as indicated by the shoulder peak (Fig. 5A). Several other unknown components are observed within the Dimetapp chromatogram. When this chromatogram is compared to the Dimetapp CL chromatogram in Fig. 5B, no interferences can be seen for brompheniramine.

We also compared chromatographic results between an UV detector and CL detector for three antihistamine-spiked urine samples. The urine matrix generated a large unretained absorbance response for UV wavelengths at both 214 and 254 nm that did not come down to

baseline until about 12 min. The unretained signal caused by this urine sample was smaller for the CL detector coming down to baseline in about 5 min. It could be attributed possibly to amino acids found in urine [20] such as histidine and tryptophan which have secondary amine groups as well as other amines that give strong signals at alkaline pH. Both urea and uric acid did not react with $\text{Ru}(\text{bpy})_3^{3+}$ to generate CL. Previously we have reported that carbonyl groups next to the nitrogen atom are electron withdrawing preventing facile oxidation of the analyte to a radical by $\text{Ru}(\text{bpy})_3^{3+}$ [7]. At 254 and 214 nm, the unretained urine components

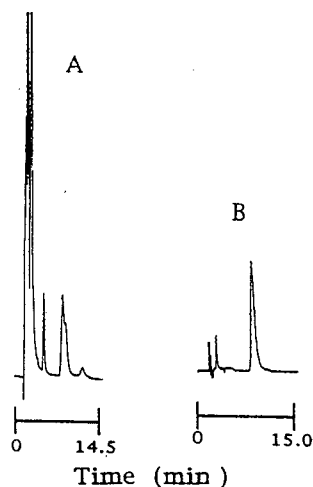


Fig. 5. Dimetapp (4.0 $\mu\text{g/ml}$ brompheniramine 8.4 min) sample chromatograms with detection at (A) 214 nm and (B) CL. Mobile phase: acetonitrile-0.01 M borate buffer, pH = 9.0 (47:53). The peak at 5.1 min in chromatogram A is the internal standard, N,N-dimethylbenzylamine.

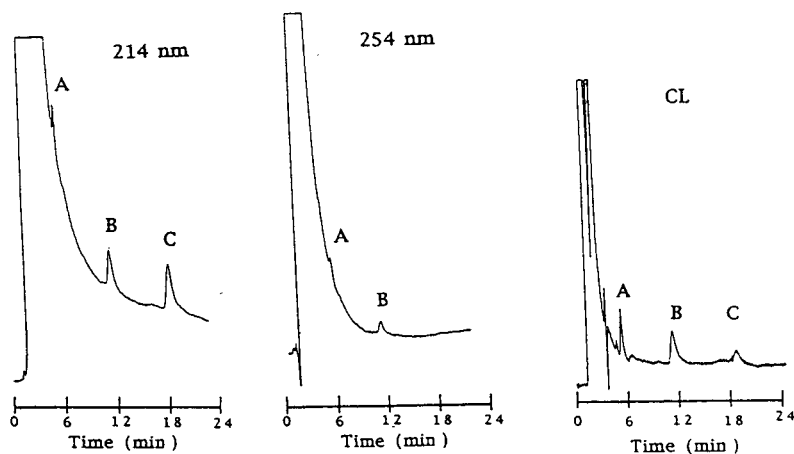


Fig. 6. Chromatograms of an undiluted urine sample spiked with 0.15 $\mu\text{g/ml}$ pheniramine (A), 0.26 $\mu\text{g/ml}$ brompheniramine (B), and 0.29 $\mu\text{g/ml}$ diphenhydramine (C) taken with UV (214 nm), UV (254 nm), and CL detection. Mobile phase: acetonitrile–0.025 M borate buffer, pH 9.0 (40:60). Flow-rate: 0.8 ml/min. Injection size: 100 μl .

such as uric acid greatly interfere with the determination of 1.1 $\mu\text{g/ml}$ of pheniramine which shows up as a shoulder peak (data not shown). Baseline resolution of pheniramine from the urine matrix peak is possible using the CL detector. This UV urine matrix problem is still evident for 5 $\mu\text{g/ml}$ brompheniramine which elutes off later than the pheniramine analyte (data not shown). Fig. 6 shows a comparison of UV 214 nm, UV 254 nm, and CL chromatograms for a urine sample spiked at low levels (0.1–0.3 $\mu\text{g/ml}$) of pheniramine, brompheniramine, and diphenhydramine. These concentrations are more typical of those found in urine for these antihistamines. No sample preconcentration using a column or extraction was done. For the chromatograms detected at 214 and 254 nm, pheniramine is almost completely obscured by the urine matrix. Diphenhydramine cannot be detected at this level at 254 nm. Complete resolution and detection of all three drugs on a non-sloping baseline was possible using the CL detector.

Acknowledgement

Financial support through a NIH AREA grant is gratefully appreciated.

References

- [1] T.A. Nieman, in J.W. Birks (Editor), *Chemiluminescence and Photochemical Reaction Detection in Chromatography*, VCH, New York, 1989, Ch. 4.
- [2] J.B. Noffsinger and N.D. Danielson, *Anal. Chem.*, 59 (1987) 865.
- [3] J.B. Noffsinger and N.D. Danielson, *J. Chromatogr.*, 387 (1987) 520.
- [4] N.D. Danielson, L. He, J.B. Noffsinger and L. Trelli, *J. Pharm. Biomed. Anal.*, 7 (1989) 1281.
- [5] M.A. Targove and N.D. Danielson, *J. Chromatogr. Sci.*, 28 (1990) 505.
- [6] J.A. Holeman and N.D. Danielson, *Anal. Chim. Acta*, 277 (1993) 55–60.
- [7] L. He, K.A. Cox and N.D. Danielson, *Anal. Lett.*, 23 (1990) 195.
- [8] K. Uchikura and M. Kirisawa, *Chem Lett.*, (1991) 1373.
- [9] S.N. Brune and D.R. Bobbitt, *Talanta*, 38 (1991) 419.
- [10] S.N. Brune and D.R. Bobbitt, *Anal. Chem.*, 64 (1992) 166.
- [11] W.-Y. Lee and T.A. Nieman, *Anal. Chem.*, 64 (1994) 111.
- [12] T.M. Downey and T.A. Nieman, *Anal. Chem.*, 64 (1992) 261.
- [13] K. Uchikura and M. Kirisawa, *Anal. Sci.*, 7 (1991) 803.
- [14] W.A. Jackson and D.R. Bobbitt, *Anal. Chim. Acta*, 285 (1994) 309.
- [15] T.H. Wiser, T.D. Guberski and M.B. Wiener, in M.B. Wiener (Editor), *Clinical Pharmacology and Therapeutics in Nursing*, McGraw-Hill, New York, 1979, Ch. 21.
- [16] D.T. Witiak, in A. Burger (Editor), *Medicinal Chemistry, Part II*, Wiley-Interscience, New York, 3rd Ed., 1970, Ch. 65.

- [17] N.K. Athanikar, G.W. Peng, R.L. Nation, S.M. Huang and W.L. Chiou, *J. Chromatogr.*, 162 (1979) 367–376.
- [18] A.S. Sidhu, J.M. Kennedy and S. Deeble, *J. Chromatogr.*, 391 (1987) 233–242.
- [19] Y. Miyamoto, *J. Chromatogr.*, 420 (1987) 63–72.
- [20] H.C Damm and J.W. King (Editors), *Handbook of Clinical Laboratory Data*, CRC, Cleveland, OH, 1965, p. 49.

Characterisation of electron beam generated transformation products of Irganox 1010 by particle beam liquid chromatography–mass spectrometry with on-line diode array detection

David W. Allen*, Malcolm R. Clench, Andrew Crowson, David A. Leathard,
Robert Saklatvala

Division of Chemistry, Sheffield Hallam University, Pond Street, Sheffield S1 1WB, UK

First received 20 August 1993; revised manuscript received 13 June 1994

Abstract

Transformation products of Irganox 1010 [pentaerythritol tetrakis-3-(3,5-di-*tert.*-butyl-4-hydroxyphenyl) propionate], in food contact polymers subjected to electron beam irradiation have been analysed by particle beam LC–MS with on-line UV diode array detection. It has been shown that the principal transformation products arise via loss of sub-units of the parent molecule, and the subsequent transformation of these sub-units. A total of 56 transformation products has been detected, for some of which structures are proposed. These results are compared to previous work on Irganox 1330 [1,3,5-trimethyl-2,4,6-tris(3',5'-di-*tert.*-butyl-4-hydroxybenzyl)benzene], where transformations to yield *p*-quinone methide type structures were shown to occur.

1. Introduction

In previous papers we have reported on the effects of both gamma and electron beam irradiation in air on various hindered phenol and related arylphosphite antioxidants present in food contact polyolefins [1–4]. The overall trend observed has been that as the exposure to radiation increases, so the amount of antioxidant remaining decreases. This decrease in available antioxidant has been attributed to its transformation to other products via reactions with peroxy and other radicals present in the oxidising polymer.

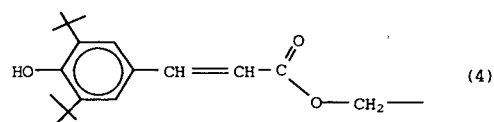
Our recent work has concentrated on the

characterisation of solvent extractable transformation products from hindered phenol and related antioxidants in polypropylene subjected to ionising radiation [5,6]. Initial studies on Irganox 1076 [octadecyl-3(3,5-di-*tert.*-butyl-4-hydroxyphenyl) propionate], Irganox 1010 [pentaerythritol tetrakis-3-(3,5-di-*tert.*-butyl-4-hydroxyphenyl) propionate] and Irganox 1330 [1,3,5-trimethyl-2,4,6-tris(3,5-di-*tert.*-butyl-4-hydroxybenzyl)benzene] were reported [5]. We employed particle beam liquid chromatography–mass spectrometry (PB-LC–MS) [7] in conjunction with data obtained using high-performance liquid chromatography (HPLC) with diode array detection (DAD) in an off-line mode to characterise the transformation products. We noted that the data obtained in our early experiments with PB-

* Corresponding author.

LC–MS in an isocratic mode were not adequate to enable characterisation of all transformation products observed [5].

A second paper reporting more detailed work on the transformation products of Irganox 1330 has been published [6]. We showed that the principal transformation products of Irganox 1330 (structure 1) under irradiation conditions arise via oxidation processes to yield quinone methide type structures and also via side chain losses arising from cleavage of *tert.*-butyl groups. Irganox 1010 (structure 2) has the potential to undergo similar transformation processes under irradiation conditions to yield one or more sub-units of structure 2 transformed into a quinone methide structure i.e., structure 3. However Irganox 1010 might also be expected to yield transformation products containing a cinnamate type sub-unit (structure 4). Transformation products containing the same number of quinone methide or cinnamate sub-units will show the same relative molecular mass (M_r). Of these isomeric structures, the cinnamate form is likely to be preferred on the grounds of aromaticity and extended conjugation.



Since these sub-units may be present in any combination the following possibilities exist where in these structures (2s) refers to one sub-unit of structure 2: $(2s)_3-C-(3)$, $(2s)_3-C-(4)$, $(2s)_2-C-(3)_2$, $(2s)_2-C-(4)_2$ etc.

We have also observed that in our previous work losses of the above sub-units from the parent antioxidant occur to yield transformation products with a variety of new substituents. In particular, cleavage of one or more of the above sub-units with the formation of alcohol or aldehyde functional group residues on what remains of the parent molecule is possible, as well as reductive cleavage to leave methyl groups [5,6].

A further class of transformation products expected would be related to the above compounds but exhibit losses of *tert.*-butyl groups.

In anticipation of such a complex mixture of transformation products it was decided to use gradient elution PB-LC–MS with the UV-DAD detector connected on line, and in this paper we report evidence for the structures of the major solvent extractable transformation products of Irganox 1010 obtained using this approach.

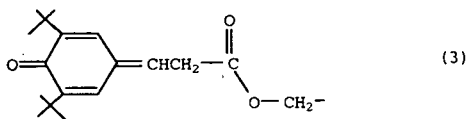
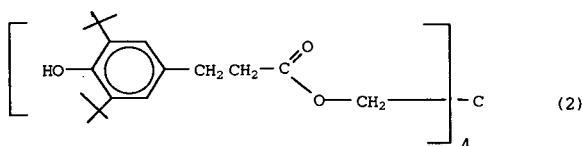
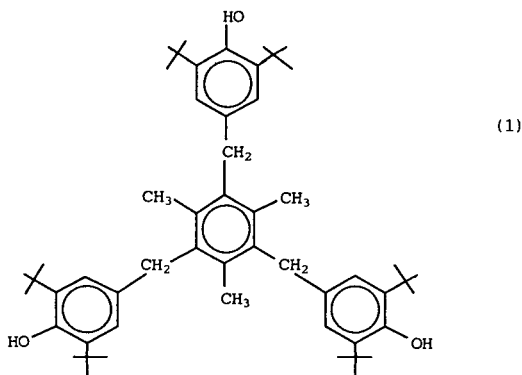
2. Experimental

2.1. Irradiation

Samples of polypropylene homopolymer stabilised with Irganox 1010 (0.25%, w/w) were prepared by sintering to produce small pellets which were then subjected to irradiation from a 4.5-MeV Dynamitron Continuous Electron Beam facility (50 kGy).

2.2. Extraction

The irradiated stabilised polypropylene (0.5 g) was heated under reflux in chloroform (10 ml) for 4.5 h to extract the transformation products. The extract was then microfiltered using a 0.45 mm pore size nylon 66 membrane filter and



1.0-cm Whatman GF/D pre-filter. The resulting extract was evaporated almost to dryness under oxygen-free nitrogen in a screw cap vial. Ethyl acetate (3 ml) was then added to the extract to precipitate oligomers. After re-microfiltration the extract was evaporated down to 0.5 ml prior to HPLC analysis.

2.3. High-performance liquid chromatography

The HPLC instrumentation comprised a Gilson binary gradient system for solvent programming and a Philips PU4021 multichannel UV–vis detector. The resulting data were processed using a Dell 210 microcomputer equipped with the Philips analytical PU 6003 Diode Array Detector system (3.0). The column employed was a 10 cm × 4.6 mm Spherisorb ODS2 analytical column fitted with a 5 cm × 4.6 mm Spherisorb ODS2 guard column.

Gradient elution was employed using the following mobile phases: (A) methanol–water (10:90, v/v); (B) ethyl acetate–methanol (57:43, v/v). Flow-rate: 0.7 ml/min. Solvent programme comprised initial 65% B for 15 min, linear gradient 65–90% B in 30 min, 90% B for 15 min and a step to 100% B which was held for 15 min. The diode array detector was set to acquire 1 spectrum/s over the range 250–390 nm.

2.4. Particle beam liquid chromatography–mass spectrometry

The HPLC system described above was connected in series with a VG Masslab (Manchester, UK) Trio 1 quadrupole mass spectrometer equipped with a VG LINC–particle beam LC–MS interface. Data were acquired in the full scan mode at 3 s/scan over the mass range 50–950 daltons under electron impact (70 eV) ionisation. All data were processed using a VG Lab Base data system.

3. Results and discussion

Our simultaneous UV–MS experiment provided three pieces of evidence for each peak: (i) the relative retention behaviour in the reversed-

phase separation, (ii) the nature of the UV spectrum, and (iii) the mass spectrum. In total we were able to detect 56 different components, on the basis of UV and/or mass spectral information (complete spectra or extracted ion chromatograms). Most of these components were present at such low concentrations, however, that it was not possible to obtain satisfactory spectra using our on-line technique. In order to identify such peaks it would be necessary to undertake significant preconcentration or to use preparative chromatography. On the basis of spectral and chromatographic information we are able to propose identities for 9 of the 56 transformation products. We have synthesised three of our proposed compounds, and obtained an authentic sample of a fourth, and shown that in each case the mass spectra are very similar to those of the transformation products.

Inspection of the complete diode array data set showed that all the major peaks absorb significantly at 275 nm. The 275 nm chromatogram Fig. 1 shows twelve peaks I to XII with absorbances above 0.05 eluting before Irganox 1010 (peak XIII). On the basis of their retention behaviour the twelve transformation products giving rise to these peaks fall into three groups: (a) peaks I to III, (b) peaks IV to VIII, and (c) peaks IX to XII.

Group (a), peaks I, II and III, elute in the initial 15-min isocratic region [65% B, i.e. methanol–ethyl acetate–water (31:37:32)]. Given the reversed-phase nature of the separation these three transformation products are therefore expected to have much the most polar structures and/or lowest relative molecular masses (M_r).

Group (b), peaks IV to VIII, elute during the gradient portion of the chromatogram with retention times between 15 and 45 min, and are expected to be of steadily decreasing polarity and/or increasing M_r .

Group (c), peaks IX to XII, with retention times between 45 and 60 min, are expected to be of significantly lower polarity and/or higher M_r , since they elute during the second isocratic portion of the run [90% B, i.e. methanol–ethyl acetate–water (40:51:9)] as does Irganox 1010 itself (peak XIII).

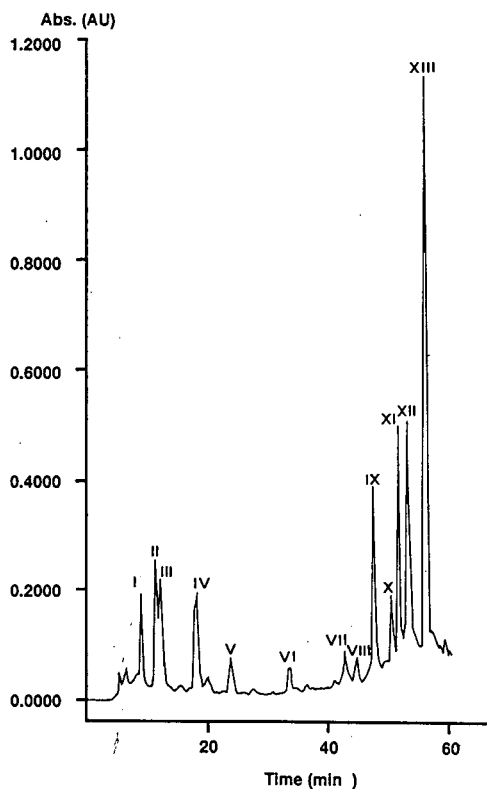


Fig. 1. UV absorption chromatogram (275 nm) of extract of irradiated polypropylene homopolymer originally stabilised with Irganox 1010.

The raw total ion chromatogram is shown in Fig. 2 scaled to 100% for the Irganox 1010 peak XIII. Peaks appear with retention times approximately 0.5 min longer than in the UV chromatogram, reflecting the fact that the diode array detector and mass spectrometer were connected in series. Although there is some deterioration in

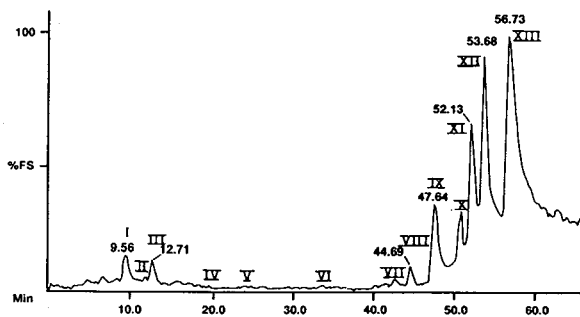
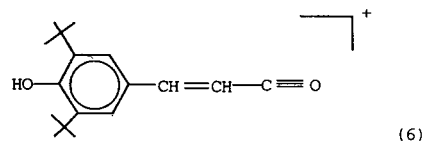
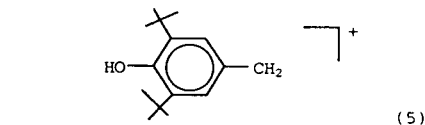


Fig. 2. Total ion chromatogram of same polypropylene extract as in Fig. 1. FS = full scale.

peak shape, the loss of chromatographic resolution compared with the UV trace is not too severe.

Peaks I and III in group (a) are clearly visible in the total ion chromatogram, but in group (b), for the gradient elution part of the run, the only obvious peak is peak VIII. All five of the peaks IX to XIII show clearly in group (c). The fact that only eight of the thirteen peaks seen in the UV chromatogram appear clearly in the total ion chromatogram is not unexpected, since without calibration neither UV absorbance nor LC-MS ion intensity give a good indication of the amount of material present. It was possible to locate peaks II, V, VI and VII using the mass spectrometer data system, but no mass spectral peak could be found for peak IV. Although peak X shows up reasonably strongly on the raw total ion chromatogram, it was not possible to obtain an interpretable mass spectrum for this component.

Fig. 3 shows the UV and mass spectra for the Irganox 1010 peak (peak XIII). The major UV absorption band in the range 260–300 nm (λ_{\max} 285 nm) is characteristic of phenolic compounds, and similar bands are found in most of the transformation products. The upper mass range of the spectrometer precludes detection of a molecular ion for Irganox 1010 (M_r 1178). The base peak at m/z 219 is attributed to the fragment ion with structure 5 formed by cleavage of the carbon-carbon bond β to the aromatic ring. Significantly this m/z 219 peak is found in many of the transformation products. Similarly, the ion at m/z 259 (tentative structure 6) which gives the second most abundant peak in the mass spectrum of Irganox 1010, is also found in the high M_r transformation products giving rise to peaks IX and XI.



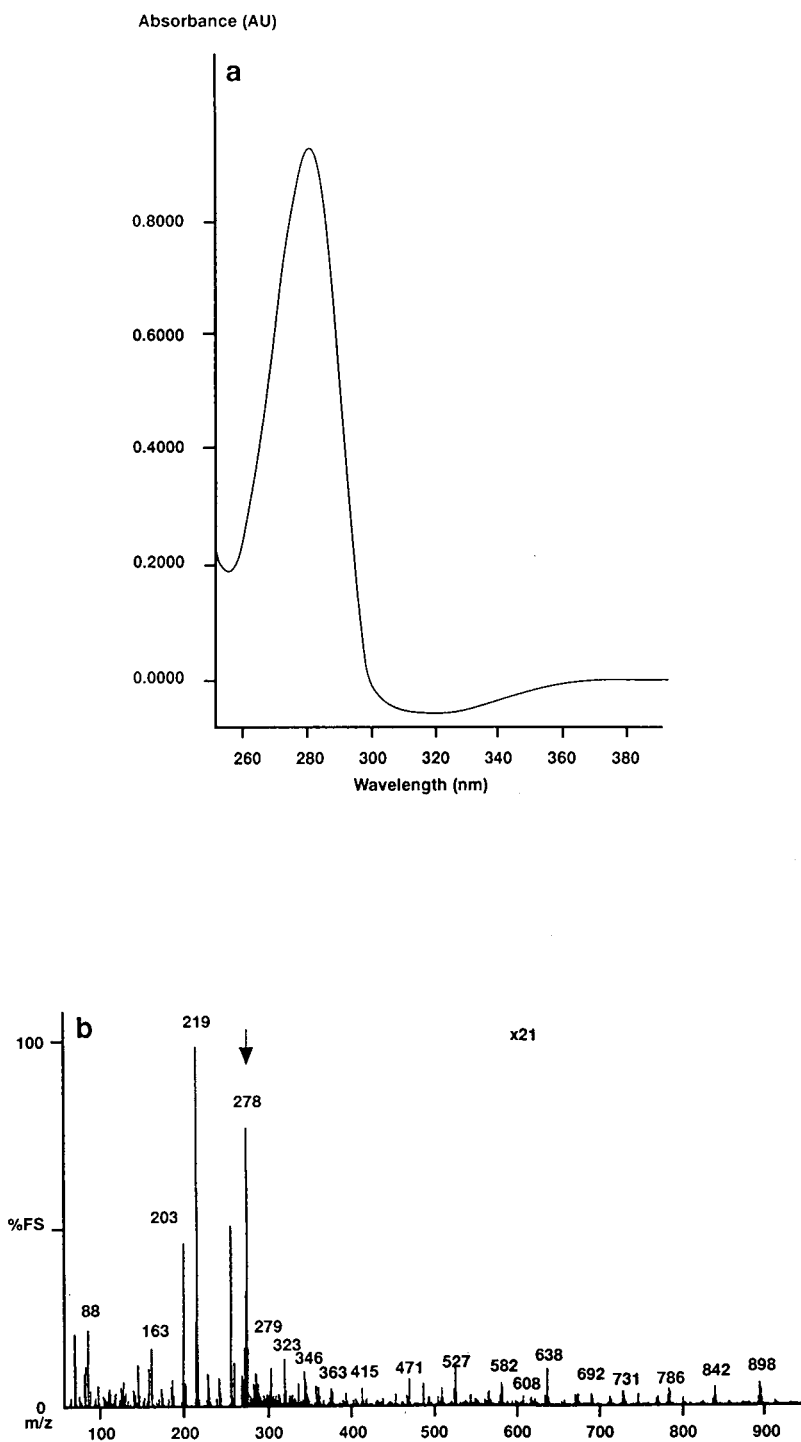
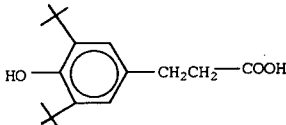
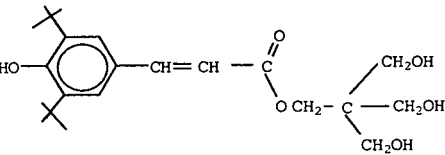
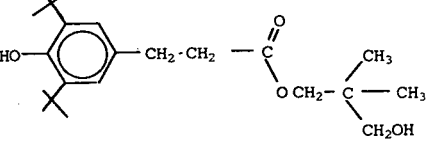
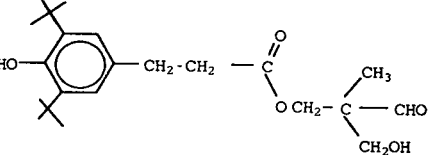
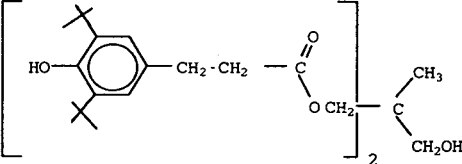
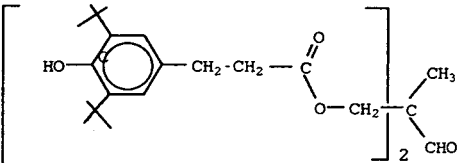
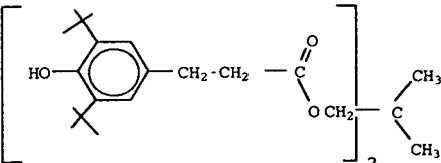
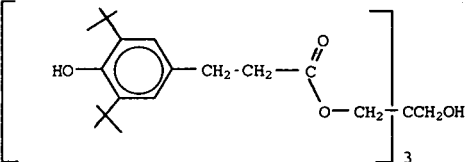
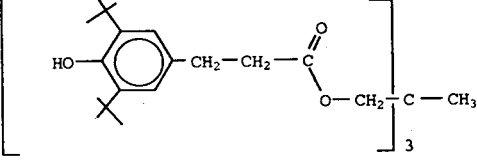


Fig. 3. (a) Diode array UV spectrum of peak XIII (Irganox 1010) for chromatogram of Fig. 1. (b) Mass spectrum of peak XIII (Irganox 1010) for chromatogram of Fig. 2.

Table 1
Proposed structures for major transformation products of Irganox 1010 after 50 kGy electron beam irradiation

Chromatographic peak number	M_r (u)	Proposed structure
I ^a	278	
II	394	
III ^a	364	
V	378	
tentative structure (see text)		
VI	640	
VII	638	
VIII ^a	624	
IX	916	
XI ^a	900	
XII	> 1000	Simple cleavage of <i>tert.</i> -butyl groups

^a Identity confirmed by synthesis or comparison with authentic standards.

Table 1 shows our proposed structures for transformation products corresponding to nine of the peaks, together with a much more tentative possible structure for peak V. All these peaks except peak II show UV spectra similar to Irganox 1010, with the main absorption band extending from 260 to 300 nm with λ_{\max} in the range 280–285 nm characteristic of phenolic compounds. Fig. 4 shows examples for peaks I and IX. We conclude that the only major chromophore in such compounds is the Irganox 1010 subgroup.

None of the UV spectra provide evidence of quinone methide structure **3** similar to those found in our work with Irganox 1330 [6]. Such structures would show a characteristic intense absorption at significantly longer wavelengths, extending to 380 nm with λ_{\max} at about 345 nm.

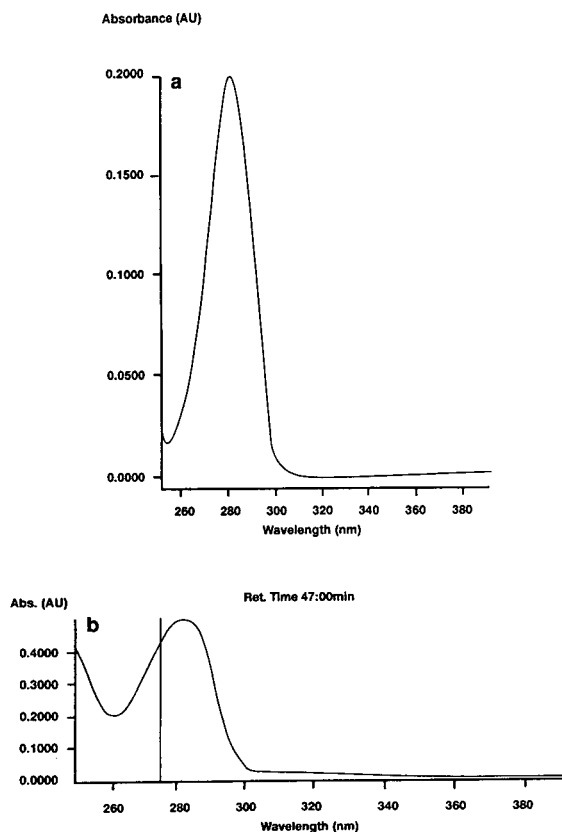


Fig. 4. (a) Diode array UV spectrum of peak I. (b) Diode array UV spectrum of peak IX.

Such quinone methide structures would have the same M_r as the corresponding cinnamate, being two mass units less than that of compound containing the fully saturated Irganox 1010 subunit.

3.1. Peak I

This peak shows a UV spectrum (Fig. 4a) which is very similar to that of Irganox 1010, indicating an intact phenolic group, without further conjugation. The mass spectrum (Fig. 5a) with a relatively intense molecular ion at m/z 278, base peak at m/z 263 due to the expected loss of CH_3 from the *tert.*-butyl groups, and significant fragment ion at m/z 219 as found in Irganox 1010 itself, is very similar to that of an authentic sample of 3-(3,5-di-*tert.*-butyl-4-hydroxyphenyl)propanoic acid (Fig. 5b). A B/E linked scan mass spectrum of the authentic sample confirmed that both m/z 263 and m/z 219 arise directly from fragmentation of the molecular ion. The low mass and relatively high polarity of this carboxylic acid are consistent with the fact that this compound has the shortest retention time of all the identified transformation products.

3.2. Peak II

The mass spectrum (Fig. 6a) shows a weak molecular ion at m/z 394. This is the only peak with a significantly different UV spectrum (Fig. 6b) to that of Irganox 1010: the absorption band is much broader, extending to beyond 320 nm, with λ_{\max} at 290 nm. This is characteristic of cinnamate type compounds (structure **4**), with extended conjugation.

3.3. Peak III

The single sub-unit structure assigned to this peak (M_r at m/z 364) is shown in Table 1.

This substance was synthesised, and comparison between the mass spectrum of the authentic sample and the transformation product was used to confirm assignments.

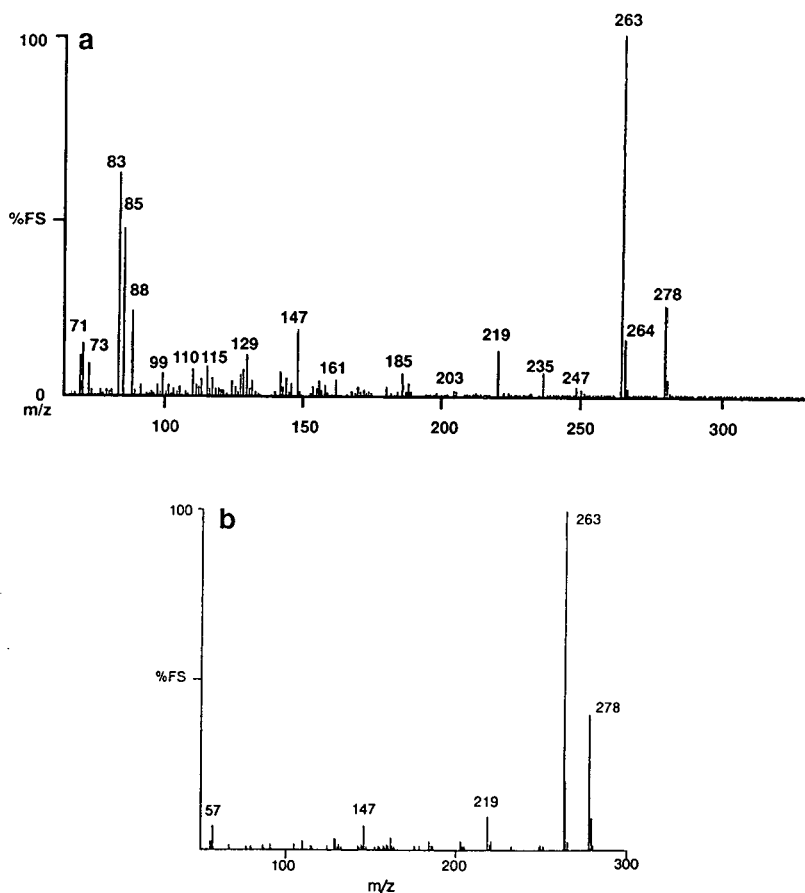


Fig. 5. (a) Mass spectrum of peak I. (b) Mass spectrum of an authentic sample of 3-(3,5-di-*tert.*-butyl-4-hydroxyphenyl) propanoic acid.

3.4. Peak V

On the basis of its UV spectrum (phenolic) and mass spectrum (apparent molecular ion at 378) peak V would be consistent with the single sub-unit structure shown in Table 1. However, such a structure is more polar than the proposed structure for peak III, and would therefore be expected to elute significantly earlier in the chromatogram. The actual identity of peak V is therefore uncertain.

3.5. Peaks VI, VII, and VIII

Peaks VI to VIII have been assigned to the structures containing two 1010 type sub-units.

The mass spectra of these three compounds show characteristic ions corresponding to structure 6 as well as the other principal fragmentation routes discussed. Confirmation of these assignments was achieved by synthesis of the compound with the structure proposed for peak VIII. The mass spectra of peak VIII and the synthetic sample are shown in Fig. 7a and b, respectively.

3.6. Peaks IX and XI

Peaks IX and XI are assigned to components containing three Irganox 1010 type sub-units. Peak IX has been assigned the structure shown in Table 1 on the basis of the mass spectral and

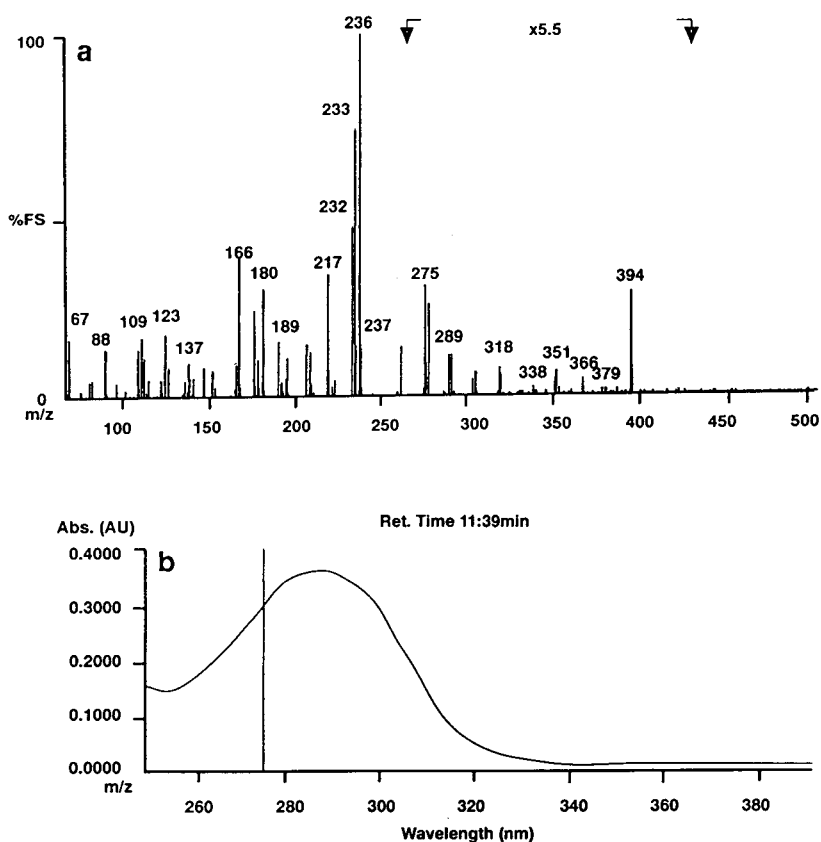


Fig. 6. (a) Mass spectrum of peak II. (b) Diode array UV spectrum of peak II.

UV evidence, Figs. 8 and 4b, respectively, and similarly for peak XI. In order to confirm these assignments an authentic sample of the compound with the structure proposed for peak XI was synthesised. A comparison between the mass spectrum obtained from peak XI and the synthetic sample is shown in Fig. 9a and b.

3.7. Peak XII

This peak elutes shortly before Irganox 1010 itself. On the basis of its high mass and the lack of any evidence of extended conjugation in the UV data we have tentatively explained it as arising via simple loss of a *tert.*-butyl group or groups from Irganox 1010, this type of transformation product having been previously identified in our work on Irganox 1330. [The relative

molecular mass of this proposed substance, in common with that of Irganox 1010 (peak XIII) is above the mass range of the instrument used.]

It was not possible to assign structures for peaks IV and X.

In summary then we conclude that peaks I to III contain a single sub-unit, while peaks VI to VIII contain two sub-units, and peaks IX, XI and XII retain three of the four sub-units of Irganox 1010.

We have also identified one of the smaller peaks, with UV absorbance of much less than 0.05. This is the small peak seen in Fig. 1 between peaks V and VI. Its mass spectrum is shown in Fig. 10a, while Fig. 10b shows the mass spectrum of a synthesised sample of 2,2-dimethylpropyl-3-(3,5-di-*tert.*-butyl-4-hydroxyphenyl) propanoate (structure 7). The similarity

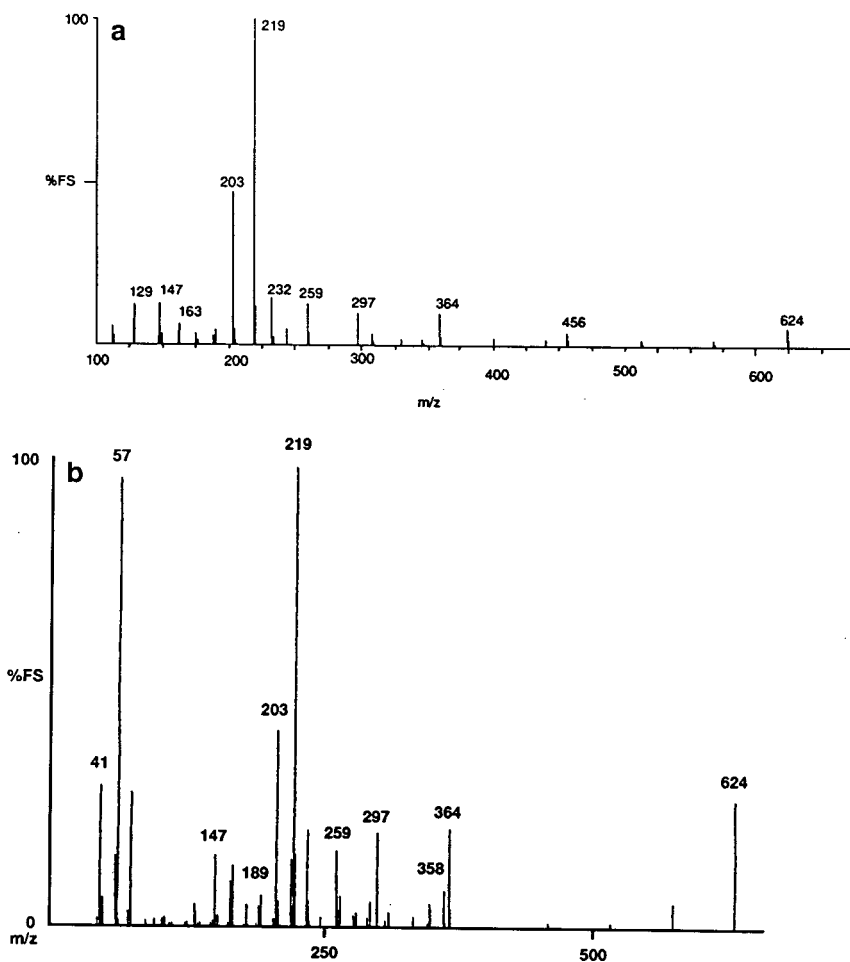


Fig. 7. (a) Mass spectrum of peak VIII. (b) Mass spectrum of a synthesised compound with the structure proposed for peak VIII.

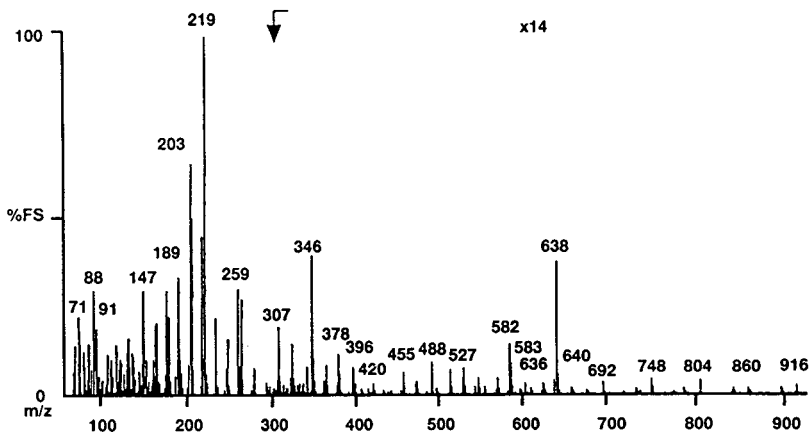


Fig. 8. Mass spectrum of peak IX.

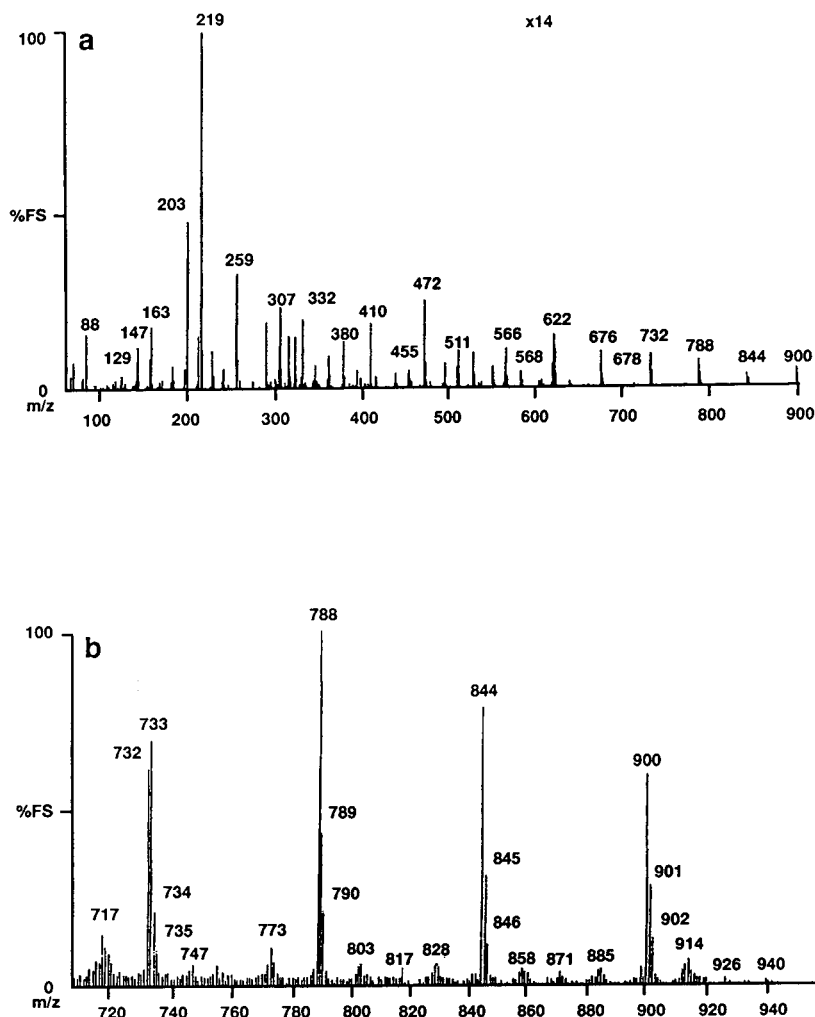
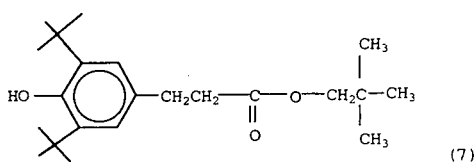


Fig. 9. (a) Mass spectrum of peak XI. (b) Mass spectrum of a synthesised compound with the structure proposed for peak XI.

between the two spectra is striking. This compound is the least polar of all the transformation products containing a single sub-unit, and is therefore the last of these to be eluted.



Overall the types of transformation products observed here appear to differ from those observed for Irganox 1330. In our work on Irganox 1330 we reported transformation to proceed via the formation of quinone methide type compounds. The difference in structure between the two antioxidants, principally the presence of the labile C–O bond in Irganox 1010 appears to lead to transformation proceeding via sub-unit losses. An overall scheme for this process is shown in Fig. 11.

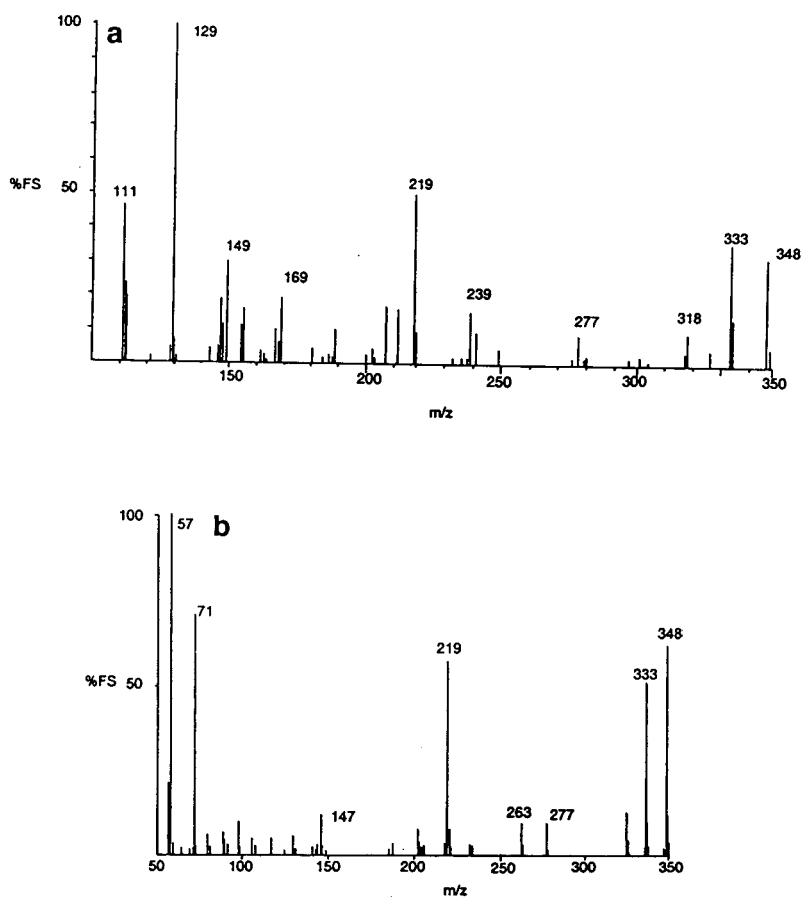


Fig. 10. (a) Mass spectrum of small peak eluting between peaks V and VI. (b) Mass spectrum of a synthesised compound with the structure proposed for the small peak eluting between Peaks V and VI.

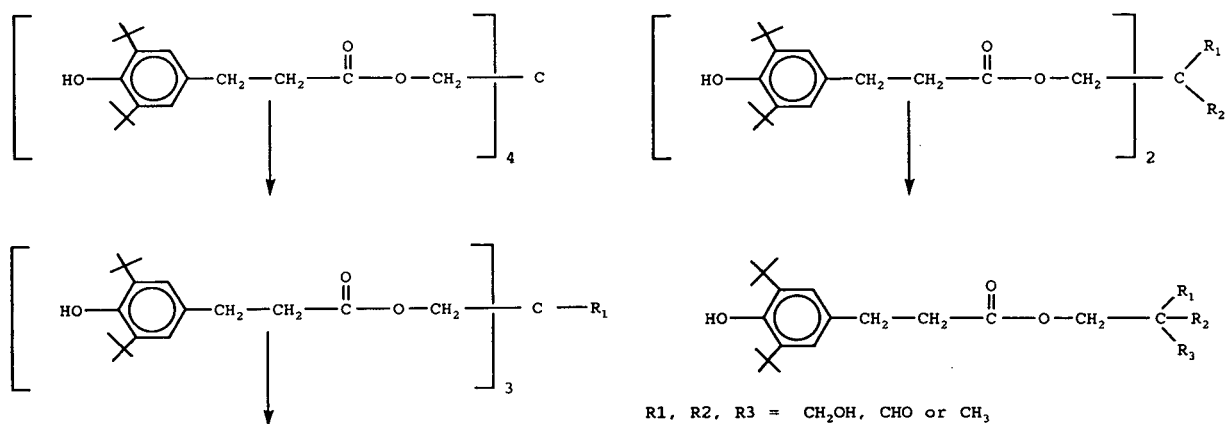


Fig. 11. Principal transformation processes for Irganox 1010 under electron beam irradiation.

4. Conclusions

Transformation of Irganox 1010 in food contact polymers subjected to electron beam irradiation gives rise to a complex mixture of products. The principal products arise via cleavage of C–O bonds leading to sub-unit losses. The formation of quinone methide species previously observed in our work on Irganox 1330 was not an important process in the transformation of Irganox 1010.

The combination of particle beam LC–MS with on-line UV diode array detection has proved a powerful analytical tool for this application.

Acknowledgements

This work was supported by the Ministry of Agriculture Fisheries and Food to whom thanks are due, and is Crown Copyright. The authors thank Dr. D. Richards, VG Masslab for his

continuing support. The authors are indebted to ICI (Chemicals and Polymers Group) plc, and Giba-Geigy plc for the provision of information and materials, and to Viritech Ltd (Swindon) for the use of their electron beam irradiation facilities.

References

- [1] D.W. Allen, D.A. Leathard, C. Smith and J.D. McGuinness, *Chem. Ind. (London)*, (1987) 198.
- [2] D.W. Allen, D.A. Leathard and C. Smith, *Chem. Ind. (London)*, (1987) 854.
- [3] D.W. Allen, A. Crowson and D.A. Leathard, *Chem. Ind. (London)*, (1990) 16.
- [4] D.W. Allen, D.A. Leathard and C. Smith, *Radiat. Phys. Chem. Int. J. Radiat. Appl. Instrum. Part C*, 38 (1991) 461.
- [5] D.W. Allen, M.R. Clench, A. Crowson and D.A. Leathard, *Polym. Degrad. Stab.*, 39 (1993) 293.
- [6] D.W. Allen, M.R. Clench, A. Crowson and D.A. Leathard, *J. Chromatogr. A*, 629 (1993) 283.
- [7] R.F. Browner and R.C. Willoughby, *Anal. Chem.*, 56 (1984) 2626.



ELSEVIER

Journal of Chromatography A, 679 (1994) 299–305

JOURNAL OF
CHROMATOGRAPHY A

Effect of detector temperature on the flame ionization detector response

M. Dressler*, M. Cigánek

Institute of Analytical Chemistry, Academy of Sciences of the Czech Republic, Veveří 97, 611 42 Brno, Czech Republic

First received 20 December 1993; revised manuscript received 26 May 1994

Abstract

The effect of the detector temperature on the flame ionization detector response of *n*-alkanes (nonane, decane, undecane, dodecane), *n*-octanol and dimethylphenol was studied for four different detector designs. Both absolute and relative response changes were found. They are dependent on the detector design and the solute type.

1. Introduction

The flame ionization detector (FID) is the most frequently used gas chromatographic detector. Since its origin [1–3] its properties have been studied many times. Parameters such as the mechanism of ion formation [4,5], carrier gas, hydrogen and air flow-rates [5–9], column temperature programme [10], carrier gas type [9,11], electrode geometry [5–8], voltage level [5–9], response linearity [6,8,12] and functional groups [5,12] have been studied in connection with FID response and noise. Only several of the oldest references are given here as examples, of course. For determinations the relative response factors have been published. The concept of effective carbon number has been developed [5], consisting in the constancy of the contribution of different carbon atom types in the solute mole-

cule to the overall solute response. The effect of hydrogen and carrier gas flow-rates on the FID relative molar response has been published [13]. Many anomalous FID responses for different types of compounds have been described (e.g., [14–16]).

The detector temperature has been considered mentioned only exceptionally. FID is generally considered not to be very sensitive to temperature changes (e.g., [17]). Only Maggs [18] and Teplý and Dressler [19] have presented some temperature response effect. Maggs found about a 1.3-fold increase in the molar and mass responses without any changes in the relative response within the temperature range 30–150°C. Teplý and Dressler found a small response increase for the FID using steam as the carrier gas within the temperature range 150–280°C.

In this work we studied the effect of the detector temperature on the FID response in greater detail within a wide temperature range and for different detector designs.

* Corresponding author.

2. Experimental

Four flame ionization detectors were studied: Carlo Erba (Milan, Italy) (HRGC 5300 Mega Series gas chromatograph), Phillips Scientific (Cambridge, UK) (PU 4400), Laboratory Instruments (Prague, Czech Republic) (Chrom 5) and Hewlett-Packard (Avondale, PA, USA) (5980 A). Their configurations are given in Fig. 1. A jet is the electrode in the Carlo Erba (Fig. 1a) and Hewlett-Packard (Fig. 1b) detectors and a coil around the jet in the Phillips detector (Fig. 1c). In the Laboratory Instruments detector (Fig. 1d) two electrodes in the form of semi-cylinders

insulated from one another are situated above the jet. Between these two electrodes and the detector wall a PTFE barrier is placed, directing the gas flow to the space between both the semi-cylinders.

The column and injector temperatures were equal for all four detectors, 110 and 220°C, respectively. Packed columns were used with the Phillips and Laboratory Instruments chromatographs and capillary columns with the Carlo Erba and Hewlett-Packard instruments. The flow-rates of hydrogen and air through all the detectors studied were similar, 25 and 350 ml min⁻¹, respectively (air in Laboratory Instru-

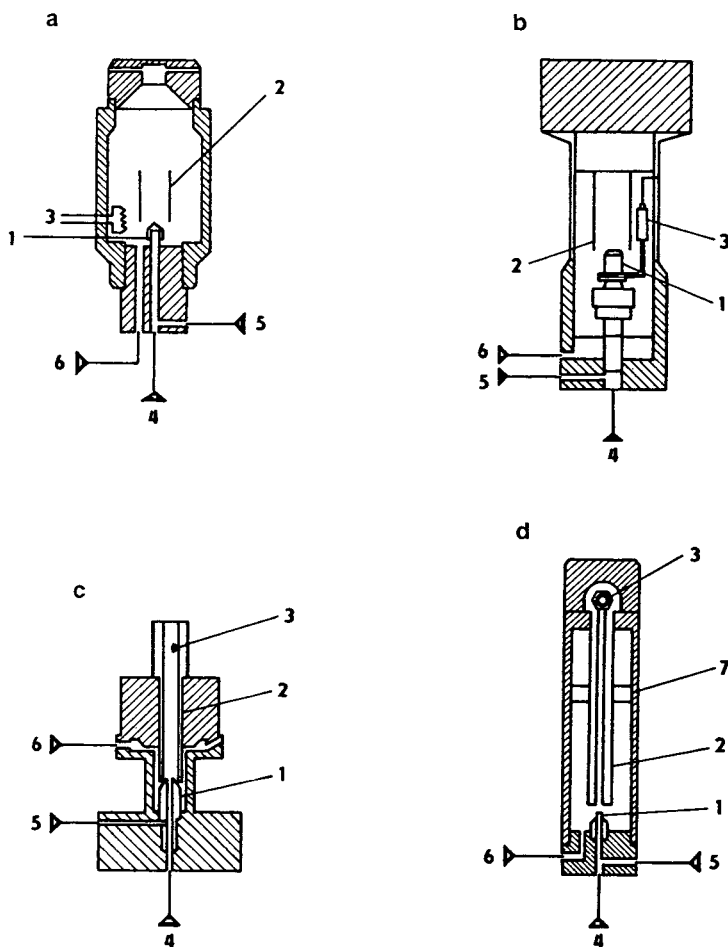


Fig. 1. Schematic diagrams of the flame ionization detectors. (a) Carlo Erba; (b) Hewlett-Packard; (c) Phillips; (d) Laboratory Instruments. 1 = Jet; 2 = collector electrode; 3 = ignition; 4 = carrier gas inlet; 5 = hydrogen inlet; 6 = air inlet; 7 = PTFE barrier.

ments chromatograph at 450 ml min⁻¹). The nitrogen make-up gas flow-rate was set in such a way as to obtain the same overall nitrogen flow-rate through the detector. The injection splitting ratio for the capillary columns was always 50:1.

The chromatographic conditions were as follows:

Carlo Erba: HP-5 column, 30 m × 0.53 mm I.D.; film thickness, 0.88 μm; flow-rates of nitrogen, carrier gas 3 ml min⁻¹, make-up gas 29 ml min⁻¹;

Hewlett-Packard: Ultra 2 column, 25 m × 0.2 mm I.D.; film thickness, 0.3 μm; flow-rates of nitrogen, carrier gas 0.9 ml min⁻¹, make-up gas 31 ml min⁻¹;

Phillips: column, 3.1 m × 4.0 mm I.D., Chromosorb W AW (149–177 μm) with 10% of SE-54; nitrogen carrier gas flow-rate, 32 ml min⁻¹;

Laboratory Instruments: column, 1.1 m × 3.0 mm I.D., Chromosorb W AW (149–177 μm) with 4% of SE-54; nitrogen carrier gas flow-rate, 32 ml min⁻¹.

Alkanes (*n*-C₉–C₁₂), *n*-octanol (OH) and dimethylphenol (DMP) were used as test solutes. A 1-μl volume of methylene chloride solution (about 0.1 μg of each solute) was always injected.

For processing the detector signals an HP 3393A integrator (Hewlett-Packard) was used. The given response values are the arithmetic averages of three parallel measurements. The relative responses are peak-area (or peak-height) ratios of the solute tested with respect to decane.

3. Results

3.1. Carlo Erba FID

The FID response for C₉–C₁₂ alkanes and octanol increases slightly within the temperature range 120–130°C. The response at 320°C is about 14% higher than that at 120°C. The DMP response increases between 240 and 280°C, the maximum response being ca. 19% higher (Fig. 2).

The alkane and OH relative responses do not

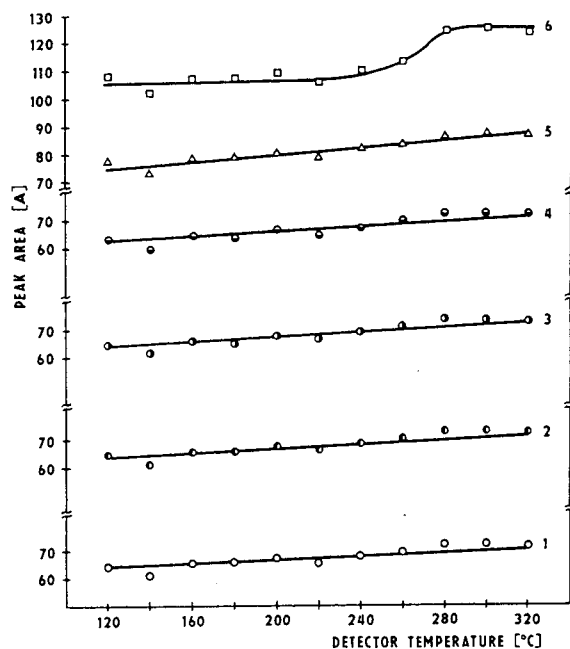


Fig. 2. Effect of detector temperature on Carlo Erba FID response. 1 = C₉; 2 = C₁₀; 3 = C₁₁; 4 = C₁₂; 5 = OH; 6 = DMP. A = arbitrary units.

change with the detector temperature. The DMP relative response decreases slightly from 120°C, having the lowest value at about 230°C, then it increases again up to 320°C. The maximum–minimum response differences are 3% and 6% for 120 and 320°C, respectively (Fig. 3).

3.2. Phillips FID

The temperature dependence of the response exhibits a maximum for all the compounds studied (Fig. 4). The temperature maximum is, however, different for alkanes and octanol plus DMP. For alkanes it is about 230°C and for octanol and DMP about 200°C. The response at 340°C is always lower than that at 120°C. The maximum response for alkanes is about 6% and 21% higher in comparison with the response at 120 and 340°C, respectively. For DMP these differences are about 20% and 39% higher and for OH about 13% and 35% higher.

The alkane relative response is the same for all detector temperatures studied (Fig. 5). It is not

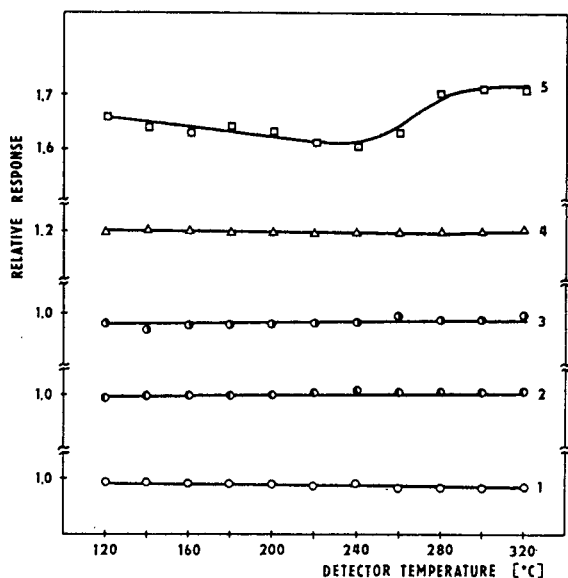


Fig. 3. Effect of detector temperature on Carlo Erba FID relative response. 1 = C_9/C_{10} ; 2 = C_{11}/C_{10} ; 3 = C_{12}/C_{10} ; 4 = OH/C_{10} ; 5 = DMP/C_{10} .

so for DMP and OH. The maximum relative response for both compounds occurs at about 190°C. It is about 14% higher than that at both 120 and 340°C for DMP and about 10% higher for OH.

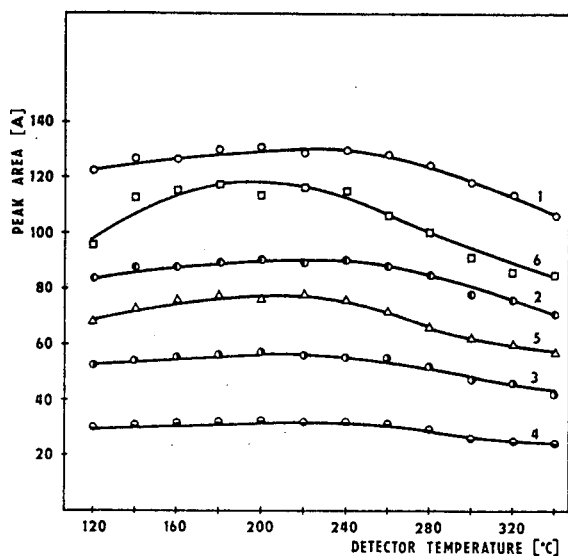


Fig. 4. Effect of detector temperature on Phillips FID response. Identification as in Fig. 2.

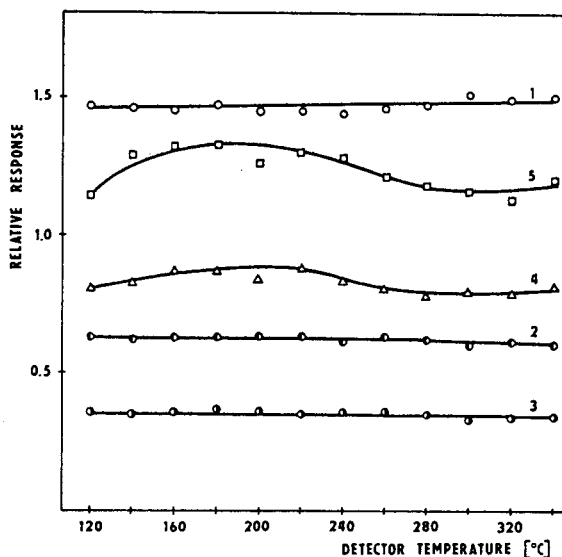


Fig. 5. Effect of detector temperature on Phillips FID relative response. Identification as in Fig. 3.

3.3. Hewlett-Packard FID

During the experiments with the Hewlett-Packard FID some time-dependent differences in the octanol and dimethylphenol responses were noticed. The first measurements are presented in Fig. 6a. The responses for C_{10} , OH and DMP increase within the temperature range studied. The highest response values were about 35% higher than the lowest values. Three months later, the responses for the same temperature range remained constant (Fig. 6b). The results obtained were compared with those for another instrument of the same type (Fig. 6c). The temperature dependences of the response for the second instrument were different. The response for all solutes increase beginning at about 160°C. The OH and C_{10} response reach a constant maximum value at about 240 and 305°C, respectively. The DMP response shows a maximum at about 250°C.

The temperature dependence of the relative response is maximum at about 230°C for both DMP and OH and the response difference to a temperature of 120°C is about 7% (Fig. 7a). Three months later, the relative responses remained constant (Fig. 7b). The temperature

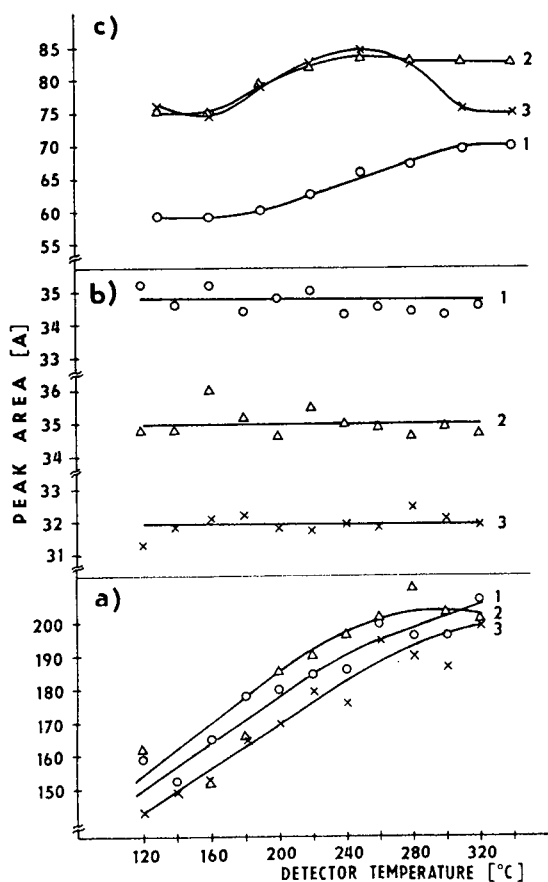


Fig. 6. Effect of detector temperature on Hewlett-Packard FID response. (a) first instrument, first measurements; (b) the same 3 months later; (c) second instrument. 1 = C₁₀; 2 = OH; 3 = DMP.

dependences are again different for the second instrument (Fig. 7c). Starting from about 250°C the relative response decreases. For a temperature of 340°C it equals 6% and 23% for OH and DMP, respectively. We have no explanation for this effect; it was not observed with the other FIDs studied.

3.4. Laboratory Instruments FID

The temperature dependences for this type of FID differ to a great extent from those for the other detectors studied (Fig. 8). Starting from 140–160°C a response decrease occurs for all the compounds studied. A very deep response de-

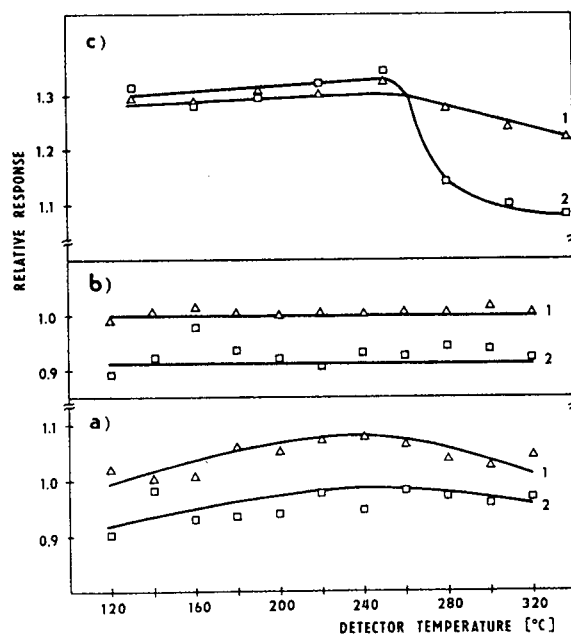


Fig. 7. Effect of detector temperature on Hewlett-Packard FID relative response. (a) First instrument, first measurements; (b) the same 3 months after; (c) second instrument. 1 = OH/C₁₀; 2 = DMP/C₁₀.

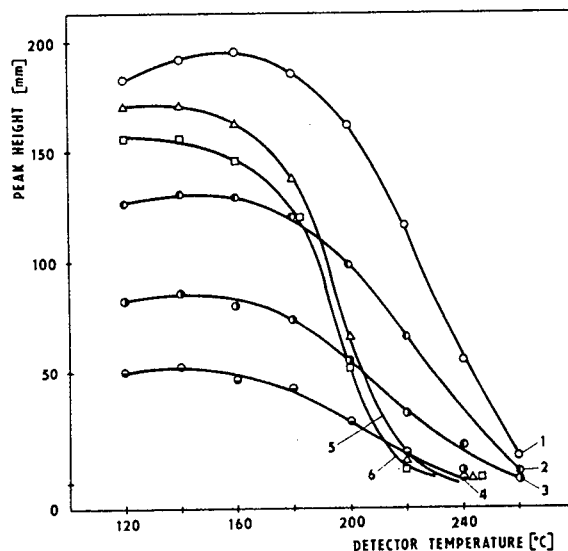


Fig. 8. Effect of detector temperature on Laboratory Instruments FID response. Identification as in Fig. 2.

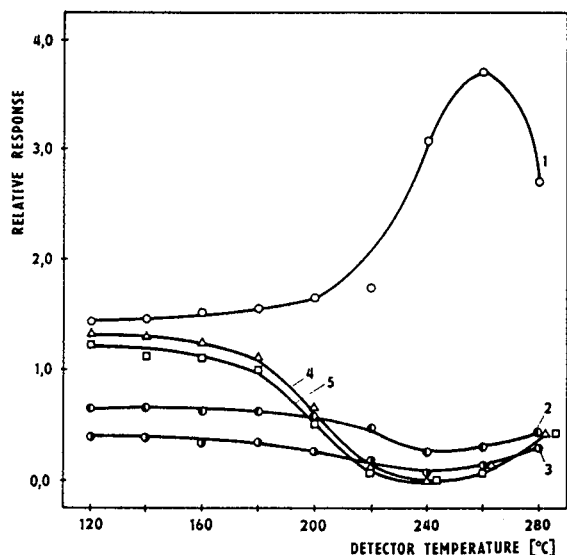


Fig. 9. Effect of detector temperature on Laboratory Instruments FID relative response. Identification as in Fig. 3.

crease, of about two orders of magnitude, appears at temperatures higher than ca. 230 and 240°C for DMP + OH and alkanes, respectively.

None of the relative responses are constant

within the temperature range studied, including *n*-alkanes (Fig. 9). Up to 160°C the relative response changes are small. The level of the relative response changes depends on the alkane used as a standard. The response behaviour of this type of FID is abnormal, especially at temperatures above ca. 160°C.

3.5. Temperature inside the detector body

The FID is not thermostated separately but is heated from its bottom base. We measured with a thin thermocouple the real temperatures inside the detector body at different distances from the detector base at different set detector temperatures for two of the detectors studied (Table 1). Real jet temperatures for one FID were also measured.

The real temperature inside both FIDs followed at each distance is always lower than the temperature set. The higher the set temperature, the higher are the relative temperature differences. The real temperature decreases with increasing distance from the detector base. A greater decrease was found with the Laboratory

Table 1
Temperature inside the detector body

Temperature set (°C)	Temperature measured (°C)				Jet	Detector
	Position					
	1	2	3	4		
120	72	69	67	65	145	I ^a
160	94	84	83	82	170	
200	112	105	103	101	201	
240	140	135	131	129	226	
280	171	165	162	160	253	
320	198	190	186	184	278	
120	101	117	125			II ^b
160	131	133	147			
200	175	167	153			
240	203	185	164			
280	230	211	170			
320	260	228	185			

^a I = Carlo Erba FID. Position = distance from the base (in the free "gas" detector volume, between the wall and the flame): 1 = 4 mm, 2 = 16 mm, 3 = 28 mm, 4 = 40 mm; jet orifice is 8 mm above the detector base.

^b II = Laboratory Instruments FID. Position: 1 = 4 mm, 2 = 24 mm, 3 = 42 mm; jet orifice is 9 mm above the detector base.

Instruments FID. The jet temperature increases with increasing detector temperature. This difference is about 130°C for a detector temperature change from 120 to 320°C.

4. Conclusions

Both the absolute and relative FID response depends on the detector temperature. The level and the character of these changes depend on the detector design and on the solute type.

The response values differ for different detector temperatures by up to several tens of per cent, and for one detector studied even by two orders of magnitude.

The relative response for *n*-alkanes seems to be constant within the temperature range 120–340°C. The relative response for DMP and OH can depend on the detector temperature. The differences are usually up to 23%, with the exception of one detector studied for which it was several hundred per cent.

The absolute and relative responses for one of the detectors studied changed during the experimental period and they were different for two different instruments.

Our results show that for compounds containing heteroatoms the effective carbon number need not be constant within the FID temperature range used. For some special FID designs it can be valid even for hydrocarbons. The effective carbon number can even depend on the detector type (with the same instrument type) and/or on the detector “life”.

It is difficult to explain why the effects of response changes with FID temperature are observed and further experiments are needed. However, the temperatures around the FID

flame (both “gas” and jet) are different at different FID set temperatures. This means that, e.g., the diffusion conditions for oxygen and other molecules and/or radicals vary.

References

- [1] I.G. McWilliam, *Aust. Pat.*, 224 504 (1957).
- [2] J. Harley, W. Nel and V. Pretorius, *Nature*, 181 (1958) 117.
- [3] I.G. McWilliam and R.A. Dewar, in D.H. Desty (Editor), *Gas Chromatography 1958*, Academic Press, New York, 1958, p. 142.
- [4] R.A. Dewar, *J. Chromatogr.*, 6 (1961) 312.
- [5] J.C. Sternberg, W.S. Gallaway and D.T.L. Jones, in N. Brenner, J.E. Callen and M.D. Weiss (Editors), *Gas Chromatography 1961*, Academic Press, New York, 1962, p. 231.
- [6] I.G. William, *J. Chromatogr.*, 6 (1961) 110.
- [7] D.H. Desty, C.J. Geach and A. Goldup, in R.P.W. Scott (Editor), *Gas Chromatography 1966*, Butterworths, London, 1961, p. 46.
- [8] J. Novák and J. Janák, *Chem. Listy*, 57 (1963) 371.
- [9] A.T. Blades, *J. Chromatogr.*, 14 (1976) 45.
- [10] K. Grob, Jr., *J. High Resolut. Chromatogr.*, 3 (1980) 286.
- [11] R.L. Hoffmann and C.D. Evans, *Science*, 153 (1966) 172.
- [12] G. Perkins, Jr., G.M. Rouayheb, L.D. Lively and W.C. Hamilton, in N. Brenner, W.C. Callen and M.D. Weiss (Editors), *Gas Chromatography 1961*, Academic Press, New York, 1961, p. 269.
- [13] O. Hainová, P. Boček, J. Novák and J. Janák, *J. Gas Chromatogr.*, 5 (1967) 401.
- [14] M. Dressler, *J. Chromatogr.*, 42 (1969) 408.
- [15] B.A. Schaefer, *Anal. Chem.*, 42 (1970) 448.
- [16] B.A. Schaefer and D.M. Douglas, *J. Chromatogr. Sci.*, 9 (1971) 612.
- [17] R. Schill, in R.L. Grob (Editor), *Modern Practice of Gas Chromatography*, Wiley, New York, 1977, p. 239.
- [18] R.J. Maggs, *Column*, 1, No. 2 (1966) 2.
- [19] J. Teplý and M. Dressler, *J. Chromatogr.*, 191 (1980) 221.

Gas chromatographic determination of vapour pressures of pheromone-like compounds

II. [☆] Alcohols

Bohumír Koutek^{a,*}, Michal Hoskovec^a, Pavlína Vrkočová^b, Karel Konečný^a,
Ladislav Feltl^b

^aDepartment of Natural Products, Institute of Organic Chemistry and Biochemistry,
Academy of Sciences of the Czech Republic, Flemingovo nám. 2, CZ-166 10 Prague 6, Czech Republic

^bDepartment of Analytical Chemistry, Faculty of Natural Sciences, Charles University, Albertov 2030,
CZ-128 40 Prague 2, Czech Republic

Received 21 April 1994

Abstract

The vapour pressures of 98 (*Z*)- and (*E*)-monounsaturated C₁₀–C₁₈ alcohols were determined using a method based on gas chromatographic retention data. This method, by utilizing a non-polar HP-1 capillary column, five experimental temperatures, four reference compounds (C₁₁, C₁₂, C₁₄ and C₁₆ alkanols) whose polarities approximated that of the test compounds and melting point corrections for compounds that are solids at ambient temperature, provided vapour pressures that agreed reasonably well with the available literature values. For alkenols belonging to structurally similar subseries, e.g., for ω -3, ω -5 and ω -7 unsaturated derivatives, the vapour pressures may be represented over a range of pressure by simple equations in which the number of carbon atoms is a parameter.

1. Introduction

The saturation properties of pure liquids play a major role in both the understanding of fluid phase behaviour and the design and operation of a multitude of industrial processes [1,2]. Such properties are essential not only when used directly in calculations, but also when

used as input to variety of models and applications.

At present, there is an increasing need for vapour pressures of high-molecular-mass organic compounds at ambient temperatures [3,4]. One of the most important reasons for this is the increased public sensitivity to the effect of chemicals on health and the environment generally. As the vapour pressure of an organic chemical exerts a large influence on its dispersal in the environment, a knowledge of the vapour pressures should allow one not only to model the fate of organic pollutants [5,6] but

* Corresponding author.

[☆] For Part I, see Ref. [20].

also to optimize the use of ecologically friendly behaviour-modifying chemicals [7]. An impetus for developing more effective design for practical applications of these compounds is the continuing value of pheromones for monitoring insect flight activity and the recent commercial success in controlling several pests by permeating the air with their sex pheromones [7]. Both the release rates and, in the case of blends, the release ratios of pheromone components from dispensers are governed, for the most part, by the vapour pressures of the compounds. It appears that environmental concerns are weighing against the use of traditional pesticides and expectations are [8] that pheromones will capture about 15–40% of the insecticide market within 10 years. Thus, an understanding of the pheromone evaporative process can aid in the optimization of selectivity conditions and the minimization of the loss of the biological activity of synthetic pheromone blends.

The vapour pressures of compounds of low volatility are commonly determined by either gas saturation [9,10] or effusion [11] methods. Gas chromatography (GC) is an alternative method for measuring vapour pressures [12,13], offering advantages in terms of speed, solute sample size, purity and stability requirements. It is based on the use of a non-polar stationary phase and isothermal conditions such that a compound's GC retention time is related directly to its vapour pressure. The GC method has been used to study polychlorinated biphenyls and dioxins [14,15], herbicide esters [12], organophosphorus pesticides [16], tetraorganostannanes [17], linear alkylbenzenes [18] and fatty acid methyl esters [19]. Using this approach, we have obtained [20] some vapour pressure data on pheromone-like acetates.

In this paper we show that the GC method yields equally good results in determining equilibrium vapour pressures of more polar compounds, viz. monounsaturated (C_{10} – C_{18}) pheromone-like alcohols. The extensive set of 98 compounds studied also allowed the influence of subtle structural differences in chain length and the positions of double bonds on vapour pressures to be revealed.

2. Experimental

2.1. Chromatography

Samples were analysed on a Hewlett-Packard HP 5890 chromatograph equipped with a 3 m \times 0.31 mm I.D. fused-silica capillary column (cross-linked 5% methylsilicone, HP-1, film thickness 0.52 μ m) with split injection and a flame ionization detector. The length of the column employed (3 m) is a compromise between the need for acceptable resolution when working with mixtures and the need to avoid prohibitively long retention times, particularly at lower temperatures. The chromatograph was operated isothermally with a hydrogen flow-rate of 5 ml/min at 10°C intervals in the range 50–160°C as specified. C_{11} , C_{12} , C_{14} and C_{16} alkanols were used as reference standards. Retention times were determined on a Hewlett-Packard HP 5895A ChemStation. Adjusted retention times were calculated by subtracting the retention time of methane from the retention time of the chemical. As recommended [13], long retention times of compounds producing unsymmetrical peaks at low temperatures were not taken at the peak maximum, but were estimated at the centre of gravity of the peak. The reproducibility of retention time measurements expressed as the relative standard deviation of at least three measurements for each compound was 0.03%.

2.2. Chemicals

The alcohols were either obtained from the Research Institute for Plant Protection (IPO-DLO) (Wageningen, Netherlands) and used as received or synthesized in our laboratory. In the latter instance, the purity of the chemicals was at least 97% as determined by capillary GC. Condensed nomenclature for alcohols is used: the letters after the colon indicate the functional type (OH = alcohol), the number between the dash and colon indicate the number of carbon atoms in the chain and the letters and numbers before the dash indicate the configuration and

position of the double bonds, e.g., Z3-10:OH is (Z)-3-decenol.

2.3. Data treatment

The method has been discussed in detail by Bidleman [13] and Hinckley et al. [21] and will therefore be only briefly reviewed here. At a constant temperature, the vapour pressures of a test and of a reference compound (subscripts T and R, respectively) are related by the ratio of their latent heats of vaporization:

$$\ln P_T = \frac{\Delta H_T}{\Delta H_R} \cdot \ln P_R + C \quad (1)$$

where ΔH is the latent heat of vaporization and C is a constant. A similar equation has been developed for the GC (adjusted) retention times t' :

$$\ln \left(\frac{t'_T}{t'_R} \right) = \left(1 - \frac{\Delta H_T}{\Delta H_R} \right) \ln P_R - C \quad (2)$$

Hence, a plot of $\ln(t'_T/t'_R)$ versus $\ln P_R$ should have a slope $1 - \Delta H_T/\Delta H_R$ and an intercept $-C$. Eq. 1 can then be used to determine the vapour pressure of the test compound at any temperature if the vapour pressure of the reference compound at that temperature is known.

Since the GC method gives the subcooled liquid vapour pressure (defined as the liquid vapour pressure extrapolated below the melting point) [22], it was necessary to convert the literature-based solid vapour pressures (P_S) into subcooled liquid vapour pressures (P_L) by using the equation developed by Mackay et al. [23]:

$$\ln \left(\frac{P_S}{P_L} \right) = -\frac{\Delta S_F}{R} \left(\frac{T_M}{T} - 1 \right) \quad (3)$$

where T_M and T are the absolute melting and ambient temperatures, respectively, R is the gas constant and ΔS_F is the entropy of fusion. The usually employed "average" value of $\Delta S_F = 56.5$ J/K·mol (or the corresponding value $\Delta S_F/R = 6.79$) seems to be too low for alcohols, however. Based on the value of enthalpy of fusion (ΔH_F) published [24] for 1-hexadecanol (34.286 kJ/mol), ΔS_F for this compound amounts 106.34

J/K·mol and, as a consequence, $\Delta S_F/R = 12.789$. Hence this constant was used to convert literature P_S values of 1-hexadecanol and 1-pentadecanol into P_L .

2.4. Statistical analysis

The data were subjected to statistical analyses utilizing the Statgraphics Plus 7.0 software package (Manugistic, Rockville, MD, USA).

3. Results and discussion

The accuracy of the GC method as represented by Eqs. 1 and 2 depends to a large extent on two factors: (i) the accuracy of the P_R values and (ii) the similarity of infinity dilution activity coefficients γ in the stationary phase between the test and reference compounds to which Eq. 2 is applied. Strictly, an additional term, $-\ln(\gamma_T/\gamma_R)$, should appear (see discussion in Ref. [21]) on the right-hand side of this equation and only when $\gamma_T \sim \gamma_R$ (or at least $\gamma_T/\gamma_R \sim \text{constant}$) can the use of Eq. 1 lead to reasonable results. As values of γ on a squalane liquid phase have been found [25] to range from 0.48 to 0.73 for hydrocarbons and from 17 to 34 for alcohols, the frequently employed reference hydrocarbons seemed to be disqualified for our purposes. Therefore, we chose to use n -alkanols (i.e., compounds of the same chemical class as the test compounds) as the reference standards. When literature vapour pressure values were being selected for the reference n -alkanols, some judgment was necessary. We favoured recent static measurements [26] that have been especially focused on the low vapour pressure field. The literature values of the four reference compounds given in Table 1 in the form of the Antoine equation are thus from a single report. In most instances vapour pressures were calculated from the Antoine constants by interpolation. In those instances where some extrapolation was necessary (14:OH, 15:OH and 16:OH), the temperature range of extrapolation was usually less than 40 K.

As the choice of the P_R is critical for the

Table 1
Vapour pressures (P_R) of the reference n -alkanols

Alkanol	Constants of the Antoine equation ^a			P_R (25°C) (Pa)
	A	B	C	
11:OH	7.094	2105.005	176.145	0.4255
12:OH	6.860	2011.634	162.769	0.1402
14:OH	6.916	2217.995	165.381	0.01844
16:OH	5.964	1781.618	120.726	0.00207 ^b

^a Ref. [26]; $\log P$ (kPa) = $A - B/(t + C)$.

^b Vapour pressure is for the subcooled liquid; it was calculated from the original solid vapour pressure ($5.4726 \cdot 10^{-4}$ Pa) using Eq. 3 and m.p. 56°C.

accuracy of vapour pressures determined by the comparative GC method, the literature P_R data were checked for internal consistency. Examination of the logarithm of vapour pressure (corrected for melting point) as a function of the number of carbon atoms in alkanol series (Fig. 1) confirms that an excellent linear correlation, $\ln P = (-1.0675 \pm 0.0058)n_C + (10.8973 \pm 0.0734)$ ($n = 7$, S.E. = 0.0374, $r^2 = 0.9999$), does exist.

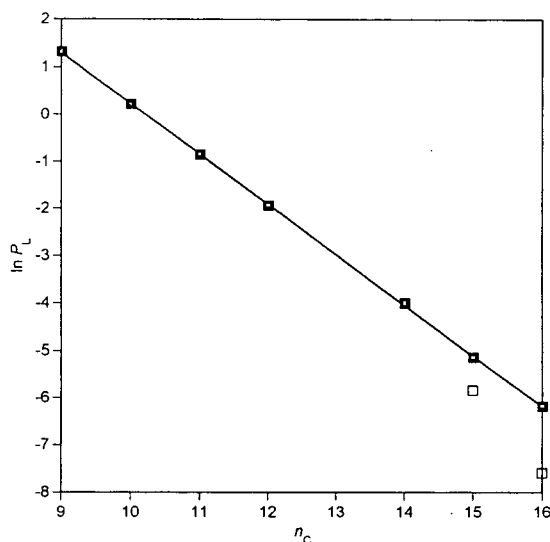


Fig. 1. Liquid vapour pressures (Pa) (25°C) of alkanols [25] as a function of the number of carbon atoms. □ = Original (solid) vapour pressures of 15:OH and 16:OH.

Table 2
Adjusted GC retention times (min) of the n -alkanols

Alkanol	80°C	90°C	100°C	110°C	120°C
9:OH	0.773	0.482	0.332	0.237	0.172
10:OH	1.553	0.926	0.605	0.409	0.283
11:OH	3.162	1.800	1.123	0.724	0.481
12:OH	6.557	3.541	2.122	1.313	0.837
14:OH	26.696	13.305	7.385	4.242	2.256
15:OH	53.448	25.600	13.698	7.600	4.379
16:OH	110.337	50.162	25.846	13.914	7.757

3.1. Validation of the method

Six n -alkanols with known P_L [26] were chromatographed along with the 14:OH reference, and P_{GC} values at 25°C were calculated from the relative retention data (Table 2) using Eqs. 1 and 2. In Fig. 2, these P_{GC} values are compared with P_L . As can be seen, the regression line obtained closely parallels the $y = x$ line. The equation of the regression line by a linear least-squares fit is

$$\ln [P_L \text{ (Pa)}] = (1.02536 \pm 0.0049) \ln P_{GC} \quad (4)$$

($n = 6$, S.E. = 0.0402, $r^2 = 0.9999$)

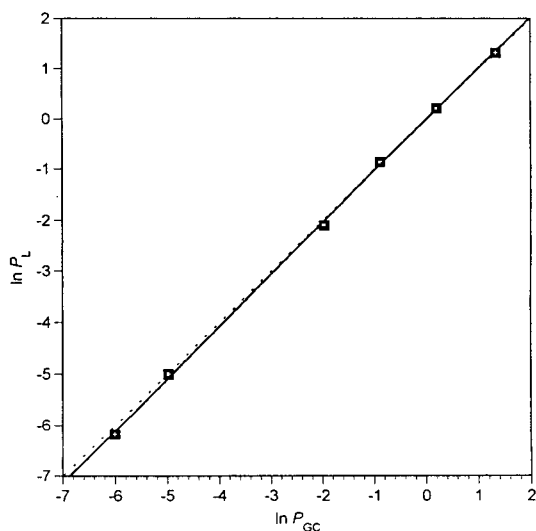


Fig. 2. Logarithmic plot of the literature vapour pressures P_L of alkanols (25°C) vs. the corresponding P_{GC} data (Eq. 1) from the present work. The regression line (solid) and $y = x$ line (dashed) are shown.

with a slope nearly equal to 1. Note that in Eq. 4 the intercept has not been included at the 0.05% probability level. The quality of fit produced by the proposed vapour pressure correlation is excellent, thus demonstrating the validity of the GC method even for polar compounds.

Another noteworthy feature of this correlation is that it appears to be applicable over a range of pressures that covers three orders of magnitude. Table 3 presents a comparison between the GC-based and literature vapour pressure data. Our corrected (Eq. 4) vapour pressures differ from those given by N'Guimbi et al. [26] by values ranging from 0.6% (for 10:OH) to 5.3% (for 12:OH). In addition to the original database [26] employed in deriving Eq. 4, Table 3 also includes a complete data set [3] obtained from the Chebyshev-type polynomial in x of degree 3 by extrapolation. This polynomial has been proposed to allow extrapolation for about 150 K with fair confidence. The slightly lower (about 10%) but consistently similar vapour pressure values following from the use of this equation might be regarded as a notable agreement between the two literature data sets. It is noticeable that vapour pressures of 10:OH (1.233 Pa) and 12:OH (0.1328 Pa) following from the use of Eq. 4 compare favourably with the values 1.190 and 0.1397 Pa obtained [27] for these compounds from a simultaneous correlation of vapour pres-

sure and thermal data. Hence it appears that the GC method is capable of yielding vapour pressures of saturated alcohols with an error below 10%.

This conclusion finds further support in the estimated heats of vaporization. In deriving vapour pressures from GC retention time data, $\Delta H_T/\Delta H_R$, the ratio of the enthalpies of vaporization of a test to that of the reference compound is obtained. Hence, by utilizing the literature [28] experimental ΔH_R value for our reference standard, 14:OH (102.2 ± 2.4 kJ mol⁻¹), the remaining enthalpies of vaporization of alkanols may be calculated from the $\Delta H_T/\Delta H_R$ ratios given in Table 3. The results calculated by this approach are 72.17 kJ mol⁻¹ for 9:OH, 79.27 kJ mol⁻¹ for 10:OH and 91.69 kJ mol⁻¹ for 12:OH. These values compare well with the corresponding calorimetric data, viz. 76.86 ± 0.75 , 81.50 ± 0.75 and 91.96 ± 0.59 kJ mol⁻¹, respectively, yielding a maximum error of 6.1%.

3.2. Vapour pressures of alkenols

Vapour pressures of all measured alkenols were determined by the same approach as described above for saturated compounds. Taking advantage of the internal consistency of the vapour pressure data for saturated derivatives demonstrated above, the test compounds were

Table 3
Parameters of Eq. 2 and vapour pressures (25°C) of the *n*-alkanols

Alkanol ^a	$\Delta H_T/\Delta H_R$	C	P · 1000 (Pa)				Error ^c (%)
			Eq. 1	Eq. 4	Exp. ^b	Exp. ^d	
9:OH	0.7062	4.1446	3760	3888	3738	3334	4.0
10:OH	0.7756	3.3008	1226	1233	1241	1087	-0.6
11:OH	0.8379	2.4614	412.9	403.7	425.0	378.1	-5.0
12:OH	0.8972	1.6137	139.6	132.8	140.2	136.1	-5.3
15:OH	1.0493	-0.7941	6.846	6.033	5.894 ^c	5.335	2.4
16:OH	1.1007	-1.6180	2.446	2.100	2.069 ^c	1.842	1.5

^a Standard 14:OH.

^b Ref. [25].

^c Corrected by using Eq. 3.

^d Ref. [3].

^e Error = $100(P_{GC} - P_{EXP})/P_{EXP}$; P_{EXP} taken from Ref. [25].

Table 4
GC data and vapour pressures (25°C) of decenols

Alcohol	Relative retention time ^a					P (Pa)	
	50°C	60°C	70°C	80°C	90°C	Eq. 1	Eq. 4
Z3-10:OH	0.128	0.146	0.168	0.189	0.210	1.669	1.691
E3-10:OH	0.125	0.142	0.163	0.183	0.204	1.704	1.727
Z4-10:OH	0.135	0.153	0.174	0.193	0.214	1.536	1.553
E4-10:OH	0.141	0.160	0.179	0.198	0.218	1.432	1.445
Z5-10:OH	0.144	0.162	0.183	0.202	0.223	1.406	1.418
E5-10:OH	0.147	0.165	0.185	0.205	0.225	1.367	1.378
Z6-10:OH	0.147	0.166	0.186	0.206	0.227	1.380	1.391
E6-10:OH	0.147	0.165	0.185	0.205	0.225	1.365	1.376
Z7-10:OH	0.153	0.171	0.192	0.212	0.232	1.311	1.320
E7-10:OH	0.153	0.171	0.191	0.210	0.229	1.294	1.303
Z8-10:OH	0.175	0.195	0.217	0.237	0.258	1.109	1.112
E8-10:OH	0.165	0.183	0.204	0.224	0.244	1.187	1.192

^a Standard 12:OH.

chromatographed using four reference standards: 11:OH (for C₁₂ alkenols), 12:OH (for C₁₀, C₁₃ and C₁₄ alkenols), 14:OH (for C₁₅ and C₁₆ alkenols) and 16:OH (for C₁₈ alkenols).

The relative retention times and calculated

vapour pressures for C₁₀, C₁₂, C₁₃, C₁₄, C₁₅, C₁₆ and C₁₈ alkenols are listed in Tables 4–10. Inspection of these tables reveals that the vapour pressures of all alkenols are similar to those of the corresponding alkanols. In spite of this, two

Table 5
GC data and vapour pressures (25°C) of dodecenols

Alcohol	Relative retention time ^a					P (Pa)	
	60°C	70°C	80°C	90°C	100°C	Eq. 1	Eq. 4
Z2-12:OH	2.034	1.961	1.894	1.827	1.780	0.167	0.160
E2-12:OH	2.083	2.002	1.933	1.854	1.806	0.162	0.155
Z3-12:OH	1.768	1.726	1.691	1.649	1.624	0.204	1.196
E3-12:OH	1.719	1.682	1.646	1.606	1.591	0.212	0.204
Z4-12:OH	1.793	1.743	1.701	1.652	1.612	0.196	0.188
E4-12:OH	1.896	1.832	1.775	1.715	1.665	0.181	0.173
Z5-12:OH	1.864	1.803	1.753	1.698	1.662	1.187	0.179
E5-12:OH	1.944	1.870	1.811	1.745	1.701	0.175	0.167
Z6-12:OH	1.867	1.800	1.753	1.697	1.664	0.187	0.179
E6-12:OH	1.913	1.839	1.787	1.726	1.673	0.178	0.170
Z7-12:OH	1.901	1.829	1.780	1.720	1.672	0.181	0.173
E7-12:OH	1.951	1.871	1.813	1.748	1.700	0.174	0.166
Z8-12:OH	2.002	1.922	1.855	1.789	1.738	1.169	0.162
E8-12:OH	2.002	1.914	1.855	1.784	1.732	0.169	0.162
Z9-12:OH	2.078	1.986	1.920	1.840	1.789	0.161	0.154
E9-12:OH	2.096	1.998	1.924	1.837	1.775	0.156	0.149
Z10-12:OH	2.402	2.273	2.171	2.065	1.979	0.132	0.125
E10-12:OH	2.246	2.128	2.041	1.946	1.886	1.145	0.138

^a Standard 11:OH.

Table 6
GC data and vapour pressures (25°C) of tridecenols

Alcohol	Relative retention time ^a					P (Pa)	
	70°C	80°C	90°C	100°C	110°C	Eq. 1	Eq. 4
Z7-13:OH	1.762	1.721	1.675	1.633	1.590	0.0673	0.0628
E7-13:OH	1.817	1.769	1.713	1.666	1.619	0.0639	0.0596
Z9-13:OH	1.890	1.839	1.776	1.719	1.674	0.0607	0.0565
E9-13:OH	1.939	1.856	1.790	1.728	1.678	0.0575	0.0534
Z11-13:OH	2.266	2.177	2.077	1.999	1.920	0.0472	0.0436
E11-13:OH	2.167	2.077	1.982	1.900	1.833	0.0491	0.0455

^a Standard 12:OH.

subtle trends are apparent in all series considering the influence of double bond position: (i) the vapour pressures of series members with a double bond located near the centre of the carbon chain are generally higher than those of the corresponding saturated compounds and (ii) the

vapour pressures of isomers with a double bond positioned on the second carbon atom of the chain (irrespective of the end of the molecule from which the numbering starts) are either close to or lower than those of the saturated compounds. It appears that the double bond position

Table 7
GC data and vapour pressures (25°C) of tetradecenols

Alcohol	Relative retention time ^a					P (Pa)	
	80°C	90°C	100°C	110°C	120°C	Eq. 1	Eq. 4
Z2-14:OH	3.820	3.538	3.299	3.113	2.911	0.0211	0.0191
E2-14:OH	3.883	3.586	3.345	3.140	2.925	0.0203	0.0184
Z3-14:OH	3.389	3.186	3.013	2.847	2.685	0.0256	0.0234
E3-14:OH	3.286	3.083	2.912	2.767	2.609	0.0267	0.0243
Z4-14:OH	3.358	3.157	2.966	2.811	2.650	0.0256	0.0233
E4-14:OH	3.526	3.289	3.079	2.902	2.723	0.0234	0.0213
Z5-14:OH	3.408	3.217	3.017	2.843	2.663	0.0246	0.0224
E5-14:OH	3.551	3.308	3.096	2.917	2.729	0.0230	0.0209
Z6-14:OH	3.343	3.138	2.954	2.798	2.634	0.0257	0.0234
E6-14:OH	3.462	3.243	3.050	2.865	2.686	0.0240	0.0218
Z7-14:OH	3.340	3.134	2.959	2.798	2.634	0.0258	0.0235
E7-14:OH	3.485	3.259	3.057	2.883	2.704	0.0239	0.0217
Z8-14:OH	3.412	3.209	3.004	2.840	2.665	0.0246	0.0224
E8-14:OH	3.616	3.301	3.087	2.922	2.719	0.0220	0.0200
Z9-14:OH	3.512	3.285	3.079	2.898	2.725	0.0236	0.0215
E9-14:OH	3.622	3.376	3.157	2.961	2.768	0.0222	0.0202
Z10-14:OH	3.682	3.473	3.223	3.016	2.819	0.0217	0.0196
E10-14:OH	3.731	3.464	3.221	3.025	2.815	0.0211	0.0191
Z11-14:OH	3.881	3.587	3.335	3.117	2.909	0.0200	0.0181
E11-14:OH	3.834	3.548	3.300	3.079	2.864	0.0201	0.0182
Z12-14:OH	4.346	4.024	3.714	3.447	3.185	0.0169	0.0153
E12-14:OH	4.102	3.774	3.495	3.250	3.004	0.0180	0.0163

^a Standard 12:OH.

Table 8
GC data and vapour pressures (25°C) of pentadecenols

Alcohol	Relative retention time ^a					P (Pa)	
	90°C	100°C	110°C	120°C	130°C	Eq. 1	Eq. 4
Z9-15:OH	1.633	1.598	1.564	1.533	1.505	0.00917	0.00814
E9-15:OH	1.692	1.649	1.605	1.568	1.536	0.00851	0.00754
Z10-15:OH	1.696	1.651	1.608	1.574	1.541	0.00845	0.00749
E10-15:OH	1.729	1.681	1.638	1.593	1.557	0.00815	0.00721
Z11-15:OH	1.768	1.721	1.676	1.629	1.590	0.00794	0.00702
E11-15:OH	1.769	1.721	1.673	1.623	1.581	0.00781	0.00691
Z12-15:OH	1.841	1.790	1.735	1.677	1.639	0.00739	0.00652
E12-15:OH	1.830	1.771	1.714	1.660	1.614	0.00730	0.00644
Z13-15:OH	2.071	1.988	1.915	1.849	1.792	0.00617	0.00542
E13-15:OH	1.955	1.880	1.811	1.744	1.695	0.00654	0.00576

^a Standard 14:OH.

Table 9
GC data and vapour pressures (25°C) of hexadecenols

Alcohol	Relative retention time ^a					P (Pa)	
	100°C	110°C	120°C	130°C	140°C	Eq. 1	Eq. 4
Z3-16:OH	2.973	2.801	2.673	2.524	2.401	0.00329	0.00285
E3-16:OH	2.900	2.741	2.605	2.465	2.343	0.00336	0.00291
Z4-16:OH	2.919	2.758	2.629	2.486	2.364	0.00337	0.00292
E4-16:OH	3.054	2.872	2.719	2.559	2.422	0.00302	0.00261
Z5-16:OH	2.944	2.779	2.639	2.494	2.369	0.00327	0.00283
E5-16:OH	3.033	2.851	2.703	2.546	2.412	0.00307	0.00265
Z6-16:OH	2.854	2.704	2.575	2.440	2.320	0.00348	0.00301
E6-16:OH	2.962	2.794	2.657	2.506	2.378	0.00323	0.00279
Z7-16:OH	2.809	2.664	2.545	2.414	2.299	0.00362	0.00314
E7-16:OH	2.993	2.798	2.659	2.507	2.377	0.00312	0.00270
Z8-16:OH	2.849	2.702	2.576	2.433	2.323	0.00350	0.00303
E8-16:OH	2.967	2.799	2.656	2.510	2.377	0.00321	0.00278
Z9-16:OH	2.880	2.711	2.586	2.447	2.335	0.00344	0.00298
E9-16:OH	3.001	2.825	2.679	2.521	2.393	0.00312	0.00270
Z10-16:OH	2.962	2.795	2.658	2.506	2.377	0.00323	0.00279
E10-16:OH	3.058	2.873	2.719	2.563	2.426	0.00302	0.00261
Z11-16:OH	3.050	2.870	2.719	2.572	2.430	0.00308	0.00266
E11-16:OH	3.125	2.930	2.757	2.604	2.457	0.00288	0.00248
Z12-16:OH	3.191	2.997	2.822	2.665	2.510	0.00282	0.00243
E12-16:OH	3.198	2.996	2.810	2.651	2.499	0.00276	0.00238
Z13-16:OH	3.330	3.110	2.922	2.746	2.588	0.00261	0.00224
E13-16:OH	3.294	3.066	2.884	2.705	2.544	0.00260	0.00224

^a Standard 14:OH.

Table 10
GC data and vapour pressures (25°C) of octadecenols

Alcohol	Relative retention time ^a					P (Pa)	
	120°C	130°C	140°C	150°C	160°C	Eq. 1	Eq. 4
Z3-18:OH	2.676	2.500	2.400	2.288	2.200	0.000377	0.000309
E3-18:OH	2.583	2.448	2.346	2.244	2.149	0.000406	0.000333
Z9-18:OH	2.465	2.339	2.254	2.160	2.083	0.000453	0.000373
E9-18:OH	2.596	2.455	2.366	2.247	2.157	0.000402	0.000330
Z11-18:OH	2.534	2.405	2.311	2.216	2.130	0.000431	0.000354
E11-18:OH	2.637	2.497	2.391	2.275	2.181	0.000386	0.000316
Z13-18:OH	2.712	2.555	2.439	2.326	2.221	0.000363	0.000296
E13-18:OH	2.753	2.585	2.463	2.342	2.234	0.000345	0.000282

^a Standard 16:OH.

relative to both the polar and non-polar ends of the molecule is significant. As illustrated in Figs. 3 and 4, these trends may be observed both for the *Z*- and *E*-isomers in all the series investigated.

For homologous subseries such as *Z*- or *E*-isomers of 7-10:OH, 9-12:OH, 11-14:OH and 13-16:OH (ω -3 unsaturation), 5-10:OH, 7-12:OH, 9-14:OH and 11-16:OH (ω -5 unsatura-

tion) and 3-10:OH, 5-12:OH, 9-14:OH and 11-16:OH (ω -7 unsaturation), the double bond is at a constant position with respect to the non-polar end of the molecule. Analysis of the double bond effect in these subseries reveals that the vapour pressures of alkenols having different positions of unsaturation decrease in the order ω -7 > ω -5 > ω -3 > saturated. The empirical relationships given by the $\ln P$ vs. n_c expression

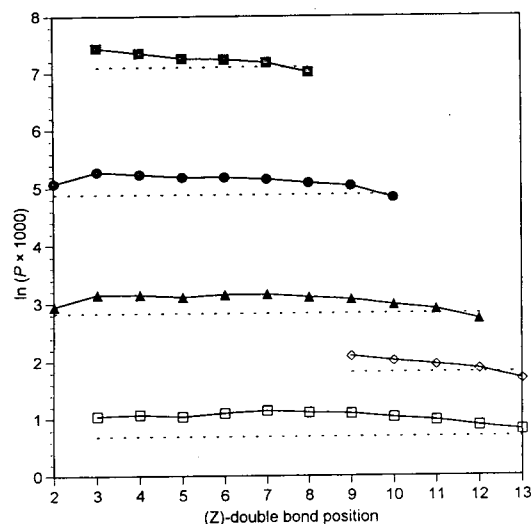


Fig. 3. Vapour pressures (Eq. 4) for (*Z*)-alkenols plotted against the respective double bond position. ■ = Decenols; ● = dodecenols; ▲ = tetradecenols; ◇ = pentadecenols; □ = hexadecenols. Dashed lines show the vapour pressures of the corresponding saturated compounds.

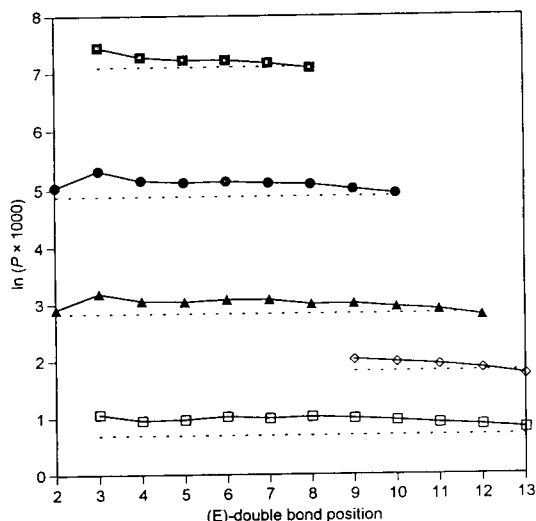


Fig. 4. Vapour pressures (Eq. 4) for (*E*)-alkenols plotted against the respective double bond position. ■ = Decenols; ● = dodecenols; ▲ = tetradecenols; ◇ = pentadecenols; □ = hexadecenols. Dashed lines show the vapour pressures of the corresponding saturated compounds.

Table 11
Proposed relationships for predicting vapour pressures at 25°C

Alcohol subseries ^a	Ln[P (Pa)] = a - bn _c		S.E. ^b	r ²
	a	b		
Saturated	10.772 ± 0.135	1.058 ± 0.010	0.0458	0.9998
ω-3-(Z)	10.904 ± 0.065	1.064 ± 0.005	0.0220	1.0000
ω-3-(E)	10.844 ± 0.081	1.060 ± 0.006	0.0276	0.9999
ω-5-(Z)	10.805 ± 0.018	1.046 ± 0.001	0.0061	1.0000
ω-5-(E)	10.849 ± 0.020	1.053 ± 0.002	0.0067	1.0000
ω-7-(Z)	10.995 ± 0.222	1.053 ± 0.017	0.0751	0.9995
ω-7-(E)	11.178 ± 0.307	1.071 ± 0.023	0.1040	0.9991

^a Number of data points, n = 6.

^b S.E. = standard error of estimate.

were obtained from analyses of the calculated (Tables 4–10) ln P data. The relevant equations, listed in Table 11, may be used to estimate vapour pressures for any set of ω-3, ω-5 and ω-7 alkenols. The quality of the fit obtained with MAD (mean average deviation) 2.3% (ω-3), 1.9% (ω-5) and 4.8% (ω-7) combined with the convenience of only one substance-specific input variable makes this an attractive approach in predicting vapour pressures of some other structurally similar derivatives.

At this point some comment should be made regarding literature vapour pressure values of unsaturated alcohols. To our knowledge, only four of the alkenols investigated in this work had literature data available for comparison. Heath and Tumlinson [29] determined the vapour pressures of Z7-12:OH, Z9-14:OH, Z11-14:OH and Z11-16:OH as 1.25, 0.177, 0.160 and 0.039 Pa, respectively. They carried out these determinations on capillary liquid crystal GC columns at “room temperature”, which probably corresponded to 30°C. At that temperature our GC method yields vapour pressures of 0.344, 0.044, 0.037 and 0.0057 Pa, respectively, for the same compounds. Hence our values are significantly (3.6–6.8 times) lower than those in Ref. [29]. Note, however, that a high degree of correlation exists between both data sets. The linear fit

may be expressed as $\ln P = (1.1716 \pm 0.0666) \ln P_{\text{Heath}} - (1.231 \pm 0.137)$ (n = 4, S.E. = 0.164, r² = 0.9936).

By utilizing the reliable literature [26] values at 30°C (see Table 1) for 12:OH (0.266 Pa) and 14:OH (0.0366 Pa), the ratio $P_{\text{alkenol}}/P_{\text{alkanol}}$ for compounds with the same number of carbon atoms may be adopted as an approximate measure of the “effect of non-terminal monounsaturation”. This vapour pressure ratio following from our data is about 1.2–1.3, which seems to be a reasonable value considering its similarity to the corresponding values common for non-terminal alkene [1] and unsaturated acetate series [20]. On the other hand, the ratio of 4.7–4.8 which follows from the use of the data from Ref. [29] appears to be unrealistically high. The reasons for this discrepancy are not clear. However, besides the imprecisely defined temperature they used, another factor might be important, viz. the use of cholesteryl p-chlorocinnamate as a stationary phase. It may be that the polar alcohols interact in a specific manner with this phase and then this factor would account for the differences in the two studies.

As the errors in the reported vapour pressures depend both on experimental uncertainties and on the accuracy of the literature vapour pressure data adopted for the reference standards, it is difficult to determine any inherent error in the present method for alcohols. Some discussion is possible, however: as to the latter error factor, recent inter-laboratory data [25,27] for 10:OH and 12:OH agree to within ±5%, which may be regarded as a very good agreement. Hence the differences between our data and those taken from the literature for alkanols are generally not greater than the experimental errors (see Table 3). On the other hand, when admitting a propagation of errors, the uncertainty might reach about 10%. Moreover, the vapour pressures for 15:OH and 16:OH were obtained by (prudent) extrapolation and additionally corrected for melting points. It is unlikely that they are in serious error (see the internal homogeneity of the alkanol data illustrated in Fig. 1), but we have to accept their lower accuracy. Taken

together, we assume that, at worst, the errors may combine to give an overall uncertainty in vapour pressures of about 15%.

4. Conclusions

This study has demonstrated the successful application of the capillary GC method to the determination of the vapour pressures of unsaturated alcohols whose generally low thermal stability causes difficulties in direct measurements by conventional physico-chemical methods. The method yields reasonable vapour pressure values for both the alkanols and alkenols at 25°C provided that a compound of similar structure and polarity is used as the reference standard. It is hoped that these new values may considerably extend the database for the vapour pressures of alcohols, and enable entomologically oriented chemists to study and model the physical behaviour of pheromone-like compounds in the environment more accurately.

The method is currently being used to determine vapour pressures of unsaturated aldehydes and will be the subject of a separate report.

Acknowledgement

This work was financially supported, in part, by Grant No. DHR-5600-G-00-1051-00, Program in Science and Technology Cooperation, from the US Agency for International Development.

References

- [1] R.C. Reid, J.M. Prausnitz and B.E. Poling, *The Properties of Gases and Liquids*, McGraw-Hill, New York, 4th ed., 1987.
- [2] R.D. Shaver, R.L. Robinson, Jr., and K.A.M. Gasem, *Fluid Phase Equilib.*, 64 (1991) 141.
- [3] D. Ambrose, J.H. Ellender and C.H.S. Sprake, *J. Chem. Thermodyn.*, 6 (1974) 909.
- [4] R.D. Gray, Jr., J.L. Heidman, R.D. Springer and C. Tsionopoulos, *Fluid Phase Equilib.*, 53 (1989) 355.
- [5] D. Mackay and S. Paterson, *Environ. Sci. Technol.*, 25 (1991) 427.
- [6] D. Mackay, S. Paterson and W.Y. Shiu, *Chemosphere*, 24 (1992) 695.
- [7] J.H. Tumlinson, in R.L. Ridgway, R.M. Silverstein and M.N. Iscoe (Editors), *Behavior-Modifying Chemicals for Insect Management—Applications of Pheromones and Other Attractants*, Marcel Dekker, New York, 1990, Ch. 5.
- [8] A. Shani, *Role of Pheromones in Integrated Pest Management*, Institutes for Applied Research, Ben-Gurion University of the Negev, Beer-Sheva, Israel, 1991.
- [9] W.F. Spencer and M.M. Cliath, *Residue Rev.*, 85 (1983) 57.
- [10] W.J. Sonnefeld, W.H. Yoller and W.E. May, *Anal. Chem.*, 55 (1983) 275.
- [11] J.J. Murray, R.F. Pottie and C. Pupp, *Can. J. Chem.*, 52 (1974) 557.
- [12] D.J. Hamilton, *J. Chromatogr.*, 195 (1980) 75.
- [13] T.F. Bidleman, *Anal. Chem.*, 56 (1984) 2490.
- [14] J.W. Westcott and T.F. Bidleman, *J. Chromatogr.*, 210 (1981) 331.
- [15] B.D. Eitzer and R.A. Hites, *Environ. Sci. Technol.*, 22 (1988) 1362.
- [16] Y.-H. Kim, J.E. Woodrow and J.N. Seiber, *J. Chromatogr.*, 314 (1984) 37.
- [17] D. Hawker, *Chemosphere*, 25 (1992) 427.
- [18] P.M. Sherblom, P.M. Gschwend and R.P. Eganhouse, *J. Chem. Eng. Data*, 37 (1992) 394.
- [19] S. Husain, P.N. Sarma, G.Y.S.K. Swamy and K. Sita Devi, *J. Am. Oil Chem. Soc.*, 70 (1993) 149.
- [20] B. Koutek, M. Hoskovec, K. Konečný and J. Vrkoč, *J. Chromatogr.*, 626 (1992) 215.
- [21] D.A. Hinckley, T.F. Bidleman, W.T. Foreman and J.R. Tushall, *J. Chem. Eng. Data*, 35 (1990) 232.
- [22] W.Y. Shin and D. Mackay, *J. Phys. Chem. Ref. Data*, 15 (1986) 911.
- [23] D. Mackay, A. Bobra, D.W. Chan and W.Y. Shin, *Environ. Sci. Technol.*, 16 (1982) 645.
- [24] D.R. Lide (Editor), *CRC Handbook of Chemistry and Physics*, CRC Press, Boca Raton, FL, 72nd ed., 1991–92.
- [25] T. Nitta, K. Morinaga and T. Katayama, *Ind. Eng. Chem. Fundam.*, 21 (1982) 296.
- [26] J. N'Guimbi, H. Kaseghari, I. Mokbel and J. Jose, *Thermochim. Acta*, 196 (1992) 367.
- [27] K. Růžička and V. Majer, *Fluid Phase Equilib.*, 28 (1986) 253.
- [28] M. Mansson, P. Sellers, G. Stridh and S. Sunner, *J. Chem. Thermodyn.*, 9 (1977) 91.
- [29] R.R. Heath and J.H. Tumlinson, *J. Chem. Ecol.*, 12 (1986) 2081.



ELSEVIER

Journal of Chromatography A, 679 (1994) 319–328

JOURNAL OF
CHROMATOGRAPHY A

Carbon dioxide supercritical fluid extraction of incinerator fly ash with a reactive solvent modifier

J.W. Hills^{a,1}, H.H. Hill, Jr.^{a,*}, D.R. Hansen^b, S.G. Metcalf^b

^a*Department of Chemistry, Washington State University, Pullman, WA 99164, USA*

^b*Westinghouse Hanford Company, Richland, WA 99352, USA*

First received 4 May 1993; revised manuscript received 30 November 1993

Abstract

Carbon dioxide supercritical fluid extraction was used to extract polycyclic aromatics, halogenated phenols, halogenated aromatics and dioxins from a municipal incinerator fly ash matrix. The extraction solvent was modified with methanol or a reactive solvent modifier, N,O-bis-trimethylsilyl-trifluoroacetamide (BSTFA), which was added to the sample before extraction. Extracts, obtained at two temperatures and with three supercritical fluid formulations, were analyzed by the US Environmental Protection Agency contract laboratory program GC-MS procedure for semi-volatile organic compounds. Average recoveries of surrogate analytes with pure carbon dioxide and carbon dioxide modified with methanol were 50% (500 atm and 100°C). Average recoveries were 82% at 100°C and 54% at 30°C with BSTFA present. Carbon dioxide modified with methanol was found to be less efficient than carbon dioxide modified with BSTFA. Unlike earlier uses of reactive modifiers, the acidic and phenolic components were determined as the free acids and phenols. Hydrolysis of trimethylsilyl derivatives of phenols, produced by the modifier during the extraction, with methanol reproduced the free phenols. At 60°C the average hydrolysis yield of the four phenols was 96.7%. This hydrolysis step also allowed analysis of free acids by standard methods.

1. Introduction

The advantages of supercritical fluid extraction (SFE) are listed elsewhere [1], but primarily include speed and reduced solvent waste. Solvents used in SFE are gases at room temperatures and pressures. This simple fact gives SFE a great speed advantage over conventional liquid

extraction techniques. Extracts produced by liquid methods using solvents such as methylene chloride must be concentrated from hundreds of milliliters to just a few milliliters. This requires time, provides an opportunity for analyte loss and release of chlorinated solvent into the atmosphere and produces waste solvent. The supercritical solvents which are gases at standard temperatures and pressures are easily removed from the extract at room pressure. However, solvents such as carbon dioxide enable extraction of only non-polar and weakly adsorbed compounds.

A major limitation of SFE is its inability to

* Corresponding author.

¹ Present address: Washington State University, Tri-Cities, Richland, WA 99352, USA.

extract polar and strongly adsorbed analytes. Common SFE solvents, like carbon dioxide, lack the intermolecular cohesive solvent strength needed to overcome the energy of adsorption binding the analyte to the sample matrix. One technique used to increase the solvent strength of the supercritical fluid is to introduce small amounts of polar solvent modifiers to the extracting solvent [2,3]. Polar modifiers act in two ways. First, the overall polarity of the extraction solvent is raised, increasing the solubility of polar analytes in the fluid. Second, the modifier competes with the analytes for the same adsorptive sites to which the analytes are adsorbed. Displacement of the analyte from the sample matrix by the solvent modifier drives the analyte into solution. Presumably the stronger a modifier's affinity with adsorptive sites of the matrix the more pronounced the displacement effect.

The objective of the project was to evaluate the potential of coupling standard US Environmental Protection Agency (EPA) methods such as the EPA contract laboratory program (CLP) gas chromatography with mass spectral detection (GC–MS) method for semi-volatile compounds with SFE using the reactive modifier approach for the determination of organic compounds from highly adsorptive matrices such as municipal incinerator fly ash. To achieve this objective, the experiments were divided into three phases.

Because the use of reactive modifiers produces derivatized analytes and the EPA CLP GC–MS method for semi-volatile compounds was designed for underivatized compounds, phase I of the project tested a collection method in which derivatized analytes were hydrolyzed back to their original form before GC–MS analysis. Phase II of the project compared the extraction efficiencies of pure supercritical carbon dioxide, carbon dioxide modified with methanol and carbon dioxide modified with a derivatizing reagent at both high (100°C) and low (30°C) temperatures. Finally phase III: identification and quantification of native compounds by the EPA CLP GC–MS method for semi-volatile compounds.

2. Experimental

2.1. Instrumentation

Supercritical fluid extractor

The extractor was purchased from ISCO (Lincoln, NE, USA) and consisted of a syringe pump (Model 260D) and a stainless-steel extraction unit (Model SFX 2-10) with heating block and two extraction cells. Each extraction cell consisted of a metal tube with an internal volume of 10 ml and was capped at both ends with threaded stainless-steel caps containing 2- μ m stainless-steel frit filters. The extraction cells were held at the extraction temperature within an aluminum heating block. Pressure was maintained in the extraction cells with a deactivated 20 cm \times 50 μ m I.D. fused-silica capillary flow restrictor and a partially opened exit valve. The low pressure end of the restrictor was placed in a solvent trap containing 0.5 ml methanol. The solvent trap has been described elsewhere [4].

Gas chromatography–mass spectrometry

The GC–MS system used in these experiments was that recommended by the EPA CLP method. It consisted of a Hewlett-Packard 5890 gas chromatograph fitted with a 5970 mass-selective detector.

Chromatographic operating conditions for all experiments in this project were as follows: The chromatographic column was a 30 m Rtx-5 fused-silica capillary column (Resteck, Bellefonte, PA, USA). The carrier gas was helium at 1 ml/min. All separations were temperature programmed with an initial column temperature of 40°C with no hold time. The oven was programmed from 40 to 270°C at 10°C/min with a final hold of 35 min. The injection port temperature was maintained at 270°C.

Operating conditions for the mass spectrometer were as follows: the ion source for the mass selective detector was held constant at 250°C. The voltage for the electron impact ion source was operated at 70 V, but was not turned on until the solvent and reagent byproducts had eluted from the chromatographic column, 8.5 min after

injection. For some samples the detector was operated in the scanning mode, for others it was operated in a selective ion monitoring mode.

Gas chromatography–flame ionization detection

Determinations concerning phase I of this project, the hydrolysis of the extracted derivatives, were made on a chromatograph identical to the one described above but fitted with a flame ionization detector. Identifications were made by matching retention times with those of standards.

2.2. Experimental procedures

The project was divided into three phases: hydrolysis of trimethylsilyl (TMS) derivatives, extraction of surrogate analytes, and, finally, the extraction and analytical determination of several native organic compounds in municipal fly ash. Experimental procedures for each phase of the project are given below.

Phase I: Hydrolysis of TMS derivatives

To determine if TMS derivatives of semi-volatiles could be quantitatively converted to their underivatized form upon collection from the supercritical fluid extractor, a mixture of surrogate compounds were derivatized and then collected and hydrolyzed upon collection in methanol. The test mixture used in this phase of the project included 1 $\mu\text{g}/\mu\text{l}$ each of the following eight compounds dissolved in methylene chloride: 2-fluorophenol (2FP), phenol- d_5 (PHL), 2-chlorophenol (2CP), dichlorobenzene- d_4 (DCB), nitrobenzene (NBZ), 2-fluorobiphenyl (FBP), tribromophenol (TBP) and terphenyl- d_{14} (TPH). A “d” at the end of a compound name indicates that the compound was deuterated, the number at the “d” is the number of protons replaced. A 10- μl aliquot of this 1 $\mu\text{g}/\mu\text{l}$ test mixture was placed in a 0.5-ml quantity of trap solvent methylene chloride and treated with 100 μl of the neat commercial grade derivatization reagent N-O-bis trimethylsilyl-trifluoroacetamide (BSTFA) (Pierce, Rockford, IL, USA). Derivatization was conducted for 15 min at 80°C.

After derivatization, the 0.5-ml aliquot of the sample was diluted to 2.0 ml with methanol to simulate the collection process. The process described above resulted in methanol solutions of the hydrolyzed surrogate compounds at the 4 $\mu\text{g}/\mu\text{l}$ level.

These hydrolyzed solutions were analyzed by GC–flame ionization detection (FID) by making a 1- μl splitless injection of the extract. The complete derivatization, hydrolysis and analysis steps were repeated three times at different temperatures to obtain the data presented in Table 1.

Phase II: Extraction of surrogate analytes

The extraction efficiency of the three solvents was compared for the extraction of a mixture of test compounds from a municipal fly ash matrix. The three solvent formulations compared were (1) pure supercritical carbon dioxide, (2) supercritical carbon dioxide modified with methanol and (3) supercritical carbon dioxide modified with a derivatizing reagent. The test mixture was the same as that used for the hydrolysis studies and corresponded to the surrogate analytes required in the EPA CLP method for the extraction of semi-volatiles from solid matrices. They were the same as listed in phase I. The municipal fly ash sample was from the municipal waste incinerator, Toronto, Canada and was obtained in bulk from samples collected by

Table 1
Derivatization and hydrolysis yields of surrogate analytes

Compound	Yield (%) at		
	25°C	60°C	80°C
2FP	96	95	96
PHL	62	83	87
2CP	95	95	95
DCB	98	96	97
NBZ	97	95	95
FBP	99	98	91
TBP	100	101	101
TPH	106	112	111

Professor K.W. Karasek and Dr. K.P. Naikwadi of the University of Waterloo, Waterloo, Canada.

Pre-extraction treatment

The procedure for all of the extractions was the same. A 6-g sample of fly ash was loaded into a 10-ml extraction cell. Then, the surrogate compounds were added to the sample matrix in two mixtures, base-neutrals (1,2-dichlorobenzene- d_4 , nitrobenzene- d_5 , 2-fluorobiphenyl and terphenyl) at a concentration of $1 \mu\text{g}/\mu\text{l}$ for each compound and acids (2-fluorophenol, phenol- d_5 , 2-chlorophenol- d_4 and 2,4,6-tribromophenol) at a concentration of $1.5 \mu\text{g}/\mu\text{l}$ for each compound. After application of the surrogate analytes, $10 \mu\text{l}$ of each solution, the solvent was allowed to evaporate at room temperature for fifteen minutes before the extraction cell was sealed or modifiers were added.

Modifiers for the extractions were added as liquids directly to the fly ash samples. When methanol was the modifier, $500 \mu\text{l}$ of pure methanol were injected onto the fly ash sample. When neat BSTFA was the modifier, $250 \mu\text{l}$ of the commercially purchased solution were injected. Additions of larger volumes, 500 and $750 \mu\text{l}$, made no significant difference in extraction efficiency. After the addition of the modifier, the sample cell was sealed and pressurized to 500 atm (1 atm = 101 325 Pa) with pure carbon dioxide.

Extraction

The extraction process was a two-step procedure. First, a static extraction was conducted for 5 min at 500 atm and at 30 or 100°C . This initial static extraction period was followed by a dynamic extraction in which carbon dioxide flowed through the cell at a rate of 0.1–0.3 ml/min measured at the pump. At this rate, approximately four cell volumes of the solvent were passed over the sample in a 3- to 4-h extraction. A partially opened exit valve was used to retard and control and carbon dioxide

flow. This low flow-rate was required in order to achieve a high trapping efficiency.

Sample collection

The analyte trap contained 1 ml of a methanol–methylene chloride (3:1, v:v) mixture into which the fused-silica capillary restrictor was placed such that the supercritical carbon dioxide was depressurized in the solution, depositing the analytes in solution. If required, the trapping solvent could be heated after collection to insure quantitative conversion of the derivatives to their underivatized form. During the sample collection process, some of the trapping solvent was evaporated. After extraction, methylene chloride was added to bring the volume back to 1.0 ml.

Internal standards

In addition, $5 \mu\text{l}$ of an internal standard solution were added to the 1.0 ml extract solution. The internal standard consisted of 1,4-dichlorobenzene- d_4 , naphthalene- d_{10} , acenaphthene- d_{14} , phenanthrene- d_{10} , chrysene- d_{12} and perylene- d_{12} at concentrations of $4 \mu\text{g}/\mu\text{l}$ for each component. Thus, the final concentration of each 1.0-ml sample extract was $20 \text{ ng}/\mu\text{l}$ of each standard. The extract was then transferred to the auto sampler where $2\text{-}\mu\text{l}$ injections were made into the GC–MS system with no further preparation.

Phase III: Extraction of native analytes

Identification of the native analytes which were adsorbed onto the fly ash was accomplished as described in EPA CLP Semi-Volatile Method. Target components were also quantified by the internal standard method. A list of the internal standards is given in the section above. The target compounds, internal standards, and surrogates were identified by direct comparison of the sample mass spectrum to the mass spectrum of a standard of the suspected compound. Before an analyte identification was verified, two criteria were satisfied: The analyte eluted from a GC at the same relative retention time as the standard and the mass spectrum of the analyte matched that of the standard.

3. Results and discussion

Recently we proposed that stronger affinity with the matrix active sites can be achieved if the modifier reacts with, rather than simply adsorbs to, the surface [4,5]. The addition of chemical reagents to the extraction solvent to act as reactive solvent modifiers has been used to extract several matrices. Reactions employed thus far are silylation [5], and methyl esterification [3]. This laboratory has shown silylation reagents are applicable to the extraction of polar and acidic compounds from biological samples, sediments and air particulates. Conversion of polar analytes, such as fatty acids and diacids, to the silyl derivatives during the extraction rendered them more soluble in the non-polar extraction fluid. The non-polar derivatized analytes were readily extracted and determined by GC. Interestingly, compounds that were inert to the derivatization reagent also benefited from the presence of the reagent. This benefit arose from the action of the reagent on the matrix. Compounds adsorbed by hydrogen bonding to the matrix surface was released when the surface moiety was converted to the TMS derivative. The strength of a hydrogen bond is about one tenth that of a covalent bond. Thus the displacement of the adsorbed molecule by a covalently bonded TMS group was energetically favored over temporary and weaker displacement by non-reactive modifiers.

While the first approach, the addition of polar modifiers, has been investigated extensively for both SFE and supercritical fluid chromatography, the second approach, the addition of reactive modifiers, has been used in the extraction of only a few matrices such as coffee beans, tea, marine sediment, agricultural soil, airborne particulate matter and sewage sludge. All of these studies have involved matrices which could be classified as moderately polar. Fly ash from incinerators, however, is a highly adsorptive and oxidized matrix and is difficult to extract using pure supercritical carbon dioxide or even supercritical carbon dioxide with polar modifiers. The difficulty of extracting municipal incinerator

fly ash has been demonstrated. In these studies matrix destruction with acid treatment was required for extraction of chlorinated dibenzo-*p*-dioxins and dibenzofurans [6].

3.1. Phase I: Hydrolysis of TMS derivatives

Simultaneous supercritical fluid chemical derivatization and extraction (SFDE) normally has been followed by analysis of the target analytes as their derivatives. However, standard analysis methods, such as EPA CLP method employed in this work, are often designed to determine the underivatized analyte. For example, the EPA CLP method used in this work is designed to monitor free phenols or acids rather than the TMS derivatives of these compounds. Thus, in order to use the EPA CLP method, an easy, quantitative conversion of the extracted analyte back into the native compound was needed. This was achieved by simply collecting the derivatized extract in methanol. Methanol hydrolysed TMS esters back to free acids and phenols during the collection of the extract.

Fig. 1a shows a total ion chromatogram for the test mixture of surrogate compounds, demonstrating retention times of these underivatized compounds. Fig. 1b shows a typical chromatogram for this mixture after derivatization with BSTFA. From these two chromatograms, it was clear that the derivatization process was nearly quantitative. Peaks for 2FP, PHL, 2CP and TBP are missing in Fig. 1b compared with Fig. 1a. Instead, four new peaks appear in Fig. 1b which correspond to the TMS derivatives of these four phenolic compounds. It was interesting to note the effect that the derivative had on chromatography. The TMS-2FP derivative eluted faster than its underivatized analogue while the derivatives of the other three phenols eluted later than their underivatized counterparts. Those test compounds which do not form derivatives, DCB, NBZ, FBP and TPH, occurred at the same elution time in both chromatograms. Note that in Fig. 1b, the relative sensitivity of the derivatized compounds is greater than the underivatized compounds. This is one advantage of derivatiza-

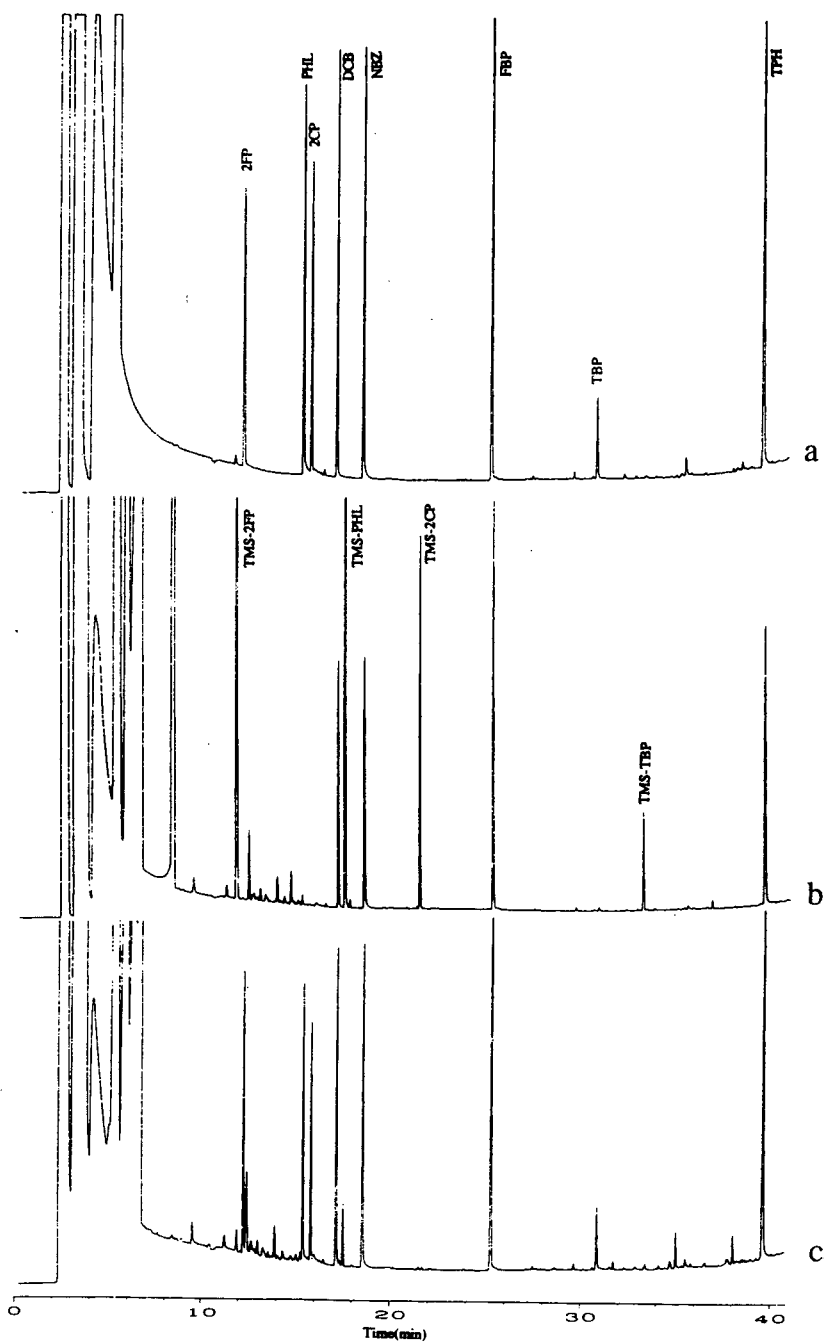


Fig. 1. Gas chromatograms of surrogate analytes. The original eight compounds: 2-fluorophenol (2FP), phenol- d_5 (PHL), 2-chlorophenol (2CP), dichlorobenzene- d_4 (DCB), nitrobenzene (NBZ), 2-fluorobiphenyl (FBP), tribromophenol (TBP), terphenyl- d_{14} (TPH) are seen in the top trace (a). The middle trace (b) is the same mixture after treatment with BSTFA. The label "TMS" indicates the trimethylsilyl derivative of the analyte. The bottom trace (c) is the derivatized mixture after hydrolysis with methanol. Analysis conditions: 1- μ l splitless injection of the extract was made on to a 30 m Rtx-5 capillary column held at 40°C. The column temperature was raised at 10°C/min to 270°C where it was held 35 min.

tion, but requires that the method be calibrated for the derivative rather than the native compound. Thus, in order to conform to previously described methods, the derivatives were hydrolyzed back to the native compound for detection as shown in Fig. 1c. In this third chromatogram, the native peaks reappear and the chromatogram resembles that of Fig. 1a. Table 1 presents the results of the hydrolysis experiments. At all temperatures the hydrolysis, except for PHL, was better than 90% complete.

3.2. Phase II: Extraction of surrogate analytes

Use of surrogate compounds to spike the fly ash matrix was not anticipated to render information on how well native compounds might be desorbed from the matrix but was expected to provide information on the efficiency at which desorbed compounds were removed from the extraction cell and trapped in the collection cell. In addition, they provide information on sample loss due to irreversible adsorption and other losses during the extraction process. Fig. 2 shows the GC-MS reconstructed ion chromatograms of the fly ash extract produced at 500 atm and 100°C with pure carbon dioxide (Fig. 2a), carbon dioxide with methanol (Fig. 2b) and carbon dioxide with BSTFA (Fig. 2c).

Table 2 compares the recoveries found for each of the surrogate compounds after extraction with pure carbon dioxide, methanol modified carbon dioxide and BSTFA modified carbon dioxide. It is interesting to note the trend in the extraction efficiency of the pure carbon dioxide. With the exception of nitrobenzene, extraction efficiency decreases as the elution time of the analyte increases (analytes are listed in order of increasing chromatographic elution time). This indicates that the extraction efficiency of pure supercritical carbon dioxide was determined primarily by the vapor pressure of the analyte. This trend is less noticeable with the methanol modified extraction and is not seen in the BSTFA-modified extraction. One explanation was that compounds with higher heats of vaporization, greater cohesive energy between themselves and

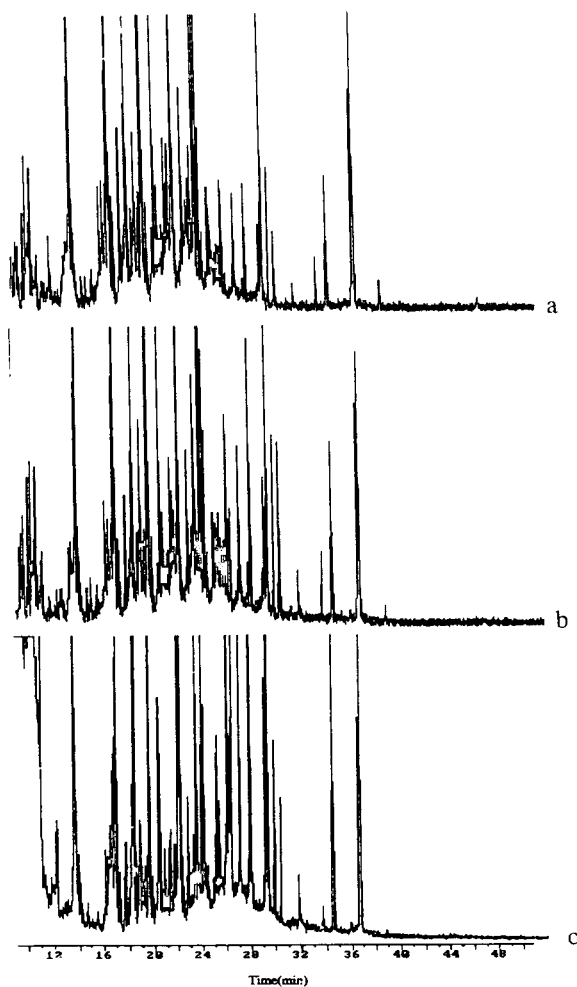


Fig. 2. Gas chromatograms of fly ash extract. Extraction conditions: 30°C, 500 atm, carbon dioxide with 250 μ l BSTFA. Analysis conditions: 2- μ l splitless injection of the extract was made on to a 30 m Rtx-5 capillary column held at 40°C. The column temperature was raised at 10°C/min to 270°C where it was held 35 min.

the matrix surface, were adsorbed to the surface more strongly. Supercritical carbon dioxide could not overcome this adsorption energy. Methanol could disrupt the matrix-analyte cohesion and thus desorbed the compounds to some extent. BSTFA completely displaced these compounds from the surface; it was able to overcome the adsorptive forces.

Table 2
Recoveries of surrogate analytes from municipal incinerator fly ash matrix

Compound	Recovery (%)			
	CO ₂ , 100°C	CO ₂ with MeOH, 100°C	CO ₂ with BSTFA	
			30°C	100°C
PHL	69 (11) ^a	80 (4)	46 (10)	100 (3)
2CP	65 (3)	35 (1)	61 (7)	86 (20)
DCB	69 (12)	55 (21)	89 (16)	102 (4)
NBZ	38 (53)	5 (3)	48 (3)	103 (5)
FBP	75 (7)	62 (26)	32 (1)	116 (5)
TBP	35 (19)	62 (14)	40 (40)	48 (17)
TPH	27 (9)	4 (2)	31 (6)	106 (2)
Average	54 (20)	43 (10)	50 (12)	94 (8)

^a Values in parentheses are % relative standard deviations.

3.3. Phase III: Extraction of native analytes

A problem in extraction studies for trace organic analysis is that spiked analytes do not necessarily mimic the adsorptive behaviour of native analytes. Native analytes which have been “weathered” often do not behave in the same manner as their spiked standards. In this section of the study, twelve native compounds were

identified on the fly ash and their extraction yields were compared for the three solvents. These semi-volatile analytes were identified in the fly ash extracts following qualitative procedures used in EPA CLP methods and are listed in Table 3. At these low levels (ng/g), isomers of the dichlorobenzenes and the trichlorophenols could not be identified separately with certainty.

Quantitative data for each of these compounds

Table 3
Native compounds identified in municipal waste incinerator fly ash

Compound	ng/g			
	CO ₂ , 100°C	CO ₂ with MeOH, 100°C	CO ₂ with BSTFA	
			30°C	100°C
Phenol	nd	32	43	110
Dichlorobenzenes	75	140	120	170
N-nitroso-di-N-propylamine	68	24	130	300
1,2,4-Trichlorobenzene	110	190	110	56
Benzoic acid	22	320	37	96
4-Methyl naphthalene	nd	10	30	37
Trichlorophenols	nd	59	nd	450
Acenaphthylene	77	54	20	101
Acenaphthene	nd	77	37	150
N-nitrosodiphenylamine	nd	29	20	47
Dibenzofuran	nd	nd	nd	13
Hexachlorobenzene	36	46	46	170

nd = Not detected.

are given for each extraction method. With pure carbon dioxide as the extraction solvent, no native phenols were detected in the sample. However, when methanol was added to the sample as a modifier, both phenol and the trichlorophenols were found. When BSTFA was used as the modifier, a several fold increase in extraction efficiency over the methanol modified extraction was observed for several compounds. Of the twelve native compounds identified, ten showed significantly better extraction yields when BSTFA was used as the modifier. This was not the case for 1,2,4-trichlorobenzene and benzoic acid. These compounds were extracted better with the methanol modified solvent. In addition to this seemingly contradictory evidence, relative standard deviations for the BSTFA extraction of these two compounds were the highest observed in this study, 140% for 1,2,4-trichlorobenzene and 100% for benzoic acid. Other relative standard deviations for the native analytes at the ng/g level ranged from 1% for acenaphthylene to 84% for phenol and dibenzofuran.

On the whole, however, the evidence is relatively clear that native compound extraction was more efficient with BSTFA than with methanol or pure carbon dioxide although extraction precision was not as high as we have come to expect with the more traditional Soxhlet extraction method.

3.4. Temperature effects

The solvation strength of a supercritical fluid is a function of density. According to Czubryt et al. [7] who used an argument based on Hildebrand solubility parameters (see Ref. [8]), the more dense and liquid-like the more solvation power the fluid has. That is, at lower temperatures the fluid could more readily overcome the affinity an adsorbed molecule has for the surface to which it is adsorbed. However, adsorbed molecules can overcome the energy barrier and desorb from a surface by thermal energy. Increasing the extraction temperature would decrease the density of the extraction fluid but at the same time give adsorbed molecules more thermal energy to

overcome the desorption energy barrier. These two views would seem to be at odds with each other. Extractions were made at two temperatures, 30°C (1.0 g/ml) and 100°C (0.80 g/ml), to determine if solvent strength or temperature controlled yields from this matrix.

The recoveries of the surrogates, Table 2, implied that the surrogates adsorbed irreversibly to the fly ash matrix at 30°C while at 100°C they eluted with much less adsorption. Concurrently, the yields at the higher temperature also suggest that it is the better extraction temperature. The total yield of quantified compounds in the 100°C extraction was determined to be 1.7 μg compared to a total yield of 0.60 μg for the 30°C extract. Although not conclusive, it appears that the higher temperature not only desorbs native compounds better but might also prevent the surrogates from adsorbing. The higher thermal energy is postulated to prevent the native analytes from re-adsorbing once solvated in the extraction solvent. The solvation strength view of supercritical fluid extraction does not address adsorption of analytes.

3.5. Chlorinated dioxins

Although these experiments were not designed to determine chlorinated dioxins, the presence of several dioxin precursors (dichlorobenzenes, trichlorobenzene and trichlorophenols) in the fly ash suggested that dioxin may also be present. However, even though chlorinated dioxins are known to form on the surface of fly ash after combustion [9], no dioxins were detected in the extracts when the mass spectrometer was operated in its less sensitive scanning mode. To increase sensitivity, single ion monitoring was used to produce the selective chromatograms shown in Fig. 3. Fig. 3a shows the selective ion chromatogram of m/z 322 that is the molecular ion for tetrachloro-dibenzo-dioxin. Five peaks can be seen in the chromatogram. The identities of the two peaks with retention times of around 27 min were confirmed as two TCDD isomers by a second selective ion chromatogram. Fig. 3b shows this m/z 257 ion chromatogram. This mass corresponds to the molecular ion minus COCl

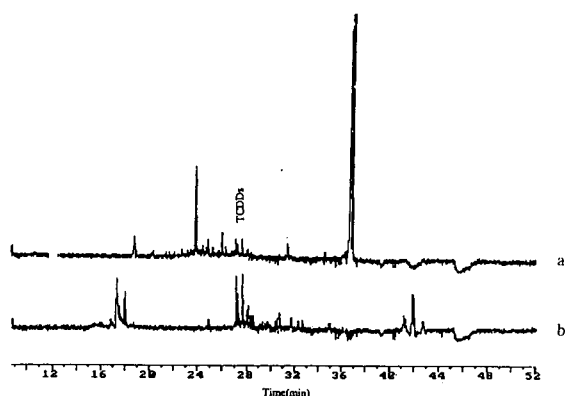


Fig. 3. Selective ion chromatograms of tetrachlorodioxins (TCDDs). (a) Selective ion chromatogram of the M^+ ion at m/z 322. Selective ion chromatogram for the $(M - COCl)^+$ ion at m/z 257. Chromatographic and analysis conditions as in Fig. 2.

($M - 63$). The relative intensities of the two ions are consistent with mass spectra of these compounds [10].

Although quantitative data were not obtained for these compounds, it is encouraging that these compounds were observed when BSTFA was used with supercritical fluid extraction even though the ash was not pretreated with HCl before extraction and no clean-up procedures were used after extraction to decrease chemical noise. Pure carbon dioxide or carbon dioxide modified with methanol is generally not sufficient to extract chlorinated dioxins unless the ash has been treated with HCl to remove heavy metals prior to extraction.

4. Conclusions

The use of a derivatizing reagent, such as BSTFA, as an additive to solid samples, even highly reactive samples such as municipal incinerator fly ash, enhanced the extraction efficiency of supercritical carbon dioxide for the many semi-volatile compounds extracted from these matrixes. For analytes which form silyl derivatives, this enhancement in extraction efficiency is attributed to both the higher solubility of the derivatives in supercritical carbon dioxide and the disruption of the analyte–matrix inter-

action by derivatization. For semi-volatile compounds, which do not form silyl derivatives, disruption of the analyte–matrix interaction enhanced extraction efficiency as well. By collecting silylated analytes in a solvent of methanol after SFE, silyl derivatives are converted back to their native form. The extracts can then be analyzed by standardized procedures such as the EPA CLP method for semi-volatile compounds. The effect of temperature on extraction efficiency was found to be significant and as effective as the solvent conditions investigated.

Acknowledgements

This research was supported in part by the Northwest College and University Association for Science under Grant DE FG06-89ER-75522 with the US Department of Energy (J.W.H.) and by the Bayerisches Institut für Abfallforschung (H.H.H.). In addition, the authors thank Ms. Cindy Jergensmeier for her contributions to the GC–MS analysis and Dr. K.P. Naikwadi and Professor F.W. Karasek of the University of Waterloo, Canada for supplying the fly ash used in this study.

References

- [1] S.B. Hawthorne, *Anal. Chem.*, 62 (1990) 633A.
- [2] J.R. Wheeler and M.E. McNally, *J. Chromatogr. Sci.*, 27 (1989) 534–539.
- [3] S.B. Hawthorne, D.J. Miller, D.E. Nivens and D.C. White, *Anal. Chem.*, 64 (1992) 405.
- [4] J.W. Hills and H.H. Hill, *J. Chromatogr. Sci.*, 30 (1993) 6–12.
- [5] J.W. Hills, H.H. Hill and T. Maeda, *Anal. Chem.*, 63 (1991) 2152–2155.
- [6] N. Alexandrou and J. Pawliszyn, *Anal. Chem.*, 61 (1989) 2770.
- [7] J.J. Czubryt, M.N. Myers and J.C. Giddings, *J. Phys. Chem.*, 74 (1970) 4260–4266.
- [8] A.F. Brown, *Chem. Rev.*, 75 (1975) 731–753.
- [9] K.P. Naikwadi, F.W. Karasek and H. Hatano, *J. Chromatogr.*, 511 (1990) 281–290.
- [10] R.A. Hites, *CRC Handbook of Mass Spectra of Environmental Contaminants*, CRC Press, Boca Raton, FL, 1990.

Supercritical fluid chromatographic determination of tocopherols on an ODS-silica gel column

Takashi Yarita^{a,*}, Akira Nomura^a, Kouichi Abe^b, Yasuhiko Takeshita^c

^a*Department of Analytical Chemistry, National Institute of Materials and Chemical Research, Tsukuba, Ibaraki 305, Japan*

^b*Tokyo Research Laboratory, Eisai Co., Ltd., Bunkyo, Tokyo 112, Japan*

^c*Faculty of Engineering, Kokushikan University, Setagaya, Tokyo 154, Japan*

First received 8 March 1994; revised manuscript received 26 May 1994

Abstract

A method for the supercritical fluid chromatographic (SFC) determination of tocopherols in vegetable oils was investigated using an ODS-silica gel column with carbon dioxide as the mobile phase. The retention of tocopherols was affected by the density of the mobile phase and the addition of methanol as a modifier. The addition of small concentrations of methanol produced a satisfactory separation of tocopherol homologues, including the positional isomers β - and γ -tocopherol. The results of the determination of tocopherols in vegetable oils by SFC were in satisfactory agreement with those obtained by normal-phase HPLC.

1. Introduction

Tocopherols are well known as components of vitamin E. Four compounds, 5,7,8-trimethyltolcol (α -tocopherol), 5,8-dimethyltolcol (β -tocopherol), 7,8-dimethyltolcol (γ -tocopherol) and 8-methyltolcol (δ -tocopherol), are widely distributed in the natural products and their biological activities as vitamin E are different from one another.

HPLC using fluorescence or UV detection is a popular technique for determining tocopherols because of the simplicity and precision [1,2]. There have been many reports on the determination of tocopherols by HPLC under normal- and reversed-phase conditions. However, the separation of the positional isomers β - and γ -

tocopherol under reversed-phase conditions has not been reported.

In recent years, supercritical fluid chromatography (SFC) has been developed as separation technique that is a bridge between GC and LC. Carbon dioxide is usually used as the mobile phase in SFC because of its critical properties and safety. However, the addition of a modifier to the mobile phase is often required in order to improve the retention and the peak shapes [3–9]. In packed-column SFC, a UV detector is widely used when an organic solvent is added to the mobile phase. A fluorescence detector can be expected to have higher sensitivity and greater selectivity than a UV detector for the detection of fluorescent species. However, the use of fluorescence detectors in SFC is not convenient owing to the pressure resistivity of the cell.

SFC has been applied to the determination of

* Corresponding author.

tocopherols. Upmoor and Brunner [10] described the retention behaviour of α -tocopherol on various stationary phases. The retention of α -tocopherol decreased with increasing methanol concentration in the mobile phase. Perrin and Prevot [11] reported the separation of tocopherols by SFC on a silica gel column. The elution order of tocopherols in this study was similar to that in normal-phase HPLC. Saito and co-workers [12,13] demonstrated the enrichment of α - and β -tocopherol from wheat germ powder by semi-preparative SFC and supercritical fluid extraction. They also demonstrated the isolation of α - and β -tocopherol using a recycle SFC system [14].

In this paper, we report the determination of tocopherols by SFC on an ODS-silica gel column. The effects of methanol used as a modifier on the retention and the separation of tocopherols and the application of the method to vegetable oil analysis are described.

2. Experimental

2.1. Equipment

SFC system

A Shimadzu (Kyoto, Japan) LC-6A pump was used to deliver carbon dioxide. The pump head was cooled so as to maintain a stable flow. An Isco (Lincoln, NE, USA) Model 100 DM pump was used to deliver methanol. A DKK (Tokyo, Japan) LSA-M mixer was used for mixing carbon dioxide and methanol. A Rheodyne (Cotati, CA, USA) Model 7125 sample injector with a 20- μ l sample loop was used for sample injection. The separation column was kept at 40°C in a column oven from a Shimadzu LC-1 system. A Shimadzu SPD-6A UV detector was used for detection at 290 nm. The flow-rate of the mobile phase was controlled by a restrictor made of a capillary tube (200 mm \times 50 μ m I.D.).

HPLC system

The HPLC system consisted of a Model 576 pump (GL Sciences, Tokyo, Japan), a Rheodyne Model 7125 sample injector with a 20- μ l sample

loop and a Shimadzu RF-535 fluorescence detector.

2.2. Materials and chemicals

The separation columns used in SFC and HPLC were an L-column ODS (250 mm \times 4.6 mm I.D., particle size 5 μ m, pore diameter 120 Å) from the Chemicals Inspection and Testing Institute Japan (Tokyo, Japan) and a Chromatorex-SI (250 mm \times 4.6 mm I.D., particle size 5 μ m, pore diameter 100 Å) from Fuji Silysia (Kasugai, Aichi, Japan), respectively. α -, β -, γ - and δ -tocopherols used as the standards and tocol used as the internal standard were obtained from Eisai (Tokyo, Japan). Wheat germ, cottonseed and soybean oils were obtained from Sigma (St. Louis, MO, USA). Rice bran oil was donated by Tokyo Oil and Fat (Tokyo, Japan). Carbon dioxide used as the mobile phase in the SFC was of standard grade. Methanol, hexane, 1,4-dioxane and 2-propanol were of HPLC grade. The other reagents used were of analytical-reagent-grade and were used as received.

2.3. Preparation of vegetable oils

Vegetable oils were prepared according to Ishikawa et al. [15] as follows. About 10 g of vegetable oil samples were saponified with potassium hydroxide after adding tocol as the internal standard and pyrogallol-ethanol solution. The unsaponifiable matter was extracted with light petroleum (b.p. 30–60°C). The extracted solutions were concentrated to about 5 ml after washing and dehydration with sodium sulfate. The recoveries of tocopherols by this method were 100% [15].

2.4. HPLC procedure

HPLC was applied to the determination of tocopherols in vegetable oils under normal-phase conditions [1]. Hexane–1,4-dioxane–2-propanol (985:10:5, v/v/v) was used as the mobile phase at a flow-rate of 1.0 ml min⁻¹. The silica gel column was used for separation at room temperature. Fluorescence detection was performed

with excitation at 290 nm and emission at 325 nm.

3. Results and discussion

3.1. Retention of tocopherols

The peak shapes of tocopherols were poor when carbon dioxide was used as the mobile phase without a modifier. The retention behaviour of tocopherols and tocol was investigated at carbon dioxide pressures of 12–30 MPa. An increase in carbon dioxide pressure decreased the retention of all the solutes. Approximately linear relationships were obtained from the relationship between $\log k'$ and density of carbon dioxide. Chloroform was used to obtain t_0 for a calculating k' with UV detection at 220 nm. A thermodynamic description of this behaviour was reported in detail by Chester and Innis [16]. The elution order remained the same in this pressure range: tocol, δ -, β -, γ and α -tocopherol. Tocopherols having fewer methyl groups in the molecules were eluted faster than those having more methyl groups. Therefore, it seems that the elution order of tocopherols in SFC on the ODS-silica gel column was based on the number of methyl groups in the molecules and was similar to that in reversed-phase LC. On the other hand, the positional isomers β - and γ -tocopherol were separated under these conditions.

The peak shapes of tocopherols improved when methanol was added as a modifier to the mobile phase. The effect of the modifier on the retention of tocopherols at a mobile phase pressure of 15 MPa was investigated by plotting $\log k'$ of tocopherols and tocol vs. the concentration of methanol in the mobile phase, as shown in Fig. 1. The addition of methanol decreases the retention of all the solutes. The elution order of tocopherols is based on the number of methyl groups in the molecules under these conditions. The elution order of β - and γ -tocopherol reverses depending on the amount of methanol added. In practice, β - and γ -tocopherol eluted as one peak when high concentrations of methanol were added to the mobile phase.

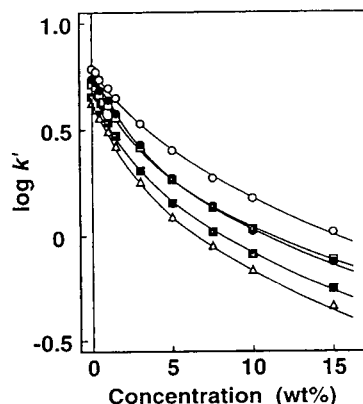


Fig. 1. Effect of the methanol modifier on k' . Samples: \circ = α -tocopherol; \bullet = γ -tocopherol; \square = β -tocopherol; \blacksquare = δ -tocopherol; \triangle = tocol.

3.2. Separation of tocopherols

The effect of methanol used as the modifier on the separation of tocopherols at a mobile phase pressure of 15 MPa was investigated. The separation factor (α) between adjacent peaks increased with increasing addition of methanol to the mobile phase, except for the positional isomers β - and γ -tocopherol. The α value between β - and γ -tocopherol approached to 1 according to the amount of methanol added. This suggests that the separation of β - and γ -tocopherol is difficult when high concentrations of methanol are added as the modifier.

Fig. 2 shows the relationship between the methanol concentration in the mobile phase and resolution (R_s) between adjacent peaks. When a small amount of methanol is added to pure carbon dioxide, the R_s values increase considerably, probably owing to the improvement of the peak shapes. At higher concentrations of methanol, on the other hand, all the R_s values decrease with increasing methanol concentration, presumably because the theoretical plate number concerning the separation of tocopherols on this separation column decreases. The theoretical plate number for α -tocopherol at methanol concentrations of 0.5 and 15% (w/w) were about 12 500 and 3200, respectively. When the methanol concentration in the mobile phase is above

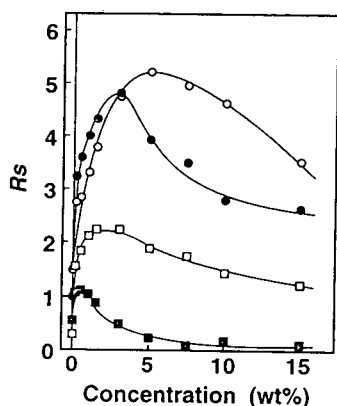


Fig. 2. Effect of the methanol modifier on R_s . The R_s values were obtained for (○) α - and γ -tocopherol, (●) β - and γ -tocopherol, (□) δ -tocopherol and tocol and (■) β - and γ -tocopherol.

3% (w/w), the R_s value between β - and γ -tocopherol is below 0.5 and suggests overlapping of their chromatographic peaks. The best separation of β - and γ -tocopherol is expected when 0.5% (w/w) of methanol is added to the mobile phase.

3.3. Application to vegetable oils

The determination of tocopherols in several kinds of vegetable oils was performed by SFC on the ODS-silica gel column, as shown in Fig. 3. The pressure of mobile phase was kept at 15 MPa and 0.5% (w/w) of methanol was added as the modifier. Some peaks were detected after 18 min and were, probably due to sterols included in the vegetable oils. The results for the determination of tocopherols in vegetable oils are given in Table 1. It is found that the compositions of tocopherols in four vegetable oils differ. The reproducibilities ($n = 5$) are good except for the components present in small amounts. The detection limit and detector linear dynamic range for α -tocopherol under these conditions were 16 ng (signal-to-noise ratio = 3) and four orders of magnitude, respectively. The detection limit is sufficient for vegetable oil analysis. However, fluorescence detection is needed for the determi-

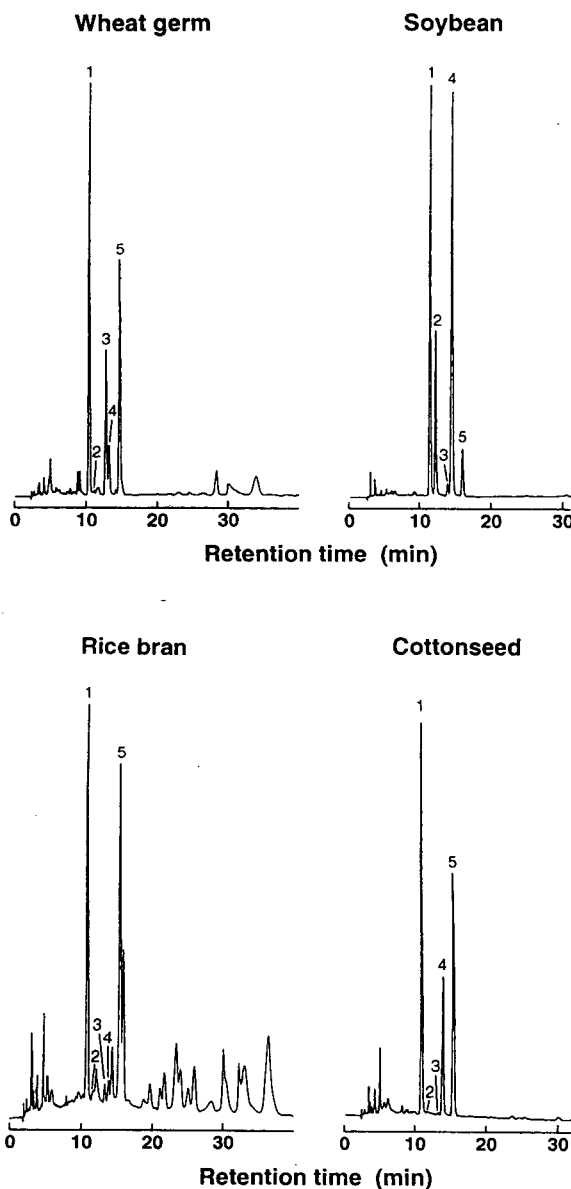


Fig. 3. SFC of tocopherols in vegetable oils. Peaks: 1 = tocol (internal standard); 2 = δ -tocopherol; 3 = β -tocopherol; 4 = γ -tocopherol; 5 = α -tocopherol.

nation of tocopherols if greater sensitivity is required, such as in plasma analysis.

Vegetable oils contain not only tocopherols but also structurally related compounds, such as tocotrienols and tocopherol esters. Determina-

Table 1
Comparison of SFC and HPLC determinations of tocopherols in vegetable oils

Oil	Method	Content of tocopherol (mg per 100 g) ^a			
		α -	β -	γ -	δ -
Wheat germ	SFC	259 ± 2	119 ± 1	41.7 ± 1.2	3.1 ± 0.5
	HPLC	267 ± 5	105 ± 1	35.5 ± 3.2	1.6 ± 0.4
Soybean	SFC	19.9 ± 0.4	3.4 ± 0.2	136 ± 2	47.0 ± 0.5
	HPLC	19.9 ± 0.6	6.4 ± 0.2	132 ± 1	46.9 ± 0.4
Rice bran	SFC	28.2 ± 0.4	1.0 ± 0.1	1.2 ± 0.1	Trace
	HPLC	27.6 ± 0.2	1.4 ± 0.2	1.3 ± 0.3	Trace
Cottonseed	SFC	133 ± 1	1.2 ± 0.2	61.4 ± 0.5	Trace
	HPLC	130 ± 1	8.6 ± 0.2	58.4 ± 0.4	Trace

^a Mean ± S.D. (*n* = 5).

tion of tocopherols in vegetable oils by normal-phase HPLC using a fluorescence detector was performed in order to compare it with SFC, as shown in Fig. 4. Tocopherols having more methyl groups in the molecules are eluted faster than those having fewer methyl groups under

these conditions. The results for the determination of tocopherols in vegetable oils by HPLC are also given in Table 1. The results obtained by SFC and HPLC show good agreement. A small difference between the SFC and HPLC results occurred for some tocopherols present in small

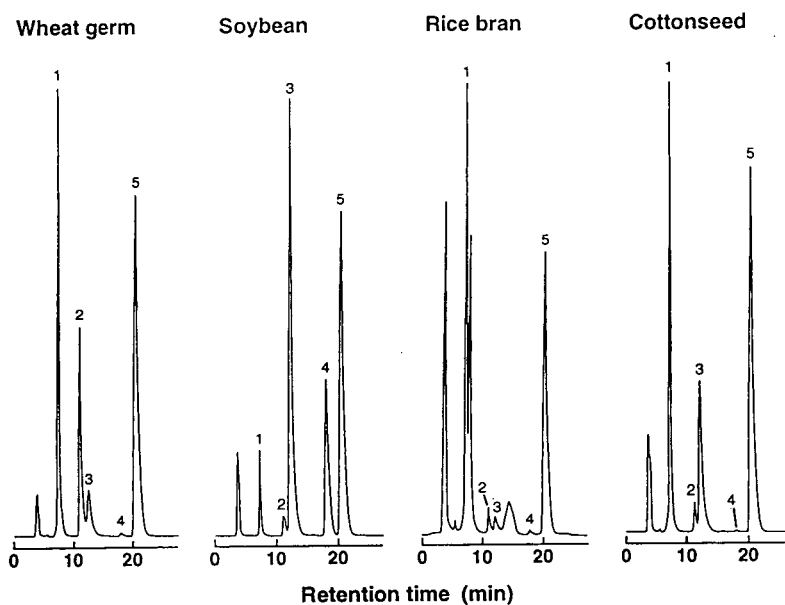


Fig. 4. HPLC of tocopherols in vegetable oils. Peaks: 1 = α -tocopherol; 2 = β -tocopherol; 3 = γ -tocopherol; 4 = δ -tocopherol; 5 = tocol (internal standard).

amounts, such as β -tocopherol in cottonseed oil. This is probably due to the peak overlap with other components in vegetable oils.

4. Conclusions

The determination of tocopherols by SFC using an ODS-silica gel column was reported. The retention behaviour of tocopherols under these conditions was similar to that in reversed-phase HPLC. However, SFC could separate tocopherols, including positional isomers. The addition of small concentrations of methanol as modifier produced satisfactory separations.

Both SFC and normal-phase HPLC were applied to the determination of tocopherols in vegetable oils. It is significant that SFC could effect separates in a different chromatographic mode to that in normal-phase HPLC because vegetable oils contain tocopherols as well as their structurally related compound. We conclude that SFC is suitable as a quantitative method for the determination of tocopherols.

Acknowledgement

The authors thank Mr. Imura of Tokyo Oil and Fat for discussions concerning vegetable oils.

References

- [1] K. Abe and A. Matsumoto, in M. Mino, H. Nakamura, A.T. Diplock and H.J. Kayden (Editors), *Vitamin E—Its Usefulness in Health and in Curing Diseases*, Japan Scientific Societies Press, Tokyo, and Karger, Basle, 1993, p. 13.
- [2] A.P. De Leenheer, H.J. Nelis, W.E. Lambert and R.M. Bauwens, *J. Chromatogr.*, 429 (1988) 3.
- [3] A.L. Blilie and T. Greibrokk, *Anal. Chem.*, 57 (1985) 2239.
- [4] J.M. Levy and W.M. Ritchey, *J. High Resolut. Chromatogr. Chromatogr. Commun.*, 8 (1985) 503.
- [5] J.M. Levy and W.M. Ritchey, *J. Chromatogr. Sci.*, 24 (1986) 242.
- [6] M.E. McNally, J.R. Wheeler and W.R. Melander, *LC-GC*, 6 (1988) 816.
- [7] T.A. Berger and J.F. Deye, *J. Chromatogr. Sci.*, 29 (1991) 141.
- [8] T.A. Berger and J.F. Deye, *J. Chromatogr. Sci.*, 29 (1991) 280.
- [9] T.A. Berger and J.F. Deye, *J. Chromatogr. Sci.*, 29 (1991) 390.
- [10] D. Upmooor and G. Brunner, *Ber. Bunsenges. Phys. Chem.*, 93 (1989) 1009.
- [11] J.L. Perrin and A. Prevot, *Rev. Fr. Corps Gras*, 35 (1988) 485.
- [12] M. Saito, T. Hondo and Y. Yamauchi, in R.E. Smith (Editor), *Supercritical Fluid Chromatography*, Royal Society of Chemistry, London, 1988, Ch. 8, p. 203.
- [13] M. Saito and Y. Yamauchi, *J. Chromatogr. Sci.*, 27 (1988) 79.
- [14] M. Saito and Y. Yamauchi, *J. Chromatogr.*, 505 (1990) 257.
- [15] S. Ishikawa, M. Sawada and G. Katui, *Vitamins*, 34 (1966) 185.
- [16] T.L. Chester and P.P. Innis, *J. High Resolut. Chromatogr. Chromatogr. Commun.*, 8 (1985) 561.



ELSEVIER

Journal of Chromatography A, 679 (1994) 335–344

JOURNAL OF
CHROMATOGRAPHY A

Suggested definition of zone resolution and zone capacity in separations of weak electrolytes or ampholytes by steady-state electrophoretic methods

Karel Šlais

Institute of Analytical Chemistry, CZ-61142 Brno, Czech Republic

First received 14 December 1993; revised manuscript received 2 May 1994

Abstract

A new definition of zone resolution in the general class of steady-state electrophoretic methods is proposed. Under certain assumptions, the limiting zone capacity can be described by a single explicit expression of wide applicability. The expressions for zone resolution and zone capacity were used to describe the separation of weak electrolytes or ampholytes in ordered series of zones with a Gaussian or square-wave concentration profile or with the profile which is the transition between these shapes.

1. Introduction

Steady-state electrophoretic methods [1–3] include powerful separation tools such as isoelectric focusing (IEF) [4–12], isotachopheresis (ITP) [13–19] and methods that can be considered as a transition between typical IEF and ITP (e.g., IEF with electrophoretic mobilization [20–27], ITP with carrier ampholytes [14,19,28,29]). Some of the transition (intermediate) methods can be regarded also as electrophoretic focusing in a steady-state moving natural pH gradient [30].

The separation power of the method can be reasonably visualized by the number of components that can be resolved into individual zones. For this purpose, the definition of zone breadth is necessary. Several such definitions could be suggested and defended; the most convenient one identifies the breadth of the

Gaussian concentration distribution with the distance between two inflection points, which is twice the standard deviation. When the concentration profiles of the separated zones can be approximated by the Gaussian curves, terms such as zone resolution, R_s , and peak capacity n_c , [3,10,30,31] are generally applicable. A search of the literature shows that a number of approaches have been suggested to describe the degree of zone separation [3,7–10,31–35]. As they describe systems composed of the Gaussian zones or boundaries characterized by a standard deviation, the relationships derived can be transferred to the description based on the R_s value [35].

Unfortunately, the steady-state electrophoretic methods mentioned above often produce zones with nearly square-wave forms of their concentration profiles which are separated by sigmoidal boundaries. Typical examples include well sepa-

rated ITP zones [1,2,13,17,36–39] or IEF zones with the use of a small number of carrier ampholytes and/or a high intensity of the electrical field [1,2,8,11,40,41]. The degree of zone separation was described with the help of the boundary width for strong electrolytes [42]. However, there is a smooth transition between Gaussian and square-wave concentration profiles [1,2,8,43]. The fundamental unity of the electrophoretic separation processes discussed so far was supported by general electrophoretic models [1,2,43–47]. Therefore, it seemed meaningful to seek some characteristics of the separation power of the steady-state electrophoretic methods that would not be sensitive to the shape of the concentration profile of the separated zones. Especially a parameter that would cover the Gaussian, square-wave and intermediate shapes would be valuable. However, a more generally applicable definition of zone resolution leading to great mathematical complexity in the calculation of resolving power would be useless.

In this paper, the resolution between neighbouring zones is considered in the array of the equidistant bands with equal mass of the considered components. The suggested description of zone separation is based on the definition of the term called the effective length of the concentration gradient which generally exists in any system with an array of steady-state zones. The simplified model enables one to define such a width for concentration profiles of various shapes.

2. Theory

2.1. Model definition

Here we discuss an idealized system of monoprotic weak electrolytes or mono-monovalent ampholytes, with equal diffusion coefficients, D_i , with a small degree of ionization, so that the component effective charge is much smaller than unity, $|z_i| \ll 1$. The solution is convection-free and stationary. Separation occurs only due to the differences in pK_a or isoelectric point, pI , dispersion due only to the diffusion. The pK_a or pI

values of compounds are evenly spaced on the pH scale. Since, for the estimation of the limiting peak capacity, a large number of the separated compounds is of interest, the difference between the neighbouring zones amounts to only a fraction of a pH unit, $\Delta(\text{pH})$. For a series of ampholyte zones, it is $\Delta(\text{pH}) = \Delta(pI)$. For all compounds considered, the derivative of the pH dependence of the effective mobility of a compound, $d\mu_i/d(\text{pH})$, is considered to be a constant within the zone and the same for all compounds.

When the zones are sufficiently overlapped, a continuous constant pH gradient, dpH/dx , can be assumed. As D_i values are equal and constant, the conductivity can also be assumed to be constant along the length of the whole series of the zones, L . This assumption includes the neglect of the contribution of the solvent ions to the conductivity, which implies that the zone pH is close to neutral. As the area of the cross-section of the channel, A , is also constant, the electrical field, E , is constant. The model may be considered as artificial but it is often used for modelling the steady state in idealized IEF [1,2,5,7–10,12,30,43,46].

As steady-state IEF can be treated as zero-velocity steady-state ITP [12,17,37], it is reasonable to examine the conditions for the applicability of above IEF model to the idealized ITP of weak electrolytes. For this treatment, the zone existence diagram [18] is useful. It appears that weak electrolytes with the same D_i can generate zones with approximately the same conductivity under steady-state conditions. For example, the series of zones can cover the pH range from 4 to 10 while the conductivity varies by only about 10% over the entire pH range. Applying the above assumptions used for IEF also to ITP of a series of weak electrolytes, we have $\Delta(\text{pH}) = \Delta(pK_a)$. Further, it follows from the model description that the pH difference, $\Delta(\text{pH})$, and the potential difference, ΔU , between the neighbouring zones are independent of whether their shape is Gaussian or square-wave and whether the steady-state zone moves or not.

As mentioned previously, owing to the change

in the field intensity, the shape of the concentration distribution curves of the zones can change from Gaussian to nearly square wave. According to the model described, the influence of this transition on the important variables, including Δx , $\Delta(\text{pH})$, $d\mu/d(\text{pH})$, mean zone mobility and zone conductivity can be neglected for the estimation of the limiting zone capacity.

Generally, a series of zones is studied (see Fig. 1). In a one-dimensional arrangement, the zones are evenly spaced by Δx , which is the distance of zone maxima or between the boundaries. When the array consists of zones of equal mass of components, m_i , equal concentrations in zone maxima, c_{mi} , result.

Common features of the series of concentration profiles of real zones include their maxima, slopes on both zone sides, inflection points at these slopes and asymptotic declination of the concentration toward both sides. At the contacts between the neighbouring zones, boundaries exist at the places of greatest mixing of separated compounds. For a series of equal zones with

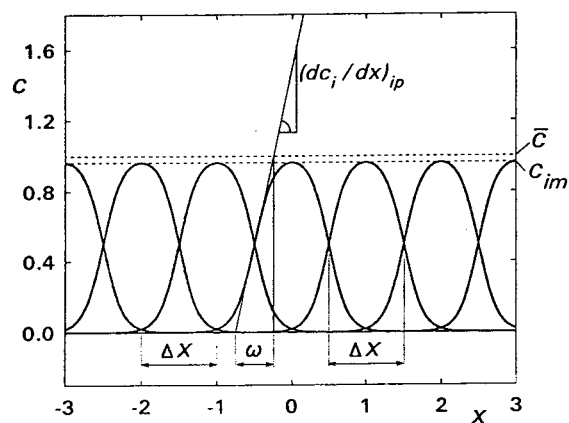


Fig. 1. Definition of the effective length of the concentration gradient. c_i = Component concentration; c_{im} = component concentration in the zone maximum; \bar{c} = average total concentration of the considered components in the zone array; x = zone array length coordinate; Δx = distance between the zone maxima or the distance between the zone boundaries; $(dc_i/dx)_{ip}$ = tangent of the concentration gradient at its inflection point; ω = effective length of the concentration gradient. The dimensions of variables c and x are bound by Eq. 2.

arbitrary shape, the tangent at the inflection point, $(dc_i/dx)_{ip}$, and the distance between the zone maxima or the distance between the boundaries, Δx , can be well defined (see Fig. 1).

Let us define the effective length of the concentration gradient, ω , as

$$\omega = \bar{c} / |dc_i/dx|_{ip} \quad (1)$$

where the total average concentration of all considered compounds, \bar{c} , (either carriers or spacers or analytes) is expressed with the help of m_i and Δx as

$$\bar{c} = m_i / A\Delta x \quad (2)$$

According to the model adopted, \bar{c} can be considered as constant within the series of zones. In Fig. 1, the dimensions of x and c variables are bound by Eq. 2 and the zone concentration profiles are shown with $\bar{c} = 1$ and $\Delta x = 1$ arbitrary unit.

It follows from the definition that ω is not concentration dependent and that the narrower the Gaussian peak, the smaller is the ω obtained. These properties are similar to those of the standard deviation of the Gaussian peak, σ . However, the parameter ω can be defined also for other forms of zone concentration profiles, which opens up the possibility for the comparison of zones with different shapes.

The resolution of the separated zones is proportional to the level of purity of the respective zone or inversely proportional to the degree of mixing of the neighbouring zones. For qualitative analysis, it is more practical to relate the resolution to the detectability of zones of the individual components. Mathematically, it can be expressed with the ratio of the distance between the zones to a suitable feature of the concentration profile of the zone. For a Gaussian profile, the curve standard deviation, σ_i , is usually chosen [3,8,10,31–33,35].

Here, the resolution in the array of evenly spaced equal zones, R_z , is defined as the dimensionless quantity by the relationship

$$R_z = (\Delta x / \omega)^{1/2} \quad (3)$$

As R_z is based on ω , a comparison of the zone resolution between series of zones of different shape can be made.

The zone capacity, n_z , is defined as the upper limit of the resolvable zones for a given technique under the prescribed conditions [3,31,32]. It is obtained by allowing each hypothetical zone occupy a distance Δx . For the overall length of the series of the zones, L , it is

$$n_z = L/\Delta x \quad (4)$$

The zone capacity is dependent on the quality of the zone separation or, in other words, on the degree of the mutual mixing of the compounds in the neighbouring bands. It is usually expressed in terms of the resolution. As long as ΔU and $\Delta(\text{pH})$ are constant along L , the translation of R_z into information on the total maximum number of resolvable components can be made by combination of Eqs. 3 and 4:

$$n_z = L/(R_z^2 \omega) \quad (5)$$

or, again by virtue of Eq. 3,

$$n_z = L/[R_z(\Delta x \omega)^{1/2}] \quad (6)$$

The use of the above-mentioned definitions can be illustrated by Fig. 2, where some important simplified cases occurring in the steady-state electromigration methods are outlined. In Fig. 2a, a series of evenly spaced, overlapping Gaussian zones models the background of carrier ampholytes in IEF and in the focusing in the moving steady-state pH gradient. In Fig. 2b, a series of well separated, evenly spaced Gaussian peaks models the separated analytes in IEF and in some transition methods. In Fig. 2c, a series of equal nearly square-wave zones separated by symmetrical boundaries models the ITP of weak electrolytes with very small differences in their $\text{p}K_a$ values and IEF with a small number of carriers and/or with a large field intensity.

2.2. Explicit expressions for ω

Series of Gaussian zones

From the properties of the Gaussian curve, for the tangent at the inflection point we have

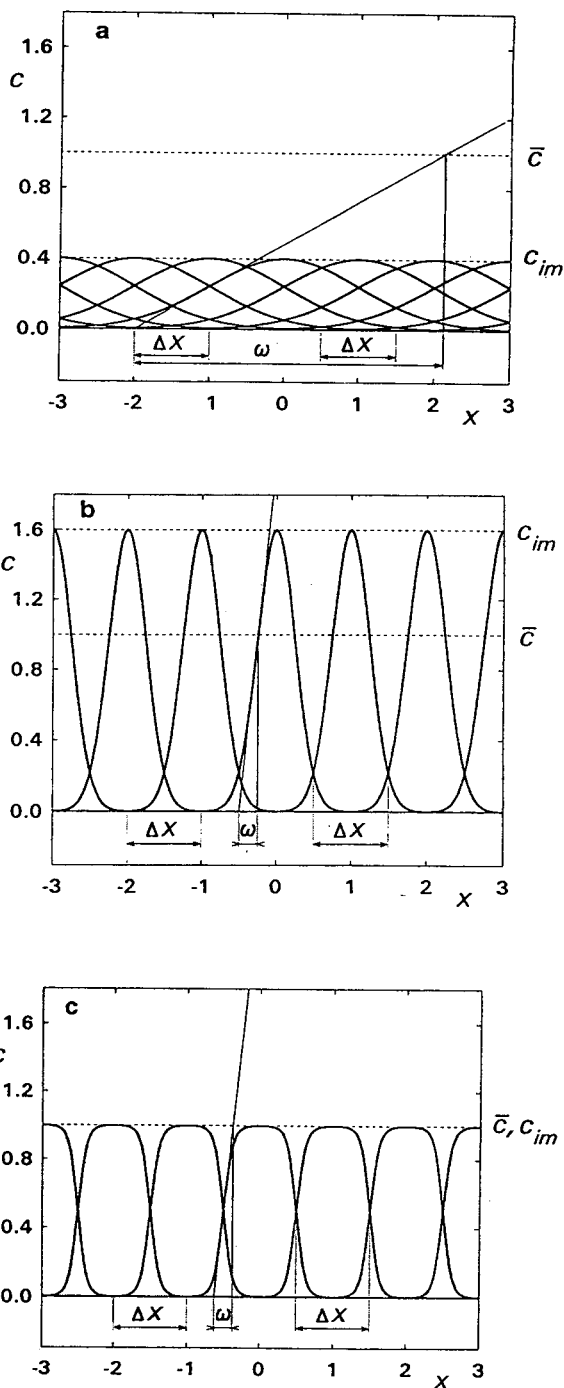


Fig. 2. Typical concentration profiles occurring in the separation of weak electrolytes by steady-state electromigration methods. (a) $\omega = 4\Delta x$; (b), (c) $\omega = 0.25\Delta x$. For explanation of symbols, see Fig. 1.

$$|dc_i/dx|_{ip} = c_{mi}/(e^{1/2}\sigma_i) \quad (7)$$

and m_i within the Gaussian peak can be calculated as

$$m_i = c_{mi}A\sigma_i(2\pi)^{1/2} \quad (8)$$

Eqs. 1, 2, 7 and 8 yield for the effective length of the concentration gradient in the series of equal Gaussian peaks, ω_p ,

$$\omega_p = (2\pi e)^{1/2}\sigma_i^2/\Delta x \quad (9)$$

According to the model adopted, for σ_i^2 in steady-state electrophoretic methods we can write [3,5,7,8,10,30]

$$\sigma_i^2 = RT/\{EF[-dz_i/d(\text{pH})][d(\text{pH})/dx]\} \quad (10)$$

where F is the Faraday charge, R is the gas constant and T is the absolute temperature. Then, by insertion of Eq. 10 in Eq. 9, we obtain for ω_p

$$\omega_p = (2\pi e)^{1/2}RT/\{FE\Delta x[-dz_i/d(\text{pH})][d(\text{pH})/dx]\} \quad (11)$$

The selectivity, or the relative difference in the mobilities of the compounds in the neighbouring zones, p , is introduced [15,18,32,42,48] as

$$p = \Delta\mu/\bar{\mu} \quad (12)$$

where $\Delta\mu$ is the difference in the effective mobilities of the compounds in the neighbouring zones and $\bar{\mu}$ is their mean. Since, in the model considered, $\bar{\mu}$ is also the effective mobility of the whole series of the zones, we have

$$p = [-d\mu_i/d(\text{pH})]\Delta(\text{pH})/\bar{\mu} \quad (13)$$

The effective mobility and effective charge of compound are bound by the Nernst relationship:

$$\mu_i = z_iFD_i/RT \quad (14)$$

Insertion of $\Delta(\text{pH}) = \Delta x[d(\text{pH})/dx]$ and Eq. 14 in Eq. 13 yields for p

$$p = \Delta x[d(\text{pH})/dx][dz_i/d(\text{pH})]/z \quad (15)$$

Then, by use of Eq. 15, Eq. 11 can be written in the form

$$\omega_p = (2\pi e)^{1/2}RT/zFEp \quad (16)$$

Series of square-wave zones separated by symmetric boundaries

For low dissociation of weak electrolytes, $|z_i| \ll 1$, the ratio of the ion mobilities may be approximated by the ratio of the respective dissociation constants. For example, for weak acids, the selectivity can be then expressed as [15,39,48]

$$p = \Delta K_a/\bar{K}_a \quad (17)$$

where ΔK_a is the difference in the acidic K_a values of the compounds in the neighbouring zones and \bar{K}_a is their geometric mean. Generally, the boundary between the zones of the weak electrolytes in ITP is unsymmetric. For $p \ll 1$, which is of practical interest for examining the separation power, it can be considered as symmetric [15,39].

Let us consider a well developed square-wave zone which is symmetrical around the origin, $x = 0$, and the sigmoidal boundaries are symmetric around the $-\Delta x/2$ and $\Delta x/2$ coordinates, respectively. The concentration profile of the considered component in such a zone (see Fig. 2c) can be expressed as

$$c_i/\bar{c} = 1/\{1 + \exp[-\beta(x + 0.5\Delta x)]\} - 1/\{1 + \exp[-\beta(x - 0.5\Delta x)]\} \quad (18)$$

where β is the reciprocal distance [39]. For both weak anions and cations with $p \ll 1$, in the present notation we have

$$\beta = (zF/RT)(v/\bar{\mu})(\Delta K_a/\bar{K}_a) \quad (19)$$

where v is the linear velocity of the whole series of steady-state zones. The derivatization of Eq. 18 yields the tangent at the inflection point of the concentration profile in the boundary as

$$|dc_i/dx|_{ip} = \bar{c}\beta/4 \quad (20)$$

From Eqs. 1 and 20, the effective length of the concentration gradient in methods giving the symmetrical boundary between the weak electrolytes, ω_b , is

$$\omega_b = 4/\beta \quad (21)$$

Since for the potential field in the considered series of the zones

$$E = v/\mu \quad (22)$$

we obtain by insertion of Eqs. 17, 19 and 22 in Eq. 21

$$\omega_b = 4RT/FEzp \quad (23)$$

By comparison of Eqs. 16 and 23, we can see that the only differences are in the expressions for selectivity (see Table 1) and in the numerical coefficients. For the same E , z and p , the ratio of the respective equations may be summarized as $\omega_p = 1.033\omega_b$. The difference can be neglected and a numerical coefficient of 4 will be adopted in further calculations. The appropriate selectivity parameters used should be consistent with the compounds and method considered (see Table 1).

Transition from Gaussian to square-wave zones

The above-mentioned concentration profiles are certain limiting cases. Computer modelling has shown a smooth transition from one to another, e.g., by a continuous increase in E [1,2,8].

Let us consider the steady state depicted in Fig. 2a, where Gaussian peaks are depicted with $\sigma_i = \Delta x$ and $\omega = 4\Delta x$. Now, on increasing E by, e.g., factor 16, two cases may occur:

(a) When the system contains the background maintaining the continuous pH gradient [5,8,10], the Gaussian shape of the considered zones continues. This situation may be exemplified by

analytes in IEF (see Fig. 2b), where Gaussian peaks are shown with $\omega = 0.25\Delta x$.

(b) Without a background, the bands acquire the square-wave zones [1,2,8,30,43] (see Fig. 2c), where also $\omega = 0.25\Delta x$. Hence, for the small ω , the zone shape appears to be dependent on the presence of the background pH gradient.

For well developed square-wave zones, Δx can be considered as composed of two parts, namely the zone of the respective component with the length, l_i , and the effective length of the concentration gradient, ω :

$$\Delta x = l_i + \omega \quad (24)$$

In Fig. 2c, $l_i = 3\omega$. The limiting case, when $l_i = 0$, or when

$$\Delta x = \omega \quad (25)$$

may also be seen as a transition between square-wave and Gaussian zone shapes. At the transition point, the linear relationship between m_i and the zone height for Gaussian peaks starts to transform into a linear relationship between m_i and the zone length for square waves. Then, ω should be intermediate between the ω of the two typical cases, ω_p and ω_b . Since they are almost identical, ω in the transition point should not be very different from either of them. With the use of Eq. (23), condition (25) for the transition point can be represented as

$$\Delta x = 4RT/EFzp \quad (26)$$

Almgren [8] estimated the transition from Gaussian zones to square-wave zones in IEF from the calculated pH and conductivity profiles. The transition point was considered as the state when the calculated smooth linear pH profile begins to change into a staircase course, where, the steepness of the pH profile at the zone maximum is 15% lower and that at the midpoint between the zone maxima by 15% higher than the average gradient steepness. In the present notation, he found for this state (Eq. 47 in Ref. 8):

$$\Delta pI = \{4RT[d(\text{pH})/dx]/FE[-dz_i/d(\text{pH})]\}^{1/2} \quad (27)$$

which, by insertion of

Table 1
Summary of expressions for the selectivity, p , in steady-state electrophoretic modes for $p \ll 1$ and $|z_i| \ll 1$

System	Expressions for p
Weak acids, bases	$\Delta\mu/\bar{\mu}$, $\Delta z/z$ $\Delta K_a/\bar{K}_a$, $\Delta K_b/\bar{K}_b$ $\Delta(\text{p}K_a)[-d\mu_i/d(\text{pH})]/\bar{\mu}$ $\Delta(\text{p}K_a)[-dz_i/d(\text{pH})]/z$
Good ampholytes	$\Delta(pI)[-d\mu_i/d(\text{pH})]/\bar{\mu}$ $\Delta(pI)[-dz_i/d(\text{pH})]/z$

$$\Delta pI = \Delta x d(\text{pH})/dx \quad (28)$$

in Eq. 27 and squaring gives, after rearrangement,

$$\Delta x = 4RT/\{FE\Delta x[-dz_i/d(\text{pH})][d(\text{pH})/dx]\} \quad (29)$$

With Eq. 15, this leads finally to an equation that is identical with Eq. 26. It indicates that the expression of ω for the Gaussian or for the square-wave concentration profiles in steady-state electrophoretic methods can be applied also for the transition between these profile forms.

The profile transition may be illustrated by Fig. 3, where the concentration courses of the single zone are shown for ω values of $0.25\Delta x$, $0.5\Delta x$ and Δx . With the background pH gradient, the Gaussian curves 1, 2 and 5, respectively, result. Without the background and the same ω values, curves 3, 4 and 5, respectively, are obtained. Without the presence of the background pH gradient, the square-wave shape starts to develop at $\omega < \Delta x$.

2.3. Zone resolution

The zone resolution, R_z , was defined for the series of zones by Eq. 6. For Gaussian peaks, from Eqs. 6 and 9 we have

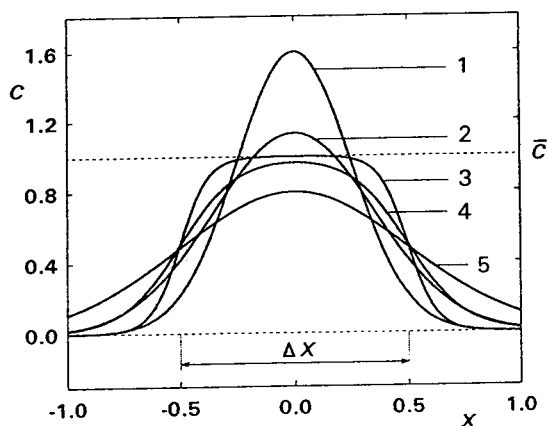


Fig. 3. Dependence of a single zone concentration profile on ω and on the presence of a background continuous pH gradient. Curves: 1, 2, 5 = with background pH gradient; 3, 4, 5 = without background; 1, 3, $\omega = 0.25\Delta x$, 2, 4, $\omega = 0.5\Delta x$; 5, $\omega = \Delta x$. For explanation of symbols, see Fig. 1.

$$R_z = (2\pi e)^{-1/4} \Delta x/\sigma_i = \Delta x/(2.033\sigma_i) \quad (30)$$

The resolution of Gaussian peaks is described in terms of R_s , defined as [3,10,32]

$$R_s = \Delta x/4\sigma_i \quad (31)$$

From Eqs. 30 and 31, the relationship between R_z and R_s for the series of Gaussian peaks is

$$R_z = R_s \cdot 2/1.016 \approx 2R_s \quad (32)$$

The ratio of R_z for peaks to R_z for the square zones is, by virtue of Eqs. 3, 16 and 23, only $(1.033)^{1/2} = 1.016$, which also justifies the common expressions for both zone forms.

For methods giving the zones modelled by Figs. 2 and 3, from Eqs. 3 and 23 we obtain

$$R_z = (FEzp\Delta x/4RT)^{1/2} \quad (33)$$

As Eqs. 15 and 28 yield

$$zp\Delta x = (\Delta pI)^2 \{[-dz_i/d(\text{pH})]/[d(\text{pH})/dx]\} \quad (34)$$

this indicates that Eq. 33 is equivalent to the previous relationships for the resolution of the Gaussian zones in IEF [3,10]. The only difference is in the numerical coefficient that relates R_z to R_s (see Eq. 32). In Fig. 2b and 2c, the zones are separated with the same $R_z = 2$. Both the Gaussian ($\Delta x = 4\sigma$) and square-wave zones ($l_i = 3\omega$, $\Delta x = 4\omega = 16/\beta$) may be considered as detectably resolved. The content of the pure compound in the respective Gaussian zone, Φ_p , is 95.4%. This content in the respective square-wave zone, Φ_b , can conveniently be calculated with the help of the boundary width, w , when the boundary is considered as a 1:1 mixed zone composed of the neighbouring pure compounds. With the help of Eq. 18, we obtain

$$\begin{aligned} w &= 4 \int_{\Delta x/2}^{\infty} dx / \{1 + \exp[-\beta(x - 0.5\Delta x)]\} \\ &= 4 \ln 2/\beta \end{aligned} \quad (35)$$

Apparently, it follows from Eqs. 21 and 35 that $w = \omega_b \ln 2$. Then, Φ_b is given by

$$\Phi_b = 1 - (w/2)/\Delta x \quad (36)$$

For $R_z = 2$, from Eqs. 3, 21, 35 and 36

$\Phi_b = 1 - \ln 2/8 = 91.3\%$. For ITP of the square-wave zones of strong electrolytes, it was suggested [42] that one can define the required resolution with the help of the same zone purity as that for the series of Gaussian peaks with $R_s = 1$. In the present notation, this means setting $\Phi_p = \Phi_b$ or $\Phi_b = 95.4\%$ of the respective compound. Then Δx should be $\Delta x = (w/2)/0.0456 = \omega \ln 2/0.0912 = 7.60\omega$ and, from Eq. 3, $R_z = 7.6^{1/2} = 2.75$.

For the definition of the just-resolved Gaussian zones in IEF, the following criterion is often used [7–9,33]:

$$\Delta x = 3.08\sigma_i \quad (37)$$

According to Eqs. 31, 32 and 37, this corresponds to $R_s = 0.77$ and $R_z = 1.54$. Φ_p is then 87.4%. When $R_z = 1.54$ is applied also for the square-wave zones, $\Phi_b = 85.4\%$. Despite the different approaches to the definition of the zone resolution, the differences in the zone purity can be considered as not critical for estimation of the separation power of the examined methods.

2.4. Zone capacity

For an array of Gaussian peaks, we obtain the known equation for estimation of the limiting peak capacity [3] by insertion of Eqs. 9 and 32 in Eq. 6:

$$n_z = L/(R_s 4\sigma_i) \quad (38)$$

It is usually accepted that $R_s = 1$ or, in the present notation, $R_z = 2$. If this value of R_z is considered adequate also for the square-wave and transition concentration profiles, we obtain by combination of Eqs. 6 and 23 for $R_z = 2$

$$n_z = [(L^2 FEz_p)/(16\Delta x RT)]^{1/2} \quad (39)$$

By insertion of Eq. 15, we can write Eq. 39 in the form known for the estimation of the peak capacity in IEF [3,10]:

$$n_z = \{L^2 FE[-dz_i/d(\text{pH})][d(\text{pH})/dx]/16RT\}^{1/2} \quad (40)$$

According to the model adopted, it is possible to introduce the potential drop across the whole

series of zones, U , as $U = -EL$ and the total pH difference across L , $\delta(\text{pH})$, as $\delta(\text{pH}) = L[d(\text{pH})/dx]$. The zone capacity can then be expressed in the form

$$n_z = \{FU\delta(\text{pH})[dz_i/d(\text{pH})]/16RT\}^{1/2} \quad (41)$$

which indicates that the maximum number of resolvable components should not be dependent on the length of the zone array. This conclusion is important for comparison of n_z in ITP and IEF, respectively. In IEF, L may theoretically be up to the whole length of the channel. In ITP, the length of the zone array is generally only a fraction of the channel length. When applying ITP to weak electrolytes with a small degree of dissociation, $|z_i| \ll 1$, the migration velocity of the steady-state zones is substantially smaller than the velocity of fully dissociated analytes in the adjusted sample zone. On the other hand, the undissociated analytes in the sample remain stationary until they are dissociated. In this way, the series of adjusted zones may occupy a substantial part of the channel length in ITP of the weakly dissociated electrolytes. Hence, according to the last-mentioned equations, the zone capacity of ITP may be close to that of IEF in the discussed cases.

As the final equations for the limiting zone capacity are based on ω , which is applicable to zones of different shapes, it is similarly valid for steady-state electrophoretic methods giving a series of Gaussian and square-wave zones and for zones with a shape that is intermediate between them.

3. Conclusions

Based on the above discussion, a comparison of the limiting zone capacities of the examined steady-state methods with the zone capacities of other electrophoretic methods can be made. Previously [3,10,49,50], the limiting peak capacities of capillary zone electrophoresis (CZE) and IEF were found to be similar. This can also be supported by Eq. 39 when the selectivity for CZE expressed as $p = \Delta x/L$ is

taken into consideration. Further, the zone capacities of ITP and CZE of strong electrolytes were found to be of the same order of magnitude [42]. Together with the relationships derived here, it can be concluded that, for the same total potential over the channel, the limiting zone capacities of IEF, ITP and CZE are comparable. Based on the zone concentration profiles discussed previously [30], similar expressions for n_z can also be expected for intermediate methods such as IEF with electrophoretic mobilization and isotachopheresis with polyampholytic spacers.

The above relationships were derived for symmetrical zones and boundaries. It can be expected that, owing to the applicability to the above-discussed different shapes of the concentration profiles, small deviations from symmetry will not cause serious changes in the estimation of the resolution or of the limiting zone capacity by the final equations.

The suggested description of the separation efficiency is fully compatible with the equations used so far. It shows that under some assumptions, the previous equations for the zone capacity can be used not only for the Gaussian peaks, but also for the square-wave zones of the weak electrolytes and the transition between the peak and the square wave. The similar expressions obtained and the values of the system parameters for the description of the separation efficiency of the different zone shapes give further support to the fundamental unity of the methods discussed.

References

- [1] W. Thormann and R.A. Mosher, in A. Chrambach, M.J. Dunn and B.J. Radola (Editors), *Advances in Electrophoresis*, Vol. 2, VCH, Weinheim, 1988, p. 45.
- [2] R.A. Mosher, D.A. Saville and W. Thormann, *The Dynamics of Electrophoresis*, VCH, Weinheim, 1992.
- [3] J.C. Giddings, *Unified Separation Science*, Wiley-Interscience, New York, 1991.
- [4] E. Schumacher, *Helv. Chim. Acta*, 40 (1957) 2322.
- [5] H. Svensson, *Acta Chem. Scand.*, 15 (1961) 325.
- [6] H. Svensson, *Acta Chem. Scand.*, 16 (1962) 456.
- [7] O. Vesterberg and H. Svensson, *Acta Chem. Scand.*, 20 (1966) 820.
- [8] M. Almgren, *Chem. Scr.*, 1 (1971) 69.
- [9] H. Rilbe, *Ann. N.Y. Acad. Sci.*, 209 (1973) 11.
- [10] J.C. Giddings and H. Dahlgren, *Sep. Sci.*, 6 (1971) 345.
- [11] W. Thorman, R.A. Mosher and M. Bier, *J. Chromatogr.*, 351 (1986) 17.
- [12] K. Shima, *Electrophoresis*, 8 (1987) 14.
- [13] E. Schumacher and T. Studer, *Helv. Chim. Acta*, 47 (1964) 957.
- [14] F.M. Everaerts, J.L. Beckers and Th.P.E.M. Verhegen, *Isotachopheresis*, Elsevier, Amsterdam, 1976.
- [15] W. Thormann, *Sep. Sci.*, 19 (1984) 455.
- [16] P. Radi and E. Schumacher, *Electrophoresis*, 6 (1985) 195.
- [17] K. Shima, *Electrophoresis*, 7 (1986) 121.
- [18] P. Boček, M. Deml, P. Gebauer and V. Dolník, *Analytical Isotachopheresis*, VCH, Weinheim, 1988.
- [19] S. Hjertén and M. Kiessling-Johansson, *J. Chromatogr.*, 550 (1991) 811.
- [20] S. Hjertén and M. Zhu, *J. Chromatogr.*, 346 (1985) 265.
- [21] S. Hjertén, J. Liao and K. Yao, *J. Chromatogr.*, 387 (1987) 127.
- [22] S. Hjertén, K. Elenbring, F. Kilár, J.L. Liao, A.J.C. Chen, C.J. Siebert and M.D. Zhu, *J. Chromatogr.*, 403 (1987) 47.
- [23] M.A. Firestone and W. Thormann, *J. Chromatogr.*, 436 (1988) 309.
- [24] F. Kilár and S. Hjertén, *Electrophoresis*, 10 (1989) 23.
- [25] M. Zhu, D.L. Hansen, S. Burd and F. Gannon, *J. Chromatogr.*, 480 (1989) 311.
- [26] B.T. Wehr, M. Zhu, R. Rodriguez, D. Burke and K. Duncan, *Am. Biotechnol. Lab.*, 22 (1990) 23.
- [27] M. Zhu, R. Rodriguez and T. Wehr, *J. Chromatogr.*, 559 (1991) 479.
- [28] F. Acevedo, *J. Chromatogr.*, 470 (1989) 407.
- [29] T. Manabe, H. Yamamoto and T. Okuyama, *Electrophoresis*, 10 (1989) 172.
- [30] K. Šlais, *J. Microcol. Sep.*, 5 (1993) 469.
- [31] J.C. Giddings, *Anal. Chem.*, 39 (1967) 1027.
- [32] J.C. Giddings, *Sep. Sci.*, 4 (1969) 181.
- [33] H. Svensson, *J. Chromatogr.*, 25 (1966) 266.
- [34] E. Glueckauf, *Trans. Faraday Soc.*, 51 (1955) 34.
- [35] A.S. Said, *Sep. Sci. Technol.*, 13 (1978) 647.
- [36] M. Bier, R.M. Cuddeback and A. Kopwillem, *J. Chromatogr.*, 132 (1977) 437.
- [37] K. Shima, *Electrophoresis*, 7 (1986) 297–303.
- [38] R.J. Routs, *Ann. N.Y. Acad. Sci.*, 209 (1973) 445.
- [39] W. Thormann and R.A. Mosher, *J. Trans. Soc. Comput. Simul.*, 1 (1984) 83.
- [40] M. Bier, R.A. Mosher and O.A. Palusinski, *J. Chromatogr.*, 211 (1981) 313.
- [41] L.M. Hjelmeland and A. Chrambach, *Electrophoresis*, 4 (1983) 20.
- [42] P. Gebauer and P. Boček, presented at the 4th International Symposium on High Performance Capillary Electrophoresis, Amsterdam, February 1992, abstracts, p. 90; *Electrophoresis*, in press.

- [43] E.V. Dose and G. Guiochon, *Anal. Chem.*, 63 (1991) 1063.
- [44] M. Bier, O.A. Palusinski, R. Mosher and D.A. Saville, *Science*, 219 (1983) 1281.
- [45] R.A. Mosher, D. Dewey, W. Thormann, D.A. Saville and M. Bier, *Anal. Chem.*, 61 (1989) 362.
- [46] V.G. Babskii, M.Yu. Zhukov and V.I. Yudovich, *Mathematical Theory of Electrophoresis*, Consultants Bureau, New York, 1989.
- [47] W. Thormann, R.A. Mosher and M. Bier, *J. Chromatogr.*, 351 (1986) 17.
- [48] P. Gebauer and P. Boček, *J. Chromatogr.*, 320 (1985) 49.
- [49] J.C. Giddings, *Anal. Chem.*, 53 (1981) 945A.
- [50] J.C. Giddings, *J. Chromatogr.*, 480 (1989) 21.

Time course of formation of inositol phosphates during enzymatic hydrolysis of phytic acid (myo-inositol hexaphosphoric acid) by phytase determined by capillary isotachophoresis

Pavel Blatný^a, František Kvasnička^b, Ernst Kenndler^{a,*}

^a*Institute of Analytical Chemistry, University of Vienna, Währingerstrasse 38, A-1090 Vienna, Austria*

^b*Department of Carbohydrate Chemistry and Technology, Institute of Chemical Technology, Prague, Technická 3, CZ-160 00 Prague, Czech Republic*

First received 28 April 1994; revised manuscript received 22 June 1994

Abstract

Capillary isotachophoresis with conductivity detection was applied to the investigation of the hydrolytic decomposition of phytic acid (myo-inositol hexaphosphoric acid) by phytase, and for the formation of the reaction products as a function of time. The quantitation of all analytes (besides phytic acid the mono- to pentaphosphorylated inositols and orthophosphate) can be carried out using two different buffer systems.

1. Introduction

The determination of the time course of the enzymatic hydrolysis of phytic acid (myo-inositol hexaphosphoric acid, IP6) has been carried out so far by an indirect method which is based on the measurement of the concentration of Fe(III) remaining in solution after the formation of an insoluble Fe–IP6 complex [1]. Fe(III) is then determined photometrically as rhodanide complex. This indirect measurement was necessary because IP6 has neither a specific reagent nor a characteristic absorption spectrum for direct determination, as pointed out in this paper.

It is obvious that the indirect method is subject to a number of errors, because not only phytic

acid, but also its degradation products may react with the Fe ions due to their chemical similarity to IP6. This method is unable to quantify these particular compounds, which is a prerequisite for the study of the reaction kinetics. Therefore a method has been introduced by the same authors [1] which allows the determination of all the compounds of interest, namely ³¹P NMR. Nevertheless, this method has a number of drawbacks. Besides its large instrumental and chemical expenditure (e.g. ²H₂O is used as a solvent for NMR measurements) no separation of the solutes is carried out, leading to superimposed signals which limit their relevance.

Isotachophoresis (ITP) with conductivity detection seems to fulfill all the demands required for the fast, simple and reliable analysis of phytic acid and its hydrolysis products (cf. e.g. [2]): it is

* Corresponding author.

a separation method of high performance for ionic components, which enables the resolution of chemically similar compounds. It combines the separation and the detection principle for these ionic separands, both based on the effective mobilities, which leads to a more or less universal detectability for these analytes, and makes the detection independent of individual properties such as UV absorbance.

ITP has been applied for the direct determination of phytic acid in food [3], where the pre-separation from the lower inositol phosphates (penta, IP5 to mono, IP1) and orthophosphate (P) was a necessity. In the present paper it is applied to separate the inositol derivatives with different degrees of phosphorylation, making it possible to observe the formation and decay of the degradation products of phytic acid during the hydrolysis with phytase.

2. Experimental

2.1. Chemicals

The following chemicals were used: hydrochloric acid (analytical-reagent grade; Merck, Darmstadt, Germany), 2-morpholinoethanesulfonic acid (99%), phytic acid (dodecasodium salt), 1,3 - bis[tris(hydroxymethyl)methylamino]propane (bis-tris-propane, 99 + %), hydroxyethyl cellulose (all from Aldrich, Steinheim, Germany); creatinine (99%), caproic acid (99–100%), phytase (crude from wheat, activity ca. 0.015 units per mg solid) (all from Sigma, Deisenhofen, Germany); ϵ -aminocaproic acid (>99%, Fluka, Buchs, Switzerland).

For the preparation of the buffers water deionised with a mixed-bed ion exchanger was used.

2.2. Apparatus

The volume-coupling instrument (Ionosep 900.1, Recman-Laboratorní Technika, Ostrava, Czech Republic) is equipped with PTFE capillaries (pre-separation part 50×1 mm, separation part 150×0.45 mm, detection part 70×0.3 mm) and a contactless high-frequency conductivity

cell. Injection is carried out by the use of a 20- μ l loop.

The constant current applied was 70 μ A initially and 30 μ A during detection.

2.3. Enzymic hydrolysis of phytic acid

A 50-mg amount of phytic acid (as dodecasodium salt) and 50 mg phytase were added to 50 ml buffer (0.04 M HCl adjusted to pH 5.15 with creatinine) and placed into a 100-ml flask. The solution was stirred on a water bath at 51°C. During the enzymic hydrolysis aliquots of the reaction mixture were taken at different times. The enzyme present in the samples was inactivated by boiling water for 1 min. Then the samples were stored at -20°C . Prior to the analysis the samples were defrosted and diluted 20-fold.

3. Results and discussion

3.1. ITP separation

In order to follow the time dependence of the hydrolytic decay of phytic acid on the one hand, and of the formation and hydrolysis of the degradation products (the lower inositol phosphates and phosphate) on the other hand the appropriate ITP conditions to separate the analytes must be found. It can be seen from Fig. 1 that system 1 (Table 1) allows the separation of most inositol phosphates and phosphate (IP4–IP1, P), but does not lead to a separation of IP6 from IP5. Therefore this system can be applied for the quantitation of these lower phosphates only. For the separation and quantitation of IP5 and IP6, however, another system has to be found. It is not likely that the separation can be enhanced by varying the pH, because it can be expected that the analytes have about the same pK values. For this reason the use of bis-tris-propane which has complex-forming properties is applied as counter ion of the leading electrolyte [2]. The resulting electropherograms, obtained by electrolyte system 2 (Table 1) are depicted in Fig. 2. It can be seen that IP6 and IP5, which

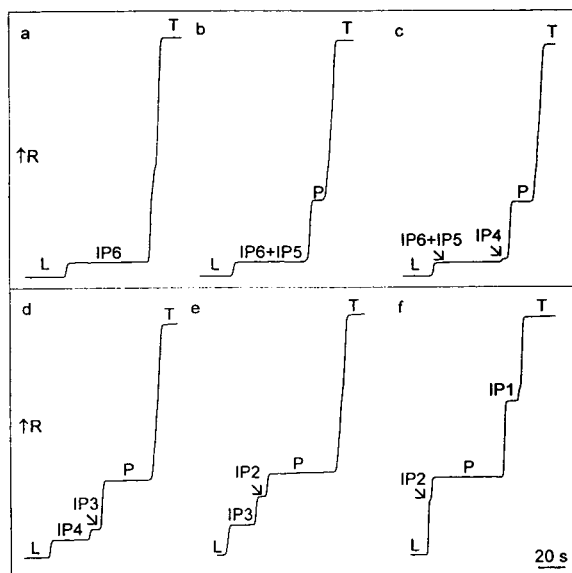


Fig. 1. Isotachopherograms of the reaction mixture of the enzymatic hydrolysis of phytic acid (IP6) after different times of reaction obtained with electrolyte system 1. IP6 and IP5 form a mixed zone. The degree of phosphorylation is indicated by the number in the symbol of the separands, e.g. IP5 for inositol pentaphosphate, etc. P = Orthophosphate; L = leading electrolyte; T = terminating electrolyte; R = electric resistance. Reaction time: (a) 0 min; (b) 2.5 min; (c) 20 min; (d) 40 min; (e) 90 min; (f) 210 min.

formed a mixed zone in system 1 are indeed migrating in two separated zones. They are also well separated from IP4 and P. It is therefore possible to quantitate all analytes by the use of these two buffering electrolyte systems.

Table 1
Buffering electrolyte systems for the determination of inositol phosphates and orthophosphate

System	Leading electrolyte ^a	pH	Terminating electrolyte
1	10 mM HCl + EACA	4.5	5 mM Caproic acid
2	10 mM HCl + BTP	6.1	5 mM MES

EACA = ϵ -Aminocaproic acid; BTP = bis-tris-propane; MES = 2-morpholinoethanesulfonic acid.

^a Leading electrolytes contain 0.1% hydroxyethyl cellulose.

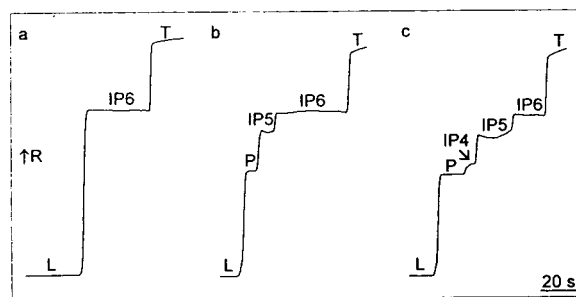


Fig. 2. Isotachopherograms of the reaction mixture of the hydrolysis of phytic acid shown in Fig. 1a, b and c, obtained with electrolyte system 2, demonstrating the separation of IP6 from IP5. Abbreviations as in Fig. 1.

3.2. Time course of the hydrolysis of phytic acid and lower inositol phosphates

The ITP results depicted in Figs. 1 and 2 allow to observe the time dependence of the formation and decay of all solutes formed during the hydrolysis. The result of the quantitation of the particular compounds is shown in Fig. 3 (where the concentration of the solutes is not given in absolute quantities, e.g. in M or in g/l, but as a relative content). This is done such that the length of the ITP zone of the particular component (which is proportional to the amount in the 20- μ l sample volume injected) is related to its maximum zone length observed during the entire time of hydrolysis. This depiction is appropriate for the goal of this investigation. A further

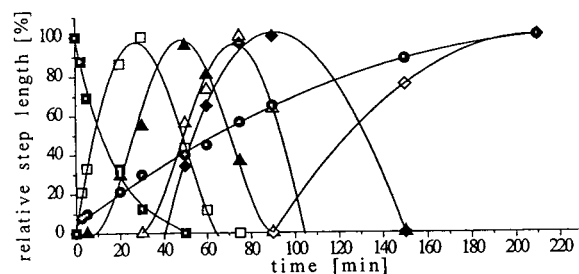


Fig. 3. Time course of the decay and formation of the inositol phosphates during the enzymatic hydrolysis of phytic acid, measured by ITP. \blacksquare = IP6; \square = IP5; \blacktriangle = IP4; \triangle = IP3; \blacklozenge = IP2; \diamond = IP1; \bullet = P. For details see text.

quantitation, e.g. by calibration with an external standard is possible. It is not obvious for the case under investigation because the decomposition products are hardly available as standards for calibration. In this case an approach could be carried out by calculating the effective mobilities from the step heights in the isotachopherograms and approximating the concentrations by the Kohlrausch “regulation function”. Even an overall mass balance could be made possible in this way. This is, however, not of interest for the problem presented here.

From Fig. 3 it can be seen that half of the initially present IP6 decays within 12 min under the given conditions, whereby the immediate formation of IP5 and P is clearly observed from the appearance of their ITP zones. The concentration of IP5 and P increases upon degradation of IP6. That of IP5 increases steeply, reaches a maximum value after 30 min, and decreases further. The gradual formation of the next reaction product, IP4, is observed after about 10 min. This product shows a nearly symmetric concentration vs. time curve of a similar shape as IP5 (in contrast to IP6, which obviously exhibits an overall decline). The curve of IP4 is, however, broader than that of IP5, an effect which is propagated for the subsequently

formed components: the curves have similar shapes but become increasingly broader.

Whereas the concentration of the higher inositol phosphates decreases after the maximum this is not longer the case for IP1: within the reaction time a maximum is approached but no decline is observed. A similar effect is found for P, the concentration of which is continuously increasing directly after the start of the hydrolysis, approaching a maximum value. The latter effect indicates a certain saturation of the hydrolysis due to the fact that the enzyme is probably not capable to hydrolyse IP1 [1].

From these results it can be concluded that ITP serves as a rapid and simple method to determine the time course of the hydrolysis of phytic acid.

References

- [1] W. Frølich, T. Drakenberg and N.-G. Asp, *J. Cereal Sci.*, 4 (1986) 325.
- [2] F.M. Everaerts, J.L. Beckers and Th.P.E.M. Verheggen, *Isotachopheresis —Theory, Instrumentation and Applications (Journal of Chromatography Library, Vol. 6)*, Elsevier, Amsterdam, 1976, Ch. 15.
- [3] P. Blatný, F. Kvasnička and E. Kenndler, *J. Food Sci.*, submitted for publication.



ELSEVIER

Journal of Chromatography A, 679 (1994) 349–357

JOURNAL OF
CHROMATOGRAPHY A

Sensitive and selective method for the separation of organic acids by capillary zone electrophoresis

Olivier Devêvre^{a,*}, Deddi Prima Putra^b, Bernard Botton^b, Jean Garbaye^a

^a*Equipe de Microbiologie Forestière, Centre INRA de Nancy, F-54280 Champenoux, France*

^b*Laboratoire de Physiologie Végétale et Forestière, Université de Nancy I, F-54500 Vandoeuvre-Les-Nancy, France*

First received 23 March 1994; revised manuscript received 1 June 1994

Abstract

A simple and rapid method was developed for the separation and determination of a large number of organic acids by using capillary zone electrophoresis, with hydrostatic injection for 30 s and UV detection at 254 nm. Electropherograms were obtained with 4-hydroxybenzoate buffer (5 mM) adjusted to pH 4.75 at 25°C. The electroosmotic flow modifier (commercial solution) was added to the buffer at a concentration of 25 ml l⁻¹. Co-migration problems could be solved by modifying the pH of the electrophoresis buffer or by addition of Ca²⁺ to the buffer.

1. Introduction

Capillary zone electrophoresis (CZE) is the simplest form of capillary electrophoresis (CE). The separation mechanism is based on differences in electrophoretic mobilities which are dependent on the charge to mass ratio. CZE has grown increasingly popular in the field of analytical chemistry, and has been successfully used to detect and measure biomolecules [1], carbohydrates [2,3], milk and soy proteins [4] and organic acids in juices from beet sugar production [5].

CZE with indirect UV detection has been shown to be a good alternative to conventional chromatographic methods such as high-performance liquid chromatography (HPLC). Indeed, CZE requires no sample preparation, other than

dilution, has a fast analysis time (less than 7 min) and consumes only limited amounts of reagents.

The objective of this work was to optimize the separation and determination of the greatest possible number of organic acids in culture filtrates of soil fungi.

2. Experimental

2.1. Apparatus

CZE was performed on a Waters Quanta 4000 capillary electrophoresis system equipped with a UV detector set at 254 nm, with an applied voltage (*V*) of 20 kV. A fused-silica capillary (Waters), 60 cm in length (*L_t*) with I.D. 75 μm, was used and the detector window was set at 52.4 cm (*L_d*). The wall of the capillary was covered with ionizable silanol groups. In order to

* Corresponding author.

ensure that the surface of the capillary was fully and uniformly charged, it was necessary to pretreat it. Before analysis, the capillary was pretreated for 10 min with 0.1 M sodium hydroxide solution, 10 min with deionized water and 30 min with running buffer until equilibrium was reached.

2.2. Power supply and electroosmotic flow

In a normal CZE system, the capillary is filled with a background electrolyte solution and the capillary ends are immersed in separate reservoirs containing this solution. The detector is located near the cathode and the electroosmotic flow (EOF) direction is from the anode to the cathode. The EOF, as a result of an applied voltage along the capillary, is the net flow of buffer solution in the direction of the negative electrode. Usually, the EOF rate is so strong that all analytes, even those with a negative charge, move to the cathode. However, when the electrophoretic mobilities of some anions are higher than the EOF mobility of the electrolyte, these anions will escape detection because they move backwards. This problem could be solved by reversing the polarity of the applied electric field. However, the organic acids with an electrophoretic mobility equal to or lower than the EOF mobility will not be detected. One way to avoid this problem is to add an appropriate surfactant to the electrolyte in order to reverse the direction of the EOF by reversing the charge of the capillary wall. Accordingly, a negative-voltage power supply was used and 25 ml of an electroosmotic flow modifier (Waters OFM Anion-BT commercial solution) was added per litre.

2.3. Injection mode

At one capillary end the background electrolyte reservoir is replaced by the sample reservoir only during sample injection. Two injection modes are usually possible under our practical experimental conditions: hydrostatic injection or electrokinetic injection (electromigration). Some workers have remarked that electrokinetic injection

involves biases [6,7]. When a voltage is applied to the capillary length during electrokinetic injection, a larger effective volume of faster ions than slower ions will be injected, because of the different mobilities of the species in the sample solution [8]. Contrary to electrokinetic injection, hydrostatic injection effected by gravity does not discriminate between the ions, and the same effective sample volume of each ion is injected. In CZE with hydrostatic injection, as in HPLC analysis, there always exists a defined injection volume. Accordingly, the hydrostatic injection mode was used.

2.4. Injection time

Selection of the injection time was based on the relative standard deviations for peak area, which were found to decrease with increasing injection time [5]. Further, as described previously [9,10], to obtain high resolution in capillary electrophoresis the volume of the injected sample must be small compared with the capillary volume. With a capillary that had a volume of about 3 μ l (as here), 5–50 nl was the injection volume required to avoid distortion by overloading [9,10]. In this work, samples were introduced hydrostatically into the capillary for 30 s, and about 30 nl were injected.

2.5. Samples

Stock standard solutions of carboxylic acids were prepared at a concentration of 10 mM, using deionized water obtained with a Milli-Q system (Millipore). Before storage at 4°C, all solutions were sterilized by filtration through a 0.2- μ m membrane.

3. Results and discussion

Optimization of the parameters was carried out by investigating the influence of electrolyte composition, pH and temperature on the mobilities. In accordance with the aims of this work, the initial selection of the background electrolyte was based on literature data ([11], Waters com-

munications) and on our experimentation. Electropherograms were obtained with a 4-hydroxybenzoate buffer, prepared with deionized water (Milli-Q), and adjusted to the appropriate pH with sodium hydroxide at 25°C. The electrolyte solution was filtered through a 0.45- μm membrane. This buffer and the OFM concentration (as noted under Experimental) were selected to optimize the separation of most organic anions, especially current organic acids from microbe metabolism.

The electrophoretic mobility of different acids and the EOF are partly dependent on the buffer viscosity. The viscosity is dependent on temperature; therefore, precise temperature control is important. As the temperature increases, the viscosity decreases, and both the EOF and electrophoretic mobility increase. The mobility of most ions increases by 2% per degree. Further, the pH of some buffers is known to be temperature sensitive. For all these reasons, the electrolyte buffer pH was adjusted to 25°C (controlled temperature). However, because we could not operate at an elevated controlled temperature (near 25°C), an alternative was to reduce the buffer concentration from 20 to about 5 mM. Thus, 4-hydroxybenzoate buffer was used at 5 mM. However, a decrease in the buffer concentration also reduces the peak efficiency by decreasing the focusing effect. At a fixed buffer

concentration, variations of pH modify the focusing effect and also the measured peak areas. Fig. 1 shows the resulting effect of electrophoresis buffer pH on the peak areas of some acids. The response depends on the species studied. However, in general, when the buffer pH increases from 4 to 6, the corrected peak areas also increase.

Fig. 2 shows the resulting electropherograms for an organic acid mixture. The effect of electrolyte pH on organic acid separation was tested. In order to make an accurate comparison between different analytical conditions, each electrolyte pH must be adjusted at a fixed temperature (25°C under our conditions). The net electric charge of an organic anion is pH dependent, and the selectivity of the separation is affected by the buffer pH. Indeed, when the molecular masses of the organic acids are approximately the same, acids with lower $\text{p}K_a$ values are eluted faster than those with higher values. At a fixed buffer pH, species mobility is partly a function of the charge to mass ratio, which depends on the $\text{p}K_a$ values. Table 1 gives the $\text{p}K_a$ values of eleven organic acids and their charge to mass ratio. In Fig. 2a, it is apparent that most acid standards cannot be separated with an electrolyte pH of 7.25 at 25°C; only gallic acid was separated at this buffer pH. A better separation can be achieved by decreasing the pH of the

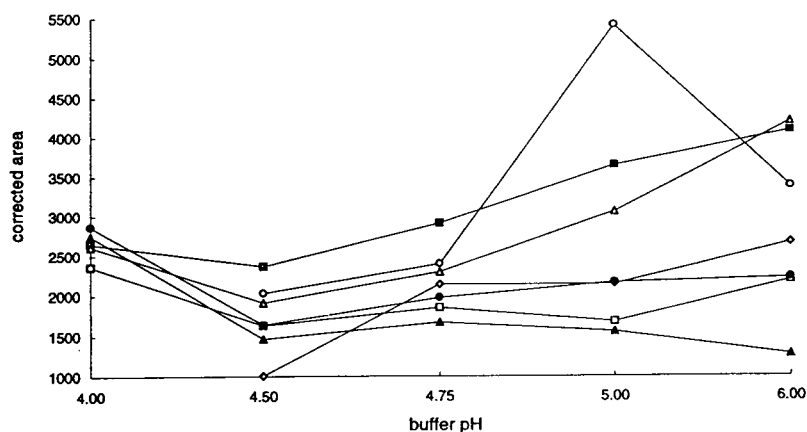


Fig. 1. Effect of buffer pH on measured peak areas which depend on the focusing effect. Each pH was adjusted at 25°C, after addition of 2.5% (v/v) OFM. Analytes: ▲ = Formic acid (0.1); ■ = fumaric acid (0.1); ○ = citric acid (0.2); ◇ = L-malic acid (0.1); □ = D-lactic acid (0.1); △ = succinic acid (0.1); ● = D-gluconic acid (0.1 mM).

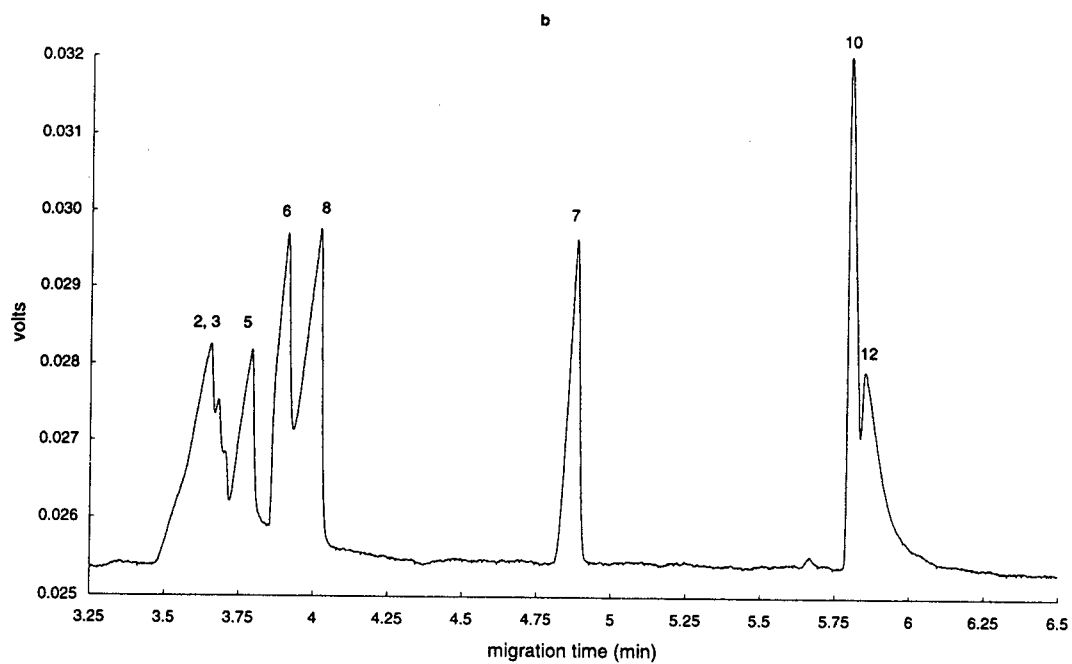
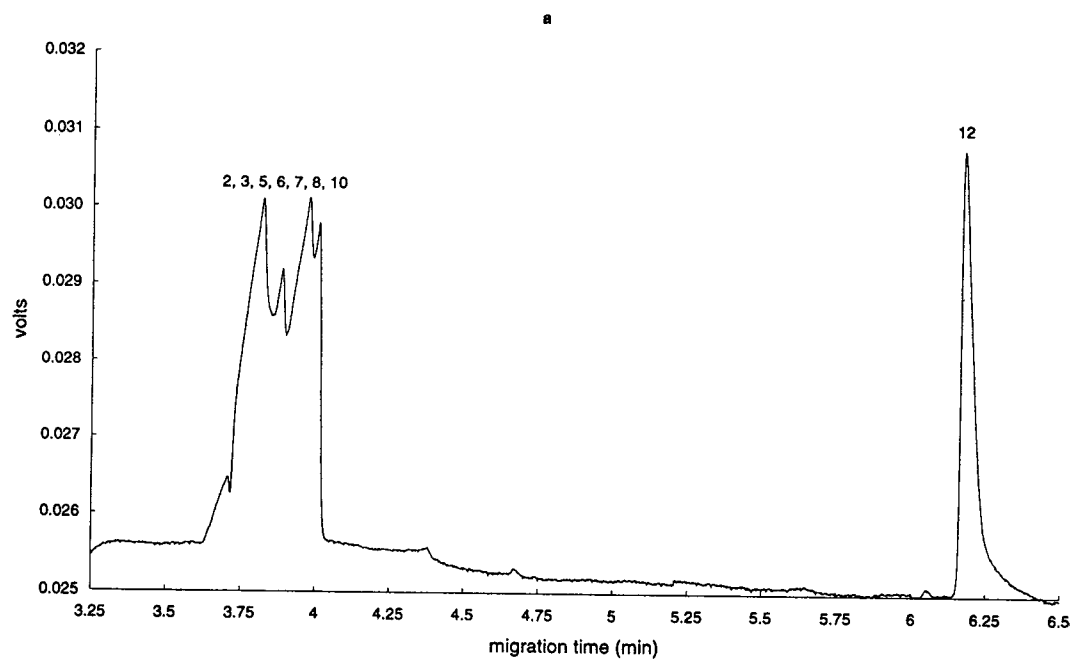


Fig. 2.

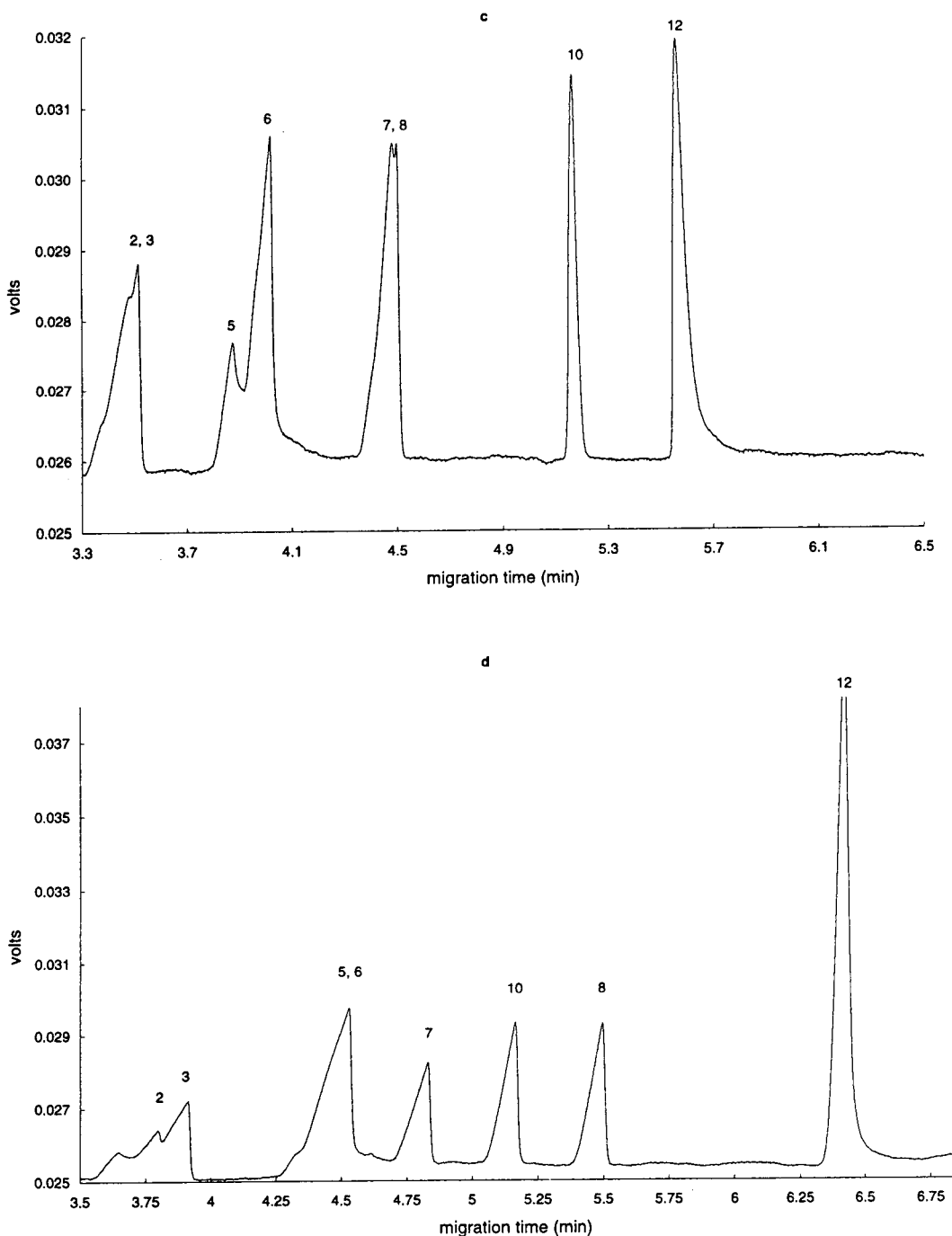


Fig. 2. Separation of eight-component organic acid mixture. pH of electrolyte: (a) 7.25 at 25°C, with 2.5% (v/v) OFM; (b) 6.00 at 25°C, with 2.5% (v/v) OFM; (c) 5.00 at 25°C, with 2.5% (v/v) OFM; (d) 4.00 at 25°C, with 2.5% (v/v) OFM. Peaks: 2 = formic acid (0.1); 3 = fumaric acid (0.1); 5 = citric acid (0.2); 6 = L-malic acid (0.1); 7 = D-lactic acid (0.1); 8 = succinic acid (0.1); 10 = D-gluconic acid (0.1); 12 = gallic acid (0.5 mM). Absorbance was measured at 254 nm.

Table 1

pK_a values of sixteen organic acids, and their relative charge to mass ratio at pH 4.75 at 25°C

Compound	M _r	pK _a at 25°C	Charge/mass ratio
Oxalic acid	90.04	pK ₁ = 1.27, pK ₂ = 4.275	0.0222
Formic acid	46.02	pK = 3.75	0.0217
Fumaric acid	116.07	pK ₁ = 2.03, pK ₂ = 4.54	0.0173
Pyruvic acid	88.1	pK = 2.49	0.0113
Maleic acid	116.07	pK ₁ = 1.97, pK ₂ = 6.24	0.0086
L-Malic acid	134.09	pK ₁ = 3.40, pK ₂ = 5.13	0.0074
Citric acid	192.12	pK ₁ = 3.13, pK ₂ = 4.76, pK ₃ = 6.39	0.0052
D-Lactic acid	90.08	pK = 3.83	0.0111
Succinic acid	118.09	pK ₁ = 4.21, pK ₂ = 5.64	0.0084
DL-Aspartic acid	133.1	pK ₁ = 1.99, pK ₂ = 3.90	0.0150
D-Gluconic acid	196.16	pK = 3.60	0.0050
Acetic acid	60.05	pK = 4.76	0.0166
L-Ascorbic acid	176.12	pK = 4.17	0.0056
Shikimic acid	174.2	pK = 4.21	0.0057
Propionic acid	74.08	pK = 4.87	0
n-Butyric acid	80.1	pK = 4.83	0

electrolyte solution (Fig. 2b–d). The electric field strength ($E \text{ V cm}^{-1}$) was constant with an applied voltage of -20 kV . At a fixed buffer concentration, when the buffer pH increases, the resulting current increases (Table 2). However, more current increases the heat produced, owing to Joule heating [12–14]. The heat is more or less readily dissipated across the silica capillary wall. Consequently, under our experimental conditions, when the pH increases the resolution decreases. A liquid cooling system [15] would be the most effective means of heat removal and thermal control. We might adjust the electrophoresis buffer pH in order to maintain both high resolution and a substantial detection level.

Fig. 3 shows the resulting electropherogram for an eighteen carboxylic acid mixture analysed

Table 2

Resulting current (μA) with different buffer pH, 5 mM 4-hydroxybenzoate and 2.5% (v/v) OFM, with an applied voltage of -20 kV

Buffer pH	Current (μA)	Buffer pH	Current (μA)
4.00	3.8	6.00	6.1
4.50	4.1	7.25	7.0
4.75	4.8	8.50	7.4
5.00	5.2		

with an electrolyte at pH 4.75; complete separation was obtained. The differences in species mobilities are greatly influenced by the pH of the electrolyte solution. Table 3 gives the electrophoretic mobilities [apparent migration rate = $(L_d/t)/(V/L_i)$] of different organic acids separated in Fig. 3. The actual mobility (electro-osmotic mobility) of a species is the sum of the EOF rate and the electrophoretic rate and is expressed in $10^{-4} \text{ cm}^2 \text{ s}^{-1} \text{ V}^{-1}$. The EOF rate is determined by measuring the migration time of a neutral marker molecule such as water. Therefore, to perform reproducible analyses, the EOF must be carefully controlled.

Some organic acids have very similar structures or the same electrophoretic behaviour, and their mobilities are not sufficiently different to allow good resolution. Under the above-defined analytical conditions, citrate and isocitrate migrate together, as do fumarate and tartrate. The relative mobility of ions can be influenced by changing their charge state through selective complexation. This principle has been used by different workers [16–18]. To optimize the separation of the fumarate–tartrate and citrate–isocitrate pairs, cationic complexation has been found to be effective. Fig. 4 shows the resulting effect of addition of calcium chloride to the

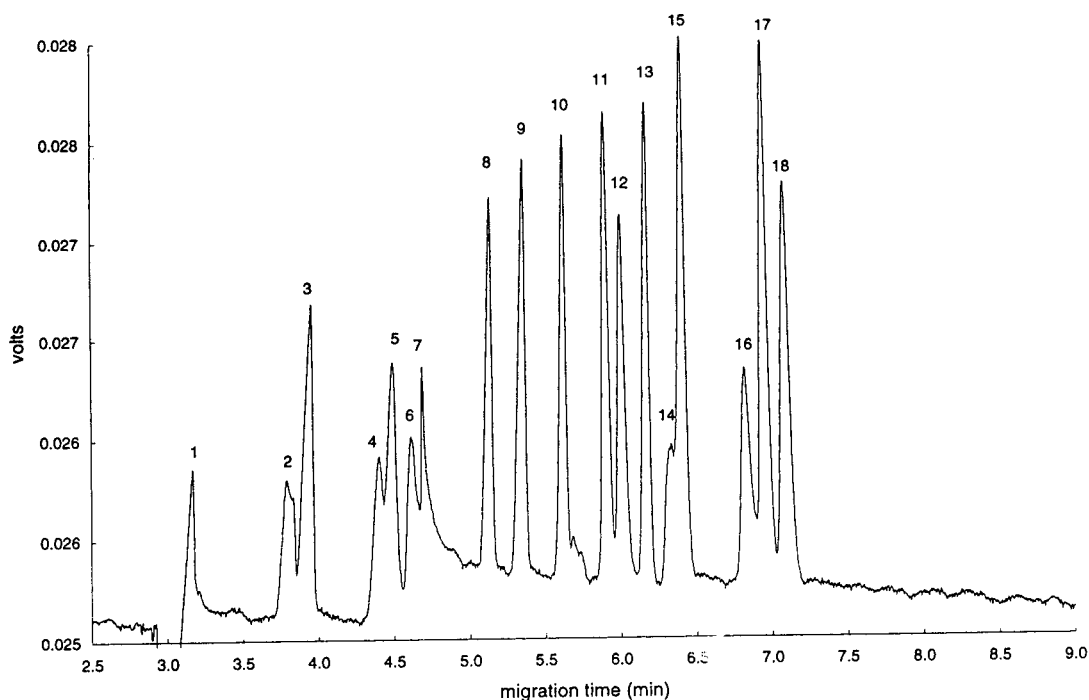


Fig. 3. Capillary electropherogram of eighteen-component organic acid mixture. 4-Hydroxybenzoate buffer at pH 4.75 at 25°C, with 2.5% (v/v) OFM. Peaks: 1 = oxalic acid (0.2); 2 = formic acid (0.1); 3 = fumaric acid (0.1); 4 = pyruvic acid (0.15); 5 = maleic acid (0.1); 6 = L-malic acid (0.1); 7 = citric acid (0.25); 8 = D-lactic acid (0.1); 9 = succinic acid (0.1); 10 = DL-aspartic acid (0.1); 11 = D-gluconic acid (0.1); 12 = D-gluconic acid (0.1); 13 = acetic acid (0.1); 14 = L-ascorbic acid (0.1); 15 = shikimic acid (0.1); 16 = gallic acid (0.2); 17 = propionic acid (0.1); 18 = *n*-butyric acid (0.1 mM).

Table 3

Calculated electrophoretic mobilities of eighteen organic acids under the following conditions: 5 mM 4-hydroxybenzoate solution containing 2.5% (v/v) OFM, adjusted to pH 4.75 at 25°C, with an applied voltage of -20 kV

Compound	Electrophoretic mobility ($10^{-4} \text{ cm}^2 \text{ s}^{-1} \text{ V}^{-1}$)	Compound	Electrophoretic mobility ($10^{-4} \text{ cm}^2 \text{ s}^{-1} \text{ V}^{-1}$)
Oxalic acid	8.26	DL-Aspartic acid	4.65
Formic acid	6.91	D-Gluconic acid	4.44
Fumaric acid	6.61	D-Gluconic acid	4.36
Pyruvic acid	5.94	Acetic acid	4.24
Maleic acid	5.82	L-Ascorbic acid	4.14
L-Malic acid	5.67	Shikimic acid	4.09
Citric acid	5.58	Gallic acid	3.84
D-Lactic acid	5.09	Propionic acid	3.77
Succinic acid	4.88	<i>n</i> -Butyric acid	3.69

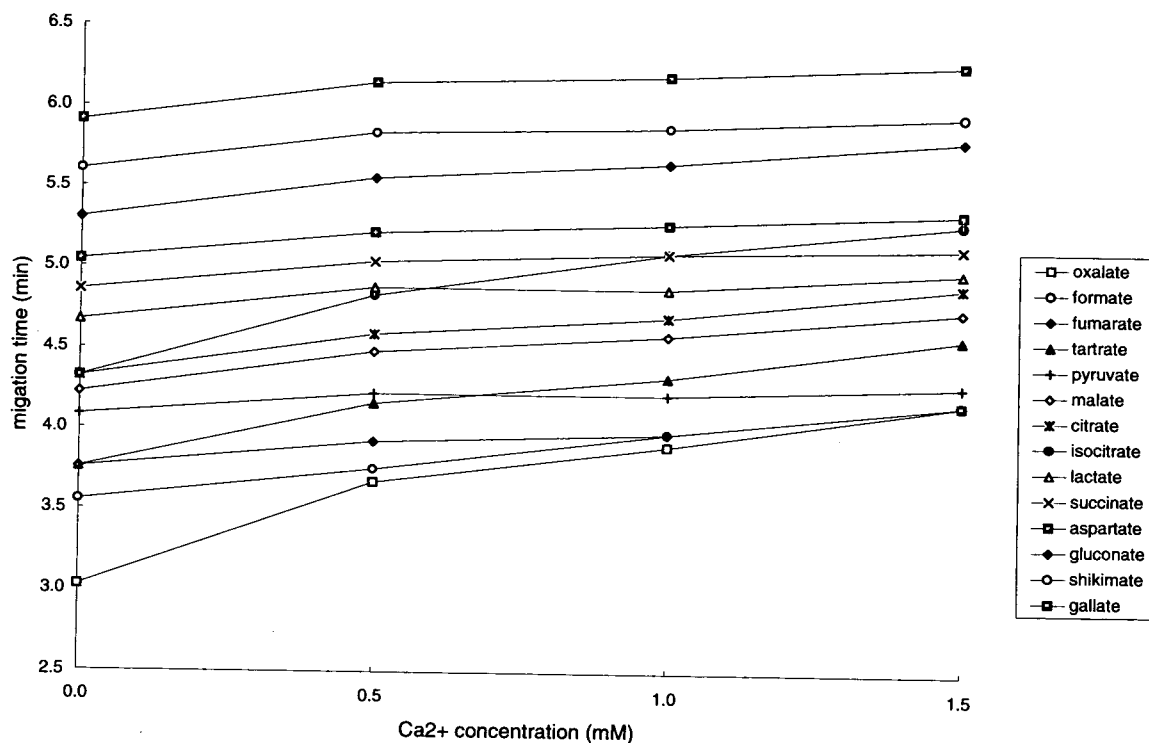


Fig. 4. Effect of Ca^{2+} concentration (calcium chloride addition) on the separation of organic acids. Conditions as in Fig. 3, except for the addition of calcium.

electrolyte buffer on the separation of fourteen organic acids. The buffer pH was adjusted to 4.75 after addition of calcium chloride. With 0.5–1.5 mM Ca^{2+} ($\text{CaCl}_2 \cdot 6\text{H}_2\text{O}$) added to the buffer, all organic acids are more or less retarded. Only oxalate, tartrate and isocitrate are significantly more retarded than the other acids tested. As shown in Fig. 4, a more effective separation was obtained with about 0.4 mM Ca^{2+} . The same results, for the separation of tartrate have been reported by Lalljie et al. [5] in work on the determination of organic acids in sugar refinery juices.

The separation and determination of oxalic acid are too difficult, if not impossible, using this method because the small oxalic acid signal could be partly or even totally obscured by the response of the accompanying inorganic anions such as chloride, sulfate, nitrite and nitrate, in a more complex medium than a standard acid mixture. This problem can be solved by using

another electrolyte buffer; separation between inorganic anions and oxalic acid is obtained with 5 mM chromate buffer at pH 6.0 (results not shown).

4. Conclusions

Analysis performed with 0.4 mM Ca^{2+} and 2.5% (v/v) OFM added to 4-hydroxybenzoate buffer adjusted to pH 4.75 at 25°C gave optimum separation between all the organic acids tested.

For organic acids from plant or fungal metabolisms, the proposed method using CZE provides good separation in a relatively short time, with a limited amount of sample. However, a considerable amount of time may have to be spent carefully selecting buffers, additives and analysis conditions in order to identify other additional species. From the separations reported here, it is apparent that CZE will become

a powerful complement to HPLC for the analysis of complex mixtures and the separation of organic acids from plant or microbe metabolism.

References

- [1] T.M. Phillips, *LC·GC Int.*, 6 (1993) 290.
- [2] P.J. Oefner, A.E. Vorndran, E. Grill, C. Huber and G.K. Bonn, *Chromatographia*, 34 (1992) 308.
- [3] A.E. Vorndran, P.J. Oefner, H. Scherz and G.K. Bonn, *Chromatographia*, 33 (1992) 163.
- [4] M. Kanning, M. Casella and C. Olieman, *LC·GC Int.*, 6 (1993) 701.
- [5] S.M.P. Lalljie, J. Vindevogel and P. Sandra, *J. Chromatogr.*, 652 (1993) 563.
- [6] T. Tsuda, T. Mizuno and J. Akiyama, *Anal. Chem.*, 59 (1987) 799.
- [7] X. Huang, M.J. Gordon and R.N. Zare, *Anal. Chem.*, 60 (1988) 375.
- [8] J. Warburton, *Int. Labmate*, (1993) 27.
- [9] F.E.P. Mikkers, F.M. Everaerts and Th.P.E.M. Verheggen, *J. Chromatogr.*, 169 (1979) 11.
- [10] M.J. Sepaniak and R.O. Cole, *Anal. Chem.*, 59 (1987) 472.
- [11] X. Huang, J.A. Luckey, M.J. Gordon and R.N. Zare, *Anal. Chem.*, 61 (1989) 766.
- [12] H. Stuppner and S. Sturm, *J. Chromatogr.*, 609 (1992) 375.
- [13] J.W. Jorgenson and K.D. Lukacs, *Anal. Chem.*, 53 (1981) 1298.
- [14] H.J. Issaq, G.M. Janini, I.Z. Atamna and G.M. Muschik, *J. Liq. Chromatogr.*, 14 (1991) 817.
- [15] M.J. Eby, *Bio/Technology*, 7 (1989) 903.
- [16] A. Weston, P.R. Brown, P. Jandik, W.R. Jones and A.L. Heckenberg, *J. Chromatogr.*, 593 (1992) 289.
- [17] T. Groh and K. Bächmann, *Electrophoresis (Weinheim)*, 13 (1992) 458.
- [18] K. Bächmann, H. Steeg, T. Groh, I. Haumann, J. Boden and H. Holthues, *J. Microcol. Sep.*, 4 (1992) 431.



ELSEVIER

Journal of Chromatography A, 679 (1994) 359–365

JOURNAL OF
CHROMATOGRAPHY A

Use of selectively methylated β -cyclodextrin derivatives in chiral separation of dansylamino acids by capillary zone electrophoresis

Masanobu Yoshinaga^a, Minoru Tanaka^{*.b}

^aKansai Technical Research Institute, Toppan Printing Co., Ltd., Ebie, Fukushima-ku, Osaka 553, Japan

^bDepartment of Applied Chemistry, Faculty of Engineering, Osaka University, Yamada-oka, Suita, Osaka 565, Japan

First received 22 February 1994; revised manuscript received 1 June 1994

Abstract

The chiral separation ability of heptakis(2-, 3- and 6-mono-O-methyl, 2,3-, 2,6- and 3,6-di-O-methyl and 2,3,6-tri-O-methyl)- β -cyclodextrins as chiral selectors in capillary zone electrophoresis was investigated using twelve dansylamino acids. Unmodified and 6-monomethylated β -cyclodextrins (β -CDs) exhibited similar high enantioselectivities. β -CD lost its high enantioselectivity after 2-methylation but still exhibited chiral separation ability after 3-methylation. In contrast to unmodified β -CD, methylation of the hydroxyl groups at the 6-position of 3-monomethylated β -CD resulted in the complete disappearance of the chiral separation ability but that of 2,3-dimethylated β -CD enhanced it. Moreover, the chemical modification of the secondary hydroxyl groups produced a reverse migration order of the enantiomers.

1. Introduction

Capillary zone electrophoresis (CZE) is attracting much attention as a method for separating a wide range of ionic and ionizable compounds owing to its rapid run times, extremely high separation efficiency, low sample requirements, etc. [1,2]. In particular, CZE is undergoing rapid development for chiral separations at the present time. In order to perform chiral separations, various chiral selectors are added to the CZE buffers. Unmodified and chemically modified cyclodextrins (CDs) have been successfully utilized for these purposes.

The chemical modification of CDs with various

functional groups has been extensively investigated in an attempt to improve the complexing and catalytic abilities of CDs. Various functional groups have been introduced on to their rims [3]. It is well known that the chemical modification of CDs brings about changes in the shape and size of their cavities, hydrogen-bonding ability and other physical properties.

Among chemically modified CD derivatives, methylated compounds have been widely used as chiral selectors in CZE [4–12]. In a previous paper [13], we reported the chiral separation of dansylamino acids by CZE using unmodified α -, β - and γ -CDs or 2,6-dimethylated and 2,3,6-trimethylated α - and β -CDs as chiral selectors. The chemical modifications of α - and β -CDs brought about remarkable changes in their enan-

* Corresponding author.

tioselectivities for dansylamino acids. To our knowledge, only 2,6-dimethylated and 2,3,6-trimethylated CDs have hitherto been applied as chiral selectors. Therefore, it was of interest to investigate the CZE enantioselectivity changes in CDs produced by selective methylation of the hydroxyl groups at their 2-, 3-, 6-, 2,3- or 3,6-positions. The results obtained may offer information concerning the evaluation of the chiral recognition of CDs.

In this paper, we describe the chiral separation of dansylamino acids by CZE in the presence of all the above-mentioned methylated β -CD derivatives.

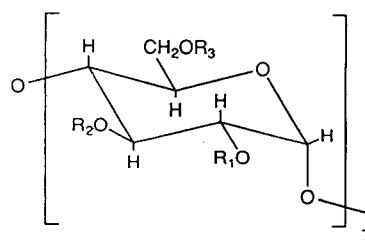
2. Experimental

2.1. Apparatus

An Applied Biosystems (Foster City, CA, USA) Model 270A fully automated CZE system was used with a 72 cm (50 cm from inlet to detector) \times 50 μ m I.D. fused-silica capillary. On-column UV detection was applied at 220 nm. The temperature and applied voltage were held constant at 30°C and 20 kV, respectively, unless specified otherwise. Sample solutions (0.2 mM) were injected by a vacuum technique (12.7 cmHg pressure difference for 1.0 s) after introducing methanol as a neutral marker to estimate the osmotic flow. Before each run, the capillary was rinsed successively with 0.1 M NaOH and the separation buffer. Electropherograms were recorded with a Hitachi (Tokyo, Japan) D-2500 Chromato-integrator. All experiments were run in duplicate to ensure reproducibility.

2.2. Reagents

Unmodified β -CD was purchased from Ensuiko Seito (Yokohama, Japan) and heptakis(2,6-di-O-methyl)- and heptakis(2,3,6-tri-O-methyl)- β -CDs were prepared by well-known methods [14,15]. Heptakis(2-, 3- and 6-mono-O-methyl and 2,3- and 3,6-di-O-methyl)- β -CDs were synthesized by modifying the literature method [16]. The mono-, di- and trimethylated β -CDs obtained are denoted by



R ₁	R ₂	R ₃	Abbreviation
CH ₃	H	H	2-MM- β -CD
H	CH ₃	H	3-MM- β -CD
H	H	CH ₃	6-MM- β -CD
CH ₃	CH ₃	H	2,3-DM- β -CD
CH ₃	H	CH ₃	2,6-DM- β -CD
H	CH ₃	CH ₃	3,6-DM- β -CD
CH ₃	CH ₃	CH ₃	2,3,6-TM- β -CD

Fig. 1. Structures of methylated β -CD derivatives used as chiral selectors.

prefixing the unmodified β -CD with MM-, DM- and TM-, respectively (Fig. 1). Dansylamino acids were obtained from Sigma (St. Louis, MO, USA) and other compounds from Wako (Osaka, Japan).

Separation buffers were prepared by dissolving each methylated β -CD at 10 mM except for 6-MM- β -CD (2 mM) in 0.1 M sodium borate–0.05 M sodium phosphate buffer (pH 9.0). They were filtered through a membrane filter after ultrasonication for 10 min prior to use.

3. Results and discussion

3.1. Characterization of methylated β -CD derivatives

After isolation, crude methylated β -CD derivatives were fractionated by silica gel column

chromatography, using chloroform–methanol as eluents [16]. The methylated β -CD derivatives thus obtained were characterized by ^1H and ^{13}C NMR spectrometry and fast atom bombardment mass spectrometry (FAB-MS). Each fractionated β -CD derivative was a mixture of heptakis(methyl)- β -CD and its under- and/or over-methylated products. Ion peaks corresponding to the methyl–oxygen bond scission products [i.e., loss of methyl group(s)] were not observed in FAB tandem mass spectra. Therefore, the composition of each methylated β -CD derivative could be estimated from the relative intensities of the $[\text{M} + \text{K}]^+$ ions (KI was adulterated with the samples).

Table 1 gives the composition of the methylated β -CD derivatives used here for CZE. It has been reported that several commercial 2,6-DM- β -CD derivatives were mixtures with broad and roughly symmetrical distributions of the degree of substitution and that the content of heptakis(2,6-di-O-methyl)- β -CD was 41% at most [17]. A higher purity of 52.6% was achieved with our 2,6-DM- β -CD (Table 1). Compared with this, the other methylated β -CDs were much more enriched in the desired heptakis(methyl)- β -CD derivatives.

3.2. Chiral separation of dansylamino acids

For a clear separation, the extent of separation of the two peaks of a racemate is represented by

$R' = 100(H - H')/H$, where H and H' are the height of the first peak and that of the valley between the two peaks, respectively. In this definition, the greater the R' value the better is the resolution, and $R' = 100$ represents a baseline separation of the two peaks.

The CZE conditions optimized for separating the dansylamino acid enantiomers were given under Experimental. The pH of the separation buffer solutions was fixed at 9.0 in order to run the solutes in the fully ionized forms. Under these CZE conditions, the β -CD derivatives having no charge are transported towards the negative electrode by electroosmotic flow (V_{eo}). In the absence of the β -CD derivatives, each negatively charged dansylamino acid migrates toward the negative electrode with the difference between V_{eo} and its electrophoretic velocity (V_{ep}) due to $V_{eo} > V_{ep}$. When included in a β -CD cavity, the solute is transported towards the negative electrode faster, because of the decrease in V_{ep} . This, therefore, indicates that a faster migrating enantiomer interacts more strongly with the β -CD cavity than the other.

Table 2 gives the migration times and the R' values for the twelve pairs of dansylamino acid enantiomers in the presence of unmodified and monomethylated β -CDs. Unmodified β -CD and 6-monomethylated β -CD (6-MM- β -CD), whose secondary hydroxyl groups at the 2- and 3-positions are not methylated, exhibited good and comparable enantioselectivities. The D-enantiomers invariably migrated faster than the corresponding L-enantiomers in the presence of β -CD or 6-MM- β -CD, indicating their stronger interaction with the D-enantiomers. These results strongly suggest the major participation of the secondary hydroxyl groups in the chiral recognition process and the minor or scarce participation of the primary hydroxyl groups.

It was of great interest to investigate which secondary hydroxyl groups play an important role in the chiral recognition process. Therefore, 2- and 3-monomethylated β -CDs (2-MM- β -CD and 3-MM- β -CD, respectively) were synthesized as chiral selectors. Methylation of the 2-hydroxyl groups (2-monomethylation) in β -CD resulted in the complete disappearance of enantioselectivity except for dansyl-DL- α -aminobutyric acid ($R' =$

Table 1
Composition of methylated β -CD derivatives

β -CD derivative	Composition (%) ^a			
	–CH ₃	0	+CH ₃	+2CH ₃
2-MM- β -CD	15.4	76.9	7.7	0
3-MM- β -CD	14.3	76.2	9.5	0
6-MM- β -CD	2.9	97.1	0	0
2,3-DM- β -CD	6.5	93.5	0	0
2,6-DM- β -CD	0	52.6	36.8	10.6
3,6-DM- β -CD	0	90.6	9.4	0
2,3,6-TM- β -CD	5.6	88.8	5.6	0

^a 0 = Desired heptakis(methyl)- β -CD; – = under-methylated β -CD derivative; + = over-methylated β -CD derivative.

Table 2
Chiral separation of dansylamino acids in the presence of unmodified and monomethylated β -CDs

Dansylamino acid	β -CD		2-MM- β -CD		3-MM- β -CD		6-MM- β -CD	
	Migration time (min)	R'	Migration time (min)	R'	Migration time (min)	R'	Migration time (min)	R'
α -Amino- <i>n</i> -butyric acid	D 9.20	12.7	D 10.20	83.6	10.26		D 11.44	62.1
	L 9.24		L 10.28				L 11.57	
Aspartic acid	D 12.84	100	20.30		19.01		D 23.02	100
	L 13.18						L 23.70	
Glutamic acid	D 12.72	100	19.09		17.78		D 21.86	93.4
	L 12.93						L 22.25	
Leucine	D 8.96	52.5	9.77		L 9.56	90.1	D 11.54	90.3
	L 9.08				D 9.64		L 11.57	
Methionine	D 9.28	31.6	10.33		L 10.06	14.2	D 11.70	11.7
	L 9.33				D 10.10		L 11.76	
Norleucine ^a	9.16	35.9	10.01		9.70	55.0	11.45	18.3
	9.22				9.76		11.54	
Norvaline	D 9.14	44.1	10.32		L 9.89	18.5	D 11.36	64.7
	L 9.20				D 9.93		L 11.49	
Phenylalanine	8.84		9.57		L 9.42	69.7	11.56	
					D 9.49			
Serine	D 9.48	38.8	11.05		10.62		12.37	
	L 9.53							
Threonine	D 9.13	94.0	10.77		10.49		D 12.05	63.8
	L 9.22						L 12.17	
Tryptophan	8.89		9.50		L 9.50	68.3	11.40	
					D 9.57			
Valine	D 9.00	76.4	10.40		10.06		D 11.56	96.5
	L 9.08						L 11.76	

^a Neither enantiomer was obtained.

83.6). On the other hand, after 3-monomethylation of β -CD, six pairs of dansylamino acid enantiomers could still be resolved. This suggests a positive contribution of the 2-hydroxyl groups to the chiral recognition. In contrast to the results for β -CD and 6-MM- β -CD, the L-enantiomers migrated faster in the presence of 3-MM- β -CD. Moreover, 3-MM- β -CD could not resolve dansyl-DL-aspartic and -glutamic acid, -serine and -threonine bearing a hydrophilic OH or a COOH group in their side-chains on asymmetric carbons, although β -CD could. However, dansyl-DL-phenylalanine and -tryptophan bearing aromatic groups in their side-chains could be resolved in the presence of 3-MM- β -CD but not in the presence of β -CD. Dansyl-DL-leucine and -norleucine bearing relatively long hydrophobic isobutyl and *n*-butyl

side-chains, respectively, could also be resolved well in the presence of 3-MM- β -CD, although dansyl-DL- α -aminobutyric acid and -valine bearing shorter ethyl and isopropyl side-chains, respectively, could not.

The reason for these remarkable changes in the chiral recognition after 3-monomethylation of β -CD may be speculated as follows. In an inclusion model where a dansyl group is included in the CD cavity and an amide and/or a COO⁻ group closely contact the secondary hydrophilic rim (2- and 3-hydroxyl groups, located inside and outside the cavity, respectively) of unmodified β -CD, the above-mentioned side-chains of the L- and D-enantiomers are located in the proximity of and far from the secondary rim of β -CD, respectively [18]. Thus the bulky side-chain is far from the hydrophilic rim in the case of the

D-enantiomer but is in the proximity of the hydrophilic rim in the case of the L-enantiomer. The approach of the side-chain to the hydrophilic rim is considered to be less favourable for the inclusion. Therefore, the D-enantiomer is included more stably than the L-enantiomer; thus, the D-enantiomer migrates faster, as mentioned previously. After 3-monomethylation of β -CD, all the 3-hydroxyl groups are replaced by OCH₃ groups. This produces a rim with both a hydrophilic and a hydrophobic ring composed of the 2-hydroxyl and 3-methoxy groups, respectively, in place of the original rim with two hydrophilic rings in unmodified β -CD. As described above, provided that a dansyl group is included in the cavity and an amide and/or a COO⁻ group closely contacts the 2-hydroxyl groups of 3-MM- β -CD, the approach of the hydrophobic side-chain to the hydrophobic ring is more favourable for the inclusion complex formation. Consequently, the complex of 3-MM-

β -CD with the L-enantiomer is stabilized more than that with the D-enantiomer. This brings about the reversal of the migration order observed in the presence of 3-MM- β -CD. Considering the high resolution of dansyl-DL-leucine ($R' = 90.1$) and the lack of resolution of dansyl-DL-valine ($R' = 0$) in the presence of 3-MM- β -CD, the longer isobutyl side-chain may closely contact the 3-methoxy groups but the shorter isopropyl side-chain may not. This trend is also true for the comparison of dansyl-DL-norleucine ($R' = 55.0$) with dansyl-DL-norvaline ($R' = 18.5$). Another drastic enantioselectivity change after 3-monomethylation of β -CD can be seen in the appearance of chiral resolution for dansyl-DL-phenylalanine ($R' = 69.7$) and -tryptophan ($R' = 68.3$) bearing the hydrophobic aromatic chains.

Similar data in the presence of dimethylated and trimethylated β -CDs are listed in Table 3. Di- or trimethylation of unmodified β -CD resulted in both a significant decrease in the chiral

Table 3
Chiral separation of dansylamino acids in the presence of di- and trimethylated β -CDs

Dansylamino acid	2,3-DM- β -CD		2,6-DM- β -CD		3,6-DM- β -CD		2,3,6-TM- β -CD	
	Migration time (min)	R'	Migration time (min)	R'	Migration time (min)	R'	Migration time (min)	R'
α -Amino- <i>n</i> -butyric acid	10.57		8.72		12.29		11.46	
Aspartic acid	21.10		L 13.68 D 13.77	31.8	22.13		22.90	
Glutamic acid	19.73		13.06		20.37		21.33	
Leucine	L 10.10 D 10.28	99.2	L 8.13 D 8.17	41.9	12.12		L 10.85 D 11.04	100
Methionine	10.57		8.45		12.56		11.40	
Norleucine ^a	10.02	26.4	8.28		12.29		10.76 10.90	92.7
Norvaline	10.34		8.42		12.24		L 11.22 D 11.32	48.0
Phenylalanine	9.97		8.04		12.08		L 10.50 D 10.69	92.1
Serine	11.08		8.82		12.57		11.88	
Threonine	10.86		8.77		12.60		11.62	
Tryptophan	L 10.38 D 10.48	21.0	8.01		12.50		L 10.90 D 11.02	76.6
Valine	L 10.37 D 10.44	25.6	8.49		12.12		L 11.06 D 11.14	38.7

^a Neither enantiomer was obtained.

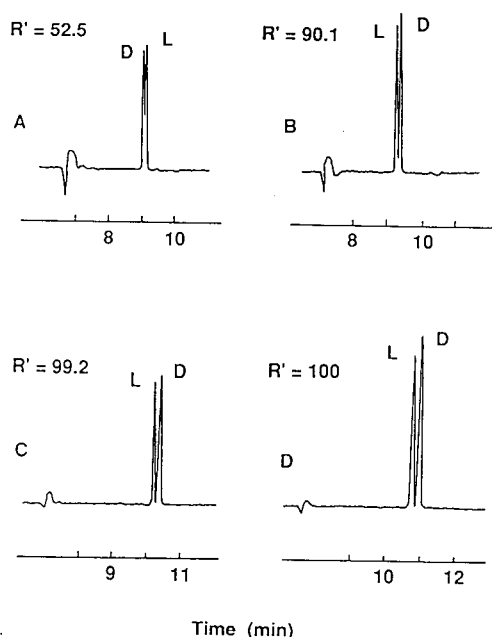


Fig. 2. Chiral separations of dansyl-DL-leucine with (A) β -CD, (B) 3-MM- β -CD, (C) 2,3-DM- β -CD and (D) 2,3,6-TM- β -CD.

recognition ability and a reversal of the migration order of the enantiomers. Fig. 2 shows typical electropherograms for dansyl-DL-leucine in the presence of 2,3-DM- and 2,3,6-TM- β -CDs, together with those in the presence of unmodified and 3-MM- β -CDs. Near and complete baseline separations of the enantiomers were obtained. The chiral separation of dansyl-DL-leucine or -norleucine is also superior to that of dansyl-DL-valine or -norvaline, respectively, with 2,3-DM- or 2,3,6-TM- β -CD as well as 3-MM- β -CD. This is probably due to the closer contact of the hydrophobic rims of methylated β -CDs with the longer *n*- and isobutyl side-chains than with the shorter *n*- and isopropyl side-chains, which is supported by the CPK molecular models.

None of the dansylamino acid enantiomers could be resolved in the presence of 3,6-DM- β -CD. After methylation of the hydroxyl groups at the 6-positions of 3-MM- β -CD, its high chiral recognition completely disappeared. On the other hand, similar 6-methylation for 2,3-DM- β -

CD enhanced the chiral recognition (2,3,6-TM- β -CDE). As already described, 6-mono-methylation of unmodified β -CD scarcely produced the enantioselectivity changes. Hence methylation of the hydroxyl groups at the 6-positions of the β -CD derivatives (unmodified, 3-MM- and 2,3-DM- β -CDs) produced different changes in the enantioselectivity. The reason for this variety is not clear at present. The penetration depth of the dansylamino acids into the cavities may be sensitively affected by 6-methylation.

3.3. Interaction of dansylamino acids with β -CD derivatives

As already described, a shorter migration time means a stronger interaction of a solute with the β -CD cavity. Strictly, all the CZE conditions for the migration time data in Tables 1 and 2 are not always the same, because their measurements required many days. Therefore, the data cannot be directly used to estimate the interaction of one dansylamino acid with the β -CD derivatives. Fig. 3 shows the migration times of dansyl-DL-leucine as a model solute in the presence of each β -CD derivative, which were measured successively under the same CZE conditions as carefully as possible. Considering the migration time values, the interaction of the solute increases in the order 2,3-DM- β -CD < 2,3,6-TM- β -CD < 6-MM- β -CD < β -CD < 2-MM- β -CD < 3,6-DM- β -

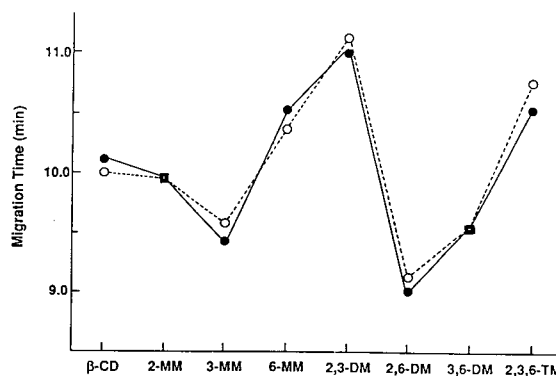


Fig. 3. Migration times of dansyl-DL-leucine in the presence of each β -CD derivative. Solutes: \circ = D-enantiomer; \bullet = L-enantiomer; \square = DL-enantiomers.

$CD \approx 3\text{-MM-}\beta\text{-CD} < 2,6\text{-DM-}\beta\text{-CD}$. On the other hand, 2,3,6-TM- and 2,3-DM- β -CDs exhibited complete and almost complete baseline separations of dansyl-DL-leucine and interacted with it more weakly than any other β -CD derivatives. 3-MM- and 6-MM- β -CD also exhibited high resolution abilities. 2,6-DM- β -CD, although it interacted most strongly, could produce only a partial resolution. Consequently, in this case, it is apparent that the chiral separation of the solute has not necessarily been correlated with its interaction strength with the CD.

In conclusion, methylation of the hydroxyl groups on the rim of each β -CD cavity produced large enantioselectivity changes for dansylamino acid enantiomers, as already described. Further work on interactions between guests and CD derivatives bearing groups different in bulkiness and/or polarity may provide more information for the chiral recognition process.

Acknowledgements

Partial support of this work by a Grant-in-Aid for Scientific Research (C) (No. 04650682) from the Ministry of Education, Science and Culture, Japan is gratefully acknowledged.

References

- [1] S.F.Y. Li, *Capillary Electrophoresis*, Elsevier, Amsterdam, 1992.
- [2] P.D. Grossman and J.C. Colburn, *Capillary Electrophoresis*, Academic Press, San Diego, 1992.
- [3] A.P. Croft and R.A. Bartsch, *Tetrahedron*, 39 (1983) 1417–1474.
- [4] S. Fanali, *J. Chromatogr.*, 474 (1989) 441–446.
- [5] J. Snopek, H. Soini, M. Novotny, E. Smolkova-Keulemansova and I. Jelinek, *J. Chromatogr.*, 559 (1991) 215–222.
- [6] T.E. Peterson and D. Trowbridge, *J. Chromatogr.*, 603 (1992) 298–301.
- [7] S. Fanali, M. Flieger, N. Steinerova and A. Nardi, *Electrophoresis*, 13 (1992) 39–43.
- [8] P. Gareil, J.P. Gramond and F. Guyon, *J. Chromatogr.*, 615 (1993) 317–325.
- [9] T.E. Peterson, *J. Chromatogr.*, 630 (1993) 353–361.
- [10] M.W.F. Nielen, *Anal. Chem.*, 65 (1993) 885–893.
- [11] S.A.C. Wren and R.C. Rowe, *J. Chromatogr.*, 635 (1993) 113–118.
- [12] M. Heuermann and G. Blaschke, *J. Chromatogr.*, 648 (1993) 267–274.
- [13] M. Tanaka, M. Yoshinaga, S. Asano, Y. Yamashoji and Y. Kawaguchi, *Fresenius' J. Anal. Chem.*, 343 (1992) 896–900.
- [14] J. Boger, R.J. Corcoran and J.-M. Lehn, *Helv. Chim. Acta*, 61 (1978) 2190–2218.
- [15] J. Szejtli, A. Lipták, I. Jodá, P. Fügedi, P. Nanási and A. Neszmélyi, *Starch/Stärke*, 32 (1980) 165–169.
- [16] K. Takeo, H. Mitoh and K. Uemura, *Carbohydr. Res.*, 187 (1989) 203–221.
- [17] T. Irie, K. Fukunaga, J. Pitha, K. Uekama, H.M. Fales and E.A. Sokolowski, *Carbohydr. Res.*, 192 (1989) 167–172.
- [18] K. Fujimura, S. Suzuki, K. Hayashi and S. Masuda, *Anal. Chem.*, 62 (1990) 2198–2205.



ELSEVIER

Journal of Chromatography A, 679 (1994) 367–374

JOURNAL OF
CHROMATOGRAPHY A

Chiral high-performance liquid chromatography methodology for quality control monitoring of dexfenfluramine

Lin Dou¹, Jia-Ning Zeng, Dante D. Gerochi, Michael P. Duda, Hans H. Stuting*
Analytical Chemistry and Clinical Trials Departments, Roche Biomedical Laboratories, 69 First Avenue, Raritan, NJ 08869, USA

First received 14 March 1994; revised manuscript received 16 May 1994

Abstract

The objective of this study was to measure the concentration of *d*-fenfluramine · HCl (the desired product) and *l*-fenfluramine · HCl (enantiomeric impurity), in the final pharmaceutical product, in the possible presence of its isomeric variants. Sensitivity, stability and specificity were enhanced by derivatizing the analytes with 3,5-dinitrophenylisocyanate utilizing a Pirkle chiral recognition approach. Analysis of the calibration curve data and quality assurance samples showed an overall inter-assay precision of 1.78 and 2.52%, for *d*-fenfluramine · HCl and *l*-fenfluramine, with an overall intra-assay precision of 4.75 and 3.67%, respectively. The minimum quantitation limit was 50 ng/ml, having a minimum signal-to-noise ratio of 10, with relative standard deviations of 2.39 and 3.62% for *d*-fenfluramine and *l*-fenfluramine. The method is capable of accurately and consistently determining as low as 0.01% *l*-fenfluramine in the *d*-fenfluramine final pharmaceutical product.

1. Introduction

After successfully developing a chiral HPLC method for the analysis of dexfenfluramine for the clinical trial involving human plasma and urine [1], we investigated adapting this methodology for application in the monitoring the final pharmaceutical product in the quality control phases.

For purposes of clarity (Fig. 1), *d,l*-fenfluramine · HCl is N-ethyl- α -methyl-*meta*-(trifluoromethyl)phenethylamine, and is referred to

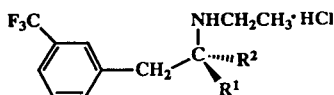
throughout this paper as m-I,II. *ortho-d,l*-Fenfluramine · HCl has the trifluoromethylphenethylamine in the *ortho* position, and is referred to as o-I,II; *para-d,l*-fenfluramine · HCl has the trifluoromethylphenethylamine in the *para* position, and is referred to as p-I,II. The roman numeral I refers to the *d*-enantiomer and the II refers to the *l*-enantiomer.

The literature appeared lacking any HPLC method for the analysis of *d*-fenfluramine in the bulk raw drug or final pharmaceutical product. Therefore, a chiral method was developed for the quantitative enantiomeric determination of m-I and m-II in the possible presence of its isomeric variants o-I,II and p-I,II. This was accomplished by derivatizing the analytes into their 3,5-dinitrophenyl urea derivatives, separat-

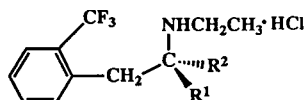
* Corresponding author.

¹ Present address: Warner Lambert, Parke-Davis Division, Building 3, Room 148, 170 Tabor Road, Morris Plains, NJ 07950, USA.

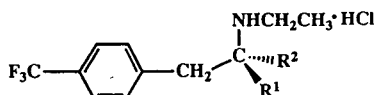
d,l-Fenfluramine-HCl (m-I,II)



Ortho-d,l-Fenfluramine-HCl (o-I,II)



Para-d,l-Fenfluramine-HCl (p-I,II)



N-Methylphenethylamine (N-MPEA)

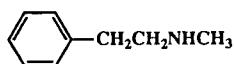


Fig. 1. Basic chemical structures. $R^1 = H$ and $R^2 = CH_3$ for the *d*-configuration; $R^1 = CH_3$ and $R^2 = H$ for the *l*-configuration.

ing them on different chiral stationary phases consisting of (*R*)- and (*S*)-1-(1-naphthyl)-ethylurea covalently bound to silica through a propyl linkage. The procedure is based on a chiral stationary phase originally described by Oi et al. [2], utilizing a convenient method for urea formation introduced by Pirkle et al. [3].

2. Experimental

2.1. Reagents

Glacial acetic acid (HPLC grade) and hydrochloric acid (reagent grade) were purchased from Fisher Scientific, Fairlawn, NJ, USA. Acetoni-

trile, hexane, methanol, methylene chloride and toluene (all HPLC grade) were purchased from Burdick & Jackson, Baxter Scientific, Edison, NJ, USA. 3,5-Dinitrobenzoylchloride (>98%) and sodium azide (>99.5%) were purchased from Fluka, Ronkonkoma, NY, USA. N-Methylphenethylamine (N-MPEA, 99%) and sodium hydroxide pellets (99.99%) were purchased from Aldrich, Milwaukee, WI, USA. m-I, m-I,II, o-I, o-I,II, p-I and p-I,II (all hydrochloride salt reference standards) were acquired through Wisconsin Analytical Research Services and Servier Technologie, Paris, France. Water, Milli-Q/HPLC grade; was produced in our laboratory.

2.2. Equipment

Similar equipment was used as previously described [1], except for the analytical columns consisting of (*R*)-naphthylurea Chiral, 250 × 4.6 mm, 5 μm particle size for system A, and the equivalent in the (*S*) configuration for system B, respectively (Supelco, Bellefonte, PA, USA).

2.3. Computerization

Similar computerization was used as previously described [1]. All concentrations were reported in the salt (HCl) form.

2.4. Preparation of reagent stock solutions

The preparation of 3,5-dinitrobenzoyl azide (DNB- N_3) and stock 3,5-dinitrophenylisocyanate (DNP-NCO) is described elsewhere [1]. A portion of this DNP-NCO stock solution was diluted with methylene chloride, 1:100 (v/v) for the m-I assay (HPLC system A) and 1:10 (v/v) for the m-II assay (HPLC system B), to give a final working solution concentration of approximately $2 \cdot 10^{-5} M$ for m-I and $2 \cdot 10^{-4} M$ for m-II. The higher concentration of DNP-NCO for the m-II assay was due to the much higher relative concentration of m-I as compared to m-II for this

assay and the reagent needed to be added in excess of all reacting species.

2.5. Placebo/blank preparation

Placebo/blank solutions were prepared by emptying one capsule (150 mg) into a 1-l class A volumetric flask. The solution was stirred, centrifuged (1500 rpm = 1250 g), and the supernatant was saved for later use.

2.6. Standard solution preparation

All sample preparations and analyses were conducted under yellow lighting in order to avoid possible sample degradation.

Analytical standard/stock and intermediate analytical standard/stock solutions were prepared in placebo solution. Concentrations were 60.0 and 6.00 $\mu\text{g/ml}$ for m-I, m-II, o-I, o-II, p-I and p-II.

Internal standard stock solutions were prepared in 1 mM HCl using HPLC-grade water. Final concentration was 6.25 $\mu\text{g/ml}$ for N-MPEA.

Working solutions were prepared in placebo solution by appropriate serial dilution of standard/stock solutions. Final concentrations were 2000, 1000, 500, 200, 100 and 50 ng/ml.

2.7. Preparation of solutions for the determination of m-II in the m-I analytical standard

Solutions of 60.00 $\mu\text{g/ml}$ of the m-I analytical standard were prepared in HPLC-grade water. This yielded relative m-II concentrations that were on the calibration curve if m-II is approximately 0.1% of m-I.

2.8. Standard curve

Each calibration curve was generated with 1.00 ml of drug-free placebo solution fortified with 50.0, 100, 200, 500, 1000 and 2000 ng/ml of m-I and m-II, in duplicate. Internal standard concentration was maintained at 1000 ng/ml.

2.9. Sample solution preparation

Determination of m-I

The contents of a 150-mg capsule were emptied into a 1000-ml class A volumetric flask, filled with HPLC-grade water, and stirred for 1 h. After the solution sat for 30 min, the colorless solution was decanted into centrifuge tubes and spun at 1500 rpm (1250 g) for 5 min. The supernatant was removed and 1.00 ml was placed in a 50-ml class A volumetric flask and filled to the mark with HPLC-grade water.

Determination of m-II

Since m-II is expected to be much lower in relative concentration to that of m-I, the following dilution scheme was used.

The contents of the 150-mg capsules containing 5, 15 or 30 mg of m-I were emptied into a 100-, 250- or 500-ml class A volumetric flask, respectively, and filled to the mark with HPLC-grade water. The solutions were stirred, allowed to settle, the colorless solutions were removed, placed in centrifuge tubes, and spun at 1500 rpm (1250 g) for 5 min. The supernatants were collected for later use. This resulted in m-I concentrations of 50, 60 and 60 $\mu\text{g/ml}$. With relative m-II concentrations expected to be in the range 0.1–3% to that of m-I, the final dilution concentrations should produce data that will fall in the linear calibration curve range of 50–2000 ng/ml.

2.10. Extraction and derivatization

Control blanks were prepared by combining 1.00 ml of placebo solution, 100 μl of HPLC-grade water and 100 μl of 0.1 M NaOH.

Standards and samples were prepared by adding 100 μl of internal standard solution (1.00 $\mu\text{g/ml}$ of N-MPEA) and 100 μl of 0.1 M NaOH to 1.00 ml of the respective solution.

A 2.00-ml volume of the appropriate concentration DNP-NCO solution was added to all and vortexed. The reaction was allowed to go to completion (15 min), the aqueous (top) layer

was removed and placed in HPLC autosampler vials ready for injection.

2.11. HPLC conditions

Our previous study [1] involved using a mobile phase composition of hexane–isopropanol–acetonitrile. However, we found better resolution, peak symmetry, and fewer interfering peaks when we substituted methylene chloride and methanol for isopropanol (IPA), especially since methylene chloride was already being used as the DNP-NCO diluent. Since alcohols also react with DNP-NCO, and not just primary and secondary amines, a previously interfering peak was removed that may now be attributed to the IPA–DNP-NCO product.

Individual solvent components were degassed under conditions of high vacuum and bumping, and then filtered through a 0.2- μ m nylon (or equivalent) membrane.

HPLC system A (quantitation of *m*-I)

Combine hexane, methylene chloride, methanol and acetonitrile, in the ratio 81.0:17.5:1.0:0.5 (v/v).

Chromatographic run time and flow-rates were 30 min at 1.50 ml/min. Detection was at 235 nm using a sensitivity of 0.005 AUFS. A 30- μ l volume of the final solution was injected. Retention times were approximately 8.3 min for *o*-I, 9.0 min for *o*-II, 10.3 min for *m*-I, 14.6 min for *p*-II and 17.6 min for N-MPEA.

HPLC system B (quantitation of *m*-II)

Combine hexane, methylene chloride, methanol and acetonitrile, in the ratio 85.0:13.5:1.0:0.5 (v/v).

Chromatographic run time, flow-rate and detection parameters were identical to that of HPLC system A. A 20- μ l volume of the final solution was injected. Retention times were approximately 7.8 min for *o*-II, 8.4 min for *o*-I (inter-system check by comparison to HPLC system A), 10.1 min for *m*-II, 14.2 min for *p*-I and 18.3 min for N-MPEA.

3. Results and discussion

The chiral *S* column yielded a favorable separation of *m*-II from *m*-I over the *R* column for this application over our previous choice [1], since *m*-II eluted prior to *m*-I and the reagent. This is preferable when analyzing a clean sample (i.e. not biological in origin) and the objective is to determine the % *m*-II in *m*-I. Two slightly different chromatographic conditions were required in order to quantitate within acceptable error limits.

Isomeric elution order was established by derivatization and chromatographing a sample of *m*-I, *m*-I,II, *o*-I, *o*-I,II, *p*-I and *p*-I,II. No peak correspondence to the antipode, in excess of the stated purity (Certificate of Analysis), was observed. This demonstrated that no racemization occurs under the extraction and/or derivatization conditions [4].

Given the present state-of-the-art in analytical chiral HPLC columns, only relatively moderate resolution and efficiency were experienced throughout these studies. Attempts at manipulating many of the customary HPLC variables (i.e. column particle size, length and temperature, mobile phase composition and linear velocity, etc.) in order to achieve adequate separation of all species in one run, were futile.

In order to determine if experimental conditions, i.e. selectivity (α), capacity factor (k'), theoretical plates (N), and subsequently resolution (R_s), were appropriate prior to the onset of any tray, test mixes (usually the high standard) were run in order to determine if the various separation factors were adequate. Typical overall physical characteristics of the separation were in the order of that expected. A range is specified to indicate the values for the first through last analytes of interest. Individual analytes should fall within the ranges specified herein. The *S* column's (HPLC system A, Fig. 2) α values ranged from 0.9 to 1.5 (analyte peak to closest neighbor), k' from 3.1 to 7.8 (using t_0 equal to the system dead volume in units of minutes), and $N_{1/2h}$ from 9600 to 12 500 plates/column. The *R* column's (HPLC system B, Fig. 3) α values ranged from 0.9 to 1.3, k' from 3.5 to 9.8, and

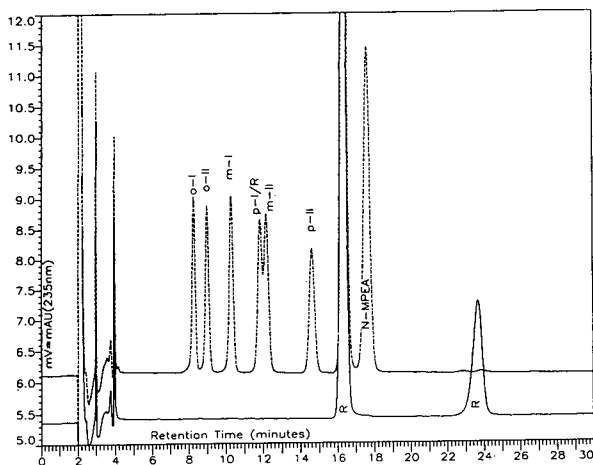


Fig. 2. Chromatographic overlays of HPLC system A showing a control blank (bottom) and 500 ng/ml m-I,II, o-I,II and p-I,II with 625 ng/ml N-MPEA (top).

$N_{1/2h}$ from 5700 to 7100 plates/column, and coincided with our previous study [1].

The calibration curves and resultant statistical data were consistent and accurate. Table 1 shows the overall inter-assay precision for standards and Table 2 shows the overall intra-assay precision. The overall relative standard deviation (R.S.D.) was less than 5%. Calibration curve data produced a minimum mean coefficient of determination, R^2 (correlation coefficient

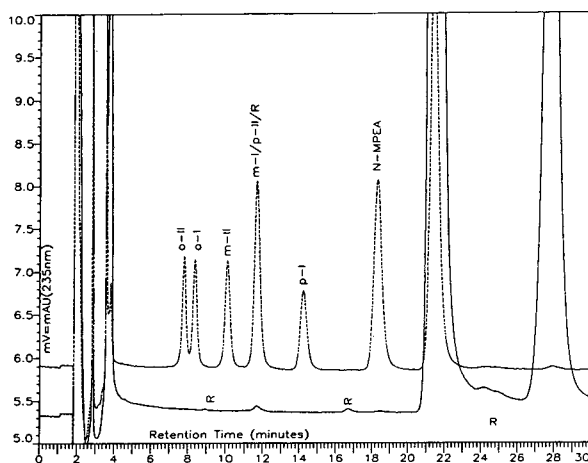


Fig. 3. Chromatographic overlays of HPLC system B showing a control blank (bottom) and 500 ng/ml m-I,II, o-I,II and p-I,II with 625 ng/ml N-MPEA (top).

squared), of >0.9992 with a slope R.S.D. of $<3\%$.

Both HPLC systems utilized high signal-to-noise (S/N) ratios when the minimum quantitation limit (MQL) of 50 ng/ml was selected. HPLC system A had typical baseline noise (maximum - minimum) equal to 10 μ V or approximately $10 \cdot 10^{-6}$ AU, while the 50 ng/ml m-I standard had a peak height of approximately 250 μ V with $N_{1/2h}$ of 10 800 plates/column. This resulted in a S/N of 25. Similar data were observed with HPLC system B, having as typical baseline noise of $8 \cdot 10^{-6}$ AU, yet the peak height was approximately 100 μ V for the 50 ng/ml m-II standard with $N_{1/2h}$ of 6400 plates/column. This resulted in a S/N of 12.5. Since efficiency was reduced for system B, the resultant decreased S/N was as expected.

Since the analytical standards employed throughout this work had stated enantiomeric purity specifications of $>99\%$ m-I and $\leq 0.12\%$ m-II (Certificate of Analysis and determined by capillary GC), we needed to determine and compare enantiopurity using this method prior to analyzing any product. High concentrations ($\geq 60.00 \mu$ g/ml) of the m-I standard were prepared so that the endogenous relative concentration of m-II in the m-I standard could be accurately evaluated. The mean m-II concentration was found to be 52.3 ng/ml, or 0.083% m-II in the m-I analytical standard, with a 1.20% R.S.D. This correction was then incorporated for all subsequent analyses on the product. Table 3 shows all data for the 5-, 15- and 30-mg capsules.

Using the sample preparation scheme herein, we were able to consistently determine that the m-I analytical standard contained 0.08% m-II, which is within the specifications listed in the Certificate of Analysis ($\leq 0.12\%$ m-II) provided by the manufacturer and determined by capillary GC. If necessary, lower, valid determinations could be made, as low as 0.01%, by altering the sample preparation scheme, e.g. increasing the initial m-I analytical standard solution concentration from 60 μ g/ml to 500 μ g/ml if m-II were as low as 0.01%.

Adequate separation of the enantiomers of the individual corresponding isomers was evidenced.

Table 1
Summary of inter-assay precision from the analysis of the calibration curve data

	STD = 50	STD = 100	STD = 200	STD = 500	STD = 1000	STD = 2000
<i>d</i> -Fenfluramine (<i>m</i> -I) (<i>n</i> = 7)						
Mean	50.94	99.39	200.58	494.25	991.11	2016.41
S.D.	1.22	0.71	3.68	3.61	8.00	14.19
R.S.D. (%)	2.39	0.71	1.83	0.73	0.81	0.70
Overall R.S.D. (%)	1.78					
<i>l</i> -Fenfluramine (<i>m</i> -II) (<i>n</i> = 8)						
Mean	51.67	98.64	198.35	493.97	1006.35	2002.18
S.D.	1.87	2.3	3.89	8.59	10.39	16.74
R.S.D. (%)	3.62	2.33	1.96	1.74	1.03	0.84
Overall R.S.D. (%)	2.52					

All concentration units are in ng/ml. STD = Analytical standard concentration.

However, when all the isomers were combined, the chromatographic requirements become more complicated, and necessitated the need for dual conditions. Fig. 2 shows the separation on HPLC system A. Note that this system can only resolve *o*-I, *o*-II, *m*-I and *p*-II (4 of the 6 analytes needed); *p*-I co-elutes with a reagent peak and *m*-II. Since it was important to be able to quantitate *m*-I and *m*-II, a second set of chromatographic conditions was required. We chose using the (*R*)-naphthylurea column for several reasons, however, mainly for reversed enantiomer elution order over that of the corresponding (*S*) column (Fig. 3). With this column in place,

and by using slightly different mobile phase composition, *m*-II and *p*-I were resolved from interfering peaks.

In addition, the percent *m*-II as compared to *m*-I in random clinical specimens 2 and 3 from our previous study [1], were approximately 1.8%. This result coincides with that determined here. This proves that physiological interconversion was not apparent in the clinical trial, since any *m*-II was coming from the product and not from metabolic origin.

This method could have been used to quantitate the isomeric variants mentioned herein, but this was beyond our need. Any evidence of any

Table 2
Summary of intra-assay precision from the analysis of the calibration curve data

	STD = 50	STD = 100	STD = 200	STD = 500	STD = 1000	STD = 2000
<i>d</i> -Fenfluramine (<i>m</i> -I) (<i>n</i> = 7)						
Mean ratio	1.014	1.022	1.003	1.007	1.007	1.009
S.D.	0.055	0.059	0.068	0.054	0.048	0.040
R.S.D. (%)	5.42	5.77	6.78	5.36	4.77	3.96
Overall R.S.D. (%)	4.75					
<i>l</i> -Fenfluramine (<i>m</i> -II) (<i>n</i> = 8)						
Mean ratio	0.992	0.990	1.000	1.078	1.043	1.031
S.D.	0.058	0.020	0.013	0.069	0.042	0.032
R.S.D. (%)	5.85	2.02	1.30	6.40	4.03	3.10
Overall R.S.D. (%)	3.67					

All concentration units are in ng/ml. STD = Analytical standard concentration.

Table 3
Verification of analytical standard purity and final product content

	Prepared m-I concentration (mg/l)	Determined m-II concentration (ng/ml)	Calculated % m-II	m-I ^a (ng/ml)	m-I ^b (mg/capsule)	m-II ^a (ng/ml)	m-II ^b (μg/capsule)	% m-II ^c
<i>m-I standard (n = 20)</i>								
Mean	63.11	52.32	0.0829					
S.D.	3.88	2.35	0.0014					
R.S.D. (%)	6.15	4.49	1.69					
<i>5-mg capsule (n = 20)</i>								
Mean				466.6	4.666	856.7	85.67	1.84
S.D.				28.9	0.289	15.8	1.58	
R.S.D. (%)				6.19	6.19	1.84	1.84	
<i>15-mg capsule (n = 20)</i>								
Mean				475.8	14.28	1037.6	260.0	1.82
S.D.				22.9	0.69	25.7	6.02	
R.S.D. (%)				4.81	4.83	2.48	2.32	
<i>30-mg capsule (n = 20)</i>								
Mean				592.7	29.64	1065.3	533.0	1.80
S.D.				25.9	1.3	22.0	11.0	
R.S.D. (%)				4.37	4.39	2.07	2.06	

^aConcentration determined by HPLC.

^bCalculated mass per capsule, calculated by multiplying HPLC concentration by appropriate dilution.

^cCalculated by dividing mass m-II by mass m-I and multiplying by 100.

of the isomeric variants of fenfluramine would show production problems.

4. Conclusions

The literature has only a few references on dexfenfluramine and all are related to its analysis from a biological matrix. The prime focus of this study was to develop and validate, an analytical stereospecific HPLC method intended to quantify the concentrations of *d*-fenfluramine (major product) and *l*-fenfluramine (impurity) in the final pharmaceutical product. Only qualitative data were required for the possible isomeric variants and their enantiomers. This new methodology has been designed for quality assurance purposes for monitoring commercial production of the drug.

Efforts addressed at producing a single HPLC

condition for resolving all the analytes of interest was futile given the resources allocated to this project and its intended use. When looking at Van der Waals models of the three isomers, and each isomer's two enantiomers, similar molecular surface characteristics were evident. Other separation approaches were considered, such as using a reversed-phase HPLC column coupled in-line to a chiral HPLC column, to separate the isomers and the enantiomers, respectively. However, solvent-stationary phase compatibility issues would be very time consuming and quite difficult to determine. Reversed-phase HPLC coupled orthogonally to chiral HPLC was another option, but we believe that such a system would have been more susceptible to error than we have demonstrated here with this system.

With the resultant statistical data shown herein, it is clear that this experimental approach is capable of providing accurate and reliable data

that can be used for monitoring the production of dexfenfluramine.

Acknowledgements

We are grateful to the following individuals, and teams behind the individuals, for seeing us through this project: Dr. Bobby Sandage of Interneuron Pharmaceuticals Inc., Lexington, MA, USA; Servier Laboratories (Paris, France) for having provided us with all the reference standards; Herb Kenny and Robert Keltgen of Thermo Separation Products, Riviera Beach, FL, USA; and especially to Philip Hamwi, Ratimir Kucan, Kevin Fallon, George Dell,

Mary Montgomery and all of the Analytical Chemistry and Clinical Trials Departments of Roche Biomedical Laboratories.

References

- [1] J.-N. Zeng, L. Dou, M. Duda and H.H. Stuting, *J. Chromatogr. B*, 654 (1994) 231–248.
- [2] N. Oi, T. Kitahara, T. Doi and S. Yamamoto, *Bunseki Kagaku (Jap. Anal.)*, 32 (1983) 345.
- [3] W.H. Pirkle, G. Mahler and M.H. Hyun, *J. Liq. Chromatogr.*, 9 (1986) 443.
- [4] T.D. Doyle, in W.J. Lough (Editor), *Chiral Liquid Chromatography*, Blackie, Glasgow, London, 1989, Ch. 6.



ELSEVIER

Journal of Chromatography A, 679 (1994) 375–380

JOURNAL OF
CHROMATOGRAPHY A

Short communication

Application of normal- and reversed-phase high-performance liquid chromatography for monitoring the progress of reactions of anthraquinone manufacturing processes[☆]

Sajid Husain*, R. Narsimha, Sara Khalid, R. Nageswara Rao

Analytical Chemistry Division, Indian Institute of Chemical Technology, Hyderabad-500 007, India

First received 3 March 1994; revised manuscript received 14 June 1994

Abstract

Two different methods for the separation and determination of the reactants, intermediates and products of anthraquinone manufacturing processes using normal- and reversed-phase high-performance liquid chromatography were developed. The separations were achieved on Spherisorb silica and reversed phase C₁₈ columns using *n*-heptane–ethanol–chloroform–acetic acid (89:5:5:1, v/v) and acetonitrile–water (65:35, v/v) as the eluents, respectively. These methods were used not only for monitoring the reaction conditions but also the yields of anthraquinone.

1. Introduction

9,10-Anthraquinone is not only an important intermediate in the manufacture of various dye-stuffs but is also used as a catalyst in the isomerization of vegetable oils [1]. It is produced in large amounts by the Friedel–Crafts reaction of phthalic anhydride and benzene in the presence of AlCl₃ catalyst [2]. Our laboratory has studied not only this process but also an alternative for the economic production of anthraquinone, involving the oxidation of toluene to benzoic acid followed by catalytic condensation [3]. The development of these two processes has required analytical methods for monitoring not

only the reaction products but also the quality of anthraquinone.

Several gravimetric, titrimetric, polarographic and spectrophotometric techniques have been used for the evaluation of anthraquinone industrially [4,5], but they lack not only specificity but also accuracy owing to the influence of impurities present in anthraquinone. Anderson [6] and Mitra and Ghosh [7] determined anthraquinone in the vapour-phase oxidation products of toluene by gas–liquid chromatography. The separation was achieved on columns packed with 5% OV-101 on Chromosorb G using temperature programming. However, these methods were tedious and time consuming. Several high-performance liquid chromatographic (HPLC) methods for the determination of anthraquinone in environmental pollutants have been reported [8–10]. However, no suitable method for moni-

* Corresponding author.

[☆] IICT Communication No. 3373.

toring the reaction conditions of anthraquinone processes is available.

In this paper, we describe two different methods for the separation, identification and determination of the reactants, intermediates, products and by-products of anthraquinone manufacturing processes by normal- and reversed-phase HPLC.

2. Experimental

2.1. Materials and reagents

All reagents were of analytical-reagent grade, unless stated otherwise. Glass-distilled water, acetonitrile, *n*-heptane, ethanol and chloroform (Spectrochem, Bombay, India) were used. Anthraquinone (BDH, Poole, UK) was used as a reference standard.

2.2. Apparatus

A Model ALC/GPC 244 high-performance liquid chromatograph (Waters, Milford, MA, USA) was used along with a U6K injector system and a Model 440 UV spectrophotometric detector. A Spherisorb silica column (250 mm × 4.6 mm I.D., particle size 5 μm) and a C₁₈ column (250 mm × 4.6 mm I.D., particle size 5 μm) (Bischoff, Leonberg, Germany) were used for separation. The chromatograms and the integrated data were recorded with an Omniscribe D 5000 recorder and a Chromatopac E1A integrator, respectively.

2.3. Chromatographic conditions

Normal-phase HPLC

The mobile phase was *n*-heptane–ethanol–chloroform–acetic acid (89:5:5:1, v/v). Samples were dissolved in the mobile phase. The analysis was carried out under isocratic conditions at a flow-rate of 1 ml/min at room temperature

(27°C). Chromatograms were recorded at 254 nm.

Reversed-phase HPLC

The mobile phase was acetonitrile–water (65:35, v/v). The flow-rate was 1 ml/min at room temperature (27°C). Chromatograms were recorded at 254 nm.

2.4. Analytical procedure

Samples of anthraquinone (10 mg) were dissolved in the mobile phase (50 ml) and 20 μl of each sample were injected and chromatographed. Synthetic and reaction mixtures were analysed under identical conditions. The amount of anthraquinone was calculated from the peak area.

3. Results and discussion

Fig. 1 shows the reaction pathways followed for the production of anthraquinone. The reaction mixtures and products of these processes were subjected to normal- and reversed-phase HPLC.

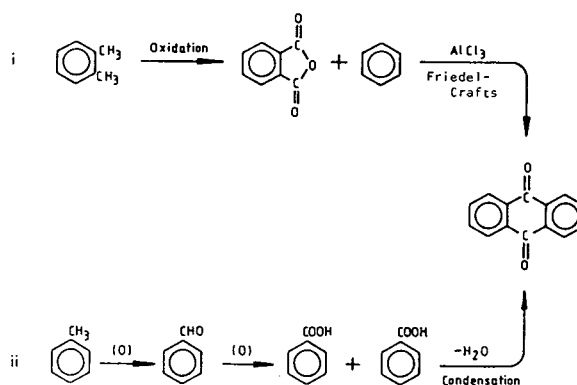


Fig. 1. Production of anthraquinone by (i) oxidation of *o*-xylene followed by Friedel-Crafts reaction of phthalic anhydride and benzene in the presence of AlCl_3 and (ii) oxidation of toluene to benzaldehyde to benzoic acid and its catalytic condensation.

3.1. Monitoring the reaction products of phthalic anhydride and benzene by normal-phase HPLC

The HPLC separation of anthraquinone and its impurities is shown in Fig. 2. The peaks were identified by injecting individual authentic compounds. It can be seen from Fig. 2 that anthraquinone is well separated from the process reactants, viz., *o*-xylene, benzene and phthalic anhydride. Maleic anhydride was used as an internal standard. It does not interfere in the determination and elutes at 6.83 min. The Spherisorb silica column was used with *n*-heptane–ethanol–chloroform–acetic acid (89:5:5:1, v/v) as mobile phase for separation. It may be noted that reversed-phase HPLC is not suitable for separation of the same reactants because phthalic anhydride is hydrolysed to phthalic acid in solvent systems containing water. The Spherisorb silica column provided the optimum resolution of peaks corresponding to the analytes under investigation. The retention data, re-

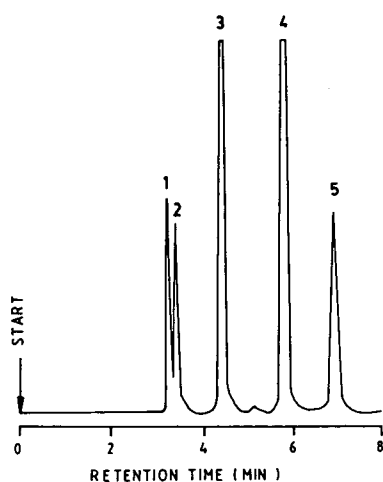


Fig. 2. Chromatogram of a mixture containing (2) benzene (1.8 μg), (1) *o*-xylene (1.6 μg), (4) phthalic anhydride (0.5 μg), (3) anthraquinone (0.1 μg) and (5) maleic anhydride (2.1 μg). Conditions: column, Spherisorb silica (250 mm \times 4.6 mm I.D., particle size 10 μm); mobile phase, *n*-heptane–ethanol–chloroform–acetic acid (89:5:5:1, v/v); flow-rate, 1 ml/min; detection, UV at 254 nm.

Table 1

Retention data for reactants involved in the synthesis of anthraquinone by reaction (i)^a

Compound	Retention time (min)	Response factor	λ_{max} (nm)
Benzene	3.35	1.00	255
<i>o</i> -Xylene	3.20	1.14	252
Phthalic anhydride	5.79	3.81	245
Anthraquinone	3.94	40.04	249
Maleic anhydride	6.83	1.28	225

^a See Fig. 1.

sponse data and wavelengths of maximum absorption of all the compounds are given in Table 1. The linearity between the mass and integral responses of anthraquinone is good. When the UV detector is set at 0.005 AUFS the limit of detection for anthraquinone is $5.0 \cdot 10^{-9}$ g with a signal-to-noise ratio of 4.0.

Standard mixtures containing known amounts of the analytes were prepared and analysed by HPLC. The accuracy of the method was determined by the standard addition technique. Subsequent additions of small amounts of the analytes were accurately reflected in their peak heights. The measured amounts agreed well with the actual values (within 2.97%). The calibration graphs are shown in Fig. 3. The relative response factors were determined for all the compounds and used to determine the compositions of reaction mixtures obtained during the process development.

The method was applied not only to monitor the reaction conditions but also to determine the quality of anthraquinone periodically. Fig. 4 shows a typical chromatogram of a reaction mixture analysed during the course of reactions. The concentrations of various reactants were determined and the composition of reaction mixture was calculated. The levels of anthraquinone formed at different stages of the reaction are given in Table 2.

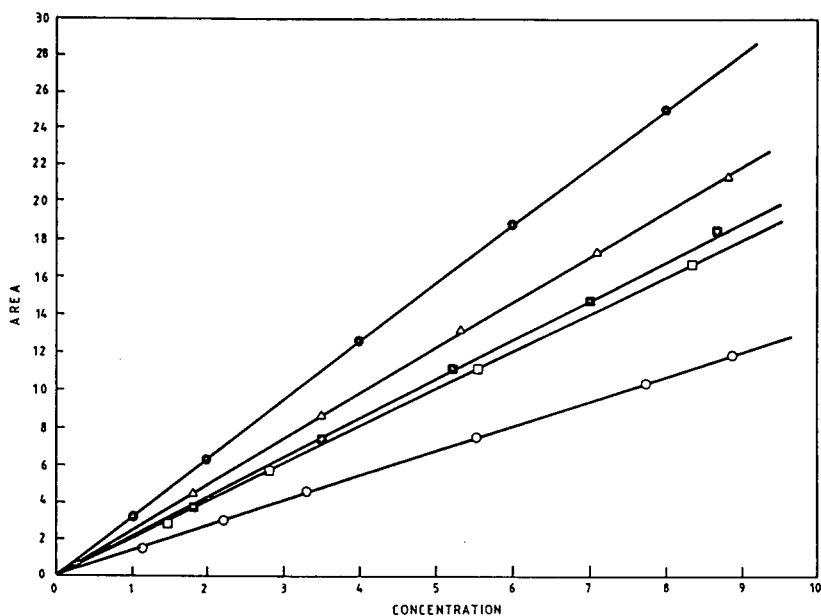


Fig. 3. Calibration graphs showing the linearity between concentration and integral response of (Δ) *o*-xylene, (\blacksquare) benzene, (\bullet) phthalic anhydride, (\square) anthraquinone and (\circ) maleic anhydride. Concentration given in μg .

3.2. Monitoring the products of catalytic oxidation of toluene by reversed-phase HPLC

The reactants and products of this process

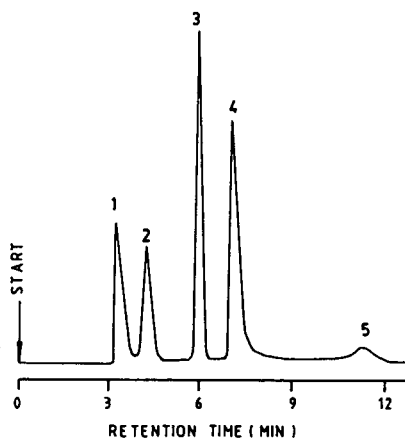


Fig. 4. Typical chromatogram of a reaction mixture collected during the course of reaction of phthalic anhydride with benzene in the presence of AlCl_3 as catalyst. Peaks: 1 = benzene; 2 = anthraquinone; 3 = phthalic anhydride; 4 = maleic anhydride; 5 = unknown. For conditions, see Fig. 2.

were subjected to HPLC and their separation is shown in Fig. 5. It can be seen that anthraquinone is well separated from all the process impurities, viz., toluene, benzaldehyde and benzoic acid. The retention data are given in Table 3. The method was well standardized and used for process development. Fig. 6 shows a typical chromatogram of anthraquinone obtained by this process. The product yields were optimized by following the reaction conditions by HPLC. The results are given in Table 4. These results indi-

Table 2
Levels of anthraquinone formed at different stages of the reaction

Sample	Time (h)	Anthraquinone (%) ^a	S.D. (%)
React mixture 1	0.5	3.92	2.45
React mixture 2	1.0	9.75	1.98
React mixture 3	2.0	22.41	1.72
React mixture 4	4.0	49.38	1.64

^a Average of three determinations.

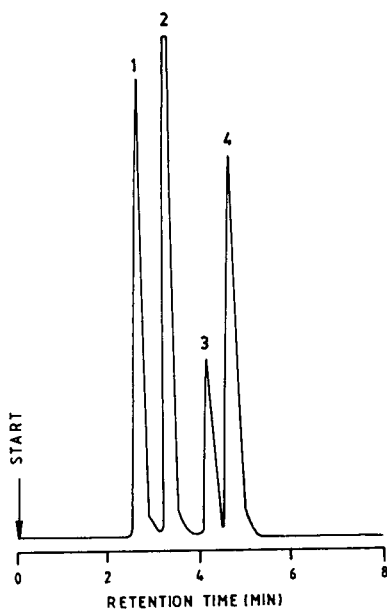


Fig. 5. Chromatogram of a typical mixture containing (1) benzoic acid (1.9 μg), (2) benzaldehyde (0.2 μg), (3) toluene (1.7 μg) and (4) anthraquinone (0.1 μg). Conditions: column, C_{18} (250 mm \times 4.6 mm I.D., particle size 5 μm); mobile phase, acetonitrile–water (65:35, v/v); flow-rate, 1 ml/min; detection, UV at 254 nm.

cate that the method is suitable for monitoring the oxidation products of toluene.

4. Conclusions

The proposed HPLC methods are simple and rapid for monitoring the reaction products of

Table 3
Retention data for reactants involved in the synthesis of anthraquinone by reaction (ii)^a

Compound	Retention time (min)	Response factor	λ_{max} (nm)
Toluene	4.22	1.00	210
Benzaldehyde	3.32	45.19	243
Benzoic acid	2.60	3.39	226
Anthraquinone	4.72	87.51	252

^a See Fig. 1.

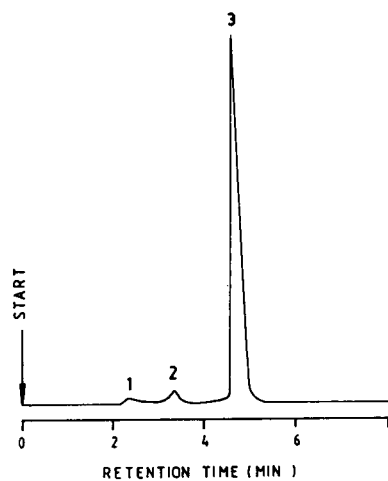


Fig. 6. Typical chromatogram of anthraquinone obtained during process development. Peaks: 1 = benzoic acid; 2 = benzaldehyde; 3 = anthraquinone. For conditions, see Fig. 5.

Table 4
Purity of anthraquinone

Sample	Purity by HPLC (%) ^a	S.D. (%)
Product 1	99.39	1.47
Product 2	98.74	1.82
Product 3	98.15	1.59

^a Average of three determinations.

anthraquinone manufacturing process. They are accurate and precise for the determination of process impurities and related products of industrial anthraquinone production.

References

- [1] A.J. Cofrancesco, in J.I. Kroschwitz and M.H. Grant (Editors), *Kirk-Othmer Encyclopedia of Chemical Technology*, Vol. 2, Wiley-Interscience, New York, 1992, pp. 801–814.
- [2] K.H. Klipstein, *Ind. Eng. Chem.*, 18 (1926) 1327.
- [3] Mistui Toatsu Chemicals, *Jpn. Kokai Tokkyo Koho*, JP 58 121 238 (1983); *C.A.*, 99 (1983) 139546.
- [4] C. Iuan, *Chem. Prum.*, 35 (1985) 638; *C.A.*, 104 (1986) 161250.

- [5] S. Egon and B. Joachim, *Arch. Pharm. (Weinheim, Ger.)*, 311 (1978) 58.
- [6] L.T. Anderson, *J. Chromatogr. Sci.*, 23 (1985) 17.
- [7] G.D. Mitra and S.K. Ghosh, *Fert. Technol.*, 17 (1980) 3.
- [8] M.A. Quillian and P.G. Sim, *J. Chromatogr. Sci.*, 26 (1988) 160.
- [9] K.H. Nelson and D.J. Cietek, *J. Chromatogr.*, 281 (1983) 237.
- [10] P. Fernandez and J. Bayana, *J. Chromatogr.*, 625 (1992) 141.



ELSEVIER

Journal of Chromatography A, 679 (1994) 381–386

JOURNAL OF
CHROMATOGRAPHY A

Short communication

High-performance liquid chromatographic determination of carnosic acid and carnosol in *Rosmarinus officinalis* and *Salvia officinalis*

Nobuyuki Okamura*, Yukako Fujimoto, Shinako Kuwabara, Akira Yagi

Faculty of Pharmacy and Pharmaceutical Sciences, Fukuyama University, Hiroshima 729-02, Japan

First received 30 March 1994; revised manuscript received 14 June 1994

Abstract

A reversed-phase high-performance liquid chromatographic method for the determination of carnosic acid and carnosol, phenolic diterpenes, which showed high antioxidative effect, is established. The analysis can be accomplished within 15 min under isocratic conditions with 0.1% phosphoric acid–60% acetonitrile as the mobile phase at a flow-rate of 1.0 ml/min, with detection at 230 nm. The detection limits of carnosic acid and carnosol are 0.104 and 0.521 ng per injection, respectively. This experimental system permits a good separation and quantification of these phenolic diterpenes in the leaves of *Rosmarinus officinalis* L. and *Salvia officinalis* L.

1. Introduction

Rosemary (*Rosmarinus officinalis* L.) and sage (*Salvia officinalis* L.) have been known to have the highest antioxidant activity among herbs [1]. Compounds responsible for these antioxidant properties isolated from rosemary were mainly the phenolic diterpenes named carnosic acid [2] and carnosol [3]. In the subsequent studies, several related phenolic diterpenes, rosmanol [4] and epirosmanol with γ -lactone were identified [5]. Carnosic acid was converted into carnosol by air-oxidation. Carnosic acid has been assumed to be the main substrate for general oxidation leading to phenolic diterpene artifacts with a δ - or γ -lactone function [6]. In practice, rosmanol,

epirosmanol and 7-methylepirosmanol containing a γ -lactone function were formed from carnosol [7]. So carnosic acid functions as the main component for the antioxidative activity of these herbs. Recently, a reversed-phased high-performance liquid chromatographic (HPLC) method for the determination of several phenolic diterpenes in rosemary and sage leaves [8] was carried out by the gradient elution with electrochemical detection. In order to determine the contents of carnosic acid and carnosol in rosemary and sage, we developed a simple and rapid method with isocratic elution and UV detection. In the present study, we described a method for the HPLC analysis of carnosic acid and carnosol and we determined these phenolic diterpenes in the different parts of rosemary and sage plants. Furthermore we determined the stability of carnosic acid by means of this HPLC method.

* Corresponding author.

2. Experimental

2.1. Materials

Dried leaves of rosemary were purchased from Mikuni (Osaka, Japan). A voucher specimen of *R. officinalis* and *S. officinalis* was available for inspection at the Herbal Garden, Fukuyama University. Reagent-grade chemicals and high-purity solvents were used except when specified otherwise. Aqueous solutions were prepared with deionized-distilled water. Acetonitrile was of HPLC grade and other solvents and chemicals were purchased from Wako (Osaka, Japan).

Ethyl acetate extract from dried leaves of rosemary (3.3 g) was partitioned between 1 M sodium hydroxide and diethyl ether, and the sodium hydroxide layer neutralized with 2 M hydrochloric acid was extracted with diethyl ether. The diethyl ether extract (95 g) was chromatographed on a silica gel column (300 mm × 200 mm I.D., 75–150 μm, Wako) using benzene–acetone (10:1) to give fractions A (46.9 g) and B (13.7 g). From fraction A carnosol (2.13 g) was crystallized with benzene. The mother liquid was applied to a polyamide column (74–149 μm, Wako) and eluted with methylene chloride and methylene chloride–methanol (4:1), successively. From the methylene chloride–methanol fraction carnosic acid (1.81 g) was obtained. The crystals (4.56 g) obtained from fraction B (13.7 g) by crystallization with benzene, were chromatographed on a silica gel column followed by a Sephadex LH-20 column (25–100 μm; Pharmacia, Uppsala, Sweden) to furnish rosmanol (54 mg). The mother liquid of fraction B (5.70 g) was chromatographed on silica gel (benzene–acetone, 10:1) and Sephadex LH-20 (methanol) columns to give epirosmanol (69 mg).

2.2. Apparatus

The HPLC system consisted of two Tosoh (Tokyo, Japan) CCPD pumps equipped with a Tosoh CCP controller connected to a dynamic mixer, a 5-μl sample loop, a Tosoh SD-8012 and

a Tosoh UV-8020 UV-Vis detector set at 230 nm. The data were processed by means of a SIC Chromatocorder-12 integrator to evaluate the peak areas. The purity of the chromatographic peaks was estimated using a Waters (Milford, MA, USA) Model 990J photodiode array detector.

2.3. Chromatographic conditions

The stainless-steel column (150 × 4.6 mm I.D.) was packed with a Wako Wakosil-II 5C18 HG (5 μm) and used at 25 ± 0.5°C. The separation was isocratically undertaken with a solvent consisting of 0.1% (v/v) aqueous phosphoric acid–acetonitrile (40:60) at a flow-rate of 1 ml/min.

2.4. Preparation of samples of dried and fresh herbs

Sample (10–1200 mg) in acetone (3 ml) was homogenized with a Polytron while being cooled in ice and the mixture was centrifuged (1500 g for 10 min) at 4°C. The acetone supernatant was then transferred to a test-tube, the residue was sonicated in a sonic cleaning bath cooling in ice for 3 min with acetone (2 ml) and centrifuged at 4°C. The residue was further extracted in the same manner. The extracts were combined and centrifuged (1500 g for 10 min) at 4°C, and then a portion (more than 20 μl) was injected into the HPLC column.

2.5. Recovery test

The powdered dried leaves (30 mg) of rosemary containing carnosic acid (1.20 mg) and carnosol (0.10 mg) were homogenized with a Polytron while being cooled in ice with two different amounts of the standard acetone solution (2 ml) in which 0.23 and 0.03 mg/ml or 0.115 and 0.015 mg/ml of carnosic acid and carnosol, respectively were added. After centrifugation the supernatant was transferred, the residue was further extracted with the standard acetone solution according to the above described procedure.

3. Results and discussion

3.1. Standard materials

The following compounds (Fig. 1) were identified by the comparison of ^1H and ^{13}C NMR spectral and the literature data [7,9]: carnosic acid, carnosol, rosmanol and epirosmanol. The purity of standard materials calculated from the peak area in the proposed method was $\geq 98\%$.

3.2. HPLC

HPLC was carried out on a Wako Wakosil-II 5C18 HG reversed-phase column, which was selected because of its large number of theoretical plates, its specific characteristics towards α -diphenolic compounds and the avoidance of poor peak shapes of these phenolic diterpenes. In order to obtain a sharp peak of carnosic acid, we

adopted an elution (60% acetonitrile) to which phosphoric acid (0.1%) was added. The retention times (and capacity factors, k') were 2.78 (rosmanol, $k' = 0.91$), 2.96 (epirosmanol, $k' = 1.03$), 6.44 (carnosol, $k' = 3.43$) and 11.28 min (carnosic acid, $k' = 6.75$). The minor phenolic diterpenes such as rosmanol and epirosmanol eluted to overlap with flavonoids. Carnosic acid and carnosol, the major constituents in rosemary, were shown to be satisfactorily separated under the isocratic conditions. These peaks were identified with the retention time and the UV spectrum obtained by photodiode array detection.

HPLC can be accomplished by applying acetone extract of rosemary and sage leaves without any prepurification. The determination of carnosic acid and carnosol can be achieved within 15 min without any clean-up of column. The detection limits (signal-to-noise ratio = 3) were 0.104 (carnosic acid) and 0.521 ng (carnosol) per injection. The calibration curves of carnosic acid and carnosol were linear over the ranges 0.07 $\mu\text{g/ml}$ –2 mg/ml and 0.20 $\mu\text{g/ml}$ –0.5 mg/ml, respectively, with correlation coefficients of 0.992–1.000. To examine the precision of this method, we injected the standard solutions of carnosic acid and carnosol at concentrations of 0.106 and 0.071 mg/ml, respectively. The relative standard deviations ($n = 10$) were 0.97 (carnosic acid) and 1.15% (carnosol). Recovery tests were performed by adding two different amounts of the standard acetone solution of carnosic acid and carnosol. The mixture was extracted and assayed according to the above procedure. The recovery of these compounds was $\geq 94.1\%$.

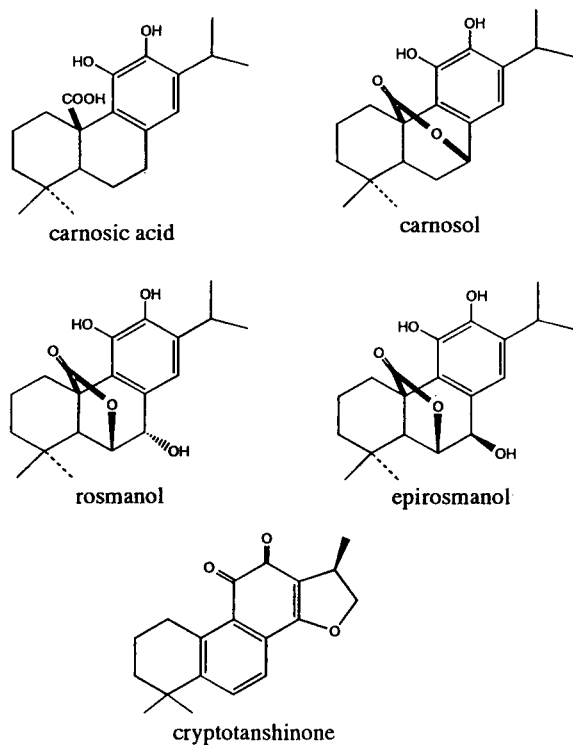


Fig. 1. Structures of phenolic diterpenes.

3.3. Stability of carnosic acid

Carnosic acid has been postulated to be the precursor of phenolic diterpene artifacts. The oxidation of carnosic acid to phenolic diterpene artifacts occurs in polar solvents, but non-polar solvents such as hexane, benzene and methylene chloride are not suited for direct injection into HPLC. As for the stability of carnosic acid in

many solvents, carnosic acid in acetone was relatively resistant to degradation at room temperature, and acetone was a suitable solvent for extraction as well as methanol or ethyl acetate.

The effect of temperature on the degradation of carnosic acid was examined in acetone solution. At -20°C in the dark, carnosic acid standard in acetone and that in rosemary acetone extract did not change at all, as shown in Figs. 2 and 3. However, when a solution of carnosic acid in acetone was left at room temperature (24°C) particularly under 12 h light condition, it decreased rapidly. The degradation of carnosic acid in the acetone extract was higher than that in acetone. Carnosic acid was transformed into carnosol followed by decomposition to form the γ -lactones, rosmanol and epirosmanol, directly [7]. Decomposition of carnosol was enhanced by light. These results indicate that raising temperature and light tend to promote the degradation of carnosic acid.

To examine whether carnosol is present in leaves of rosemary or not, fresh leaves (ca. 0.5 g) dipped in liquid nitrogen immediately after harvesting were transferred into acetone and were allowed to stand in the dark for 4 days at -20°C . Carnosol was found to be 1.7% of the content of carnosic acid. On the other hand, the ratio was

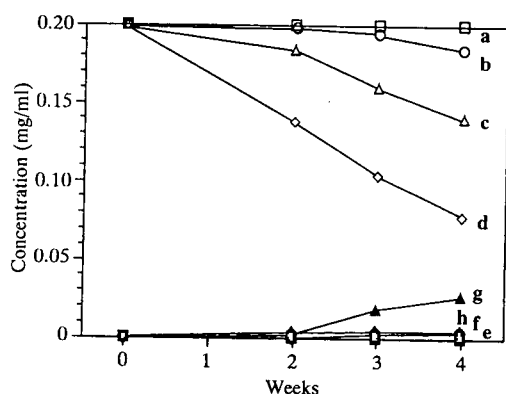


Fig. 2. Degradation of carnosic acid in acetone. Carnosic acid: a = at -20°C (dark); b = at 4°C (dark); c = at room temperature (dark); d = at room temperature (light). Carnosol: e = at -20°C (dark); f = at 4°C (dark); g = at room temperature (dark); h = at room temperature (light).

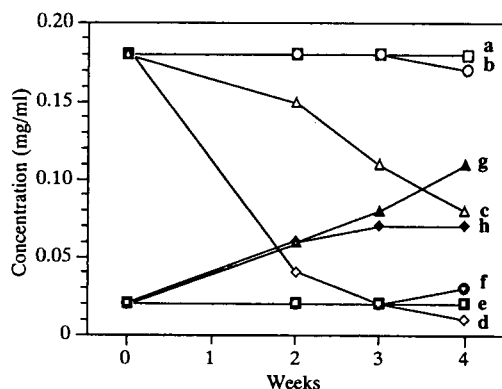


Fig. 3. Degradation of carnosic acid and carnosol in rosemary acetone solution. Carnosic acid: a = at -20°C (dark); b = at 4°C (dark); c = at room temperature (dark); d = at room temperature (light). Carnosol: e = at -20°C (dark); f = at 4°C (dark); g = at room temperature (dark); h = at room temperature (light).

5.9% in another procedure in which fresh leaves were dipped in acetone immediately after harvesting were permitted to stand in the dark for 4 days at room temperature. According to the procedure described in the Experimental section, these ratios were approximately 10%. These results suggest that the content difference between carnosic acid and carnosol in these procedures comes from the conditions of the temperature

Table 1

Content of carnosic acid and carnosol in *Rosmarinus officinalis* and *Salvia officinalis*

Material	Content (mg/g) ^a	
	Carnosic acid	Carnosol
<i>Rosmarinus officinalis</i>		
Dried leaves	42.05 ± 0.19	3.87 ± 0.10
Fresh leaves	22.79 ± 0.40	2.38 ± 0.04
Fresh stems	0.13 ± 0.01	0.10 ± 0.01
Fresh roots	nd ^b	nd
<i>Salvia officinalis</i>		
Fresh leaves	12.40 ± 0.43	1.66 ± 0.21

^a Results are means ± standard deviations from three independent experiments.

^b Not detected.

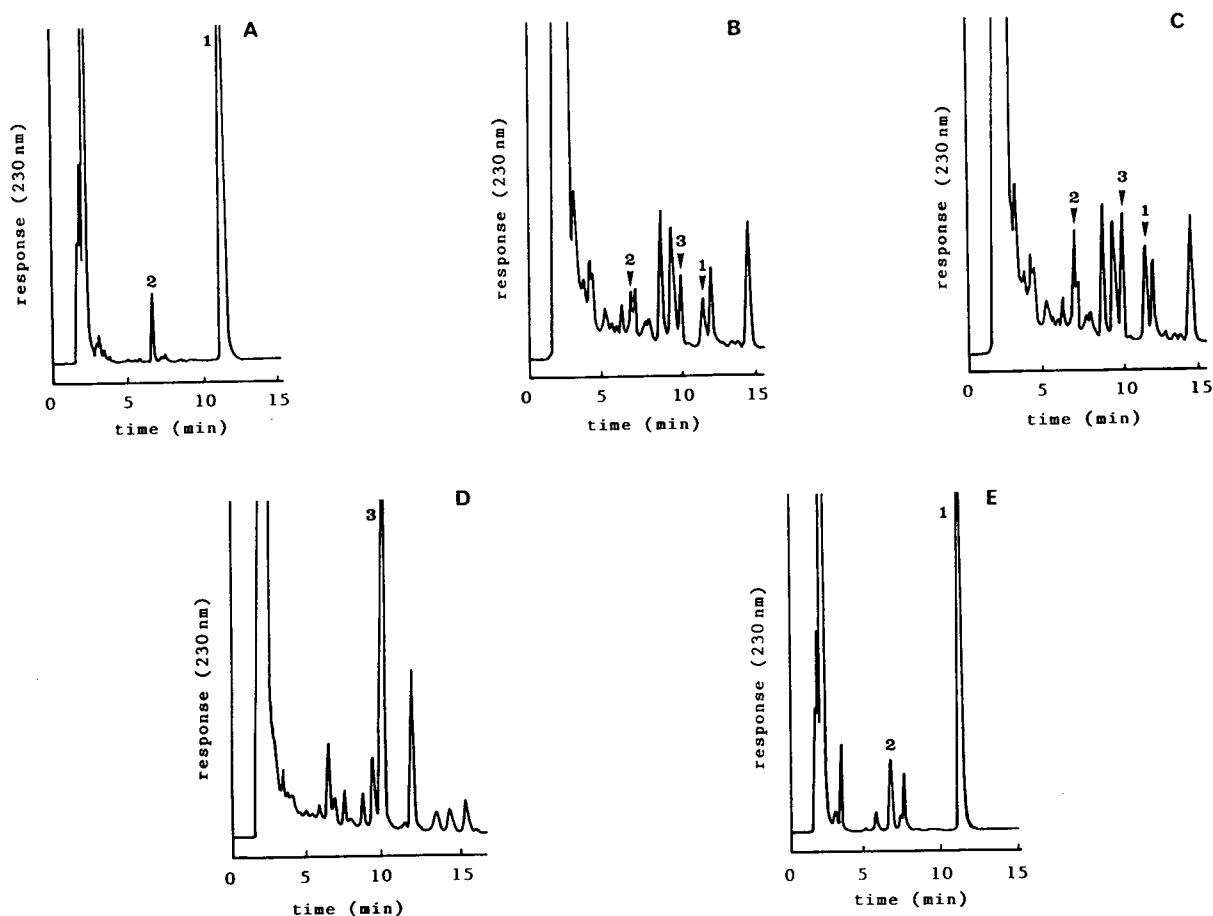


Fig. 4. Chromatograms of carnosic acid and carnosol in (A) fresh leaves, (B) fresh stems, (C) fresh stems spiked with carnosic acid, carnosol and cryptotanshinone, (D) fresh roots of rosemary and (E) fresh leaves of sage. Peaks: 1 = carnosic acid; 2 = carnosol; 3 = cryptotanshinone.

employed and air-oxidation. However, the question still remains whether carnosol is an artifact or not.

3.4. Determination of carnosic acid and carnosol

Carnosic acid and carnosol in dried and fresh leaves, fresh stems and roots of rosemary, and fresh leaves of sage were determined by the proposed method. The chromatograms are displayed in Fig. 4. The HPLC pattern of rosemary

leaves was similar to that of sage, suggesting that these plants have a close botanical and biosynthetic relationship. As shown in Table 1, carnosic acid represents a main constituent (1.24–4.21%) of the leaves extract. Although carnosic acid and carnosol are not observed in the extract of roots, cryptotanshinone, an abietane-type diterpene, existed as a main constituent instead of these compounds. The roots of *Salvia miltiorrhiza* Bung are known to contain cryptotanshinone [10] which accounted for 0.36% of fresh weight as a main compound [11]. Further study is necessary to examine the bio-

synthetic relationship of carnosic acid with cryptotanshinone, an abietane-type diterpene.

Acknowledgement

The authors are grateful to Professor Yasuto Tsuruta for valuable advice.

References

- [1] J.R. Chipault, G.R. Mizuno, J.M. Hawkins and W.O. Lundberg, *Food Res.*, 17 (1952) 42.
- [2] H. Linde, *Helv. Chim. Acta*, 47 (1964) 1234.
- [3] C.H. Briekorn, A. Fuchs, J.B. Bredenberg, J.D. McChesney and E. Wenkert, *J. Org. Chem.*, 29 (1964) 2293.
- [4] N. Nakatani and R. Inatani, *Agric. Biol. Chem.*, 45 (1981) 2385.
- [5] N. Nakatani and R. Inatani, *Agric. Biol. Chem.*, 48 (1984) 2081.
- [6] E. Wenkert, A. Fuchs and J.D. McChesney, *J. Org. Chem.*, 30 (1965) 2931.
- [7] K. Schwarz and W. Ternes, *Z. Lebensm.-Unters.-Forsch.*, 195 (1992) 99.
- [8] K. Schwarz and W. Ternes, *Z. Lebensm.-Unters.-Forsch.*, 195 (1992) 95.
- [9] R. Inatani, N. Nakatani, H. Fuwa and H. Seto, *Agric. Biol. Chem.*, 46 (1982) 1661.
- [10] K. Takiura, *Yakugaku Zasshi*, 61 (1941) 475.
- [11] N. Okamura, K. Kobayashi, A. Yagi, T. Kitazawa and K. Shimomura, *J. Chromatogr.*, 236 (1991) 317.

Short communication

Dynamic ion-exchange chromatography for the determination of lanthanides in rock standards

Noemia M.P. Moraes*, Helena M. Shihomatsu

Coordenadoria de Caracterização de Materiais, Instituto de Pesquisas Energéticas e Nucleares, Comissão Nacional de Energia Nuclear, Caixa Postal 11049, CEP 05422-970, São Paulo, Brasil

First received 14 March 1994; revised manuscript received 8 June 1994

Abstract

A high-performance liquid chromatographic procedure has been developed and tested for the determination of rare earth element (REE) concentrations in United States Geological Survey rock standards AGV-1, GSP-1 and G-2.

The procedure involved acid digestion of sample in PTFE pressure bombs, group separation of REEs, followed by elution of individual lanthanides using α -hydroxyisobutyric acid in the presence of hydrophobic ions on a C_{18} bonded silica reversed-phase column. The eluted REEs were monitored by visible spectrophotometry at 520 nm after post-column reaction with pyridylazoresorcinol. This reversed-phase partition system is suited to separate and detect all lanthanides elements in less than 20 min with good reproducibility.

Comparison of the results with literature values shows an agreement of $\pm 5\%$ for all elements. An internal standard deviation of $\pm 0.5\%$ was found for a single analysis, while triplicate analysis showed a standard deviation of 1–2%.

1. Introduction

The increasing utilization of the rare earth elements (REEs) and interest in their geological, nuclear and environmental roles [1,2] have enhanced the need for rapid, sensitive methods of determination.

Rare earth metals have been a difficult group of elements to separate individually due to their similar chemical properties. It is difficult to determine individual REEs in mixtures by standard analytical methods.

In general, REE determination in rock standards is carried out by instrumental and radio-

chemical neutron activation [3], mass spectrometry [4,5] and inductively coupled plasma [6]. In these techniques ion exchange using a complexing agent is generally employed. However this is time consuming with respect to elution and quantitation. Further, such a procedure requires large quantities of high-purity reagents and results in a high volume of acid wastes.

Studies have shown that dynamic ion exchange can be used for the high-performance liquid chromatographic (HPLC) separation and determination of metal ion in complex matrices [7–9].

In this technique a modifier is added to the mobile phase in the form of a hydrophobic ion to create a charged surface on the reversed-phase column packing material. Metals in the sample

* Corresponding author.

are separated when they interact with the charged particles of the packing material. This method gave improved column efficiency for metal ions, and greater flexibility in the choice of separation conditions.

The application of the dynamic ion exchangers for the determination of rare earths in United States Geological Survey (USGS) rocks standards in a wide range of concentrations, and the comparison with reference results, form the basis of this study.

2. Experimental

2.1. Reagents and materials

The reagents used for solutions and eluents were freshly prepared.

All solutions were prepared with distilled water that had been purified in a Milli-Q unit (Millipore). Eluents were filtered through 0.2- μm filters.

The following reagent-grade chemicals were used: 40% hydrofluoric acid; 70% perchloric acid; 37% hydrochloric acid; 65% nitric acid; 2 M hydrochloric acid; 8 M nitric acid; a quartz column of I.D. 0.8 cm containing 14 cm of Dowex 50W-X8 (200–400 mesh, 37–74 μm , hydrogen form); 4-(2-pyridylazo)resorcinol monosodium salt (PAR), 0.05 mg/l in 2 M ammonium hydroxide and 1 M acetic acid; α -hydroxyisobutyric acid (α -HIBA), 0.07 and 0.4 M aqueous solutions buffered at pH 3.8 with ammonium hydroxide; 0.01 M sodium octanesulfonate (OS); Waters Nova-Pak C₁₈ column (150 \times 3.9 mm I.D.); Waters C₁₈ Guard-Pak (5.0 \times 6.0 mm I.D.); housed in a Waters Guard-Pak (precolumn module); REE standard solutions, obtained by dissolving pure oxides (Johnson Matthey) in mineral acids.

2.2. HPLC apparatus

The liquid chromatograph used in this work was a 625 LC from Waters equipped with a linear gradient programmer, a Rheodyne 9125 load injection valve, a constant-flow peristaltic pump,

a Waters 490 programmable multiwavelength spectrophotometric detector, a Waters RDM module (post-column reagent) used to transfer the PAR complexing solution and a Spectra-Physics 4400 computing integrator–recorder.

2.3. Procedure

Sample dissolution

REEs are generally concentrated in minor mineral phases resistant to acid digestion, which can be overcome by dissolution in PTFE pressure bombs [10]. We have replaced the decomposition technique, at ambient pressure, by high-pressure decomposition, because this procedure is less time consuming and permits by its higher reaction temperature a more effective decomposition. Samples of about 200 mg were digested in PTFE bombs with 8 ml of 40% hydrofluoric acid and 0.5 ml of 65% nitric acid at 160°C for 18 h. After the dissolution the acids were evaporated and a further dissolution and evaporation were done with 5 ml of 70% perchloric acid and 10 ml of 65% nitric acid in order to eliminate hydrofluoric acid and organic materials. Finally, the residue was dissolved in 2 M hydrochloric acid, the solution was evaporated and the residue was dissolved in 2 ml of 2 M hydrochloric acid for chemical separation.

Group separation of REEs [11,12]

A quartz column of I.D. 0.8 cm containing 14 cm of Dowex 50W-X8 cation-exchange resin was conditioned with 2 M hydrochloric acid. Sample dissolved in 2 ml of 2 M hydrochloric acid was passed through the column and the interfering matrix elements were eluted with 80 ml of 2 M hydrochloric acid. The column was subsequently neutralized with 7 ml of water and the REEs, as a group, were eluted with 40 ml of 8 M nitric acid. This REE fraction was evaporated to dryness, and dissolved in the mobile phase (2 ml) prior to injection into the HPLC system.

HPLC procedure

Samples (30 to 300 μl) of the REE fraction from the group separation were injected into the mobile phase and the α -HIBA concentration was

then programmed linearly from 0.07 to 0.4 M over 15 min. The OS concentration (0.01 M), the pH (3.8) and flow-rate (1 ml/min) were maintained constant during the gradient program. The eluted REEs were detected after a post-column reaction with PAR. These post-column reactant was added to the eluent in a PTFE mixing tee at 0.5 ml/min flow-rate, and the eluted metal ions were monitored by a programmable multiwavelength detector at 520 nm. The concentrations of the REEs in the samples were calculated with the non-linear regression program in the Spectra-Physics integrator. The regression equations were generated with peak areas from three standards covering the concentration range expected for the samples.

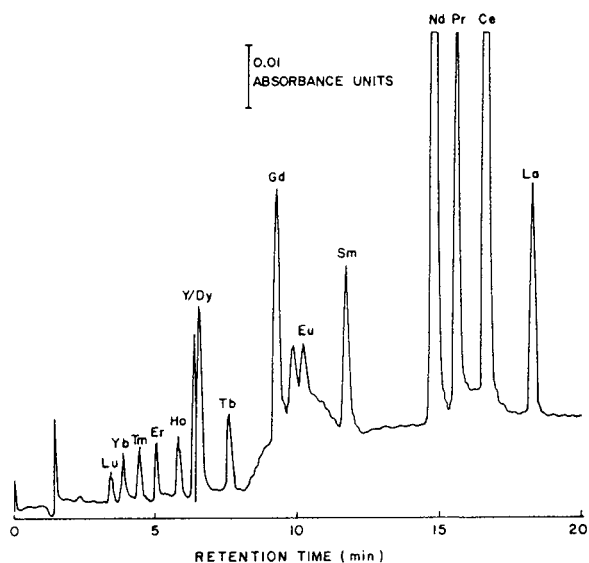


Fig. 1. Separation of rare earths in the standard solution SS2 by gradient elution. Experimental conditions: Waters Nova-Pak C₁₈ column (150 × 3.9 mm I.D.); gradient separation at 1 ml/min from 0.07 to 0.4 M α -HIBA at pH 3.8 over 20 min with 0.01 M OS. Injection volume 100 μ l.

3. Results and discussion

The REE concentrations were determined on the USGS rock standards [13] andesite AGV-1, granodiorite GSP-1 and granite G-2. Many REE analyses have been reported for these samples in the literature [13–15] and the data of Gladney et al. [15] and Hooker et al. [16] are included in this study for comparison. The data of Gladney

are based on different techniques and these values are called “consensus” values.

To evaluate the separations a calibration has been carried out by employing known standard

Table 1
REE detection limit and analyses data for the calibration solutions

Element	SS1 (ppb)		SS2 (ppb)		SS3 (ppb)		Detection limit (ppb, w/w)
	Injected	Found	Injected	Found	Injected	Found	
La	179.22	180.57	399.32	399.44	1194.94	1200.19	1
Ce	71.38	71.33	869.61	833.68	2608.83	2618.06	1
Pr	47.16	46.72	158.58	159.18	475.74	477.64	1
Nd	70.54	69.50	300.74	300.92	902.74	902.88	1
Sm	15.61	15.58	34.78	34.49	104.34	104.74	1
Eu	4.93	5.44	9.15	9.16	27.45	27.66	1
Gd	18.00	17.96	40.11	43.45	120.33	120.34	1
Tb	4.69	4.49	10.46	10.93	31.38	31.39	1
Dy	18.59	19.31	20.71	19.81	62.13	62.15	1
Ho	5.05	4.81	9.38	9.62	28.14	27.87	1
Er	5.34	5.51	9.91	9.92	29.73	29.60	3
Tm	4.46	4.82	9.94	10.07	29.82	29.83	3
Yb	5.91	5.88	10.97	11.07	32.90	33.00	3
Lu	5.13	4.66	8.53	8.49	25.59	25.73	3
Y	20.00	20.74	19.74	19.81	59.22	59.91	1

Table 2
Results of REE abundances in USGS rock standard AGV-1

Element	REE ($\mu\text{g/g}$)		
	HPLC	Lit. [15]	Lit. [16]
La	36 \pm 2	38 \pm 3	38
Ce	69 \pm 3	66 \pm 6	68.7
Pr	6.7 \pm 0.5	6.5 \pm 0.9	–
Nd	35 \pm 4	34 \pm 5	32.1
Sm	5.4 \pm 0.2	5.9 \pm 0.5	5.83
Eu	1.57 \pm 0.07	1.66 \pm 0.11	1.54
Gd	5.17 \pm 0.05	5.2 \pm 0.6	4.76
Tb	0.66 \pm 0.04	0.71 \pm 0.11	–
Ho	0.71 \pm 0.06	0.73 \pm 0.08	–
Er	1.7 \pm 0.1	1.61 \pm 0.22	1.82
Yb	1.69 \pm 0.04	1.67 \pm 0.17	1.68

REE mixtures. The data of Table 1 list the results for three standards REEs (SS1, SS2 and SS3) mixture injected and the chromatogram for the SS2 is shown in Fig. 1. The results obtained demonstrate the total elution of individual REEs. The REE concentrations of USGS standards obtained in the present study are shown in Tables 2, 3 and 4.

The REE concentrations determined are the averages of three totally independent analyses involving separated dissolution, chemical separation and HPLC procedure. The internal relative standard deviation (R.S.D.) of the elemental values calculated for a single analysis was found

Table 3
Results of REE abundances in USGS rock standard GSP-1

Element	REE ($\mu\text{g/g}$)		
	HPLC	Lit. [15]	Lit. [16]
La	183 \pm 11	183 \pm 13	182
Ce	426 \pm 15	406 \pm 20	419
Pr	51.9 \pm 0.3	51 \pm 8	–
Nd	180 \pm 3	190 \pm 17	201
Sm	27.1 \pm 0.2	26.8 \pm 2.5	25.8
Eu	2.4 \pm 0.1	2.36 \pm 0.22	2.21
Gd	12.9 \pm 0.3	13 \pm 2	10.2
Tb	1.38 \pm 0.04	1.36 \pm 0.14	–
Ho	1.20 \pm 0.06	1.2 \pm 0.5	–
Er	2.4 \pm 0.1	2.5 \pm 0.4	2.11
Yb	1.74 \pm 0.03	1.7 \pm 0.4	1.5

Table 4
Results of REE abundances in USGS rock standard G-2

Element	REE ($\mu\text{g/g}$)		
	HPLC	Lit. [15]	Lit. [16]
La	96 \pm 2	86 \pm 5	97.7
Ce	161.2 \pm 12	159 \pm 11	160
Pr	19.2 \pm 0.6	19 \pm 2	–
Nd	50 \pm 2	53 \pm 8	54.8
Sm	7.1 \pm 0.6	7.2 \pm 0.6	7.27
Eu	1.4 \pm 0.03	1.41 \pm 0.12	1.34
Gd	4.14 \pm 0.09	4.1 \pm 0.8	3.97
Tb	0.38 \pm 0.01	0.48 \pm 0.07	–
Dy	1.8 \pm 0.2	2.5 \pm 0.5	2.11
Ho	0.37 \pm 0.09	0.37 \pm 0.02	–
Er	0.81 \pm 0.07	1.2 \pm 0.3	0.83
Yb	0.70 \pm 0.06	0.78 \pm 0.14	0.6
Y	10.9 \pm 0.6	11.4 \pm 2.3	–

to be in the order of 0.5%. The total R.S.D. based on triplicate analyses, was found to be in the range 1–2% for most of the elements.

Because of the appreciable overlap between the Dy and Y peaks in the sample G-2 it was not possible to obtain reliable peak areas for these elements. In the case of samples AGV-1 and GSP-1 it is not possible to separate the two elements (Dy and Y). For the three samples it was not possible to determine Lu and Tm because the concentrations of these elements was below the detection limit.

A comparison of the REE values obtained by HPLC in this study with the literature values [15,16] shows agreement to within 5% for most of the elements for GSP-1, AGV-1 and G-2.

A typical chromatogram obtained for a rock sample (AGV-1) after group REE separation is shown in Fig. 2.

5. Conclusions

The results showed that the method employed is efficient and has adequate sensitivity and reproducibility for the determination of REEs in complex matrices.

The use of α -HIBA as an eluting agent combined with dynamic ion exchangers for the sepa-

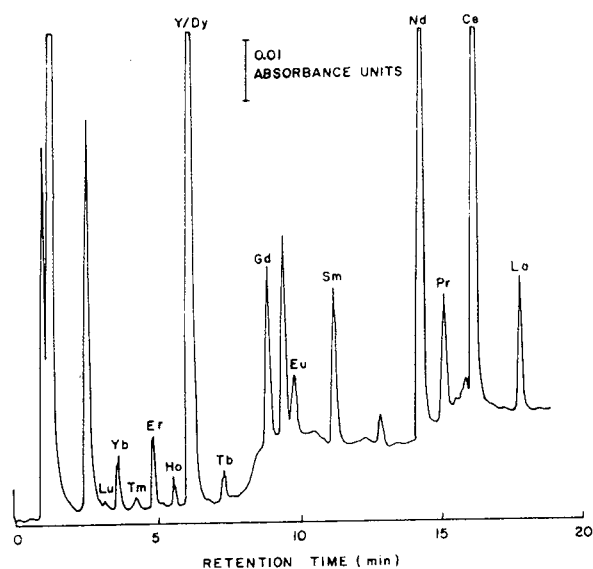


Fig. 2. Separation of rare earths in the rock solution AGV-1 by gradient elution. Experimental conditions as in Fig. 1.

ration of individual REEs have a number of advantages relative to conventional ion-exchange resins. Some of them are its high sensitivity, that little sample is required and multi-elements analyses can be carried out with a single injection.

HPLC has been shown to provide rapid and accurate methods for the analyses of REEs, as compared to the other techniques like isotope dilution mass spectrometry [4,16] and inductively coupled plasma mass spectrometry [17]. The major advantages of the technique are speed and low cost of analyses

Acknowledgement

The authors are grateful to the authorities of Comissão Nacional de Energia Nuclear for

providing all the facilities. and financial support was provided by the Fundação de Amparo à Pesquisa do Estado de São Paulo (FAPESP).

References

- [1] P. Henderson (Editor), *Rare Earth Element Geochemistry*, Elsevier, Amsterdam, 1984.
- [2] P. Linsalata, R.S. Morse, H. Ford, M. Elsenbud, E.P. France, M.B. de Castro, N. Lobão, I. Sachett and M. Carlos, *Health Phys.*, 56 (1983) 33.
- [3] K.C. Condie, G.P. Bowhry and P. Allen, *Contrib. Mineral. Petrol.*, 92 (1986) 93.
- [4] N.M.P. Moraes and S.S. Iyer, *Anal. Chim. Acta*, 236 (1990) 487
- [5] M.J.M. Duke and A. Smith, *J. Radioanal. Nucl. Chem.*, 110 (1987) 207.
- [6] K.E. Jarvis and I. Jarvis, *Geostand. Newsl.*, 12 (1988) 1.
- [7] R.M. Cassidy, F.C. Miller, C.H. Knight, J.C. Roddick and R.W. Sullivan, *Anal. Chem.*, 58 (1986) 1389.
- [8] R.M. Cassidy, S. Elchuk and P.K. Dasgupta, *Anal. Chem.*, 59 (1987) 85.
- [9] R.M. Cassidy, *Chem. Geol.*, 67 (1988) 185.
- [10] H.M. Shihomatsu and S.S. Iyer, *Anal. Chim. Acta*, 288 (1990) 333.
- [11] J.C. Crock and F.E. Lichte, *Anal. Chem.*, 54 (1982) 1329.
- [12] J.C. Crock, F.E. Lichte and T.W. Wildeman, *Chem. Geol.*, 45 (1984) 149.
- [13] S. Abbey, *Pap. -Geol. Surv. Canada*, Paper 83, 1983, p. 15.
- [14] S. Abbey, *Geostand. Newsl.*, 4 (1980) 163.
- [15] E.S. Gladney, C.E. Buns and I. Rollandts, *Geostand. Newsl.*, 7 (1983) 226.
- [16] P.J. Hooker, R.K. O'Nions and R.J. Pankhurst, *Chem. Geol.*, 45 (1984) 149.
- [17] K.E. Jarvis, *Chem. Geol.*, 68 (1988) 31.

Short communication

Experimental method to distinguish column dead time from system dead time for the accurate determination of gas chromatographic void volumes: simultaneous pre- and post-column injection

Yongqing Liu, Kwang S. Yun, Jon F. Parcher*

Chemistry Department, University of Mississippi, University, MS 38677, USA

First received 26 April 1994; revised manuscript received 28 June 1994

Abstract

A new experimental technique for the accurate determination of the dead time of a chromatographic column is described. The technique involves simultaneous pre- and post-column injections of an unretained probe solute. The method allows the accurate determination of the *column* void volume as opposed to the *system* void volume which includes extracolumn volumes. The procedure also eliminates the uncertainties in void volume measurements caused by splitters, multiple flow paths, or auxiliary gas flows required for some detectors or certain types of chromatography such as supercritical fluid chromatography.

1. Introduction

Accurate measurement of the dead time and hence the void volume of a chromatographic column is critical to the experimental determination of thermodynamic parameters from any chromatographic experiment. The problem is very complex and troublesome as evidenced by the multitude of discussions and reviews in the literature [1–10]. Moreover, most of these papers cite multiple prior studies: Kazakevich and McNair [8] for example cite 28 previous investigations involving different methods for the evaluation and definition of the void volume of chromatographic columns in liquid and gas chromatography.

Currently, there are at least four commonly used strategies for measuring this critical parameter, viz., (i) gravimetric determination of the weight of mobile phase of known density in a column, (ii) selection of a dead time which gives the “best” linear fit for a plot of the log of the adjusted retention time of a homologous series of solutes vs. carbon number or some other linearization parameter, (iii) measurement of the retention volume of a dead time probe solute *which is unretained and unexcluded by the stationary phase*, and (iv) measurement of the retention times of isotopically labeled components of the mobile phase or system peaks.

In addition to the experimental difficulties, the exact definition of the void volume is often ambiguous especially for liquid systems in which the mobile phase may solvate the stationary

* Corresponding author.

phase, as well as low-temperature GC or high-pressure SFC systems in which the stationary phase may consist primarily of adsorbed components of the mobile phase. RP-HPLC with alkane-bonded stationary phases also presents conceptual problems because of the uncertain role of the bonded phase in the retention mechanism(s). In such cases, precise definition as well as accurate measurement of the void volume is imperative before any meaningful thermodynamic measurements can be reported or interpreted.

Accurate void volume measurements are particularly difficult if the flow stream of the mobile phase is split or augmented at some point in the apparatus. Inlet splitters are common with capillary GC systems, outlet splitters are sometimes used with mass specific detectors, and other detectors require a makeup gas. Some more complex multidimensional chromatography instruments [11,12] use multiple columns with makeup gas or flow splitting for each column. These configurations with variable flow paths and rates exacerbate the difficulties of accurately measuring the void volume of a given column.

In the present work, a new experimental technique for the determination of void volumes using strategy iii is described. The method involves the injection of the same sample simultaneously at the inlet and outlet of the analytical column. The dead time of the column is obtained from the residence time of the dead time probe *between the two injection sites*, i.e., in the column not the extracolumn plumbing or the detector.

2. Experimental

A simplified schematic diagram of the dual injection technique is illustrated in Fig. 1 for a typical system with a detection system which requires a splitter or auxiliary gas. Pneumatically actuated valves Nos. 1 and 2 are switched simultaneously to provide two sample pulses, only one of which passes through the analytical column. The sample injected via valve No. 2 remains undifferentiated and serves only as a marker for the residence time of any solute in

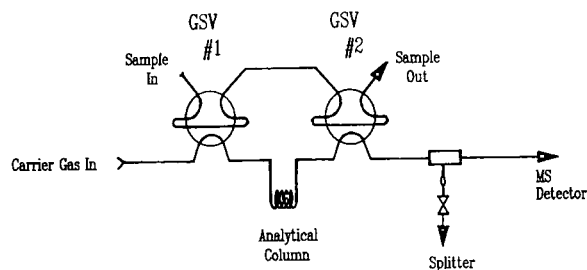


Fig. 1. Schematic diagram of a dual injection system with an outlet splitter. GSV = Gas sampling valve.

the extracolumn regions of the instrument. This residence time may be influenced by the split ratio if a splitter is used or by the flow-rate of the auxiliary or makeup gas if the detector requires such flows. In any case, the extracolumn residence times of the samples injected from both valves will be the same and can be factored out of the column dead time measurements.

3. Results and discussion

A typical chromatogram [13] obtained with a GC-MS system configured as shown in Fig. 1 is given in Fig. 2. Each line in the drawing represents the detector response for a different solute in a carrier gas composed of natural helium, ^4He . The mass selective detector was used to monitor various m/z values, viz., $m/z = 3$ for the dead time probe, ^3He , $m/z = 20$ for neon and $m/z = 47$ for isotopically labeled carbon dioxide. The first peaks in the chromatogram are due to the coelution of all of the sample components injected from sampling valve No. 2. The retention time of these samples gives the residence time of any solute in the extracolumn segments of the system. The time from injection to elution of the dead time probe injected from valve No. 1 is the dead time of the entire system. Whereas, the difference between the elution time of the ^3He probe injected from valve No. 1 and that injected from valve No. 2 gives an accurate measure of the dead time of the analytical column.

Such an instrument has been used to measure very small changes in the measured void volume of a gas-solid chromatographic column as a

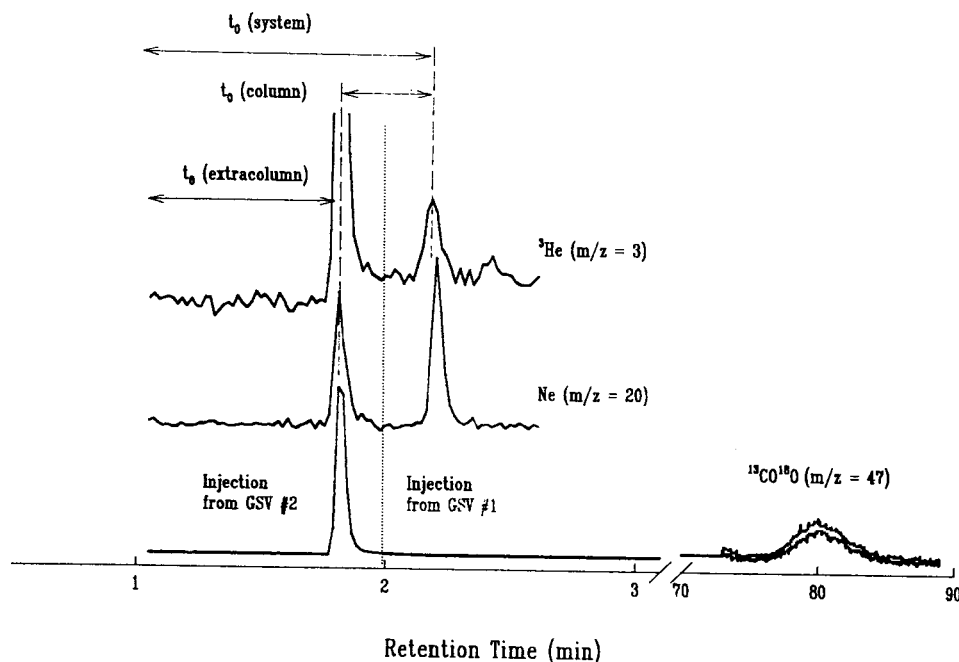


Fig. 2. Example chromatogram obtained from a dual injection instrument [13]. The solutes were injected simultaneously at both sampling valve at 1 min.

function of the amount of material adsorbed from the mobile phase at low temperatures (77 K) [13]. Fig. 2 represents a typical chromatogram obtained from that investigation involving the adsorption of carbon dioxide on silica gel. In this example, the residence time of the solutes in the extracolumn regions of the flow path was 1.80 min compared to the residence time of the ^3He probe in the column of only 0.17 min. That is, if the volume flow-rates were equal in the two regions, the measured extracolumn volume would be approximately ten times as large as the column void volume. The proposed dual injection technique allows the extraction of the latter quantity from the much larger system void volume and thus small changes in the column dead time and void volume could be accurately measured. The results for carbon dioxide adsorbed at 77 K are shown in Fig. 3. The precision of the measurements is sufficient to allow an accurate measurement of the decrease in void volume with increasing amounts of carbon dioxide adsorbed to give a direct measure of the molar

volume of adsorbed carbon dioxide. Thus, it was also possible to measure the volume of material adsorbed as a function of the relative pressure of adsorbate in the mobile phase to produce a truly "volumetric" isotherm [13].

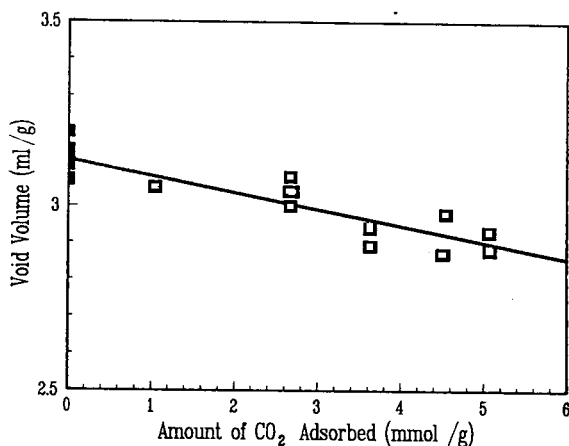


Fig. 3. Void volume measured with dual injection method with various amounts of CO₂ adsorbed on silica gel at 77 K.

4. Conclusions

There are several advantages as well as concomitant disadvantages of the proposed dual injection scheme. Some of the advantages are:

- The technique can be used to distinguish the *column* void volume from the ordinarily much larger and more uncertain *system* void volume.

- Accurate determination of the absolute injection time is not critical. Measurement of a relative retention difference rather than an absolute retention time from injection minimizes the uncertainty from the specification of the exact time of injection. Such uncertainty is especially large for manual syringe injections.

- The technique can be used with any type of chromatography, i.e., GC, SFC, and HPLC.

- The peak profile of the post-column injection peak gives a snapshot of the pre-column injection peak. Thus, changes originating in the column can be distinguished from those occurring in other parts of the system such as the detector. Relevant changes include band spreading, chemical reactions, and isotope exchange processes.

An unforeseen advantage of the dual injection scheme is the fact that the detector response to the sample injected via valve No. 2 gives an undifferentiated profile of the sample injected at valve No. 1. This is especially valuable with a mass specific detector because it provides knowledge of exactly what was injected into the analytical column even if all or part of the sample does not elute in a reasonable time or elutes with the dead time marker.

There are also a number of disadvantages to the proposed method:

- The added complexity and expense of two pneumatically controlled sampling valves may be significant.

- The method still requires a viable dead time probe solute, i.e. a solute which is not retained by the stationary phase.

- Peak overlap may become a limiting problem with non-specific detectors especially for columns with very low void volumes.

- The experimental technique does not elimi-

nate the ambiguities of, or the need for, an exact definition of the void volume and mobile phase volume of a given column.

- Dual injections of a scarce sample is undesirable. This can be overcome by injection of only the dead time marker in the post-column injector; however, some of the advantages cited above will be lost in this case.

- The post-column sampling valve will itself contribute to peak spreading because of its crucial position between the exit of the column and the detector.

- The dual-injection technique is only valuable for instruments in which either the system void volume is significantly larger than the column void volume or there are multiple flow paths for the mobile phase.

The proposed injection scheme will solve some but certainly not all the problems encountered in the accurate assessment or even the exact definition(s) of the void volume and the mobile phase volume of a chromatographic column. In many cases, these two volumes are not equivalent, and extraordinary care must be exercised in the presentation and interpretation of chromatographic retention data and thermodynamic information derived from such data.

Acknowledgements

Acknowledgement is made to the National Science Foundation and to the donors of the Petroleum Research Fund, administered by the American Chemical Society, for support of this research.

References

- [1] M.S. Wainwright, C.S. Nieass, J.H. Haken and R.P. Chaplin, *J. Chromatogr.*, 321 (1985) 287–293.
- [2] R.J. Smith, J.K. Haken and M.S. Wainwright, *J. Chromatogr.*, 334 (1985) 95–127.
- [3] R.J. Smith, C.S. Nieass and M.S. Wainwright, *J. Liq. Chromatogr.*, 9 (1986) 1387–1430.
- [4] A. Malik and K. Jinno, *Chromatographia*, 30 (1990) 135–137.

- [5] B.A. Bidlingmeyer, F.V. Warren, A. Weston, C. Nugent and P.M. Froehlich, *J. Chromatogr. Sci.*, 29 (1991) 275–279.
- [6] E.H. Slaats, W. Markovski, J. Fekete and H. Poppe, *J. Chromatogr.*, 207 (1981) 299–323.
- [7] J.H. Knox and R. Kaliszan, *J. Chromatogr.*, 349 (1985) 211–234.
- [8] Y.V. Kazakevich and H.M. McNair, *J. Chromatogr. Sci.*, 31 (1993) 317–322.
- [9] P.L. Zhu, *Chromatographia*, 20 (1985) 425–433.
- [10] A. Alvarez-Zepeda and D.E. Martire, *J. Chromatogr.*, 550 (1991) 285–300.
- [11] K.A. Krock, N. Rangunathan and C.L. Wilkins, *Anal. Chem.*, 66 (1994) 425–430.
- [12] Z. Liu and J.B. Phillips, *J. Chromatogr.*, 29 (1991) 227–231.
- [13] Y. Liu, L. Liu, K.S. Yun, C. Zhu, B. Yu and J.F. Parcher, *Anal. Chem.*, 66 (1994), in press.

chromatography (HPLC) [12]. Most of these procedures require derivatization in non-aqueous environments or extensive organic workup.

The GC method reported herein is based on an application for volatile organic acids that appeared in the product catalog of J & W Scientific [13]. No derivatization is needed and aqueous samples can be injected directly. The temperature program was modified to slow the rate of temperature increase to allow greater resolution between compounds with similar boiling points. Additionally, the maximum oven temperature was reduced from 250 to 170°C as no further substances were observed at higher temperatures. Experimentation has determined that isovaleric acid is the best choice as an internal standard, as it does not coelute with any of the analyte or system peaks. The GC method reported herein permits quantitative determination of PVL.

2. Experimental

2.1. Apparatus

The GC system consisted of the following: an HP5890 Series II gas chromatograph with a flame-ionization detector (Hewlett-Packard, Wilmington, DE, USA); an HP7673 autoinjector (Hewlett-Packard); an HP Cyclosplitter inlet sleeve (Restek); a deactivated fused-silica guard capillary, 10 m × 0.25 mm (J & W Scientific, Folsom, CA, USA); and a DB-FFAP fused-silica capillary column (0.25 μm film), 30 m × 0.25 mm I.D. with USP Packing Type G25 (J & W Scientific). The DB-FFAP stationary phase is an acid-modified polyethylene glycol similar to the Stabilwax-DA (Restek), Nukol (Supelco) and HP-FFAP (Hewlett-Packard). PE Nelson Access*Chrom GC/LC data system (Perkin-Elmer Nelson Systems, Cupertino, CA, USA) running on a VAX 6410 computer with VMS 5.5-2 was used for data acquisition and analysis.

2.2. Materials and reagents

Acetonitrile (HPLC grade) was obtained from Baxter (McGraw Park, IL, USA). Hydrochloric

acid (ACS reagent grade) was obtained from Mallinckrodt (Paris, KY, USA). Water was distilled twice from an all-glass apparatus then deionized and filtered through activated carbon through a Milli-Q system (Millipore, Waters). A solution of 0.0018 M HCl was prepared by diluting 15 ml hydrochloric acid 1:100 000 in water. Compressed air (hydrocarbon-free grade), compressed hydrogen (high-purity grade) and compressed helium (high-purity grade) were obtained from the Linde Division of Union Carbide (Danbury, CT, USA).

2.3. Standards and samples

An internal standard solution (ISTD) was prepared of 50 ppm isovaleric acid (Aldrich, Milwaukee, WI, USA) in acetonitrile. The working standard solution was 0.01 mg/ml PVL (Aldrich) in 0.0018 M HCl. Both working standard and sample are mixed 1:1 with ISTD prior to analysis.

2.4. GC analysis

Helium was used as the carrier gas. The system had the following parameters: gas flow-rates of 1.5 ml/min for helium, 200 ml/min for air and 20 ml/min for hydrogen; a 1-μl injection volume; injector temperature of 250°C; detector temperature of 250°C; an oven temperature program starting at 100°C for 2 min, followed by a 5°C/min thermal gradient to a maximum of 170°C; an analysis time of 16 min; and the purge valve set OFF at time 0.0 min, ON at 1.2 min and back OFF at 12.2 min (time must be less than run time). Calculations for the samples were based on peak area measurements.

3. Results and discussion

The analysis procedure for PVL was validated for two different DPE-containing ophthalmic solutions. Formula 1 contained DPE, benzalkonium chloride, sodium edetate and salts. Formula 2 contained DPE, levobunolol hydrochloride, polyvinyl alcohol, benzalkonium chloride, sodium edetate and salts. Typical chromato-

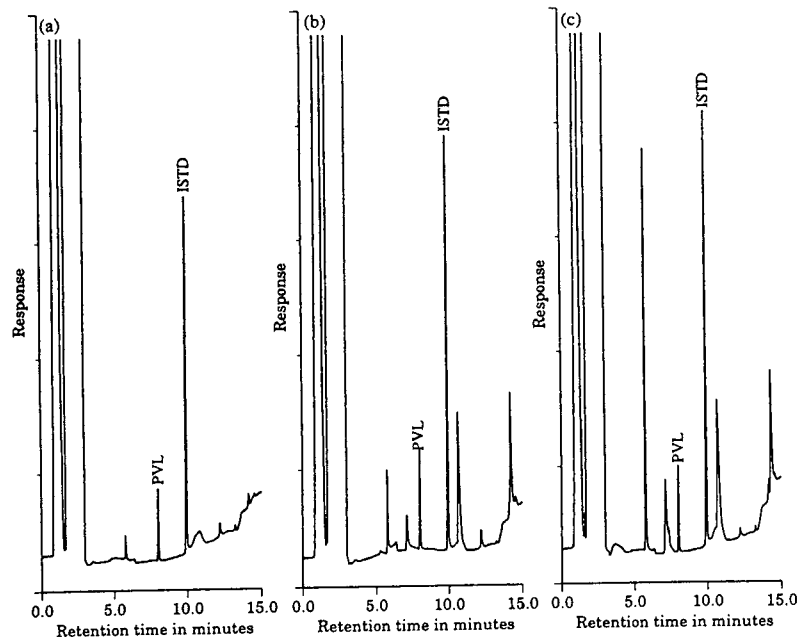


Fig. 2. Chromatograms of PVL standard (a), degraded Formula 1 (b) and degraded Formula 2 (c).

grams of PVL standard and of stability samples at expiry are shown in Fig. 2. Samples of undegraded ophthalmic solutions containing no PVL showed no interferences at the location of the PVL peak (Fig 3).

Linearity in standard diluent was checked from 1.02 to 102 $\mu\text{g/ml}$ [equivalent to 0.0968% (w/w) to 9.68% (w/w) of DPE label claim after dilution for analysis]. The correlation coefficient was 0.999 for both peak area and peak height data. ANOVA results for both peak area and peak height data gave p values less than 0.0001. Therefore, a single-point standard was used.

In addition, linearity in sample matrix was checked from 5.08 to 20.3 $\mu\text{g/ml}$ [equivalent to 0.484% (w/w) to 1.94% (w/w) of DPE label claim after dilution for analysis]. This range corresponds to 1.8 to 7.4% loss of DPE, consistent with the amount of degradation observed in manufactured lots during on-going stability studies. The correlation coefficient was 0.999 for both peak area and peak height data in Formula 1 and 0.998 for peak area data and 0.999 for peak height data in Formula 2. ANOVA results for both formulas and for both peak area and peak height data gave p values less than 0.0001.

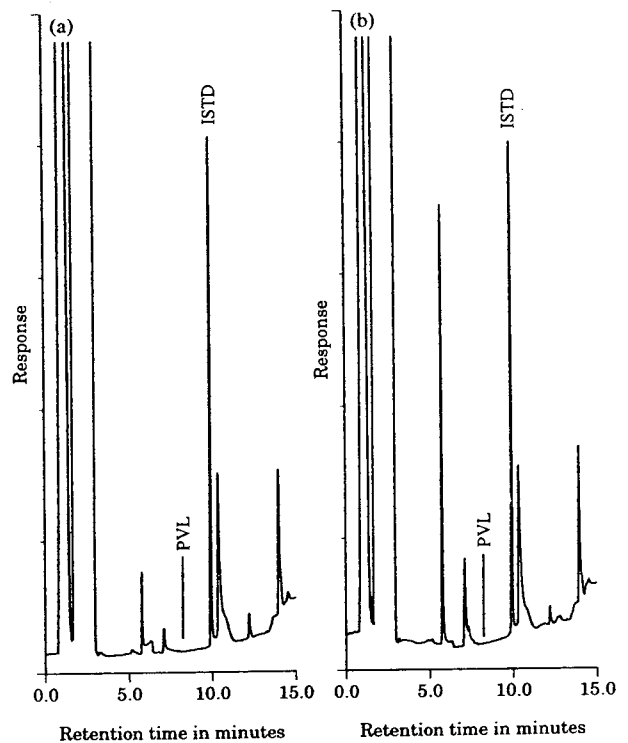


Fig. 3. Chromatograms of undegraded Formula 1 (a) and undegraded Formula 2 (b).

Table 1
Recovery of PVL from spiked samples

		1.94% (w/w)		0.968% (w/w)		0.484% (w/w)	
		Peak area	Peak height	Peak area	Peak height	Peak area	Peak height
Formula 1	Mean (%)	100.9	104.5	99.5	101.9	100.1	100.3
	S.D.	1.1	1.3	3.2	3.5	4.2	1.8
	R.S.D. (% , ±)	1.1	1.3	3.2	3.5	4.2	1.8
	<i>n</i>	3	3	3	3	3	3
Formula 2	Mean (%)	99.2	98.0	99.0	100.7	98.2	100.5
	S.D.	2.9	1.3	1.2	1.9	3.3	2.1
	R.S.D. (% , ±)	2.9	1.4	1.2	1.9	3.4	2.1
	<i>n</i>	3	3	3	3	3	3

Recovery studies to show method accuracy were completed at levels equivalent to 0.484% (w/w), 0.968% (w/w) and 1.94% (w/w) of DPE label claim. Results are summarized in Table 1.

The limit of PVL quantitation is less than 0.255 µg/ml [equivalent to 0.0242% (w/w) of DPE label claim after dilution for analysis]. An average of three peak area measurements at this concentration gave a recovery of 131%, a signal-to-noise ratio greater than 10:1 and a relative standard deviation (R.S.D.) of ± 3.6%.

Three replicates of each 0.968% (w/w) spike used in the accuracy studies were obtained to determine single-day precision. The PVL as % (w/w) of DPE label claim was calculated. On a second day, three replicates each of the same

samples were obtained to provide information concerning day-to-day precision values. Person-to-person precision experiments were run on the same samples to provide information about precision values between different analysts as well as providing feedback with respect to clarity of method write-up. Peak area data are summarized in Table 2.

The following parameters for system suitability are guidelines: tailing factor ≤ 1.25 for PVL and ≤ 1.65 for ISTD; and a resolution of ≥ 1.0 between PVL and system peak 1 (SP1) and between ISTD and system peak 2 (SP2) [2]. See Fig. 4 for a chromatogram illustrating the relevant peaks.

Plate counts and capacity factors are not

Table 2
Summary of day-to-day and operator-to-operator precision

		Operator A		Operator B
		Day 1	Day 2	
Formula 1	Mean (% , w/w)	0.962	0.972	0.977
	S.D.	0.031	0.010	0.021
	R.S.D. (% , ±)	3.2	1.0	2.2
	<i>n</i>	3	3	3
Formula 2	Mean (% , w/w)	0.958	0.985	0.968
	S.D.	0.011	0.030	0.041
	R.S.D. (% , ±)	1.2	3.0	4.2
	<i>n</i>	3	3	3

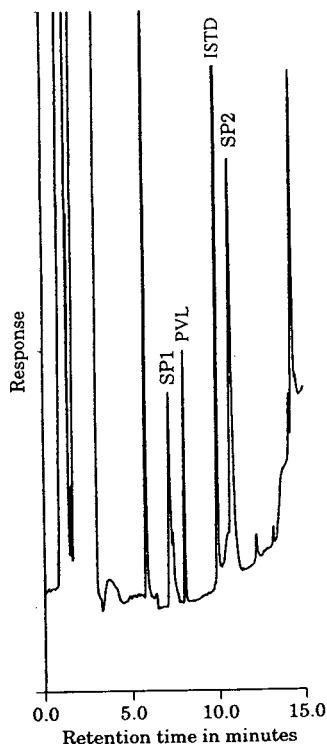


Fig. 4. Potential interfering system peaks in a chromatogram of PVL standard.

critical system suitability parameters. Both will vary considerably over the lifetime of a particular capillary as ends are cut off to removed oxidized or contaminated portions. Because the stationary phase is a stable nitroterephthalic acid-modified polyethylene glycol and both PVL and isovaleric acid (ISTD) are volatile free fatty acids with the same molecular mass, any variation in the system will result in similar changes in plate count and capacity factor for both substances. The tailing factor is a good control for capillary functionality as increases in this parameter are indicative of the formation of activated sites in the capillary. The tailing factor for the ISTD peak is particularly important, as values above 1.65 are likely to indicate that the system has not resolved ISTD and SP2. The resolution factors are essential controls to assure adequate separation of PVL and ISTD from interfering peaks. These interfering peaks, SP1

and SP2, were shown to be from the Milli-Q water used.

4. Conclusions

A simple, accurate, sensitive and precise GC method was developed to determine PVL in DPE-containing ophthalmic solutions. With this method, the PVL resulting from the degradation of DPE can be monitored accurately at concentrations representing 0.0968 to 9.68% (w/w) of DPE label claim.

Acknowledgements

I wish to thank Carl Martin for analytical assistance.

References

- [1] C.A. Weisbecker, M. Naidoff and R. Tippermann (Editors), *Physician's Desk Reference for Ophthalmology*, Medical Economics Co., Montvale, NJ, 21st ed., 1993.
- [2] *United States Pharmacopeia, USP XXII*, Mack Publ. Co., Easton, PA, 22nd revision, 1990.
- [3] G.R. Allen and M.J. Saxby, *J. Chromatogr.*, 37 (1968) 312.
- [4] D.L. Corina and K. Isaac, *J. Chromatogr.*, 260 (1983) 51.
- [5] D.L. Corina and K. Platt, *J. Chromatogr.*, 291 (1984) 127.
- [6] G. Gray and A.C. Olson, *J. Agric. Food Chem.*, 33 (1985) 192.
- [7] J. Hrivňák, L. Soják, E. Beška and J. Janák, *J. Chromatogr.*, 68 (1972) 55.
- [8] V. Palo, P. Valachovic and J. Hrivňák, *Zb. Pr. Chemickotechnol. Fak. SVST, 1979-1981* (1986) 125.
- [9] T.S. Thompson and F.W. Karasek, *J. Chromatogr.*, 388 (1987) 351.
- [10] H. Itoh and Y. Shinbori, *Bull. Chem. Soc. Jpn.*, 60 (1987) 1327.
- [11] A.A. Ivanov, O.A. Shpigun and Y.A. Zolotov, *Zh. Anal. Khim.*, 41 (1986) 134.
- [12] J.M. Miller, I.D. Brindle, S.R. Cater, K.-H. So and J.H. Clark, *Anal. Chem.*, 52 (1980) 2430.
- [13] *High Resolution Chromatography Products*, J & W Scientific, Folsom, CA, 1990, p. 79.

Book Review

Electrophoresis in Practice — A Guide to Theory and Practice, by R. Westermeier, VCH, Weinheim, New York, 1993, XVI + 277 pp., price DM 68.00, £28.00, ISBN 3-527-30012-0 (Weinheim), 1-56081-705-4 (New York).

The book is organized in three parts: Part I, Fundamentals; Part II, Methods, and an Appendix.

Part I has the following chapters: the Introduction explains the basic terms and the classification of existing electrophoretic methods. Electrophoresis (Ch. 1) gives a brief description of electrophoresis in free solution, also including a page on continuous free flow electrophoresis and a page on capillary electrophoresis; a brief description of electrophoresis in supporting media; an explanation of sieving in gels; principles of immunoelectrophoresis, pulsed field technique, DNA sequencing, and two-dimensional electrophoresis. Isotachopheresis (Ch. 2) describes briefly on three pages the principle of this technique. Isoelectric focusing (Ch. 3) gives the description of this technique carried out with free carrier ampholytes and in immobilized pH gradients. The chapter on Blotting (Ch. 4) describes the principles, possible problems and remedies. The chapters on Instrumentation (Ch. 5) and on the interpretation of electropherograms (Ch. 6) are devoted to instrumental aspects, and especially to densitometry of electrophoretic bands. Valuable is the review of commercial instrumentation and laboratory equipment guide summarized in tables.

Part II, devoted to methods, may be characterized as a cook-book, where one can find recipes organized in the following scheme: sample preparation, stock solutions required, casting of gels, preparation of a cassette, setting of electrophoretic operational conditions, staining, and an example of the separation. Method 1 is

on polyacrylamide gel electrophoresis (PAGE) of dyes and shows PAGE of low-molecular-mass substances. Method 2 is on PAGE of DNA fragments and shows the separation of oligonucleotides. Method 3 is on agarose and immunoelectrophoresis and brings the separation of protein standard makers. Method 4 is on titration curve analysis and shows the determination of the *pI* values of proteins. Method 5 is on native PAGE in amphoteric buffers and describes the cationic separation of proteins in meat extracts. Methods 6 and 7 are on agarose isoelectric focusing (IEF) and PAGIEF in rehydrated gels, respectively, and they describe IEF of the same samples as in method 5. Method 8 is on sodium dodecyl sulfate (SDS)-polyacrylamide electrophoresis and describes the determination of M_r of proteins denaturated by SDS with evaluation of results by commercial software UltroScan XL. Method 9 is on semi-dry blotting of proteins and shows blotting of SDS-denaturated proteins on nitrocellulose. Method 10 is on IEF in immobilized pH gradients and method 11 is high-resolution two-dimensional electrophoresis; schemes and detailed recipes are given of how to analyse proteins by IEF in immobilized pH gradients and by a two-dimensional technique.

Finally, the Appendix brings a clear troubleshooting guide organized as follows: symptom, cause and remedy; it gives rules and advises on what to do when something does not work or the bands are not good. IEF (A1), SDS electrophoresis (A2), semi-dry blotting (A3) and two-dimensional electrophoresis (A4) are covered.

The book is nice handbook and textbook on classical electrophoresis for a wide range of chemists covering newcomers, practitioners, scientists and experts. The text of the book is clearly written and well organized, where, by reading several related pages one can grasp a principle and a method never touched before, and, by following the step-by-step description one can practice a procedure never done before. The text is well illustrated with self-explaining

figures, and, parallel to the main text, the margins give important references and excellent glossaries.

The book may be recommended as a reference book on classical electrophoretic techniques and the readers may strongly regret that the book does not cover capillary electrophoresis at a relevant level.

Brno (Czech Republic)

Petr Boček



ELSEVIER

Journal of Chromatography A, 679 (1994) 404–405

JOURNAL OF
CHROMATOGRAPHY A

Book Review

Mass Spectrometry for the Characterization of Microorganisms (ACS Symposium Series, No. 541), edited by C. Fenselau, Washington, DC, 1994, VIII + 240 pp., price US\$ 64.95, ISBN 0-8412-2737-3.

This new volume of the *ACS Symposium Series* is truly a comprehensive snapshot in time of current research by well known authors on the mass spectrometric characterization of microorganisms. The book is divided into 14 chapters covering 232 pages with additional pages for author, affiliation and subject indexes.

A nice feature preceding all of the specialized chapters is the informative overview provided by the Editor, Professor C. Fenselau, evaluating the advantages and disadvantages of mass spectrometry (MS) for this purpose. This chapter summarizes the new possibilities offered by modern desorption techniques for the characterization of chemotaxonomic markers and defines the structural molecular prerequisites for this task. Chapters 2 and 3 describe the identification of lipid biomarkers to characterize changes in the environment of a given organism and the use of fast atom bombardment (FAB) for the analysis of phospholipids, including the possibilities of differentiating between species and the taxonomic value of these data. Phospholipid profiling by tandem MS is further discussed in Chapter 4. This chapter provides useful information on the effect of growth temperature, time, media and culturing on these profiles. The authors describe how the large data sets obtained in this way may limit in practice the evaluation of the potential information derived from the use of this instrumental technique.

The proper role of pyrolysis–GC–MS for microorganism detection and characterization is described in Chapter 5. Chapters 6 and 7 discuss the use of GC–MS of volatile metabolites for the detection of microscopic fungi and microorganisms in general. In the latter case the approach in similar but instead of headspace methods, the authors use the rapidly growing technique of membrane inlet MS (MIMS). It is indicated that although the present literature does not contain examples of the use of MIMS for the determination of metabolites in microorganism identification, there are promising possibilities for the identification of metabolites produced by known organisms. Interestingly, larger molecules may be amenable to this type of approach in the near future. Chapter 8 deals with derivatization GC–MS of carbohydrate markers for specific bacterial strains or genera. The approach is fairly comprehensive with useful practical information and examples. This is followed by a good review chapter on analytical methods for candidiasis using blood, serum or urine samples. Chiral chromatography is used for the separation of arabinitol enantiomers, which are then identified by CI-SIM-MS. Chapter 10 is an authoritative description of the occurrence, role and phylogenetic significance of modified nucleosides in microorganisms determined by thermospray LC–MS. Finally, Chapter 11 provides examples of the use of MS (FAB and electrospray) for the

study of viral proteins in a strain of HIV-1 virus. This chapter clearly shows how MS can provide definitive structural information on proteins from a given microorganism. This is nicely complemented by the examples on the use of FAB and laser and plasma desorption MS to obtain structural information on lipid A of Gram-negative bacteria. As indicated by the authors, bacterial strains could thus be identified and differentiated. The book closes with two timely and informative additional chapters on glycolipid analysis by MS techniques as applied to pathogenic *Haemophilus* and *Nisseria* species, as well as mycobacteria in general.

In summary, this volume of the *ACS Symposium Series* contains information that should be very valuable to students and also to established researchers as it presents a condensed overview of the possibilities and challenges existing in this field. The various chapters are not too extensive but contain just enough data to get anybody properly started on this topic. The only problem is that perhaps it appeared rather late for a camera-ready type of production of the presentations given in a symposium held August 1992.

Barcelona, Spain

Emilio Gelpí

Author Index

- Abe, K., see Yarita, T. 679(1994)329
- Abu-Lafi, S., Sterin, M. and Levin, S.
Role of hydroxyl groups in chiral recognition of cannabinoids by carbamated amylose 679(1994)47
- Abu-Lafi, S., see Levin, S. 679(1994)213
- Akiyama, A., see Straub, J.A. 679(1994)85
- Allen, D.W., Clench, M.R., Crowson, A., Leathard, D.A. and Saklatvala, R.
Characterisation of electron beam generated transformation products of Irganox 1010 by particle beam liquid chromatography-mass spectrometry with on-line diode array detection 679(1994)285
- Almqvist, S.R., Petersson, P., Walther, W. and Markides, K.E.
Direct and indirect approaches to enantiomeric separation of benzodiazepines using micro column techniques 679(1994)139
- Beckers, J.L.
UV detection in capillary zone electrophoresis. Peaks or dips - that is the question 679(1994)153
- Belew, M., Zhou, Y., Wang, S., Nyström, L.-E. and Janson, J.-C.
Purification of recombinant human granulocyte-macrophage colony-stimulating factor from the inclusion bodies produced by transformed *Escherichia coli* cells 679(1994)67
- Betzel, C., see Weber, W. 679(1994)181
- Blatný, P., Kvasnička, F. and Kenndler, E.
Time course of formation of inositol phosphates during enzymatic hydrolysis of phytic acid (myo-inositol hexaphosphoric acid) by phytase determined by capillary isotachopheresis 679(1994)345
- Boček, P.
Electrophoresis in Practice—A Guide to Theory and Practice (by R. Westermeier) (Book Review) 679(1994)402
- Boschetti, E., see Horvath, J. 679(1994)11
- Botton, B., see Devèvre, O. 679(1994)349
- Bruno, T.J. and Caciari, M.
Retention of halocarbons on a hexafluoropropylene epoxide-modified graphitized carbon black. II. Ethane-based compounds 679(1994)123
- Bryan, T.G., see Mourey, T.H. 679(1994)201
- Caciari, M., see Bruno, T.J. 679(1994)123
- Cai, J., see Hsieh, F.Y.L. 679(1994)206
- Cao, X.-L., Hewitt, C.N. and Waterhouse, K.S.
Determination of reactive hydrocarbons by capillary gas chromatography with the reduction gas detector 679(1994)115
- Chambers, J.Q., see Farkas, T. 679(1994)231
- Chung, M.C.M., see Yao, Z.J. 679(1994)190
- Cigánek, M., see Dressler, M. 679(1994)299
- Clench, M.R., see Allen, D.W. 679(1994)285
- Cleveland, J.A., Martin, C.L. and Gluck, S.J.
Spectrophotometric determination of ionization constants by capillary zone electrophoresis 679(1994)167
- Cooke, N., see Horvath, J. 679(1994)11
- Crowson, A., see Allen, D.W. 679(1994)285
- Danielson, N.D., see Holeman, J.A. 679(1994)277
- De Boer, A.J., see Mesters, J.R. 679(1994)93
- Devèvre, O., Putra, D.P., Botton, B. and Garbaye, J.
Sensitive and selective method for the separation of organic acids by capillary zone electrophoresis 679(1994)349
- Dou, L., Zeng, J.-N., Gerochi, D.D., Duda, M.P. and Stuting, H.H.
Chiral high-performance liquid chromatography methodology for quality control monitoring of dexfenfluramine 679(1994)367
- Dressler, M. and Cigánek, M.
Effect of detector temperature on the flame ionization detector response 679(1994)299
- Duda, M.P., see Dou, L. 679(1994)367
- Dusbábek, F., see Šimek, P. 679(1994)195
- Dzido, T.H. and Smolarz, H.D.
Preliminary computer simulation for fine tuning of the high-performance liquid chromatography of some phenolic acids 679(1994)59
- Engasser, J.-M., see Gaillard, I. 679(1994)261
- Engelhardt, H.
Practical High-Performance Liquid Chromatography (by V.R. Meyer) (Book Review) 679(1994)212
- Farkas, T., Chambers, J.Q. and Guiochon, G.
Column efficiency and radial homogeneity in liquid chromatography 679(1994)231
- Feltl, L., see Koutek, B. 679(1994)307
- Fick, M., see Gaillard, I. 679(1994)261
- Fujimoto, Y., see Okamura, N. 679(1994)381
- Furuya, K., see Inoue, H. 679(1994)99
- Gaillard, I., Martial, A., Marc, A., Engasser, J.-M. and Fick, M.
Analytical method optimization for protein determination by fast high-performance liquid chromatography 679(1994)261
- Garbaye, J., see Devèvre, O. 679(1994)349
- Gelpí, E.
Mass Spectrometry for the Characterization of Microorganisms (edited by ACS) (Book Review) 679(1994)404
- Gerochi, D.D., see Dou, L. 679(1994)367
- Gluck, S.J., see Cleveland, J.A. 679(1994)167
- Golshan-Shirazi, S., see Levin, S. 679(1994)213
- Goto, M., see Shiosaki, A. 679(1994)1
- Graf, A., see Grimm, R. 679(1994)173
- Grimm, R., Graf, A. and Heiger, D.N.
Identification of tryptophan and tyrosine residues in peptides separated by capillary electrophoresis by their second-derivative spectra using diode-array detection 679(1994)173
- Guerrier, L., see Horvath, J. 679(1994)11
- Guiochon, G., see Farkas, T. 679(1994)231
- Guiochon, G., see Levin, S. 679(1994)213
- Günther, N., see Weber, W. 679(1994)181

Author Index

- Hall, L.
Quantitative determination of pivalic acid in dipivefrin-containing ophthalmic solutions by gas chromatography 679(1994)397
- Hansen, D.R., see Hills, J.W. 679(1994)319
- Heiger, D.N., see Grimm, R. 679(1994)173
- Henion, J., see Hsieh, F.Y.L. 679(1994)206
- Hewitt, C.N., see Cao, X.-L. 679(1994)115
- Hill, H.H., see Hills, J.W. 679(1994)319
- Hills, J.W., Hill, H.H., Hansen, D.R. and Metcalf, S.G.
Carbon dioxide supercritical fluid extraction of incinerator fly ash with a reactive solvent modifier 679(1994)319
- Hirose, T., see Shiosaki, A. 679(1994)1
- Holeman, J.A. and Danielson, N.D.
Liquid chromatography of antihistamines using post-column tris(2,2'-bipyridine) ruthenium(III) chemiluminescence detection 679(1994)277
- Horvath, J., Boschetti, E., Guerrier, L. and Cooke, N.
High-performance protein separations with novel strong ion exchangers 679(1994)11
- Hoskovec, M., see Koutek, B. 679(1994)307
- Hsieh, F.Y.L., Cai, J. and Henion, J.
Determination of trace impurities of peptides and alkaloids by capillary electrophoresis-ion spray mass spectrometry 679(1994)206
- Husain, S., Narsimha, R., Khalid, S. and Nageswara Rao, R.
Application of normal- and reversed-phase high-performance liquid chromatography for monitoring the progress of reactions of anthraquinone manufacturing processes 679(1994)375
- Inoue, H., Yamashita, H., Furuya, K., Nonomura, Y., Yoshioka, N. and Li, S.
Determination of copper(II) chlorophyllin by reversed-phase high-performance liquid chromatography 679(1994)99
- Inoue, S. and Ohtaki, N.
Metaphosphates as packing materials for biochromatography 679(1994)247
- Janson, J.-C., see Belew, M. 679(1994)67
- Jegorov, A., see Šimek, P. 679(1994)195
- Jiménez, A., see Vilaplana, J. 679(1994)133
- Just, U., see Mellor, F. 679(1994)147
- Kao, M.C.C., see Yao, Z.J. 679(1994)190
- Kavanagh, P.E., see Shalliker, R.A. 679(1994)105
- Kennndler, E., see Blatný, P. 679(1994)345
- Khalid, S., see Husain, S. 679(1994)375
- Konečný, K., see Koutek, B. 679(1994)307
- Koutek, B., Hoskovec, M., Vrkočová, P., Konečný, K. and Feltl, L.
Gas chromatographic determination of vapour pressures of pheromone-like compounds. II. Alcohols 679(1994)307
- Kraal, B., see Mesters, J.R. 679(1994)93
- Kuwabara, S., see Okamura, N. 679(1994)381
- Kvasnička, F., see Blatný, P. 679(1994)345
- Lameloise, M.-L. and Viard, V.
Choice of a tracer for external porosity measurement in ion-exchange resin beds 679(1994)255
- Leathard, D.A., see Allen, D.W. 679(1994)285
- Levin, S., Abu-Lafi, S., Golshan-Shirazi, S. and Guiochon, G.
Use of system peaks for the determination of the distribution of resorcinol, catechol and phenol in liquid chromatography 679(1994)213
- Levin, S., see Abu-Lafi, S. 679(1994)47
- Li, S., see Inoue, H. 679(1994)99
- Liu, Y., Yun, K.S. and Parcher, J.F.
Experimental method to distinguish column dead time from system dead time for the accurate determination of gas chromatographic void volumes: simultaneous pre- and post-column injection 679(1994)392
- Loh, K.C., see Yao, Z.J. 679(1994)190
- López, J., see Vilaplana, J. 679(1994)133
- MacEachern, G.J., see Mattina, M.J.I. 679(1994)269
- Marc, A., see Gaillard, I. 679(1994)261
- Markides, K.E., see Almquist, S.R. 679(1994)139
- Marnitz, U., see Weber, W. 679(1994)181
- Martial, A., see Gaillard, I. 679(1994)261
- Martin, C.L., see Cleveland, J.A. 679(1994)167
- Mattina, M.J.I. and MacEachern, G.J.
Extraction, purification by solid-phase extraction and high-performance liquid chromatographic analysis of taxanes from ornamental *Taxus* needles 679(1994)269
- Mellor, F., Just, U. and Strumpf, Th.
Supercritical fluid extraction using a new restrictor design 679(1994)147
- Mesters, J.R., Vorstenbosch, E.L.H., de Boer, A.J. and Kraal, B.
Complete purification of tRNA, charged or modified with hydrophobic groups, by reversed-phase high-performance liquid chromatography on a C₄/C₁₈ column system 679(1994)93
- Metcalf, S.G., see Hills, J.W. 679(1994)319
- Miyano, S., see Oi, S. 679(1994)35
- Moraes, N.M.P. and Shihomatsu, H.M.
Dynamic ion-exchange chromatography for the determination of lanthanides in rock standards 679(1994)387
- Mourey, T.H. and Bryan, T.G.
Size-exclusion chromatography of nylons in methylene chloride-dichloroacetic acid 679(1994)201
- Musso, G.F., see Straub, J.A. 679(1994)85
- Nageswara Rao, R., see Husain, S. 679(1994)375
- Narsimha, R., see Husain, S. 679(1994)375
- Nomura, A., see Yarita, T. 679(1994)329
- Nonomura, Y., see Inoue, H. 679(1994)99
- Nyström, L.-E., see Belew, M. 679(1994)67
- Ohtaki, N., see Inoue, S. 679(1994)247
- Oi, S., Ono, H., Tanaka, H., Shijo, M. and Miyano, S.
Axially dissymmetric bianthracene-based chiral stationary phase for the high-performance liquid chromatographic separation of enantiomers 679(1994)35
- Okamura, N., Fujimoto, Y., Kuwabara, S. and Yagi, A.
High-performance liquid chromatographic determination of carnolic acid and carnosol in *Rosmarinus officinalis* and *Salvia officinalis* 679(1994)381

- Ono, H., see Oi, S. 679(1994)35
Parcher, J.F., see Liu, Y. 679(1994)392
Parmar, P., see Straub, J.A. 679(1994)85
Petersson, P., see Almquist, S.R. 679(1994)139
Pirkle, W.H., see Schleimer, M. 679(1994)23
Putra, D.P., see Devèvre, O. 679(1994)349
Righetti, P.G., see Weber, W. 679(1994)181
Russell, I.M., see Shalliker, R.A. 679(1994)105
Saklatvala, R., see Allen, D.W. 679(1994)285
Schleimer, M., Pirkle, W.H. and Schurig, V.
 Enantiomer separation by high-performance liquid chromatography on polysiloxane-based chiral stationary phases 679(1994)23
Schurig, V., see Schleimer, M. 679(1994)23
Shalliker, R.A., Kavanagh, P.E. and Russell, I.M.
 Comparison of isocratic and gradient elution reversed-phase behaviour of high-molecular-mass polystyrenes in dichloromethane and acetonitrile 679(1994)105
Shihomatsu, H.M., see Moraes, N.M.P. 679(1994)387
Shijo, M., see Oi, S. 679(1994)35
Shiosaki, A., Goto, M. and Hirose, T.
 Frontal analysis of protein adsorption on a membrane adsorber 679(1994)1
Šimek, P., Jegorov, A. and Dusbábek, F.
 Determination of purine bases and nucleosides by conventional and microbore high-performance liquid chromatography and gas chromatography with an ion-trap detector 679(1994)195
Šlais, K.
 Suggested definition of zone resolution and zone capacity in separations of weak electrolytes or ampholytes by steady-state electrophoretic methods 679(1994)335
Smolarz, H.D., see Dzido, T.H. 679(1994)59
Sterin, M., see Abu-Lafi, S. 679(1994)47
Straub, J.A., Akiyama, A., Parmar, P. and Musso, G.F.
 Limited enzymatic digestion for the determination of the quantities of minor diastereomeric impurities in preparations of RMP-7, a peptide containing a reduced peptide bond 679(1994)85
Strumpf, Th., see Mellor, F. 679(1994)147
Stuting, H.H., see Dou, L. 679(1994)367
Takeshita, Y., see Yarita, T. 679(1994)329
Tanaka, H., see Oi, S. 679(1994)35
Tanaka, M., see Yoshinaga, M. 679(1994)359
Viard, V., see Lameloise, M.-L. 679(1994)255
Vilaplana, J., López, J. and Jiménez, A.
 Combined solvent extraction-mass spectrometry determination of free phenol traces in poly(vinyl chloride) products 679(1994)133
Vorstenbosch, E.L.H., see Mesters, J.R. 679(1994)93
Vrkočová, P., see Koutek, B. 679(1994)307
Walther, W., see Almquist, S.R. 679(1994)139
Wang, S., see Belew, M. 679(1994)67
Waterhouse, K.S., see Cao, X.-L. 679(1994)115
Weber, W., Wenisch, E., Günther, N., Marnitz, U., Betzel, C. and Righetti, P.G.
 Protein microheterogeneity and crystal habits: the case of epidermal growth factor receptor isoforms as isolated in a multicompartiment electrolyzer with isoelectric membranes 679(1994)181
Wenisch, E., see Weber, W. 679(1994)181
Yagi, A., see Okamura, N. 679(1994)381
Yamashita, H., see Inoue, H. 679(1994)99
Yao, Z.J., Kao, M.C.C., Loh, K.C. and Chung, M.C.M.
 Antibody against branched epitope as an affinity ligand to separate the parent protein 679(1994)190
Yarita, T., Nomura, A., Abe, K. and Takeshita, Y.
 Supercritical fluid chromatographic determination of tocopherols on an ODS-silica gel column 679(1994)329
Yoshinaga, M. and Tanaka, M.
 Use of selectively methylated β -cyclodextrin derivatives in chiral separation of dansylamino acids by capillary zone electrophoresis 679(1994)359
Yoshioka, N., see Inoue, H. 679(1994)99
Yun, K.S., see Liu, Y. 679(1994)392
Zeng, J.-N., see Dou, L. 679(1994)367
Zhou, Y., see Belew, M. 679(1994)67

Capillary Electrophoresis

Principles, Practice and Applications

By S.F.Y. Li

Journal of Chromatography Library Volume 52

"Everything seems to be there, any detection system you have ever dreamed of, any capillary coating, enough electrolyte systems to saturate your wits, and more, and more.

...by far the most thorough book in the field yet to appear."

Journal of Chromatography

"It is almost encyclopaedic in its coverage and all chapters are extremely well referenced. This will facilitate any search for original information on any aspect of CE."

Talanta

"This is a useful book that serves several audiences. The author is to be commended for putting together a thoughtful, complete, and thoroughly useful reference."

Analytical Chemistry

This book covers all aspects of CE, from the principles and technical aspects to the most important applications. It is intended to meet the growing need for a thorough and balanced treatment of CE. The book will serve as a comprehensive reference work. Both the experienced analyst and the newcomer will find the text useful.

Contents: **1. Introduction.** Historical Background. Overview of High Performance CE. Principles of Separations. Comparison with Other Separation Techniques. **2. Sample Injection Methods.** Introduction. Electrokinetic Injection. Hydrodynamic Injection. Electric Sample Splitter. Split Flow Sy-

ringe Injection System. Rotary Type Injector. Freeze Plug Injection. Sampling Device with Feeder. Microinjectors. Optical Gating. **3. Detection Techniques.** Introduction. UV-Visible Absorbance Detectors. Photo-diode Array Detectors. Fluorescence Detectors. Laser-based Thermo-optical and Refractive Index Detectors. Indirect Detection. Conductivity Detection. Electrochemical Detection. Mass Spectrometric Detection. **4. Column Technology.** Uncoated Capillary Columns. Coated Columns. Gel-filled Columns. Packed Columns. Combining Packed and Open-Tubular Column. **5. Electrophoretic Media.** Electrophoretic Buffer Systems. Micellar Electrokinetic Capillary Chromatography. Inclusion Pseudophases. Metal-complexing Pseudophases. Other Types of Electrophoretic Media. **6. Special Systems and Methods.** Buffer Programming. Fraction Collection. Hyphenated Techniques. Field Effect Electroosmosis. Systematic Optimization of Separation.



ELSEVIER

An imprint of Elsevier Science

7. Applications of Capillary Electrophoresis. Biomolecules. Pharmaceutical and Clinical Analysis. Inorganic Ions. Hydrocarbons. Foods and Drinks. Environmental Pollutants. Carbohydrates. Toxins. Polymers and Particles. Natural Products. Fuel. Metal Chelates. Industrial Waste Water. Explosives. Miscellaneous Applications.

8. Recent Advances and Prospect for Growth. Recent Reviews on CE. Advances in Injection Techniques. Novel Detection Techniques. Advances in Column Technology. Progress in Electrolyte Systems. New Systems and Methods. Additional Applications Based on CE. Future Trends. Subject index.

©1992 1st reprint 1993 608 pages
Hardbound

Price: Dfl. 395.00 (US\$225.75)
ISBN 0-444-89433-0

1st repr. as a Paperback 1993
Price: Dfl. 200.00 (US\$114.25)
ISBN 0-444-81590-2

ORDER INFORMATION

ELSEVIER SCIENCE B.V.

P.O. Box 330
1000 AH Amsterdam
The Netherlands
Fax: +31 (20) 5862 845

For USA and Canada

P.O. Box 945
Madison Square Station
New York, NY 10159-0945
Fax: +1 (212) 633 3680

US\$ prices are valid only for the USA & Canada and are subject to exchange rate fluctuations; in all other countries the Dutch guilder price (Dfl.) is definitive. Customers in the European Union should add the appropriate VAT rate applicable in their country to the price(s). Books are sent postfree if prepaid.

Analytical Applications of Circular Dichroism

Edited by **N. Purdie** and **H.G. Brittain**

Techniques and Instrumentation in Analytical Chemistry Volume 14

Circular dichroism is a special technique which provides unique information on dissymmetric molecules. Such compounds are becoming increasingly important in a wide variety of fields, such as natural products chemistry, pharmaceuticals, molecular biology, etc. The content of this book has been selected in order to feature the unique aspects of circular dichroism, and how these strengths can be of assistance to workers in the field.

Substantial discussions have been provided regarding the particular phenomena associated with dissymmetric compounds which give rise to the circular dichroism effect. Reviews are also given of the type of instrumentation available for the measurement of these effects. A number of chapters cover the wide range of applications illustrating the power of the method.

Owing to its broad appeal, the book will be of interest to workers in all areas of chemistry and pharmaceutical science.

Contents:

1. Introduction to chiroptical phenomena (H.G. Brittain).
 2. Instrumentation for the measurement of circular dichroism; past, present and future developments (D.R. Bobbitt).
 3. Instrumental methods of infrared and Raman vibrational optical activity (L.A. Nafie *et al.*).
 4. Application of infrared CD to the analysis of the solution conformation of biological molecules (M. Diem).
 5. Determination of absolute configuration by CD. Applications of the octant rule and the exciton chirality rule (D.A. Lightner).
 6. Analysis of protein structure by circular dichroism spectroscopy (J.F. Towell III, M.C. Manning).
 7. Chiroptical studies of molecules in electronically excited states (J.P. Riehl).
 8. Analytical applications of CD to forensic, pharmaceutical, clinical, and food sciences (N. Purdie).
 9. The use of circular dichroism as a liquid chromatographic detector (A. Gergely).
 10. Applications of circular dichroism spectropolarimetry to the determination of steroids (A. Gergely).
 11. Circular dichroism studies of the optical activity induced in achiral molecules through association with chiral substances (H.G. Brittain).
- Subject index.

© 1994 360 pages Hardbound
Price: Dfl. 355.00 (US \$ 202.75)
ISBN 0-444-89508-6

ORDER INFORMATION

For USA and Canada
ELSEVIER SCIENCE INC.

P.O. Box 945
Madison Square Station
New York, NY 10160-0757
Fax: (212) 633 3880

In all other countries
ELSEVIER SCIENCE B.V.

P.O. Box 330
1000 AH Amsterdam
The Netherlands
Fax: (+31-20) 5862 845

US\$ prices are valid only for the USA & Canada and are subject to exchange rate fluctuations; in all other countries the Dutch guilder price (Dfl.) is definitive. Customers in the European Community should add the appropriate VAT rate applicable in their country to the price(s). Books are sent postfree if prepaid.



**ELSEVIER
SCIENCE** B.V.

PUBLICATION SCHEDULE FOR THE 1994 SUBSCRIPTION

Journal of Chromatography A and *Journal of Chromatography B: Biomedical Applications*

MONTH	1993	J-J	J	A	S	O	
Journal of Chromatography A	652-657	Vols. 658-672	673/1 673/2 674/1 + 2 675/1 + 2 676/1	676/2 677/1 677/2 678/1	678/2 679/1 679/2 680/1	680/2	The publication schedule for further issues will be published later.
Bibliography Section		Vol. 681			682/1		
Journal of Chromatography B: Biomedical Applications		Vols. 652-656	657/1 657/2	658/1 658/2	659	660/1 660/2	

INFORMATION FOR AUTHORS

(Detailed *Instructions to Authors* were published in *J. Chromatogr. A*, Vol. 657, pp. 463-469. A free reprint can be obtained by application to the publisher, Elsevier Science B.V., P.O. Box 330, 1000 AH Amsterdam, Netherlands.)

Types of Contributions. The following types of papers are published: Regular research papers (full-length papers), Review articles, Short Communications and Discussions. Short Communications are usually descriptions of short investigations, or they can report minor technical improvements of previously published procedures; they reflect the same quality of research as full-length papers, but should preferably not exceed five printed pages. Discussions (one or two pages) should explain, amplify, correct or otherwise comment substantively upon an article recently published in the journal. For Review articles, see inside front cover under Submission of Papers.

Submission. Every paper must be accompanied by a letter from the senior author, stating that he/she is submitting the paper for publication in the *Journal of Chromatography A* or *B*.

Manuscripts. Manuscripts should be typed in **double spacing** on consecutively numbered pages of uniform size. The manuscript should be preceded by a sheet of manuscript paper carrying the title of the paper and the name and full postal address of the person to whom the proofs are to be sent. As a rule, papers should be divided into sections, headed by a caption (e.g., Abstract, Introduction, Experimental, Results, Discussion, etc.). All illustrations, photographs, tables, etc., should be on separate sheets.

Abstract. All articles should have an abstract of 50-100 words which clearly and briefly indicates what is new, different and significant. No references should be given.

Introduction. Every paper must have a concise introduction mentioning what has been done before on the topic described, and stating clearly what is new in the paper now submitted.

Experimental conditions should preferably be given on a *separate* sheet, headed "Conditions". These conditions will, if appropriate, be printed in a block, directly following the heading "Experimental".

Illustrations. The figures should be submitted in a form suitable for reproduction, drawn in Indian ink on drawing or tracing paper. Each illustration should have a caption, all the *captions* being typed (with double spacing) together on a *separate sheet*. If structures are given in the text, the original drawings should be provided. Coloured illustrations are reproduced at the author's expense, the cost being determined by the number of pages and by the number of colours needed. The written permission of the author and publisher must be obtained for the use of any figure already published. Its source must be indicated in the legend.

References. References should be numbered in the order in which they are cited in the text, and listed in numerical sequence on a separate sheet at the end of the article. Please check a recent issue for the layout of the reference list. Abbreviations for the titles of journals should follow the system used by *Chemical Abstracts*. Articles not yet published should be given as "in press" (journal should be specified), "submitted for publication" (journal should be specified), "in preparation" or "personal communication".

Vols. 1-651 of the *Journal of Chromatography*; *Journal of Chromatography, Biomedical Applications* and *Journal of Chromatography, Symposium Volumes* should be cited as *J. Chromatogr.* From Vol. 652 on, *Journal of Chromatography A* (incl. Symposium Volumes) should be cited as *J. Chromatogr. A* and *Journal of Chromatography B: Biomedical Applications* as *J. Chromatogr. B*.

Dispatch. Before sending the manuscript to the Editor please check that the envelope contains four copies of the paper complete with references, captions and figures. One of the sets of figures must be the originals suitable for direct reproduction. Please also ensure that permission to publish has been obtained from your institute.

Proofs. One set of proofs will be sent to the author to be carefully checked for printer's errors. Corrections must be restricted to instances in which the proof is at variance with the manuscript.

Reprints. Fifty reprints will be supplied free of charge. Additional reprints can be ordered by the authors. An order form containing price quotations will be sent to the authors together with the proofs of their article.

Advertisements. The Editors of the journal accept no responsibility for the contents of the advertisements. Advertisement rates are available on request. Advertising orders and enquiries can be sent to the Advertising Manager, Elsevier Science B.V., Advertising Department, P.O. Box 211, 1000 AE Amsterdam, Netherlands; courier shipments to: Van de Sande Bakhuyzenstraat 4, 1061 AG Amsterdam, Netherlands; Tel. (+31-20) 515 3220/515 3222, Telefax (+31-20) 6833 041, Telex 16479 els vi nl. UK: T.G. Scott & Son Ltd., Tim Blake, Portland House, 21 Narborough Road, Cosby, Leics. LE9 5TA, UK; Tel. (+44-533) 753 333, Telefax (+44-533) 750 522. USA and Canada: Weston Media Associates, Daniel S. Lipner, P.O. Box 1110, Greens Farms, CT 06436-1110, USA; Tel. (+1-203) 261 2500, Telefax (+1-203) 261 0101.

Specialists in
Chromatography

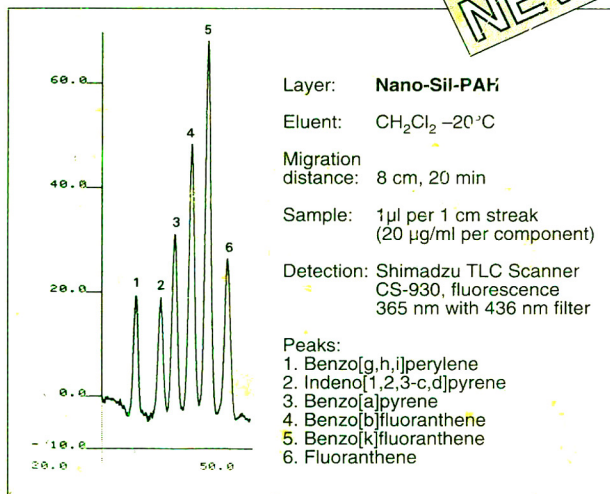
TLC

— a method with future —



- TLC ready-to-use layers with silica, RP silica, aluminium oxide, cellulose
- glass, aluminium, polyester supports
- special ready-to-use layers e.g. Nano-SIL-PAH

NEW



Please ask for further information!

MACHEREY-NAGEL



MACHEREY-NAGEL GmbH & Co. KG · P.O. Box 10 13 52
D-52313 Düren · Germany · Tel. (02421) 698-0 · Telefax (02421) 620 54
Switzerland: MACHEREY-NAGEL AG · P.O. Box 224 · CH-4702 Oensingen · Tel. (062) 762066
France: MACHEREY-NAGEL S.à.r.l. · B.P. 135 · F-67722 Hoerdt · Tel. 88.51.79.89

**FOR ADVERTISING
INFORMATION
PLEASE CONTACT OUR
ADVERTISING
REPRESENTATIVES**

USA/CANADA

Weston Media Associates

Mr. Daniel S. Lipner

P.O. Box 1110, GREENS FARMS, CT 06436-1110
Tel: (203) 261-2500, Fax: (203) 261-0101

GREAT BRITAIN

T.G. Scott & Son Ltd.

Tim Blake/Vanessa Bird

Portland House, 21 Narborough Road
COSBY, Leicestershire LE9 5TA
Tel: (0533) 753-333, Fax: (0533) 750-522

JAPAN

ESP - Tokyo Branch

Mr. S. Onoda

20-12 Yushima, 3 chome, Bunkyo-Ku
TOKYO 113
Tel: (03) 3836 0810, Fax: (03) 3839-4344
Telex: 02657617



REST OF WORLD

**ELSEVIER
SCIENCE**

Ms. W. van Cattenburch
Advertising Department

P.O. Box 211, 1000 AE AMSTERDAM,
The Netherlands

Tel: (20) 515.3220/21/22, Telex: 16479 els vi nl
Fax: (20) 683.3041